# AB INITIO INVESTIGATION OF THE THERMOCHEMISTRY, SPECTROSCOPY AND DYNAMICS OF REACTIONS BETWEEN MERCURY AND REACTIVE HALOGEN SPECIES

By

BENJAMIN C. SHEPLER

A dissertation submitted in partial fulfillment of the requirements for the degree of

DOCTOR OF PHILOSOPHY

WASHINGTON STATE UNIVERSITY
Department of Chemistry

AUGUST 2006

To the Faculty of Washington State University:

The members of the Committee appointed to examine the dissertation of BENJAMIN C. SHEPLER find it satisfactory and recommend that it be accepted.

_____
Chair

_____

_____

_____

ACKNOWLEGEMENTS

First and foremost, I would like to express my deepest thanks to my advisor Professor Kirk A. Peterson. Dr. Peterson's guidance and support throughout my time at Washington State University has been more than any graduate student could hope for. I would also like to thank a post-doctoral fellow who was at WSU for much of my tenure and worked with me on the mercury-halogen reactions, Dr. Nikolai B. Balabanov. Without Dr. Balabanov's insight and contributions the success of our research would not have been possible. A number of researchers have provided invaluable help and insight with the various projects involved in this thesis and I would like to express my appreciation to Professor B. Ramachandran (Louisiana Tech University), Dr. B.C. Garrett (Pacific Northwest National Laboratory-Environmental Molecular Sciences Laboratory), Professor R. Duchovic (Indiana University-Purdue University Ft. Wayne), Professor H. Stoll (University of Stuttgart), Dr. David Feller, and Dr. W. de Jong (Pacific Northwest National Laboratory-Environmental Molecular Sciences Laboratory). I would also like to thank my committee members: Professor Kerry W. Hipps, Professor George H. Mount, and Professor Ronald D. Poshusta whose help and contributions over the years have been invaluable. I would also like to express my gratitude to Professors Hipps and Poshusta for their instruction in the bulk of my physical chemistry course work at WSU.

I would also like to acknowledge my family without whom I would not be where I am today.

AB INITIO INVESTIGATION OF THE THERMOCHEMISTRY, SPECTROSCOPY AND DYNAMICS OF REACTIONS BETWEEN MERCURY AND REACTIVE HALOGEN SPECIES

Abstract

by Benjamin C. Shepler, Ph.D.
Washington State University
August 2006

Chair: Kirk A. Peterson

Recent measurements in the Arctic troposphere have revealed episodic depletions of mercury during polar sunrise. The depletion events are thought to be the result of reactions between gas phase elemental mercury with reactive halogen species. The goal of this work has been to characterize reactions between mercury and reactive halogen species with accurate ab initio calculations.

The main body of the thesis is divided into eight chapters and two appendices with Chapter 1 being an introduction and summary.

Chapter 2 discusses the calculation of potential energy curves for the ground and low-lying excited states of the BrCl molecule. BrCl is thought to be a major source of photolyzable halogens in the arctic troposphere.

In Chapter 3 the characterization of the ground state of HgO is discussed. The accurate dissociation energy that was calculated rules out the involvement of HgO in the mercury depletion events.

The recombination of Hg + Br atoms may be the first step in the mercury depletion events and Chapter 4 discusses ab initio calculations and quasiclassical trajectory calculations that were used to calculate the rate constant for this process.

The thermochemistry of reactions between mercury and iodine containing species is covered in Chapter 5.

It has been hypothesized that BrO plays a significant role in the mercury depletion events. The reaction of HgBr (HgCl) with BrO (ClO) can lead to the formation of mercury hypohalite species and calculations on these molecules are discussed in Chapter 6.

Heterogeneous chemistry may play a role in mercury depletion events and the effect of aqueous microsolvation on a number of mercury-halogen reactions is investigated in Chapter 7.

Cadmium should undergo similar reactions with halogen species, but little is known about gas phase reactions involving cadmium. Chapter 8 details accurate calculations on the thermochemistry of reactions between mercury and reactive halogen species.

The appendices are manuscripts on which the dissertation's author was a contributor, but not the primary author. Appendix 1 details accurate characterization of the halogen oxide molecules ClO, BrO, IO and their anions. Appendix 2 describes calculations carried out on the rate of the HgBr + Br reaction.

TABLE OF CONTENTS


| | Page |
|---|---|
| Acknowledgements . . . . . | iii |
| Abstract . . . . . | iv |
| Table of Contents . . . . . | vi |
| List of Tables . . . . . | x |
| List of Figures . . . . . | xiii |
| Dedication . . . . . | xv |
| 1. Introduction . . . . . | 1 |
| I. Mercury in the atmosphere . . . . . | 2 |
| II. Atmospheric mercury depletion events . . . . | 2 |
| III. Previous work on the reactions between mercury and reactive Halogens . | 9 |
| IV. Summary of present work . . . . . | 11 |
| V. Conclusion . . . . . | 19 |
| References . . . . . | 21 |
| 2. Ab Initio Study of the Ground and Low-Lying Excited States of BrCl . | 28 |
| I. Introduction . . . . . | 29 |
| II. Methodology . . . . . | 33 |
| III. Results and Discussion . . . . . | 39 |
| IV. Conclusions . . . . . | 45 |
| References . . . . . | 47 |

3. Mercury monoxide: a systematic investigation of its ground electronic state . 63

I. Introduction . . . . . 64

II. Methodology . . . . . 65

III. Results . . . . . 69

IV. Discussion . . . . . 73

V. Acknowledgements . . . . . 73

References . . . . . 75

4. Hg + Br → HgBr recombination and collision-induced dissociation dynamics state 83

I. Introduction . . . . . 84

II. Methodology . . . . . 87

III. Results and Discussion . . . . . 97

IV. Conclusions . . . . . 102

V. Acknowledgements . . . . . 104

References . . . . . 104

5. Ab initio thermochemistry involving heavy atoms: An investigation of the reactions Hg + IX (X = I, Br, Cl, O) 116

I. Introduction . . . . . 117

II. Methodology . . . . . 119

III. Results and Discussion . . . . . 127

IV. Conclusions . . . . . 137

V. Acknowledgements . . . . . 140

References . . . . . 141

6. Ab initio characterization of the mercury hypohalites: XHgOY . . 153

(X, Y = Br, Cl)

I. Introduction . . . . . 154

II. Methodology . . . . . 155

III. Results and Discussion . . . . . 157

IV. Conclusions . . . . . 161

References . . . . . 163

7. Micro-Solvation of Mercury Halide Species . . . . 173

I. Introduction . . . . . 174

II. Methodology . . . . . 175

III. Results and Discussion . . . . . 178

IV. Conclusions . . . . . 188

References . . . . . 189

8. Chemically Accurate Thermochemistry of Cadmium: An ab initio study of 203

Cd + XY (X = H, O, Cl, Br; Y = Cl, Br)

I. Introduction . . . . . 204

II. Methodology . . . . . 207

III. Results and Discussion . . . . . 211

IV. Conclusions . . . . . 222

V. Acknowledgements . . . . . 224

References . . . . . 225

9. Appendix 1: On the spectroscopic and thermochemical properties of ClO, BrO, IO and their anions 241

10. Appendix 2: Accurate Global Potential Energy Surface and Reaction Dynamics for the Ground State of $HgBr_2$ 265

LIST OF TABLES

2.1 Contributions and final predicted values for the equilibrium bond lengths, harmonic frequencies an dissociation energies of the $X1^1\Sigma^+(0^+)$ state of BrCl 51

2.2 Contributions and final predicted values for the equilibrium bond length, harmonic frequency, and dissociation energy of the $B^3\Pi(0^+)$ state of BrCl 52

2.3 Spectroscopic Constants of the remaining bound excited states 53

2.4 Composition of the $0^+$ states in the Λ-S basis states: short bond length and avoided crossing 1 54

2.5 Composition of the $0^+$ states in the Λ-S basis states: avoided crossing 2 55

2.6 Composition of the $0^+$ states in the Λ-S basis states: asymptotic region 56

2.7 Calculated vertical excitation energies and transition dipole moments from the ground state 57

3.1 Calculated spectroscopic constants of $1^1\Sigma^+$ and $1^3\Pi$ HgO neglecting spin-orbit coupling 78

3.2 Effects of scalar relativity on the spectroscopic constants of $1^1\Sigma^+$ at the CCSD(T) level of theory in all-electron calculations. 79

4.1 Calculated and experimental spectroscopic constants of the ground state of HgBr 108

4.2 Spectroscopic constants for the ground state of HgAr 109

4.3 Spectroscopic constants for the ground state of ArBr 109

4.4 Calculated temperature dependent rate constants for collision-induced dissociation and recombination 110

4.5 Comparison of rate constants of the 2nd order recombination of Hg and Br atoms at 298 K and 1 bar pressure ($cm^3$ $molecules^{-1}$ $s^{-1}$) 110

5.1 Equilibrium Bond Lengths (Å) and Harmonic Frequencies ($cm^{-1}$) 148

5.2 Relativistic effects on dissociation energies (kcal/mol) 149

5.3 Dissociation energies for the diatomic molecules of this study (kcal/mol) 150

5.4 0K Enthalpies of reaction, $\Delta H_r$, with constituent energy contributions 151

5.5 Dissociation energies and 0K heats of formation in kcal/mol for HgIX species 152

6.1 Bond lengths ($a_0$) and angles of the mercury hypohalites computed at the CCSD(T)/aVQZ level of theory 166

6.2 Harmonic vibrational frequencies ($cm^{-1}$) of the mercury hypohalites computed at the MP2/aVTZ level of theory 166

6.3 Enthalpies of reaction (0 K) for HgX + YO → XHgOY in kcal/mol. Computed at the CCSD(T)/CBS+CV+SO level of theory 167

6.4 Reaction enthalpies (0 K) for formation of mercury hypohalites and other competing reactions[a] (kcal/mol) 167

6.5 Excitation energies and oscillator strengths for the transitions from the ground state ($X^1A'$) of BrHgOBr to excited states at wavelengths greater than 230 nm 168

7.1 Incremental binding energies ($D_0$) for HgXY + $nH_2O$ (kcal/mol) 193

7.2 Incremental binding energies ($D_0$) for HgX and XY + $nH_2O$ (kcal/mol) 194

7.3 Incremental binding energies ($D_0$) for atoms + $nH_2O$ (kcal/mol) 195

7.4 Effects of microsolvation on reaction enthalpies (kcal/mol) 196

8.1 Basis Set and Pseudopotential Details 231

8.2 Calculated CCSD(T) Equilibrium Bond Lengths 232

8.3 Harmonic Vibrational Frequencies and Zero Point Energies 234

8.4 CCSD(T) Dissociation Energies of the Diatomic Molecules of the Present Work Compared to the Available Experimental Values 236

8.5 Calculated 0K reaction enthalpies compared to the available experimental values 238

8.6 Dissociation energies and 0K heats of formation in kcal/mol for triatomic cadmium halides 240

LIST OF FIGURES

2.1 Λ-S states of BrCl correlating with ground-state atoms 58

2.2 $\Omega = 0^+$ states 59

2.3 $\Omega = 0^-$ states 60

2.4 $\Omega = 1$ states 61

2.5 $\Omega = 2$ and 3 states 62

3.1 Potential energy curves for the lowest two electronic states of HgO calculated as a function of basis set at the MRCI+Q level of theory (neglecting spin-orbit coupling) 80

3.2 Potential energy curves at the MRCI+Q/aug-cc-pVQZ level of theory for the low-lying electronic states of HgO used in the calculation of spin-orbit coupling effects. The Hg 5*d* electrons were not correlated in these calculations. 81

3.3 Potential energy curves for the lowest *spin-orbit coupled* electronic states of HgO calculated at the MRCI+Q/CBS level of theory. The states are labeled by their Ω quantum numbers. 82

4.1 Pseudo-Jacobi coordinates used to fit the three-body potential 111

4.2 Ground state potential energy curve of HgBr and centrifugally distorted effective potential corresponding to J=200. Horizontal lines correspond to the v=25 level on each potential 111

4.3 Ground state potential energy curve of HgAr with and without the corrections for spin-orbit coupling and core-valence correlation 112

4.4 Ground state potential energy curve of ArBr with and without the 112

corrections for spin-orbit coupling and core-valencecorrelation

4.5 Contour plot of HgBr-Ar. r(HgBr)=2.494 Å 113

4.6 Contour plot of HgBr-Ar. r(HgBr)=3.440 Å 113

4.7 Surface plot of HgBr-Ar with $\alpha$=75° 114

4.8 Thermally averaged cross section as a function of collision energy 114

4.9 Boltzmann weighted cross sections as a function of j for various collision energies and v=36 115

4.10 Boltzmann weighted cross sections as a function of v for various collision energies and j=100 115

6.1 Structure of BrHgOBr 169

6.2 Energy level diagram [$\Delta H_r$(0K)] for the ground state of the HgBr+BrO reaction (kcal/mol) 170

6.3 MCSCF/aVTZ Potential energy curves for the ground and low-lying excited states in the dissociation of BrHgOBr → BrHg + OBr 171

6.4 MCSCF/aVTZ Potential energy curves for the ground and low-lying excited states in the dissociation of BrHgOBr → BrHgO + Br 172

7.1 Microsolvated structures of $HgBr_2$ 197

7.2 Microsolvated structures of HgBr 198

7.3 Microsolvated structures of $Br_2$ 199

7.4 Microsolvated structures of Br atom 200

7.5 Microsolvated structures of Hg atom 201

7.6 Alternate conformers 202

# DEDICATION

This dissertation is dedicated to my wife, Dr. Carrie G. Shepler.

# Introduction

**Benjamin C. Shepler**

*Department of Chemistry, Washington State University, Pullman, Washington 99164-4630*

## I. MERCURY IN THE ATMOSPHERE

Mercury is unique among heavy metals in the atmosphere in that it exists predominately (>90%) in the gas phase and zero oxidation state ($Hg^0$).[1-3] Gaseous elemental mercury (GEM) exhibits long atmospheric residence times on the order of 6-24 months.[1,4] This long lifetime allows for the transport of $Hg^0$ tens of thousands of kilometers from its natural and anthropogenic sources.[1] In addition to its long residence times, the high volatility of $Hg^0$ allows it to be easily reemitted to the atmosphere following deposition.[5] These long residence times and high volatility give atmospheric mercury nearly constant background concentrations of 1.8 ng/m$^3$ in the more industrialized northern hemisphere and 1.3 ng/m$^3$ in the southern hemisphere.[6-8] Reactive gaseous mercury (RGM), which is mostly divalent mercury species ($Hg^{+2}$), and particulate mercury ($Hg_p$) make up a small fraction of atmospheric mercury but have significantly shorter lifetimes and thus play a disproportionately large role in the deposition processes of mercury.[1,9]

The toxic nature of mercury makes it a significant environmental problem, and its long-range transport capabilities allow for contamination of regions remote from its natural and anthropogenic sources. Of particular concern is the highly toxic methyl mercury species whose long biological half-life can result in bioaccumulation of more than a million fold in the aquatic food chain.[1] The less toxic $Hg^0$ is able to be transformed into methyl mercury by bacteria and other natural phenomena.[10-12]

## II. ATMOSPHERIC MERCURY DEPLETION EVENTS

Throughout the fall and dark winter months the concentration of total gaseous mercury (TGM) in the polar tropospheres remains near the global background concentration. However,

in 1995 Schroeder et al.[13] were the first to observe rapid decreases in the Arctic TGM concentration during the polar spring at Alert, Nunavut, Canada. These mercury depletion events (MDEs) have since been observed elsewhere in the Arctic at Barrow, Alaska;[14] Nord, Greenland;[15] Ny-Ålesund, Svalbard;[16] and also in the Antarctic.[17] MDEs are characterized by a sudden drop in the background mercury concentration from ~1.7 ng/m$^3$ to concentrations below 1 ng/m$^3$ and frequently falling lower than 0.1 ng/m$^3$.[1,14,18,19] It only takes a few hours for the concentration to drop and can remain low for several hours up to a few days.[13,14,20] The mercury depletion events are not observed after the snowmelt, and the background concentration of mercury peaks during the summer with a median concentration slightly higher than global background concentrations before falling to normal levels again in the fall.[21]

The mercury depletion events are highly correlated with similar tropospheric ozone depletion events.[13,14] The low ozone events (LOEs) were first observed in the Arctic spring of 1985 and like the MDEs they were first observed at the Alert research station.[22] Since those first measurements the LOEs have been observed in other Arctic locations, as well as the Antarctic.[23-26] Barrie et al.[23] first proposed the link between the LOEs and bromine chemistry based on high levels of filterable bromine collected during the ozone depletion events. The role of halogens in the ozone depletion phenomena has since been largely accepted (see for example references 27-33 and references therein). It is generally believed that the tropospheric ozone depletions are the result of some combination of the catalytic reactions:[6,28,29,32]

$$Br_2 + h\nu \rightarrow 2Br \quad (1)$$

$$Br + O_3 \rightarrow BrO + O_2 \quad (2)$$

$$BrO + BrO \rightarrow 2Br + O \quad (3)$$

$$BrO + HO_2 \rightarrow HOBr + O \quad (4)$$

$$Br + RH \rightarrow HBr + R \quad (5)$$

While bromine chemistry is thought to be dominant, it is thought that iodine and to a lesser extent chlorine could also be involved.[28,30,33] Recent studies suggest that $Br_2$ and BrCl are the major sources of photolizable bromine during polar springtime.[28,30] What is less clear is how the photolizable bromine is released into the troposphere. One of the most likely scenarios involves heterogeneous reactions that activate $Br^-$ from aerosol[34] and surface snow and ice.[35] The surface/condensed phase reaction most often cited is[6,27,28,30,33]

$$HOBr + H^+ + Br^- \rightarrow Br_2 + H_2O \quad (6)$$

where again $I^-$ and $Cl^-$ are likely involved to a lesser extent. This autocatalytic release of halogens is often referred to as the "bromine explosion." There is mounting evidence[29,32,36] that indicates new sea-ice surfaces and cold temperatures that favor formation of "frost flowers" are important for the occurrence of bromine explosions. Frost flowers are fragile ice crystals that tend to be highly saline in nature and are common on the ice surfaces of open leads (breaks in sea ice).[32]

While the LOEs were originally thought to be confined to the polar regions during springtime, there have been recent measurements (see Ref. 33 and references therein) at sites outside the polar regions that have found elevated levels of BrO, ClO, IO, $Cl_2$ and Cl atoms. This suggests that the chemistry responsible for tropospheric ozone depletion may be more common outside the Arctic and Antarctic than originally assumed. In fact low ozone levels recorded at the same time as high BrO concentrations have been observed in the Dead Sea basin.[37,38] However, while this chemistry may be active outside the polar regions it is likely the lack of a strong inversion layer and the sea ice necessary for the "bromine explosions" would

preclude frequent observation of drastically low ozone levels outside the Arctic and Antarctic. If the halogen reactants necessary for the ozone depletion are present at lower latitudes, then it is also likely that the mercury depletion chemistry is also not isolated to the polar regions.

Due to the similarity of the ozone and mercury phenomena, it has been proposed that the mercury depletions are also caused by reactions between $Hg^0$ and reactive halogen species that result in the formation of oxidized Hg(II).[13,14,39] It is commonly suggested that the Br and BrO radicals are the most likely halogen reactants.[6,14,16,40-42] While the involvement of halogen species is generally accepted, the mechanism of the MDEs and the ultimate fate of the mercury is still very uncertain. One of the complications in elucidating the mechanism is that some of the observed MDEs are due to transport of already depleted air masses while others are the result of local chemistry.[20] During measurements in the Arctic and Antarctic it has been found that as the GEM concentration drops during the MDEs, the concentration of reactive gaseous mercury and particulate mercury increases.[14,16,18,20,39] RGM has been found to increase from ~2 pg/m$^3$ before MDEs to as high as 280 and 900 pg/m$^3$ during the mercury depletion events.[14,18] Early in the investigations of the MDEs there was considerable debate about whether the primary mechanism for Hg oxidation involved purely gas phase reactions and the formation of RGM[14] or heterogeneous reactions and the formation of $Hg_p$[13,39]. It now seems to be generally accepted that gas phase reactions involving formation of RGM play a significant role, but the role of $Hg_p$ is still largely in doubt.[18,20] It is possible that some of the oxidation occurs heterogeneously, but it is also likely that the oxidation only occurs in the gas phase and then the initially formed RGM becomes associated with atmospheric particles.[14,18,20,21] It has been proposed that under certain conditions icy clouds may be involved in the heterogeneous oxidation of Hg.[20]

Regardless of the mechanism for oxidation, both RGM and $Hg_p$ have significantly shorter lifetimes than GEM and are rapidly deposited on the snow pack.[9] The fate of the mercury once it has been deposited is still under considerable debate. Measurements of mercury concentration in snow have found drastic increases from the dark winter months until just prior to the snowmelt. A study at Alert in 1998 found a four-fold increase from 7.8 ng/L in January to 34 ng/L in May.[39] A similar investigation at Point Barrow saw an even more drastic increase from <1 ng/L to >90 ng/L.[14] One common hypothesis is that the increase of mercury in the snow throughout the spring is the result of mercury depletion events. A modeling study[15] has estimated that the deposition of mercury to the Arctic when not including MDEs in the simulation is 89 tons/year and this increases to 208 tons/year when MDEs are included.

However, some studies have suggested that the MDEs themselves are not responsible for the increase in mercury concentrations in the snowpack. These studies indicate that following some mercury depletion events the Hg that is initially deposited is reemitted to the atmosphere in the days following the MDE.[43-45] This hypothesis is supported by increases in GEM concentration over the snowpack and decreases in Hg concentration in snow in the days following some MDEs. It has been suggested that this emission of Hg from snow is the result of photoinduced reduction of $Hg^{+2}$ to the more volatile $Hg^0$ and involves the quasi-liquid layer on the surface of snow grains.[43-46] However, there is also evidence to suggest that the $Hg^0$ formed from the photoreduction is just as rapidly photooxidized and then redeposited when local conditions change.[45] Regardless, it is clear the deposition fluxes are being underestimated because the estimated emission flux from snow to air of 2-5 ng $m^{-2}$ $h^{-1}$ would result in complete emptying of the snowpack of Hg in a single month,[43] when in fact the concentration is known to increase during the spring months.[14,16,39] It is possible that the role of MDEs on the

concentration of Hg in snow differs in various locations and times due to different and variable meteorological and chemical conditions.[43] One other possibility is that the chemistry responsible for the MDEs is occurring even during times when bromine explosions are observed, and this is partially responsible for the increases of Hg in snow.

It does seem clear that the elevated mercury levels in the snowpack do correspond to a net increase of mercury io the Arctic ecosystem.[14,21,39,40,46] The higher concentrations of mercury in the Arctic troposphere in the summer could be an indication that the mercury in the snow is simply volatized and returned to the atmosphere. However, preliminary results suggest that the jump in summer concentrations is not sufficient to account for the loss associated with the low concentrations in the spring.[21] Another study found that during the snowmelt the concentration of Hg in the snow decreased, but measurements of GEM above the snowpack indicated that 90% of the Hg was not released to the atmosphere. It was hypothesized that the relatively soluble Hg(II) species were dissolved and carried out with the melt water.[46]

One concern about this large influx of mercury to the Arctic ecosystem is that it occurs at a time when biological activity is at a peak. To determine the fraction of mercury that is bioavailable, researchers have used genetically engineered bacteria that emit light when divalent mercury ($Hg^{+2}$) enters their cells. This measurement is of interest because bacteria are known to convert $Hg^0$ to $Hg^{+2}$ and also $Hg^{+2}$ to methyl mercury. These investigations[14,47] determined that in the spring prior to snowmelt 13% of the mercury was bioavailable. During the early snowmelt the total concentration of Hg in snow decreases, but the fraction of bioavailable Hg increases from 13% to 55%.[14,47] This result suggests differences in the behavior of the inorganic mercury species in the snowpack and could be the result of the more bioavailable Hg being either harder to photoreduce or reflect a lower water solubility.

There is reason to believe that the occurrence of mercury depletion events has been increasing over the years, as has the load of mercury to the Arctic.[14] Tarasick and Bottenheim[32] have reported an increase in the ozone depletion events from 1966-2000. Based on the strong positive correlation between the mercury and ozone depletions, it is likely that the mercury depletion events have also been increasing. The bromine explosions are thought to be enhanced by open leads (cracks) in the ice pack. The increase in open leads as a result of warming global temperatures has been suggested as a contributing factor in the increased level of ozone loss phenomena.[32] Further evidence of the role leads play in MDEs comes from a recent study of mercury concentration in snow that found mercury concentrations near open leads to be 9 times greater than in snow away from leads.[36] An investigation of sediment cores from Arctic lakes suggest a three-fold increase in mercury deposition from the onset of the industrial revolution and suggest this increase may be due to a combination of springtime mercury depletions and more general mercury deposition.[48] The increase in mercury contamination in Arctic biota since the early 1990's despite decreases in anthropogenic emissions suggest some new chemistry. If mercury depletion events or similar chemistry does significantly contribute to the load of mercury in the Arctic and have been increasing, it could help explain the increased contamination.[14]

While reactions between mercury and reactive halogen molecules have been hypothesized to be responsible for the mercury depletion events, very little was known about the gas phase reactions between these species at the start of this work. The goal of this project has been to use accurate ab initio calculations to characterize the thermochemistry, spectroscopy and dynamics of the reactions that may be involved in the mercury depletion events.

## III. PREVIOUS WORK ON THE REACTIONS BETWEEN MERCURY AND REACTIVE HALOGENS

Before the observation of MDEs, the primary interest in gaseous mercury halides was in connection with laser applications. The UV absorption[49-52] and dissociation[53-58] of $HgX_2$ and the $B^2\Sigma^+ \rightarrow X^2\Sigma^+$ transitions of HgX (X=Br, Cl, I)[59-68] have received a fair amount of attention. The infrared and Raman spectra of matrix isolated[69-72] and gas-phase[73-75] HgIX (X=Br, Cl, I) have also been characterized. Additionally, $HgI_2$ has been the focus of crossed molecular beam experiments[76-78] and femtosecond transition-state spectroscopy that focused on its photodissociation[79-82].

The first kinetic data for gas phase reactions between mercury and reactive halogen species was a rate constant for the reaction of $Hg^0$ with $Cl_2$ of $4x10^{-16}$ $cm^3$ $molec^{-1}$ $s^{-1}$ reported by Schroeder et al.[2]. More recently rate constants for reactions of mercury with a number of halogen species have been reported by Aryia and co-workers.[42,83,84] who used cold-vapor atomic absorption spectroscopy (CVAAS) and gas chromatography with mass spectrometric detection (GC-MS). They determined rate constants at 298 K and 1 atm for the reaction of mercury with $Cl_2$ ($k = 2.6 \times 10^{-18}$ $cm^3$ $molecule^{-1}$ $s^{-1}$), $Br_2$ ($k \leq 0.9 \times 10^{-16}$ $cm^3$ $molecule^{-1}$ $s^{-1}$), Cl ($k = 1.0 \times 10^{-11}$ $cm^3$ $molecule^{-1}$ $s^{-1}$), and Br ($k = 3.2 \times 10^{-12}$ $cm^3$ $molecule^{-1}$ $s^{-1}$). These researchers suggest that the reason their rate constant for the reaction with $Cl_2$ is significantly smaller than the previous result is due to surface catalyzed reactions in the earlier measurement. Ariya et al.[83] also had difficulty with surface catalyzed reactions and for this reason the $Br_2$ reaction rate constant is only an upper limit. They suggest the reactions with $Cl_2$ and $Br_2$ are two slow to play an important role in the MDEs. Even though the Cl reaction has a fairly large rate constant, they estimated that the tropospheric concentration of Cl radicals is too small for this reaction to be very important.

However, they do suggest there is sufficient concentraion of the Br radical and that the rate constant is large enough for this reaction to be of major importance in the chemistry of tropospheric mercury. A rate constant for the reaction of Hg with BrO has also been reported by the Ariya group to be between $1.0 \times 10^{-13} - 1.0 \times 10^{-15}$ $cm^3$ $molecules^{-1}$ $s^{-1}$.[42,84] Donohoue et al.[85] recently reported a rate constant for the recombination of Hg + Cl atoms of $5.3 \times 10^{-13}$ $cm^3$ $molecules^{-1}$ $s^{-1}$ that is considerably smaller than the first estimate.

In addition to these experimental investigations there has been a small number of theoretical studies by other groups. The first calculations on mercury halides were performed by Wadt in the early 1980's using relativistic effective core potentials (RECPs) in small multireference configuration interaction (MRCI) calculations employing double-ζ quality basis sets. Wadt studied the near-equilibrium ground and low-lying excited state potential curves for HgBr and HgCl[59] and near-equilibrium portions of the potential energy surfaces of the ground states of the $HgBr_2$ and $HgCl_2$ molecules[86]. Kaupp and von Schnering[87,88] used large core RECPs and nonrelativistic ECPs with 2nd-order Møller-Plesset perturbation theory (MP2) and quadratic configuration interaction (QCI) to investigate mercury compounds such as HgX, $HgX_2$, $Hg_2X_2$, and $(HgX_2)_2$ (X=F,Cl,Br,H,I). Liao et al.[89] used quasi-relativistic density functional theory (DFT) to study similar molecules as Kaupp and von Schnering. Howard[90] used RECPs and MP2 calculations to investigate $HgI_2$, while Akesson et al.[91] used RECPs with the modified coupled pair functional method for calculations on $HgCl_2$. More recently Tossell[92] carried out coupled cluster doubles (CCD) and singles and doubles coupled cluster with perturbative triples [CCSD(T)] calculations with double-zeta quality basis sets for a number of different mercury-halogen systems. Khalizov et al.[93] carried out similar quality calculations using QCISD and CCSD(T) wavefunctions with a number of different basis sets.

## IV. SUMMARY OF PRESENT WORK

The work included in this thesis has touched on a wide range of issues related to the gas phase chemistry of mercury and halogen species in hopes of better understanding the nature of the atmospheric mercury depletion events. These issues include the production of gas phase halogen species. As discussed in the background it is thought that $Br_2$ and BrCl are the major photolyzable halide species and are produced from sea salt aerosols. The $Br_2$ and BrCl are quickly photodissociated following their production and the resulting halogen radicals go on to react with ozone or mercury producing the mercury depletion events and low ozone events. The photodissociation dynamics of BrCl has also been the focus of a number of recent studies that have used resonance-enhanced multiphoton ionization (REMPI) and photofragment ion imaging.[94-99] Chapter 2 discusses calculations carried out to aid in the interpretation of these experiments in which potential energy curves were computed for the 23 low-lying excited states that dissociate to the four lowest atomic asymptotes corresponding to Br and Cl in their $^2P_{3/2}$ or $^2P_{1/2}$ states. These potentials were computed with the internally contracted multireference configuration interaction method (MRCI)[100,101] and employed series of correlation consistent basis sets[102,103] that were used to extrapolate energies to the complete basis set (CBS) limit. Spin-orbit matrix elements and transition dipole moments between all states have been computed. The potential energy curves and matrix elements have been collected in a series of subroutines that can easily be interfaced to programs for carrying out wavepacket quantum dynamics calculations. The ab inito potential curves confirm the presence of two spin-orbit-induced avoided crossings in the $\Omega = 0^+$ states that are believed to play an important role in the

photodissociation dynamics. These calculations represent the first time the low-lying excited states have been characterized by ab initio calculations.

After halogen radicals are produced from the photdissociation of $Br_2$ and/or BrCl in the atmosphere, it is believed they react with ozone, $Br + O_3 \rightarrow BrO + O_2$. It was originally thought that the BrO was then responsible for the mercury depletion events. Early studies on the dissociation energy of HgO predicted it was bound by 53±8 kcal/mol[104] or 64±15 kcal/mol.[105] Prior ab initio calculations of the dissociation energy of mercury monoxide showed even greater disparity with values ranging from ~40 kcal/mol[106] to -14 kcal/mol.[107,108] Chapter three discusses the calculations that were carried out to unambiguously determine the dissociation energy of HgO and the reaction enthalpy of the Hg+BrO reaction.[109] The large scale ab initio calculations carried out on HgO involved highly correlated wave functions and sequences of correlation consistent basis sets. In the absence of spin-orbit coupling, the electronic ground state was predicted to be a $^3\Pi$ state with a $^1\Sigma^+$ state lying above by only 0.6 kcal/mol. The inclusion of spin-orbit coupling resulted in an $\Omega=0^+$ ground state that is bound with respect to $Hg(^1S_0) + O(^3P_2)$ products by only 4.0 kcal/mol ($D_0$). This results in a $Hg+BrO \rightarrow HgO+Br$ gas phase reaction enthalpy that is strongly endothermic and implies this reaction will not occur under atmospheric conditions.

Another possible product of a reaction between Hg and BrO is BrHgO, and accurate ab intio calculations by others in this research group[110] have determined this reaction is in fact exothermic by -20.2 kcal/mol. However, the barrier to insertion was found to be on the order of 40 kcal/mol, which would make this reaction far to slow to be involved in the mercury depletion events. The geometric isomers of BrHgO (HgBrO and HgOBr) were investigated with both CCSD(T)[111-113] and multiconfigurational self-consistent field wavefunctions (MCSCF),[114,115] but

were found to only have shallow van der Waals minima. Therefore, despite the recent experimental kinetics studies[42,84] that suggest the rate of Hg + BrO → products is fast enough to be involved in the mercury depletion events, the ab initio calculations carried out by this group show conclusively that this reaction will be slow in the gas phase under atmospheric conditions.

If reaction with BrO is not the first step in the mercury depletion events then the other likely candidate is the bromine radical. The dissociation energy of HgBr was known experimentally to be 15.5±0.3 kcal/mol,[116] so at least it was known to be relatively strongly bound. Therefore, the potential role of HgBr was dependant on the rate of the Hg+Br recombination reaction. The goal of the project discussed in Chapter 4 was to determine the rate constant for this process using accurate ab inito methods for comparison to the available experimental data. To this end an accurate global potential energy surface was constructed for the reaction HgBr + Ar → Hg + Br + Ar. The calculation of the surface involved CCSD(T) and multireference configuration interaction (MRCI)[100,101] wave functions, the use of correlation consistent basis sets so the energies could be extrapolated to the CBS limit, and corrections were added for core-valence correlation, spin-orbit coupling, and the Lamb shift.

Quasiclassical trajectories (QCT) were carried out on this surface to determine the rate constant for collision-induced dissociation of HgBr by Ar atoms. All relevant initial ro-vibrational energy levels were considered up to the dissociation limit for collision energies up to 10 kcal/mol. The principle of detailed balance was then used to determine the 3$^{rd}$ order recombination rate constant for Hg + Br + Ar → HgBr + Ar and the effective second order rate constant for Hg + Br → HgBr. The calculated rate constants for collision-induced dissociation and recombination were somewhat smaller than previous experimental[83] and theoretical[93,117] determinations. The effective second order rate constant for Hg + Br recombination at

representative Arctic conditions (260 K and 1 bar pressure) was calculated to be 1.20 x $10^{-12}$ $cm^3$ $molecule^{-1}$ $s^{-1}$. The concentration of bromine radicals during mercury depletion events has been estimated to be between $10^7$-$10^8$ molecules $cm^{-3}$.[33] If the bromine concentration is considered fixed at these values then an effective half-life for Hg is calculated to be 1.6-16 hours. Despite the slower rate constant calculated for HgBr recombination, the QCT rate constant would still allow for a sufficiently fast oxidation of Hg by Br radicals for this process to play a significant role in the mercury depletion events.

If the atmospheric oxidation of Hg involves the initial oxididation to HgBr (and to a lesser extent HgCl), then there are a large number of subsequent reactions that could lead to the formation of divalent mercury, which is believed to be the major component of RGM and the species most likely to be deposited on the snow pack. Therefore, the thermochemistry of a large number of reactions between mercury and various halide species has been calculated. In general, these calculations were carried out with a composite approach that involved the use of CCSD(T) wavefunctions, correlation consistent basis sets including extrapolations to the CBS limit, and corrections for core-valence correlation, scalar relativistic effects, spin-orbit coupling, the pseuodpotential approximation, higher orders of electron correlation, and the leading quantum electrodynamic (QED) terms. Part of this overall effort was the study of the thermochemistry for reactions between mercury and iodine-containing species, and these calculations are discussed in Chapter 5. In addition to their thermochemistry, the structures and vibrational frequencies of the diatomic and triatomic mercury halide species involved have been characterized. For the structures in particular, these ab initio calculations have produced the most accurate values to date for most of the mercury halide species studied. Some representatives of the reactions that have been studied are (see also Ref 110, enthalpies are for 0 K):

$$\mathrm{Hg} + \mathrm{BrCl} \rightarrow \begin{cases} \mathrm{HgBr} + \mathrm{Cl} & \Delta H_r = 36.5\ \mathrm{kcal/mol} \quad (7) \\ \mathrm{HgCl} + \mathrm{Br} & \Delta H_r = 29.7\ \mathrm{kcal/mol} \quad (8) \\ \mathrm{BrHgCl} & \Delta H_r = -45.3\ \mathrm{kcal/mol} \quad (9) \end{cases}$$

$$\mathrm{Hg} + \mathrm{BrO} \rightarrow \begin{cases} \mathrm{HgBr} + \mathrm{O} & \Delta H_r = 39.5\ \mathrm{kcal/mol} \quad (10) \\ \mathrm{HgO} + \mathrm{Br} & \Delta H_r = 50.2\ \mathrm{kcal/mol} \quad (11) \\ \mathrm{BrHgO} & \Delta H_r = -20.2\ \mathrm{kcal/mol} \quad (12) \end{cases}$$

$$\mathrm{HgBr} + \mathrm{Br} \rightarrow \begin{cases} \mathrm{Hg} + \mathrm{Br_2} & \Delta H_r = -30.6\ \mathrm{kcal/mol} \quad (13) \\ \mathrm{BrHgBr} & \Delta H_r = -73.0\ \mathrm{kcal/mol} \quad (14) \end{cases}$$

$$\mathrm{HgBr} + \mathrm{ICl} \rightarrow \begin{cases} \mathrm{BrHgI} + \mathrm{Cl} & \Delta H_r = -14.9\ \mathrm{kcal/mol} \quad (15) \\ \mathrm{BrHgCl} + \mathrm{I} & \Delta H_r = -32.3\ \mathrm{kcal/mol} \quad (16) \end{cases}$$

$$\mathrm{HgBr} + \mathrm{BrO} \rightarrow \begin{cases} \mathrm{BrHgBr} + \mathrm{O} & \Delta H_r = -17.6\ \mathrm{kcal/mol} \quad (17) \\ \mathrm{BrHgO} + \mathrm{Br} & \Delta H_r = -4.3\ \mathrm{kcal/mol} \quad (18) \end{cases}$$

All of the abstraction reactions that resemble reactions (7), (8), (10), and (11) are significantly endothermic. The insertion reactions represented by reactions (9) and (12) are exothermic, but all have large barriers to the insertion of Hg into the X-Y or X-O bond. The direct reaction of mercury with XY and XO species is thus unlikely to occur in the Arctic troposphere. However, the reaction of initially formed HgBr and HgCl species can undergo several reactions, as represented by reactions (14)-(18), to form stable divalent mercury species. In all cases reactions of the type (14)-(17) are exothermic, and reactions similar to (18) are either slightly exothermic or slightly endothermic. Recombination reactions that form divalent mercury represented by reaction (14) will have to compete with the abstraction reactions represented by reaction (13).

Not only has the thermochemistry of these reactions been investigated, but the dynamics of the system HgBr + Br have been studied by quasiclassical trajectories and variational transition state theory (VTST). The present author was not the primary investigator on this

project, but was primarily involved in the QCT calculations. This manuscript is therefore not included in the main body of the dissertation, but is included as Appendix 2. The rate constant determined with the QCT method for the recombination of HgBr + Br → $HgBr_2$ was found to be 3.0 x $10^{-11}$ $cm^3$ $molecule^{-1}$ $s^{-1}$ at 298 K, and the HgBr + Br → Hg + $Br_2$ abstraction reaction was found to be slightly faster with a rate constant of 3.9 x $10^{-11}$ $cm^3$ $molecule^{-1}$ $s^{-1}$, as was the exchange reaction HgBr + Br′ → HgBr′ + Br, with a rate constant of 4.0 x $10^{-11}$ $cm^3$ $molecule^{-1}$ $s^{-1}$. The insertion reaction Hg + $Br_2$ → $HgBr_2$ is very slow due to a 27.2 kcal/mol barrier and the rate constant was calculated to be 2.74 x $10^{-31}$ $cm^3$ $molecule^{-1}$ $s^{-1}$. The large rate constant for the HgBr + Br recombination reaction supports the idea that subsequent oxidation of initially formed HgBr by halogen species is not only thermodynamically favorable, but also fast enough to be involved in the mercury depletion events.

It was discussed earlier that the reaction between Hg and BrO is unlikely to occur in the gas phase under atmospheric conditions, but the reaction between HgBr + BrO to form BrHgBr + O and BrHgO + Br were shown to be exothermic. Another possible product of this reaction is the formation of the mercury hypohalite BrHgOBr. Calvert and Lindberg[41] were the first to propose that mercury hypohalite species (XHgOY) could be involved in mercury depletion events and be a major component of RGM, but prior to this work these molecules had never been characterized in the gas phase. Therefore, it was the aim of the work discussed in Chapter 6 to characterize the XHgOY (X, Y = Br, Cl) molecules and compare the enthalpies of the various reactions between HgBr and BrO. Calculations were carried out in a similar composite approach to the one discussed above. It was found that for all combinations of X, Y = Br, Cl the reaction HgX + YO was *exothermic* by greater than 50 kcal/mol to yield hypohalites, and the formation

of XHgY + O products was *exothermic* by approximately 20 kcal/mol. The pathway resulting in XHgO + Y was found to be nearly isoenergetic with the HgX + YO reactants. Another route that can lead to the formation of mercury hypohalites is the reaction between XHgO + Y. Preliminary MCSCF calculations indicate that both the HgX + YO and XHgO + Y reactions leading to the formation of XHgOY are barrierless. These results support the hypothesis of Calvert and Lindberg[41] that the mercury hypohalite species could be a major component of RGM. The MCSCF and linear response CCSD calculations [118] also indicate that the excited $1^3A''$ state in BrHgOBr is also bound with respect to HgBr + BrO and BrHgO + Br. Hence it could be involved in the dynamics of the formation of the mercury hypohalites.

So far only the gas phase reactions between mercury and halogen-containing species have been discussed. However, it is likely that both gas phase and heterogeneous reactions are involved in the mercury depletion events. The deposition of mercury species on snow and ice surfaces obviously involves water, and it is also possible that clouds, water droplets and ice surfaces may catalyze the mercury oxidation. In Chapter 7 the effect of microsolvation on a number of mercury-halogen reactions is investigated. The structures and binding energies were determined for the complexes between one, two and three water molecules with mercury and halogen-containing species: $HgBr_2$, HgBrCl, $HgCl_2$, HgBr, HgCl, $Br_2$, BrCl, $Cl_2$, Hg, Br, and Cl. The calculations were carried out with the B3LYP,[119,120] MP2,[121] and CCSD(T) methods using correlation consistent basis sets. The counterpoise correction was applied to all binding energies to account for basis set superpostion error (BSSE). These calculations are the first to characterize these mercury halide-water clusters. The effects of solvation on four series of reactions have been calculated. The atom-atom recombination reactions, ie, Hg + X → HgX (X = Br, Cl) were found to increase in exothermicity by 3-4 kcal/mol due to the presence of three

water molecules. Likewise, the atom-diatom recombination reactions of the form HgX + Y → XHgY (X, Y = Br, Cl) were also found to increase in exothermicity by 1-2 kcal/mol with the addition of water molecules. HgX + Y → Hg + XY abstraction reactions that may compete with the atom-diatom recombination processes were found to be more *endothermic* by 4-7 kcal/mol when water molecules were present. Finally, the insertion reactions Hg + XY → XHgY were found to be significantly more exothermic (6-8 kcal/mol) when microsolvation was included. The barriers to these reactions are likely to also be reduced by the presence of water molecules, and heterogeneous chemistry may be a way in which these insertion reactions are involved in the MDEs.

Gas phase reactions between cadmium and halogen species are likely to be important in combustion chemistry, and also in the formation of particulate cadmium in the atmophere. The reactions between cadmium and reactive halogen species should be similar to the analagous mercury reactions that have been discussed, but prior to this work almost nothing was known about these reactions. Chapter 8 details the accurate ab initio calculations that have been carried out to determine the thermochemistry of some of these reactions, as well as to determine the structures and vibrational frequencies of all the species involved. The specific reactions that have been investigated were Cd + XY where X = Cl, Br and Y = H, O, Cl and Br. The calculations were again carried out with the composite approach described for the mercury thermochemistry. With the exception of the reaction Cd + HBr → CdH + Br and Cd + HCl → CdH + Cl, the calculated enthalpies are believed to be the most accurate to date. With the exception of CdH, the bond lengths for the cadmium-containing molecules of this study were determined to within ±0.005 Å and are the most reliable values available.

The cadmium halide reaction enthalpies are qualitatively similar to those for the mercury cases. All of the abstraction reactions considered are endothermic, while the insertion reactions are strongly exothermic. The abstraction reactions involving cadmium, however, are several kcal/mol less endothermic than the corresponding mercury reactions, while the cadmium insertion reactions are more exothermic than their mercury counterparts. The mercury abstraction reactions are known to proceed without a barrier while the insertion reactions have relatively large barriers. It is probable that the cadmium reactions follow this same trend.

## V. CONCLUSION

Accurate ab initio calculations have been carried out on reactions between mercury and small halogen containing species. The goal of this work has been to help elucidate the mechanism of episodic mercury depletion events that have been observed in the Arctic and Antarctic surface level troposphere during polar sunrise. The results of these calculations should also be relevant more generally to the whole of mercury's atmospheric chemistry. These calculations have helped to push the boundaries of highly accurate ab initio calculations involving heavy elements. The composite approach adopted in these calculations is expected to yield reaction enthalpies with an uncertainty of ±1.0 kcal/mol or better and structures accurate to ±0.005 Å or better.

Prior to this work it had been thought that the primary reaction that resulted in the mercury depletion events was between gaseous elemental mercury and BrO radicals to produce either HgO or some form of HgBrO. The present work has shown that in fact all of the potential reactions between Hg and BrO are either highly endothermic or involve large barriers on the

potential energy surface separating reactants and products. It is therefore highly unlikely that the reaction between Hg and BrO is involved in the mercury depletion events.

The other reaction that has been proposed to be involved in the mercury depletion events is the recombination of Hg and Br atoms to form HgBr. The rate constant for this process has been calculated as part of this work. Despite being slower than previous estimates, the calculated rate constant would correspond to a half-life for Hg between 2-20 hours during the mercury depletion events. This is fast enough for the recombination of Hg and Br atoms to be a first step in the mercury depletion events.

Several pathways exist for the conversion of HgBr into divalent mercury species through further reactions with halogen species. The thermochemistry of a large number of these possible reactions has been determined and many have been shown to be both exothermic and barrierless. This should allow these reactions to occur quickly in the atmosphere, and are therefore likely to be involved in the mercury depletion events. The reaction of HgBr with $O_3$ to form BrHgO and $O_2$ is another candidate reaction for the formation of divalent mercury species and BrHgO could be one of the major components of the reactive gaseous mercury formed during the Arctic depletion events. Another intriguing reaction is that between HgBr and BrO which can lead to the formation of mercury hypohalites that are another candidate for reactive gaseous mercury. As part of this work it has also been shown that snow and ice surfaces as well as interaction with aerosols may help catalyze the oxidation of mercury by the reactive halogen species.

## REFERENCES


(1) Schroeder, W. H.; Munthe, J. *Atmospheric Environment* **1998**, *32*, 809.

(2) Schroeder, W. H.; Yarwood, G.; Niki, H. *Water, Air, and Soil Pollution* **1991**, *56*, 653.

(3) Slemr, F.; Schuster, G.; Seiler, W. *Journal of Atmospheric Chemistry* **1985**, *3*, 407.

(4) Lin, C.-J.; Pehkonen, S. O. *Atmospheric Environment* **1999**, *33*, 2067.

(5) Schroeder, W. H.; Munthe, J.; Lindqvist, O. *Water, Air, and Soil Pollution* **1989**, *48*, 337.

(6) Ebinghaus, R.; Temme, C.; Lindberg, S. E.; Scott, K. J. *Journal de physique. IV, Proceedings* **2004**, *121*, 195.

(7) Slemr, F.; Brunke, E.-G.; Ebinghaus, R.; Temme, C.; Munthe, J.; Waengberg, I.; Schroeder, W. H.; Steffen, A.; Berg, T. *Geophysical Research Letters* **2003**, *30*, 1516.

(8) Temme, C.; Slemr, F.; Ebinghaus, R.; Einax, J. W. *Atmospheric Environment* **2003**, *37*, 1889.

(9) Lindberg, S. E.; Stratton, W. J. *Environmental Science and Technology* **1998**, *32*, 49.

(10) Boening. *Chemosphere* **2000**, *40*, 1335.

(11) Jernelov, A. Factors in the Transformation of Mercury to Methylmercury. In *Environmental Mercury Contamination*; Hartung, R., Dinman, B. D., Eds.; Ann Arbor Science Publishers Inc.: Ann Arbor, 1972; pp 167.

(12) Pongratz, R.; Heumann, K. G. *Chemosphere* **1999**, *39*, 89.

(13) Schroeder, W. H.; Anlauf, K. G.; Barrie, L. A.; Lu, J. Y.; Steffen, A.; Schneeberger, D. R.; Berg, T. *Nature* **1998**, *394*, 331.

(14) Lindberg, S. E.; Brooks, S.; Lin, C.-J.; Scott, K. J.; Landis, M. S.; Stevens, R. K.; Goodsite, M.; Richter, A. *Environmental Science and Technology* **2002**, *36*, 1245.

(15) Skov, H.; Christensen, J. H.; Goodsite, M. E.; Heidam, N. Z.; Jensen, B.; Wahlin, P.; Geernaert, G. *Environmental Science and Technology* **2004**, *38*, 2373.

(16) Berg, T.; Sekkesaeter, S.; Steinnes, E.; Valdal, A.-K.; Wibetoe, G. *The Science of the Total Environment* **2003**, *304*, 43.

(17) Ebinghaus, R.; Kock, H. H.; Temme, C.; Einax, J. W.; Lowe, A. G.; Richter, A.; Burrows, J. P.; Schroeder, W. H. *Environmental Science and Technology* **2002**, *36*, 1238.

(18) Sprovieri, F.; Pirrone, N.; Landis, M. S.; Stevens, R. K. *Environmental Science and Technology* **2005**, *39*, 9156.

(19) Steffen, A.; Schroeder, W. H.; Bottenheim, J.; Narayan, J.; Fuentes, J. D. *Atmospheric Environment* **2002**, *36*, 2653.

(20) Gauchard, P.-A.; Aspmo, K.; Temme, C.; Steffen, A.; Ferrari, C.; Berg, T.; Strom, J.; Kaleschke, L.; Dommergue, A.; Bahlman, E.; Magand, O.; Planchon, F.; Ebinghaus, R.; Banic, C.; Nagorski, S.; Baussand, P.; Boutron, C. *Atmospheric Environment* **2005**, *39*, 7620.

(21) Steffen, A.; Schroeder, W. H.; Macdonald, R.; Poissant, L.; Konoplev, A. *Science of the Total Environment* **2005**, *342*, 185.

(22) Bottenheim, J. W.; Gallant, A. G.; Brice, K. A. *Geophysical Research Letters* **1986**, *13*, 113.

(23) Barrie, L. A.; Bottenheim, J. W.; Schnell, R. C.; Crutzen, P. J.; Rasmussen, R. A. *Nature* **1988**, *334*, 138.

(24) Solberg, S.; Schmidbauer, N.; Semb, A.; Stordal, F.; Hov, O. *Journal of Atmospheric Chemistry* **1996**, *23*, 301.

(25) Wessel, S.; Aoki, S.; Winkler, P.; Weller, R.; Herber, A.; Gernandt, H.; Schrems, O. *Tellus, Series B* **1998**, *50*, 34.

(26) Rasmussen, A.; Kilisholm, S.; Sorensen, J. H.; Mikkelsen, I. S. *Tellus* **1997**, *49B*, 510.

(27) Bottenheim, J. W.; Fuentes, J. D.; Tarasick, D. W.; Anlauf, K. G. *Atmospheric Environment* **2002**, *36*, 2535.

(28) Foster, K. L.; Plastridge, R. A.; Bottenheim, J. W.; Shepson, P. B.; Finlayson-Pitts, B. J.; Spicer, C. W. *Science* **2001**, *291*, 471.

(29) Lehrer, E.; Honninger, G.; Platt, U. *Atmospheric Chemistry and Physics* **2004**, *4*, 2427.

(30) Spicer, C. W.; Plastridge, R. A.; Foster, K. L.; Finlayson-Pitts, B. J.; Bottenheim, J. W.; Grannas, A. M.; Shepson, P. B. *Atmospheric Environment* **2002**, *36*, 2721.

(31) Strong, C.; Fuentes, J. D.; Davis, R. E.; Bottenheim, J. W. *Atmospheric Environment* **2002**, *36*, 2641.

(32) Tarasick, D. W.; Bottenheim, J. W. *Atmospheric Chemistry and Physics* **2002**, *2*, 197.

(33) Platt, U.; Honninger, G. *Chemosphere* **2003**, *52*, 325.

(34) Fan, S.-M.; Jacob, D. J. *Nature* **1992**, *359*, 522.

(35) Tang, T.; McConnell, J. C. *Geophysical Research Letters* **1996**, *23*, 2633.

(36) Douglas, T. A.; Sturm, M.; Simpson, W. R.; Brooks, S.; Lindberg, S. E.; Perovich, D. K. *Geophysical Research Letters* **2005**, *32*, L04502.

(37) Hebestreit, K.; Stutz, J.; Rosen, D.; Matveev, V.; Peleg, M.; Luria, M.; Platt, U. *Science* **1999**, *283*.

(38) Matveev, V.; Peleg, M.; Rosen, D.; Tov-Alper, D. S.; Stutz, J.; Hebestreit, K.; Platt, U.; Blake, D.; Luria, M. *Journal of Geophysical Research* **2001**, *106*, 10375.

(39) Lu, J. Y.; Schroeder, W. H.; Barrie, L. A.; Steffen, A.; Welch, H. E.; Martin, K.; Lockhart, L.; Hunt, R. V.; Boila, G.; Richter, A. *Geophysical Research Letters* **2001**, *28*, 3219.

(40) Ariya, P. A.; Dastoor, A. P.; Amyot, M.; Schroeder, W. H.; Barrie, L.; Anlauf, K.; Raofie, F.; Ryzhkov, A.; Davignon, D.; Lalonde, J.; Steffen, A. *Tellus* **2004**, *56B*, 397.

(41) Calvert, J. G.; Lindberg, S. E. *Atmospheric Environment* **2003**, *37*, 4467.

(42) Raofie, F.; Ariya, P. A. *Environmental Science and Technology* **2004**, *38*, 4319.

(43) Ferrari, C. P.; Gauchard, P.-A.; Aspmo, K.; Dommergue, A.; Magand, O.; Bahlman, E.; Nagorski, S.; Temme, C.; Ebinghaus, R.; Steffen, A.; Banic, C.; Berg, T.; Planchon, F.; Barbante, C.; Cescon, P.; Boutron, C. F. *Atmospheric Environment* **2005**, *39*.

(44) Lalonde, J. D.; Poulain, A. J.; Amyot, M. *Environmental Science and Technology* **2002**, *36*, 174.

(45) Poulain, A. J.; Lalonde, J. D.; Amyot, M.; Shead, J. A.; Raofie, F.; Ariya, P. A. *Atmospheric Environment* **2004**, *38*, 6763.

(46) Dommergue, A.; Ferrari, C. P.; Gauchard, P.-A.; Boutron, C. F.; Poissant, L.; Pilote, M.; Jitaru, P.; Adams, F. C. *Geophysical Research Letters* **2003**, *30*, 1621.

(47) Scott, K. J. *Arctic* **2001**, *54*, 92.

(48) Fitzgerald, W. F.; Engstrom, D. R.; Lamborg, C. H.; Tseng, C.-M.; Balcom, P. H.; Hammerschmidt, C. R. *Environmental Science and Technology* **2005**, *39*, 557.

(49) Maya, J. *J. Chem. Phys.* **1977**, *67*, 4976.

(50) Wilcomb, B. E.; Burnham, R.; Djeu, N. *Chem. Phys. Lett.* **1980**, *75*, 239.

(51) Gedanken, A.; Raz, B.; Even, U.; Eliezer, I. *J. Mol. Spectrosc.* **1969**, *32*, 287.

(52) Bell, S.; McKenzie, R. D.; Coon, J. B. *J. Mol. Spectrosc.* **1966**, *20*, 217.

(53) Whitehurst, C.; King, T. A. *J. Phys. D: Appl. Phys.* **1987**, *20*, 1577.

(54) Wadt, W. R. *J. Chem. Phys.* **1980**, *72*, 2469.

(55) Kushawaha, V.; Mahmood, M. *J. Appl. Phys.* **1987**, *62*, 2173.

(56) Kushawaha, V.; Michael, A.; Mahmood, M. *J. Phys. B: At., Mol. Opt. Phys.* **1988**, *21*, 2507.

(57) Azria, R.; Ziesel, J. P.; Abouaf, R.; Bouby, L.; Tronc, M. *J. Phys. B: At. Mol. Phys.* **1983**, *16*, L7.

(58) Husain, J.; Wiesenfeld, J. R.; Zare, R. N. *J. Chem. Phys.* **1980**, *72*, 2479.

(59) Wadt, W. R. *Appl. Phys. Lett.* **1979**, *34*, 658.

(60) Viswanathan, K. S.; Tellinghuisen, J. *J. Mol. Spectrosc.* **1983**, *98*, 185.

(61) Wieland, K. *Z. Elektrochem.* **1960**, *64*, 761.

(62) Tellinghuisen, J.; Ashmore, J. G. *Appl. Phys. Lett.* **1982**, *40*, 867.

(63) Tellinghuisen, J.; Tellinghuisen, P. C.; Davies, S. A.; Berwanger, P.; Viswanathan, K. S. *Appl. Phys. Lett.* **1982**, *41*, 789.

(64) Salter, C.; Tellinghuisen, P. C.; Ashmore, J. G.; Tellinghuisen, J. *J. Mol. Spectrosc.* **1986**, *120*, 334.

(65) Rai, A. K.; Singh, V. B. *Indian J. Phys.* **1987**, *61B*, 522.

(66) Cheung, N. H.; Cool, T. A. *J. Quant. Spectrosc. Radiat. Transfer* **1979**, *21*, 397.

(67) Dreiling, T. D.; Setser, D. W. *J. Chem. Phys.* **1983**, *79*, 5423.

(68) Greene, D. P.; Kileen, K. P.; Eden, J. G. *J. Opt. Soc. Am. B: Opt. Phys.* **1986**, *3*, 1282.

(69) Loewenschuss, A.; Ron, A.; Schnepp, O. *J. Chem. Phys.* **1969**, *50*, 2502.

(70) Givan, A.; Loewenschuss, A. *J. Chem. Phys.* **1976**, *65*, 1851.

(71) Givan, A.; Loewenschuss, A. *J. Chem. Phys.* **1976**, *64*, 1967.

(72) Givan, A.; Loewenschuss, A. *J. Mol. Struct.* **1978**, *48*, 325.

(73) Beattie, I. R.; Horder, J. R. *J. Chem. Soc. A. Inorg. Phys. Theor.* **1970**, *14*, 2433.

(74) Clark, R. J. H.; Rippon, D. M. *J. Chem. Soc. Faraday trans. II* **1973**, *69*, 1496.

(75) Klemperer, W. *J. Chem. Phys.* **1956**, *25*, 1066.

(76) Wilcomb, B. E.; Mayer, T. M.; Bernstein, R. B.; Bickes, R. W., Jr. *J. Am. Chem. Soc.* **1976**, *98*, 4676.

(77) Wilcomb, B. E.; Haberman, J. A.; Bickes, R. W. J.; Mayer, T. M.; Bernstein, R. B. *J. Chem. Phys.* **1976**, *64*, 3501.

(78) Mayer, T. M.; Wilcomb, B. E.; Bernstein, R. B. *J. Chem. Phys.* **1977**, *67*, 3507.

(79) Baskin, J. S.; Zewail, A. H. *J. Phys. Chem.* **1994**, *98*, 3337.

(80) Baumert, T.; Pedersen, S.; Zewail, A. H. *J. Phys. Chem.* **1993**, *76*, 12447.

(81) Dantus, M.; Bowman, R. M.; Gruebele, M.; Zewail, A. H. *J. Chem. Phys.* **1989**, *91*, 7437.

(82) Pedersen, S.; Baumert, T.; Zewail, A. H. *J. Phys. Chem.* **1993**, *97*, 12460.

(83) Ariya, P. A.; Khalizov, A.; Gidas, A. *Journal of Physical Chemistry A* **2002**, *106*, 7310.

(84) Raofie, F.; Ariya, P. A. *Journal de physique. IV, Proceedings* **2003**, *107*, 1119.

(85) Donohoue, D. L.; Bauer, D.; Hynes, A. J. *Journal of Physical Chemistry* **2005**, *109*, 7732.

(86) Wadt, W. R. *Journal of Chemical Physics* **1980**, *72*, 2469.

(87) Kaupp, M.; von Schnering, H. G. *Inorganic Chemistry* **1994**, *33*, 4179.

(88) Kaupp, M.; von Schnering, H. G. *Inorganic Chemistry* **1994**, *33*, 2555.

(89) Liao, M.-s.; Zhang, Q.-e.; Schwartz, W. H. E. *Inorganic Chemistry* **1995**, *34*, 5597.

(90) Howard, S. T. *Journal of Physical Chemistry* **1994**, *98*, 6110.

(91) Akesson, R.; Persson, I.; Sandstrom, M.; Wahlgren, U. *Inorganic Chemistry* **1994**, *33*, 3715.

(92) Tossell, J. A. *Journal of Physical Chemistry A* **2003**, *107*, 7804.

(93) Khalizov, A. F.; Viswanathan, B.; Larregaray, P.; Ariya, P. A. *Journal of Physical Chemistry A* **2003**, *107*, 6360.

(94) Beckert, M.; Wouters, E. R.; Ashfold, M. N. R.; Wrede, E. *Journal of Chemical Physics* **2003**, *119*, 9576.

(95) Cao, J.; Loock, H.-P.; Qian, C. X. W. *Canadian Journal of Chemistry* **1994**, *72*, 758.

(96) Cooper, M. J.; Jackson, P. J.; Rogers, L. J.; Orr-Ewing, A. J.; Ashfold, M. N. R.; Whitaker, B. J. *Journal of Chemical Physics* **1998**, *109*, 4367.

(97) Park, M.-S.; Jung, Y.-J.; Lee, S.-H.; Kim, D.-C.; Jung, K.-H. *Chemical Physics Letters* **2000**, *322*, 429.

(98) Smolin, A. G.; Vasyutinskii, O. S.; Vieuxmaire, O. P. J.; Ashfold, M. N. R.; Balint-Kurti, G. G.; Orr-Ewing, A. J. *Journal of Chemical Physics* **2006**, *124*, 094305.

(99) Wouters, E. R.; Beckert, M.; Russell, L. J.; Rosser, K. N.; Orr-Ewing, A. J.; Ashfold, M. N. R.; Vasyutinskii, O. S. *Journal of Chemical Physics* **2002**, *117*, 2087.

(100) Knowles, P. J.; Werner, H.-J. *Chemical Physics Letters* **1988**, *145*, 514.

(101) Werner, H.-J.; Knowles, P. J. *Journal of Chemical Physics* **1988**, *89*, 5803.

(102) Dunning, T. H. J.; Peterson, K. A.; Wilson, A. K. *Journal of Chemical Physics* **2001**, *114*, 9244.

(103) Peterson, K. A.; Figgen, D.; Goll, E.; Stoll, H.; Dolg, M. *Journal of Chemical Physics* **2003**, *119*, 11113.

(104) Grade, M.; Hirschwald, H. *Ber. Bunsen-Ges. Phys. Chem.* **1982**, *86*, 899.

(105) Chase, M. W., Jr.; Davies, C. A.; Downey, J. R., Jr.; Frurip, D. J.; McDonald, R. A.; Syverud, A. N. *Journal of Physical and Chemical Reference Data* **1985**, *14*, Suppl. No. 1.

(106) Hu, A.; Otto, P.; Ladik, J. *Journal of Molecular Structure* **1999**, *468*, 163.

(107) Cundari, T. R.; Moody, E. W. *Journal of Molecular Structure* **1998**, *425*, 43.

(108) Stömberg, D.; Gropen, O.; Wahlgren, U. *Chemical Physics* **1989**, *133*, 207.

(109) Shepler, B. C.; Peterson, K. A. *Journal of Physical Chemistry A* **2003**, *107*, 1783.

(110) Balabanov, N. B.; Peterson, K. A. *Journal of Physical Chemistry A* **2003**, *107*, 7465.

(111) Purvis, G. D. I.; Bartlett, R. J. *Journal of Chemical Physics* **1982**, *76*, 1910.

(112) Raghavachari, K.; Trucks, G. W.; Pople, J. A.; Head-Gordon, M. *Chemical Physics Letters* **1989**, *156*, 479.

(113) Watts, J. D.; Gauss, J.; Bartlett, R. J. *Journal of Chemical Physics* **1993**, *98*, 8718.

(114) Knowles, P. J.; Werner, H.-J. *Chemical Physics Letters* **1985**, *115*, 259.

(115) Werner, H.-J.; Knowles, P. J. *Journal of Chemical Physics* **1985**, *82*, 5053.

(116) Tellinghuisen, J.; Ashmore, J. G. *Chemical Physics Letters* **1983**, *102*, 10.

(117) Goodsite, M. E.; Plane, J. M. C.; Skov, H. *Environmental Science and Technology* **2004**, *38*, 1772.

(118) Christiansen, O.; Koch, H.; Halkier, A.; Jorgensen, P.; Helgaker, T.; Meras, D. *Journal of Chemical Physics* **1996**, *105*, 6921.

(119) Becke, A. D. *Journal of Chemical Physics* **1993**, *98*, 5648.

(120) Stephens, P. J.; Devlin, F. J.; Chabalowski, C. F.; Frisch, M. J. *Journal of Physical Chemistry* **1994**, *98*, 11623.

(121) Møller, C.; Plesset, M. S. *Physical Reviews* **1934**, *46*, 618.

# An ab Initio Study of the Ground and Low-Lying Excited Electronic States of BrCl

**Benjamin C. Shepler and Kirk A. Peterson***

*Department of Chemistry, Washington State University, Pullman, Washington 99164-4630*

**Abstract**

The goal of this work has been to calculate ab initio potential energy curves for all states of the BrCl molecule that correlate with the four lowest asymptotic atomic product channels. The potential curves were determined using MRCI wavefunctions and correlation consistent basis sets. Special care has been taken to include the effects of scalar relativity and spin-orbit coupling. A small number of large active space MRCI calculations were performed to account for electron correlation due to higher order excitations. Spin-orbit matrix elements and transition dipole moments have also been computed and saved. It is hoped that these potentials can be used in future wavepacket calculations to further investigate the photodissociation of BrCl. In addition, highly accurate coupled-cluster calculations with corrections for full iterative triple and quadruple excitations, core-valence correlation, and spin-orbit coupling have been carried out for the ground electronic state.

## I. INTRODUCTION

The ultraviolet and visible spectroscopy and dynamics of bromine monochloride have been investigated experimentally for decades. Most recently, the photodissociation dynamics have been of particular interest. The photodissociation of BrCl is of strong interest since this process in the atmosphere results in the formation of Br and Cl radicals. It is well known that halogen radicals are involved in the destruction of stratospheric ozone,[1] and BrCl is a likely product of the heterogeneous activation of stratospheric chlorine and bromine.[2-5] More recently halogen species have been shown to play a large role in tropospheric ozone depletion events during polar sunrise in the arctic.[6-8] In fact BrCl along with $Br_2$ have recently been proposed as the major sources of atmospheric photolyzable bromine responsible for these tropospheric ozone depletions events.[9,10] Similar tropospheric mercury depletion events have also been observed during polar sunrise in the Arctic.[11,12] They are also thought to be the result of reactions with halogen species and have been implicated in the high concentration of mercury found in arctic biota.[11,13] In addition to its relevance to atmospheric chemistry, the UV-visible spectrum of BrCl has also received interest for its possible use as a chemical laser system.[14,15]

The electronic spectra of BrCl and the other diatomic halogens is made both interesting and complex due to the fact that 23 electronic states (5 x $\Omega = 0^+$, 5 x $\Omega = 0^-$, 8 x $\Omega = 1$, 4 x $\Omega = 2$, and 1 x $\Omega = 3$) correlate to the four low-lying electronic asymptotes of separated Br and Cl atoms:

| | | | | |
|---|---|---|---|---|
| BrCl $[X^1\Sigma^+(0^+)]$ | → | Br + Cl | $\Delta E = 18026\ cm^{-1}$ (51.53 kcal/mol or 554.8 nm) | (1) |
| | | Br + Cl* | $\Delta E = 18907\ cm^{-1}$ (54.06 kcal/mol or 529.0 nm) | (2) |
| | | Br* + Cl | $\Delta E = 21711\ cm^{-1}$ (62.07 kcal/mol or 460.6 nm) | (3) |
| | | Br* + Cl* | $\Delta E = 22594\ cm^{-1}$ (64.60 kcal/mol or 442.6 nm) | (4) |

In the above expressions Br/Cl corresponds to the $^2P_{3/2}$ level and Br*/Cl* to the $^2P_{1/2}$ level, where the zero field spin-orbit splittings are 3685.2 $cm^{-1}$ and 882.4 $cm^{-1}$ for Br and Cl, respectively.[16]

BrCl displays a continuous absorption band in the UV-visible region with 4 peaks at 228 nm, 376 nm, 454 nm and a weak absorption at 533 nm that have been primarily attributed to excitation from the ground $X^1\Sigma^+(0^+)$ state to the $D(0^+)$, $C^1\Pi(1)$, $B^3\Pi(0^+)$ and $A^3\Pi(1)$ excited states respectively.[17,18] The first observation of the electronic spectra was reported in the 1930s,[19] but then not picked up again until Clyne and Coxon's observations of the emission[20] and absorption[21] bands in the 1960s.

Since these first studies a number of the BrCl excited states have been at least partially characterized. The first high resolution studies of the $B^3\Pi(0^+) - X^1\Sigma^+(0^+)$ absorption band system was reported by Coxon.[22] The lifetime and relaxation kinetics of vibrational levels in the B state were determined from a number of laser induced fluorescence studies on the B-X transition by Wright et al.[23] and Clyne and co-workers.[24-26] These initial studies indicated the parallel ($\Delta\Omega$=0) nature of the B-X transition, a barrier in the B-state potential curve, and the occurrence of predissociation in the higher vibrational levels. The barrier in the potential curve is thought to be the result of a strongly avoided crossing with higher lying repulsive $0^+$ states. A study by Tellinghuisen[27] found the barrier height to lie 275 $cm^{-1}$ above the first dissociation limit and in the same study reported a closed-form potential for the B-state. As a result of the avoided crossing, the B-state correlates adiabatically with ground state atomic products (channel 1) while correlating diabatically with either excited Br* or Cl* atomic products (channels 2 or 3 above). Predissociation in the highest vibrational levels is likely attributable to the interactions

responsible for the avoided crossing, but predissociation is also observed in the lower vibrational levels so long as they lie above the first dissociation limit. The predissociation in these lower levels was found to scale with J′(J′+1) indicating a rotational-electronic coupling with an Ω=1 state that likely corresponds to the $A^3\Pi(1)$ or $C^1\Pi(1)$ states.[28,29]

The excited B-state of BrCl has certainly received the most attention, but other excited states have also been observed. A study of the emission of the ion-pair D′ (2) state [dissociates to $Br^+(^3P_2) + Cl^-(^1S_0)$] to the A′ (2) state [dissociates to ground state atoms] allowed for the determination of spectroscopic constants including $T_e$, $\omega_e$, $r_e$, and $D_e$ for both the A′ and D′ states. The emission of the E ion-pair state, which correlates with the same asymptote as the D′ state, to the ground $X^1\Sigma^+(0^+)$[30] and excited $B^3\Pi(0^+)$[31,32] has also been observed and spectroscopic constants are available for this ion-pair state as well.[31] Spectroscopic constants for the ground state are known to high resolution. The best spectroscopic determination[29] of $D_e$ for the ground state of BrCl yielded a value of 18244±5 $cm^{-1}$. Tellinghuisen recently refined his own spectroscopic value in recent spectrophotometric determinations of the equilibrium constant for $Br_2 + Cl_2 \rightarrow 2BrCl$ to get a current best estimate of $D_e$ = 18248±2 $cm^{-1}$.[33] The first high resolution determination of the equilibrium bond length and harmonic frequency was carried out by Coxon[22] and these values were later improved upon by Uehara et al.[34]

Much of the recent work on BrCl has been study of its photodissociation dynamics with resonance-enhanced multiphoton ionization (REMPI) and photofragment ion imaging following photolysis at wavelengths ranging between 235-570 nm.[28,35-39] With these excitation wavelengths the three lowest dissociation channels 1-3 were observed, but in no cases were both the Br and Cl atoms found in their excited states (channel 4). In the long wavelength region

between 330-570 nm it was found that only channels 1 and 2 were produced. Excited Cl atoms were produced at the longest wavelengths, with the branching ratio for channel 2 increasing to a maximum between ~520-450 nm (depending on initial vibrational level of the parent BrCl) and then decreasing at shorter wavelengths.[35] This was thought to be due to excitation to the $B^3\Pi(0^+)$ state followed by dissociation along the diabatic potential curve to excited Cl products.[35] Formation of ground state products at shorter wavelengths was ascribed primarily to perpendicular excitation to the $C^1\Pi(1)$ state and that at longer wavelengths was also due to contributions from parallel excitation to the $B^3\Pi(0^+)$ followed by adiabatic dissociation.[28,35] Perpendicular excitation to the $A^3\Pi(1)$ is also expected to contribute to formation of ground state products.[28,35] The third dissociation channel (Br* + Cl) is only observed at wavelengths shorter than 260 nm.[28,37] At these shorter wavelengths each of the first three dissociation channels is observed. Production of the upper channel is associated with the parallel excitation to the $D(0^+)$ state which may be a $^3\Sigma^-(0^+)$ state, and may also be due to a smaller contribution from the $2^3\Pi(0^+)$ state (often designated the Y state).[28] The Y state is believed to be responsible for the avoided crossing and subsequent barrier in the B state. This upper channel also has a perpendicular component from an $\Omega$=1 state that was not specified. At these shorter wavelengths production of the Br + Cl* channel is thought to occur only through perpendicular excitations and a likely candidate is the $2^1\Pi(1)$ state.[37] Production of ground state atoms at the shorter wavelengths is due primarily to parallel excitations to the $^3\Sigma^-(0^+)$ and $2^3\Pi(0^+)$ states and involves a number of avoided crossings.[37] One recent experimental study included the parameterization of empirical potential curves for the $A^3\Pi(1)$, $B^3\Pi(0^+)$, $C^1\Pi(1)$, and Y electronic states.[35]

The goal of the current project has been to calculate high quality ab initio potential energy curves for each of the 23 electronic states that correlate to the four lowest dissociation channels of BrCl. The motivation for this work is to help interpret the electronic spectra and dissociation dynamics discussed above. It is hoped the potential curves can be used in wave packet dynamics calculations for rigorous comparison with the available experimental data. The potential curves were computed with multireference configuration interaction (MRCI) wavefunctions and extrapolations were made to the complete basis set (CBS) limit. Corrections to account for the effects of spin-orbit coupling, scalar relativity and higher order correlation have been included. While there have been a number of previous accurate calculations on the BrCl ground state,[40-43] there has been no previous reports of ab initio calculations on the excited states of BrCl.

## II. METHODOLOGY

The inherent multireference character of the molecular excited states precluded the use of standard single reference wavefunction methods. Therefore, the method used to compute the potential energy curves (PEC) for the excited states of BrCl was the internally contracted multireference singles and doubles configuration interaction[44,45] (MRCI) method. The first series of calculations were based on molecular orbitals determined in state-averaged full-valence complete active space self consistent field[46,47] (CASSCF) calculations. Four series of CASSCF calculations were carried out in $C_{2v}$ symmetry for the 12 Λ-S states of BrCl correlating with ground state atoms (18 including the degeneracies of the Π and Δ states). The first state-averaged all components of the states of $^1A_1$ and $^1A_2$ symmetry (2 x $^1\Sigma^+$, $^1\Sigma^-$, $^1\Delta$); the second series averaged $^1B_1$ and $^1B_2$ symmetry (2 x $^1\Pi$); the third series averaged $^3A_1$ and $^3A_2$ (2 x $^3\Sigma^+$,

$^3\Sigma^-$, $^3\Delta$); and the fourth averaged states of $^3B_1$ and $^3B_2$ symmetry (2 x $^3\Pi$). Each CASSCF calculation was followed by a MRCI calculation also employing a full-valence active space and in which only the valence electrons are correlated. These full-valence active spaces contained 8 active orbitals: 4 $a_1$, 2 $b_1$, 2 $b_2$, and 0 $a_2$ (this corresponds to 4 $\sigma$ and 4 $\pi$ in $C_{\infty v}$). The MRCI calculations included the multireference analog of the Davidson correction[48-50] (MRCI+Q) to approximately account for the effects of higher excitations. For each state 25 points on the PEC were computed between 3.5 and 50 bohr. Except where otherwise noted all calculations were carried out with the MOLPRO suite of ab initio programs.[51]

The basis sets used in this work were from the correlation consistent family of basis sets. On chlorine the aug-cc-pV($n$+$d$)Z sets that contain modified $d$-shells containing additional tight exponents[52] were used and on bromine the aug-cc-pV$n$Z-PP sets[53] were used that are optimized for use with small-core relativistic pseudopotentials (PPs) of the Stuttgart/Köln groups.[53] The pseudopotential replaces the $1s^2 2s^2 2p^6$ electrons of the bromine atom. These basis sets will henceforth be denoted aVnZ and the MRCI calculations just described were carried out with both the aVQZ and aV5Z basis sets. The total energies were then extrapolated with the formula in equation 5 to get an estimate of the potentials at the complete basis set limit.

$$E(n) = E_{\mathrm{CBS}} + B / n^3. \tag{5}$$

Unfortunately, full valence active spaces on diatomic halogen and interhalogen molecules do not yield a large number reference configurations due to the fact that the atoms have only 1 half-empty valence orbital. To account for additional electron correlation a number of larger active space MRCI calculations were carried out for each state. These larger MRCI calculations included 16 orbitals in the active space (7 $a_1$, 4 $b_1$, 4 $b_2$, and 1 $a_2$) and were chosen since they had the highest natural orbital occupations in the smaller active space MRCISD calculations on the

$X^1\Sigma^+$ and $B^3\Pi$ states. Restrictions were placed on the reference configurations to allow no more than 2 electrons in the non-valence orbitals. These larger MRCI calculations were based on CI natural orbitals taken from the smaller active space MRCIs and in the case of Π and Δ states the orbitals were state-averaged between the two components. The aVTZ basis sets were employed with these larger MRCIs. These calculations included as many as 21 million contracted configurations in the case of the $^3\Pi$ states, which would correspond to 236 million uncontracted configurations. This can be contrasted to the full-valence CAS MRCI calculations which yield 134 thousand/1 million contracted/uncontracted variational parameters with the same basis set.

MRCI calculations using both the large and small active spaces and the aVTZ basis set were carried out at 3.9, 4.6, 5.2, and 5.8 Bohr. These data were then used to compute scaling factors for each state at each geometry in a manner similar to the scaling of the external correlation energy approach of Truhlar and co-workers.[54] This scaling factor is defined as:

$$f = \frac{E_{MRCI2} - E_{MRCI1}}{E_{MRCI1} - E_{CASSCF}} \tag{6}$$

where $E_{MRCI2}$ and $E_{MRCI1}$ are the two-body energies of the large and small active space MRCI+Q calculations, respectively, and $E_{CASSCF}$ is the two-body CASSCF energy. Scale factors were calculated via Eq. (6) for each state at 4 geometries, which were then fit with second order polynomials. The scale factor was extrapolated for the bond lengths shorter than 3.9 $a_o$ and was held fixed at their 5.8 $a_o$ value for the longer bond lengths. These scaling factors were then applied to the small active space MRCI+Q/CBS energies via

$$E_{scaled} = f(E_{MRCI1} - E_{CASSCF}) + E_{MRCI1}. \tag{7}$$

Scalar relativistic effects are accounted for on the Br atom by the use of the relativistic pseudopotential. To account for scalar relativity in the Cl atom the expectation values of the

mass-velocity plus Darwin terms of the Breit-Pauli Hamiltonian were evaluated with uncontracted aVTZ basis sets and MRCI wave functions using the smaller active space described above. These scalar relativistic corrections, ΔSR, were then added to the scaled-MRCI+Q/CBS energies.

The effects of spin-orbit coupling were determined within the interacting states method as employed in MOLPRO. The effective 1-electron spin-orbit operator on Br was taken from the pseudopotential and a relativistic PP was also used on chlorine[55,56] for these calculations. The chlorine PP leaves the $3s^2 3p^5$ electrons to be treated explicitly and employs the same aVnZ basis sets described above only they have been recontracted in the presence of the pseudopotential. The spin-orbit coupled eigenstates were obtained by diagonalizing a matrix of $H_{el}+H_{so}$ in a basis of all 18 pure Λ-S states correlating to ground state atoms. The spin-orbit matrix elements were calculated at the MRCI/aVTZ level of theory using the same smaller active space described above, and used orbitals from state-averaged CASSCF calculations. Additionally, all permanent dipole moments and non-zero transition dipole moments between all 18 Λ-S states were computed at this level of theory.

The Λ-S states computed at the scaled-MRCI+Q/CBS+ΔSR level have been fit with the modified Lennard-Jones potential of Leroy and co-workers,[57] which has the form

$$V(R) = D_e \left[ 1 - \left( \frac{R_e}{R} \right)^n e^{-\beta^S_{MLJ}(z) z} \right]^2 \tag{8}$$

where

$$\beta^S_{MLJ}(z) = f_S(R) \left[ \sum_{m=0} \beta_m z^m - \beta_\infty \right] + \beta_\infty , \tag{9}$$

$$z = \frac{(R - R_e)}{(R + R_e)}, \tag{10}$$

$$\beta_\infty = \ln\left[2D_e(R_e)^n / C_n\right] \tag{11}$$

where $C_n$ is the London dispersion constant and $f_S$ is a switching function of the form

$$f_S(R) = 1 / \left[e^{\alpha_S (R - R_S)} + 1\right] \tag{12}$$

and $\alpha_S$ is a damping strength parameter and $R_S$ is the distance where the damping is half-complete. The off-diagonal spin-orbit matrix elements described above were saved for each geometry and along with the permanent and transition dipole moments were interpolated with the reproducing kernel Hilbert space (RKHS) method[58] using the distance-like kernel[58]:

$$q(x, x') = \frac{1}{14} x_>^{-7} \left(1 - \frac{7}{9} \frac{x_<}{x_>}\right) \tag{13}$$

where $x_<$ = Min(x,x') and $x_>$ = Max(x,x'). To aid in future wave packet calculations a number of subroutines were written in Fortran 77. These subroutines load the potentials, dipole moments, and SO matrix elements from which it constructs $H_{el} + H_{SO}$ and the dipole moment matrices. The off-diagonal elements of $H_{el} + H_{SO}$ are taken from the spin-orbit calculations and the diagonal elements are the scaled-MRCI+Q/CBS+ΔSR energies. The program then symmetry adapts and sorts both $H_{SO}$ and the dipole moment matrices. This step is followed by a block-diagonalization of $H_{el} + H_{SO}$ and transformation of the dipole matrices into the spin-orbit coupled basis. This suite of programs requires the user to supply a bond length and returns the spin-orbit coupled eigenstates and transition dipole moments from the ground state at the specified geometry.

Finally, to obtain an estimate for the remaining error in the potential curves an additional series of calculations were carried out only on the BrCl ground state. These calculations are analogous to a similar study carried out by this group on the halogen oxides[59] (ClO, BrO, IO and their anions) and will only be described briefly here. Coupled cluster singles and doubles calculations with a perturbative treatment of connected triple excitations[60-62] [CCSD(T)] were carried out with aVTZ, aVQZ and aV5Z basis sets followed by extrapolation to the CBS limit. A core-valence correction, ΔCV, was determined from calculations with valence-only correlation and where both the valence and core electrons were correlated in CCSD(T) calculations. These used aug-cc-pwCVQZ[63] basis sets (aug-cc-pwCVQZ-PP on Br[64]). Spin-orbit coupling effects, ΔSO, were determined from MRCISD/aVTZ calculations using the spin-orbit CI method[65] as implemented in the Columbus[66] suite of ab initio programs. The third correction was to account for scalar relativity on Cl and for the pseudopotential used on Br. This correction, ΔDK, was determined as the difference between CCSD(T)/aug-cc-pwCVTZ-PP and CCSD(T)/aug-cc-pwCVTZ-DK where in the second all-electron calculation the DKH[67,68] Hamiltonian was employed and the basis sets were recontracted for use with this Hamiltonian. Finally, higher order correlation effects were determined from CCSDT/aVTZ and CCSDTQ/aVDZ calculations carried out using the MOLPRO interface to the MRCC[69] code of Kallay and co-workers. In addition, these energies from the full iterative triple and quadruple calculations were used along with CCSD energies to obtain an estimate of the full configuration interaction (FCI) limit with the aVDZ basis set using the continued fraction extrapolation technique.[70]

## III. RESULTS AND DISCUSSION

The potential curves for the pure Λ-S states can be seen in Figure 1 while those of the spin-orbit coupled eigenstates are pictured in Figures 2-5. The spin-orbit states with different Ω values are shown separately for clarity.

The calculated bond lengths, harmonic frequencies, and dissociation energies ($D_e$) along with the contributions from the various applied corrections for the $X^1\Sigma^+(0^+)$ and $B\ ^3\Pi(0^+)$ states are shown in Tables 1 and 2 together with their corresponding experimental values. Among the calculated states these are the only two for which there exist accurate experimental values. The calculated spectroscopic constants were determined by fitting the potential curves to polynomial functions and then applying the usual Dunham analysis.[71] The most reliable calculated spectroscopic constants for the X state are the CCSD(T)/CBS + ΔCV + ΔSO + ΔDK + ΔT + ΔQ + ΔFCI values. However, both sets of calculated spectroscopic constants agree very well with experiment. The best CCSD(T) values differ from experiment by only 0.001 Å, 0.9 $cm^{-1}$ and 0.1 kcal/mol for $r_e$, $\omega_e$ and $D_e$ respectively and the best MRCI+Q differences are only slightly higher at 0.003 Å, 4 $cm^{-1}$ and 0.1 kcal/mol. The agreement between the best MRCI+Q values and experiment for the B state is also good, but not as close as for the ground state. The calculated bond length is considerably shorter than experiment with a difference of 0.020 Å and the harmonic frequency is nearly 10 $cm^{-1}$ larger than experiment. However, the MRCI+Q calculations on the B state do reproduce the experimental energetics very well with the dissociation energy differing from experiment by only 0.1 kcal/mol and the excitation energy by 0.2 kcal/mol. The calculated barrier height in the B state potential was 1.2 kcal/mol compared to

an experimental value of 0.8 kcal/mol. This quantity is difficult to predict theoretically because of its sensitivity to the position of the avoided crossing that gives rise to it.

The errors in the MRCI+Q estimates are likely due to core-valence correlation, which is not included in the MRCI+Q potential energy functions and higher order correlation effects. Examination of the ground state corrections indicate core valence correlation results in a shortening of the bond length by a considerable -0.007 Å. Also, while the CV effects on the dissociation energy for the ground state of BrCl is negligible this is often not the case and is likely not true for all of the excited states. CCSD(T) calculations and ΔCV were not included for the B-state because the multireference character near $r_e$ make the Hartree-Fock and resulting CCSD(T) wavefunctions unreliable. It is likely the scaling carried out in this work on the MRCI+Q potential curves overestimates the effects of higher order electron correlation. It is well known that the size-extensivity error in MRCI calculations increases with larger active spaces[72] and that the Davidson correction may overestimate this error. The excellent agreement between experiment and theory for the energetics of the B state may benefit from this over estimation because it may counteract the neglect of core-valence correlation. The poor agreement for the bond length may suffer from this overestimation as the scaling decreases the MRCI+Q bond length by a very considerable -0.025 Å. CCSDT and CCSDTQ calculations carried out on the B state seem to confirm this as they suggest a more modest decrease in the bond length of -0.013 Å and an increase in $D_e$ of only 0.8 kcal/mol. Several other scaling techniques were tested to see if the agreement with experiment could be improved. Among these, it was found neglecting the Davidson correction altogether resulted in a dissociation energy that was much smaller than experiment and bond lengths that were significantly too long.

Also, using the Pople[73] correction for higher order excitations in place of the Davidson correction gave results comparable to those given in Table 2.

Another potential source of error is in the treatment of spin-orbit coupling. The spin-orbit corrections to the spectroscopic constants when using the interacting states approach in Molpro or the much larger CIs in the SOCI approach of Columbus gave very similar corrections to the spectroscopic constants of the ground state. More specifically the corrections to the dissociation energy are -4.0 and -3.9 for Molpro and Columbus, respectively. It is also possible to compare the calculated and experimental zero-field splittings. The experimental $^2P_{3/2} - {}^2P_{1/2}$ splitting of Br atom is 10.54 kcal/mol and the theoretical values are in relatively good agreement at 9.73 kcal/mol for the SOCI approach and 9.76 for the interacting states approach. For Cl atom the experimental splitting is 2.52 kcal/mol compared to theoretical values of 2.59 and 2.64 kcal/mol. The interacting states approach yields excellent agreement in these comparisons with the more robust SOCI method and gives further confidence in the spin-orbit corrections applied to the full potential curves. The present spin-orbit corrections are also in good agreement with a previous study that compared Dirac-Hatree-Fock based CCSD(T) calculations with nonrelativistic CCSD(T) calculations using triple-zeta basis sets.[40] This study found relativistic effects increased the ground state BrCl bond length by 0.001 Å, decreased the harmonic frequency by 4 $cm^{-1}$, and decreased the dissociation energy by 4.3 kcal/mol. This is in qualitative agreement with the current results of +0.001 Å, -1.8 $cm^{-1}$ and -4.0 kcal/mol with the current corrections being slightly smaller because the previous study's corrections also included scalar relativistic effects.

One final note to make is about the full iterative triple and quadruple excitations in the coupled cluster calculations. As is often the case for wavefunctions dominated by a single

configuration, such as the X state of BrCl, the CCSD(T) method is very accurate. The higher order corrections do have a small effect on the bond length (+0.003 Å) and harmonic frequency (-4 $cm^{-1}$), but even without these corrections the agreement between the CCSD(T) values with experiment are quite good. It can also be seen that the full triple and full quadruple corrections to the dissociation energy are of similar magnitude but opposite in sign. This is a not uncommon occurrence in which partly through cancellation of errors the perturbative estimate of triple excitations can agree better with experiment than do the full iterative triple excitations. When possible it is always recommended to include corrections due to full quadruple excitations with full triple excitations.

The current best estimate for the spectroscopic constants of the ground state are in good agreement with the previous highly accurate study by Feller et al.[41] These authors employed a composite approach very similar to the one carried out in this work using slightly different basis sets, pseudopotentials, spin-orbit corrections, and extrapolation procedures. Their reported spectroscopic constants for the ground state of BrCl were (the present results follow in parenthesis): $r_e$ = 2.133 Å (2.137); $\omega_e$ = 451.9 $cm^{-1}$ (445.2); and $D_e$= 52.4 kcal/mol (52.3).

Table 3 contains the five spin-orbit coupled eigenstates that are bound with respect to their corresponding dissociation channels. The first three states listed in the table correlate adiabatically with ground state atomic products, while the fourth and fifth states correlate with the second and third dissociation channels, respectively. The dissociation energies listed are with respect to their particular dissociation channels. The only one of these five states that has been observed experimentally is the $A'^3\Pi(2)$ state and approximate spectroscopic constants have been reported.[32] It is not surprising that the calculated bond length is quite a bit shorter than the experimental value because this A′ state is the Ω =2 component of the same $^3\Pi$ state for which

the B state is the $0^+$ component. The energetics of the A′ state do not agree as well with experiment as do the energetics for the X and B states. This is likely a combination of theoretical and experimental error since this state has not yet been observed in high-resolution experiments. While the $A^3\Pi(1)$ state has not been observed experimentally, Beckert et al.[35] have reported an empirical potential surface that was parameterized to match the results of wavepacket calculations with experimentally observed branching ratios from BrCl photodissociation experiments. The bond length and dissociation energy these authors report for the A state are 2.540 Å and 8.53 kcal/mol which again agree qualitatively with the current values of 2.530 Å and 7.3 kcal/mol. One discrepancy between the calculated potentials and the empirical ones of Beckert et al. is that the calculations predict the X state has a shorter bond length than the A state while the empirical potentials predict the opposite. A recent study employing equation of motion coupled cluster and spin-orbit MRCI on IBr found that the X state of IBr also has a somewhat shorter bond length than the A state.[74] There exists no prior data either experimental or theoretical to which the other two states in Table 3 can be compared.

Five of the 7 total bound spin-orbit states are (at short bond lengths) composed primarily of the $X^1\Sigma^+$ and $B^3\Pi$ Λ-S basis states, which are the only two basis states that are bound with respect to ground state atoms. The other two bound spin-orbit states are here designated $2^3\Pi(0^+)$ and $1^3\Sigma^-(0^+)$, and these two states are bound with respect to their respective dissociation channels due to the two avoided crossings between the $0^+$ states. These avoided crossings are likely to play a significant role in the photodissociation dynamics of BrCl and may be of interest here to examine more closely. To this end the compositions of the five $0^+$ states in the Λ-S basis are given for a number of bond lengths in tables 4-6. By examining the compositions at 4.0 bohr

(the minimum of the X state potential) it is clear that labeling of the spin-orbit states with the Λ and S quantum numbers in the Frank-Condon region is reasonable as each state is composed almost entirely of a single basis state. The geometries at $r$ = 5.2 bohr and 5.6 bohr are shown as representative points surrounding the 1st avoided crossing (AC1). It is clear that between these two points the characters of the 3rd and 4th $0^+$ states have swapped. It is also apparent at these two geometries that Λ and S are considerably poorer quantum numbers, especially for states 3-5. Table 5 gives the compositions before, near, and after the second avoided crossing (AC2). Again, one can clearly see that between 6.0 and 6.8 $a_o$ the character of states 2 and 3 have swapped, but that many states are involved in this avoided crossing. The final point at 10.0 $a_o$ is included in Table 6 to show that in the asymptotic region all of the spin-orbit eigenstates are mixtures of several basis states.

Table 7 lists the allowed vertical excitation energies from the ground state with their transition dipole moments at the equilibrium geometry of the ground state (4.042 bohr). Examination of this table and the spin-orbit potential curves provides some further insight into the experimental observations of BrCl photodissociation. The studies at shorter wavelength by Park et al.[37] suggested production of products in the third dissociation channel was due to a parallel excitation to a $D(0^+)$, which might be of $^3\Sigma^-$ or possibly $^3\Pi$ character. Both of these states are probable contributors with adiabatic dissociation to channel 3 on the $^3\Sigma^-$ state or diabatic dissociation of the $^3\Pi$ state. The $^3\Pi$ state may be a larger contributor than previously suggested, as it has a significantly larger transition dipole moment than the $^3\Sigma^-$ state. Excitation to either of these states can also account for the observation of the first two product channels depending on the dynamics at AC1 and AC2. Production of channel 3 is known to have a

perpendicular component, but no state has been specified. Figure 4 indicates that there are two $\Omega = 1$ states that could be responsible, the $1^3\Sigma^-(1)$ and $2^3\Sigma^+(1)$, but the $2^3\Sigma^+(1)$ state has a considerably smaller transition dipole moment. The production of channel 2 via perpendicular excitation at the shorter wavelengths has been attributed to the $2^1\Pi(1)$ state, but the $1^3\Sigma^+(1)$ could also be a small contributor. At longer wavelengths, perpendicular excitation to the $C^1\Pi_1$ state is thought to be more important than excitation to the $A^1\Pi_1$ state and the magnitudes of their transition dipole moments bears that out. It has also been suggested that a third $\Omega = 1$ state is involved in the long wavelength production of ground state atoms, and while it was not specified, the current results suggest it should be the $2^3\Pi_1$ state.

The $\Omega = 2$ and $\Omega = 0^-$ states are shown in Figures 3 and 5, but they are not thought to be involved in the photodissociation dynamics. While the 2 states have relatively little structure, the $0^-$ states are more interesting in that they exhibit two avoided crossings much like the $0^+$ states.

**IV. CONCLUSIONS**

The goal of this work has been to calculate ab initio potential energy curves for all states of the BrCl molecule that correlate with the four lowest asymptotic atomic product channels (ground state atoms if spin-orbit coupling is neglected). All 23 states have been computed at 25 geometries between 3.5 and 50 bohr using the MRCI method. The correlation consistent family of basis sets were used, which allowed for extrapolation to the complete basis set limit. A small number of very large active space MRCI calculations were carried out for each state and were used to scale the potential curves to correct for higher order electron correlation effects. Spin-orbit coupling was treated with the interacting states approach and all spin-orbit matrix elements

and transition dipole moments have been saved. Most of the excited states of BrCl have not been previously observed by experiment.

A number of subroutines have been written to help organize the data and aid in the use of the ab inito potentials. It is hoped these will be useful in future wavepacket calculations to further investigate the photodissociation of BrCl. This suite of programs requires the user to supply the bond length and will then return the spin-orbit coupled eigenstates and transition dipole moments from the ground state at the specified geometry.

Finally, highly accurate spectroscopic constants have been calculated for the ground state of BrCl. This involved CCSD(T) calculations with extrapolations to the CBS limit. To this corrections were added based on CCSDT and CCSDTQ calculations and extrapolations to the FCI limit. Corrections to account for core-valence correlation, spin-orbit coupling, scalar relativity and the pseudopotential approximation were also included.

## REFERENCES


(1) Solomon, S. *Nature* **1990**, *347*, 347.

(2) Abbatt, J. P. D. *Journal of Geophysical Research-Atmospheres* **1995**, *100(D7)*, 14009.

(3) Chu, L.; Chu, L. T. *Journal of Physical Chemistry A* **1999**, *103*, 691.

(4) Danilin, M. Y.; McConnell, J. C. *Journal of Geophysical Research-Atmospheres* **1995**, *100(D6)*, 237.

(5) Hanson, D. R.; Ravishankara, A. R. *Geophysical Research Letters* **1995**, *22*, 385.

(6) Barrie, L. A.; Bottenheim, J. W.; Schnell, R. C.; Crutzen, P. J.; Rasmussen, R. A. *Nature* **1988**, *334*, 138.

(7) Bottenheim, J. W.; Gallant, A. G.; Brice, K. A. *Geophysical Research Letters* **1986**, *13*, 113.

(8) Platt, U.; Honninger, G. *Chemosphere* **2003**, *52*, 325.

(9) Foster, K. L.; Plastridge, R. A.; Bottenheim, J. W.; Shepson, P. B.; Finlayson-Pitts, B. J.; Spicer, C. W. *Science* **2001**, *291*, 471.

(10) Spicer, C. W.; Plastridge, R. A.; Foster, K. L.; Finlayson-Pitts, B. J.; Bottenheim, J. W.; Grannas, A. M.; Shepson, P. B. *Atmospheric Environment* **2002**, *36*, 2721.

(11) Lindberg, S. E.; Brooks, S.; Lin, C.-J.; Scott, K. J.; Landis, M. S.; Stevens, R. K.; Goodsite, M.; Richter, A. *Environmental Science and Technology* **2002**, *36*, 1245.

(12) Schroeder, W. H.; Anlauf, K. G.; Barrie, L. A.; Lu, J. Y.; Steffen, A.; Schneeberger, D. R.; Berg, T. *Nature* **1998**, *394*, 331.

(13) Tarasick, D. W.; Bottenheim, J. W. *Atmospheric Chemistry and Physics* **2002**, *2*, 197.

(14) Hadley, S. G.; Bina, M. J.; Brabson, G. D. *Journal of Physical Chemistry* **1974**, *78*, 1833.

(15) Perram, G. P.; Davis, S. J. *Journal of Chemical Physics* **1990**, *93*, 1720.

(16) Moore, C. E. *Atomic Energy Levels*; NSRDS-NBS 35; Office of Standard Reference Data, National Bureau of Standards: Washington DC, 1971; Vol. 1.

(17) Hubinger, S.; Nee, J. B. *Journal of Photochemistry and Photobiology A: Chemistry* **1995**, *86*, 1.

(18) Maric, D.; Burrows, J. P. *Journal of Physical Chemistry* **1996**, *100*, 8645.

(19) Cordes, H.; Sponer, H. *Zeitschrift fuer Physik* **1932**, *79*, 170.

(20) Clyne, M. A. A.; Coxon, J. A. *Proceedings of the Royal Society of London, Series A: Mathematical, Physical and Engineering Sciences* **1967**, *298*.

(21) Clyne, M. A. A.; Coxon, J. A. *Nature* **1968**, *217*, 448.

(22) Coxon, J. A. *Journal of Molecular Spectroscopy* **1974**, *50*, 142.

(23) Wright, J. J.; Spates, W. S.; Davis, S. J. *Journal of Chemical Physics* **1977**, *66*, 1566.

(24) Clyne, M. A. A.; McDermid, I. S. *Journal of the Chemical Society, Faraday Transactions 2: Molecular and Chemical Physics* **1978**, *74*, 807.

(25) Clyne, M. A. A.; McDermid, I. S. *Faraday Discussions of the Chemical Society* **1979**, *67*, 316.

(26) Clyne, M. A. A.; Zai, L. C. *Journal of the Chemical Society, Faraday Transactions 2: Molecular and Chemical Physics* **1982**, *78*, 1221.

(27) Tellinghuisen, J. *Journal of Molecular Spectroscopy* **1995**, *173*, 223.

(28) Cooper, M. J.; Jackson, P. J.; Rogers, L. J.; Orr-Ewing, A. J.; Ashfold, M. N. R.; Whitaker, B. J. *Journal of Chemical Physics* **1998**, *109*, 4367.

(29) Tellinghuisen, J. *Journal of Chemical Physics* **1988**, *89*, 6150.

(30) Wang, P.; Dimov, S. S.; Lipson, R. H. *Journal of Chemical Physics* **1997**, *107*, 3345.

(31) Brown, S. W.; Dowd, C. J.; Tellinghuisen, J. *Journal of Molecular Spectroscopy* **1988**, *132*, 178.

(32) Chakraborty, D. K.; Tellinghuisen, P. C.; Tellinghuisen, J. *Chemical Physics Letters* **1987**, *141*, 36.

(33) Tellinghuisen, J. *Journal of Physical Chemistry A* **2003**, *107*, 753.

(34) Uehara, H.; Konno, T.; Ozaki, Y.; Horiai, K.; Nakagawa, K.; Johns, J. W. C. *Canadian Journal of Physics* **1994**, *72*, 1145.

(35) Beckert, M.; Wouters, E. R.; Ashfold, M. N. R.; Wrede, E. *Journal of Chemical Physics* **2003**, *119*, 9576.

(36) Cao, J.; Loock, H.-P.; Qian, C. X. W. *Canadian Journal of Chemistry* **1994**, *72*, 758.

(37) Park, M.-S.; Jung, Y.-J.; Lee, S.-H.; Kim, D.-C.; Jung, K.-H. *Chemical Physics Letters* **2000**, *322*, 429.

(38) Smolin, A. G.; Vasyutinskii, O. S.; Vieuxmaire, O. P. J.; Ashfold, M. N. R.; Balint-Kurti, G. G.; Orr-Ewing, A. J. *Journal of Chemical Physics* **2006**, *124*, 094305.

(39) Wouters, E. R.; Beckert, M.; Russell, L. J.; Rosser, K. N.; Orr-Ewing, A. J.; Ashfold, M. N. R.; Vasyutinskii, O. S. *Journal of Chemical Physics* **2002**, *117*, 2087.

(40) de Jong, W. A.; Styszynski, J.; Visscher, L.; Nieuwpoort, W. C. *Journal of Chemical Physics* **1998**, *108*, 5177.

(41) Feller, D.; Peterson, K. A.; de Jong, W. A.; Dixon, D. A. *Journal of Chemical Physics* **2003**, *118*, 3510.

(42) Lazarou, Y. G.; Prosmitis, A. V.; Papadimitriou, V. C.; Papagiannakopoulos, P. *Journal of Physical Chemistry A* **2001**, *105*, 6729.

(43) Shepler, B. C.; Peterson, K. A. *Journal of Physical Chemistry A* **2006**, submitted.

(44) Knowles, P. J.; Werner, H.-J. *Chemical Physics Letters* **1988**, *145*, 514.

(45) Werner, H.-J.; Knowles, P. J. *Journal of Chemical Physics* **1988**, *89*, 5803.

(46) Knowles, P. J.; Werner, H.-J. *Chemical Physics Letters* **1985**, *115*, 259.

(47) Werner, H.-J.; Knowles, P. J. *Journal of Chemical Physics* **1985**, *82*, 5053.

(48) Blomberg, M. R. A.; Siegbahn, P. E. M. *Journal of Chemical Physics* **1983**, *78*, 5682.

(49) Langhoff, S. R.; Davidson, E. R. *Int. J. Quantum Chem.* **1974**, *8*, 61.

(50) Simons, J. *Journal of Physical Chemistry* **1989**, *93*, 626.

(51) Werner, H.-J. MOLPRO is a package of ab initio programs written by H.-J. Werner and P.J. Knowles, version 2002.6, R.D. Amos, A. Bernhardsson, A. Berning, P. Celani, D.L. Cooper, M.J.O. Deegan, A.J. Dobbyn, F. Eckert, C. Hampel, G. Hetzer, P.J. Knowles, T. Korona, R. Lindh, A.W. Lloyd, S.J. McNicholas, F.R. Manby, W. Meyer, M.E. Mura, A. Nicklass, P. Palmieri, R. Pitzer, G. Rauhut, M. Schütz, U. Schumann, H. Stoll, A.J. Stone, R. Tarroni, T. Thorsteinsson, and H.-J. Werner.

(52) Dunning, T. H. J.; Peterson, K. A.; Wilson, A. K. *Journal of Chemical Physics* **2001**, *114*, 9244.

(53) Peterson, K. A.; Figgen, D.; Goll, E.; Stoll, H.; Dolg, M. *Journal of Chemical Physics* **2003**, *119*, 11113.

(54) Brown, F. B.; Truhlar, D. G. *Chemical Physics Letters* **1985**, *117*, 307.

(55) Bergner, A.; Dolg, M.; Küchle, W.; Stoll, H.; Preuß, H. *Mol. Phys.* **1993**, *80*, 1431.

(56) Dolg, M. PhD. thesis, Universität Stuttgart, Stuttgart, Germany, 1989.

(57) Hajigeorgiou, P. G.; Le Roy, R. J. *Journal of Chemical Physics* **2000**, *112*, 3949.

(58) Ho, T.-S.; Rabitz, H. *Journal of Chemical Physics* **1996**, *104*, 2584.

(59) Shepler, B. C.; Peterson, K. A. **2006**, (in preparation).

(60) Purvis, G. D. I.; Bartlett, R. J. *Journal of Chemical Physics* **1982**, *76*, 1910.

(61) Raghavachari, K.; Trucks, G. W.; Pople, J. A.; Head-Gordon, M. *Chemical Physics Letters* **1989**, *156*, 479.

(62) Watts, J. D.; Gauss, J.; Bartlett, R. J. *Journal of Chemical Physics* **1993**, *98*, 8718.

(63) Peterson, K. A.; Dunning, T. H. J. *Journal of Chemical Physics* **2002**, *117*, 1.

(64) Peterson, K. A., (unpublished and available upon request).

(65) Yabushita, S.; Zhang, Z.; Pitzer, R. M. *Journal of Physical Chemistry A* **1999**, *103*, 5791.

(66) Lischka, H. H. Lischka, R. Shepard, I. Shavitt, R. M. Pitzer, M. Dallos, Th. Müller, P. G. Szalay, F. B. Brown, R. Ahlrichs, H. J. Böhm, A. Chang, D. C. Comeau, R. Gdanitz, H. Dachsel, C. Ehrhardt, M. Ernzerhof, P. Höchtl, S. Irle, G. Kedziora, T. Kovar, V. Parasuk, M. J. M. Pepper, P. Scharf, H. Schiffer, M. Schindler, M. Schüler, M. Seth, E. A. Stahlberg, J.-G. Zhao, S. Yabushita, and Z. Zhang, COLUMBUS, an ab initio electronic structure program, release 5.8 (2001).

(67) Douglas, M.; Kroll, N. M. *Annals of Physics* **1974**, *82*, 89.

(68) Jansen, G.; Hess, B. A. *Physical Review A* **1989**, *39*, 6016.

(69) Kallay, M.; Surjan, P. R. *Journal of Chemical Physics* **2001**, *115*, 2945.

(70) Goodson, D. Z. *Journal of Chemical Physics* **2002**, *116*, 6948.

(71) Dunham, J. L. *Physical Review* **1932**, *41*, 721.

(72) Duch, W.; Diercksen, G. H. F. *Journal of Chemical Physics* **1994**, *101*, 3018.

(73) Pople, J. A.; Seeger, R.; Krishnan, R. *Int. J. Quantum Chem., Quantum Chem. Symp.* **1977**, *11*, 149.

(74) Pittner, J.; Jungwirth, P. *Chemical Physics Letters* **2000**, *321*, 281.

Table 1: Contributions and final predicted values for equilibrium bond lengths (Å), harmonic frequencies ($cm^{-1}$), and dissociation energies (kcal/mol) of the $X^1\Sigma^+(0^+)$ state of BrCl.[a]

| CCSD(T) | aV5Z | ΔCBS | ΔCV | ΔSO | ΔDK | ΔT | ΔQ | ΔFCI | Total | Expt. |
|---|---|---|---|---|---|---|---|---|---|---|
| $r_e$ | 2.143 | -0.004 | -0.007 | 0.001 | 0.000 | 0.001 | 0.002 | 0.000 | 2.137 | 2.136[34] |
| $\omega_e$ | 446.1 | 3.0 | 2.7 | -1.8 | -0.7 | -1.3 | -2.3 | -0.4 | 445.2 | 444.3[34] |
| $D_e$ | 55.3 | 0.9 | 0.0 | -4.0 | -0.1 | -0.3 | 0.3 | 0.0 | 52.3 | 52.2[33] |

| MRCI+Q | aV5Z | ΔCBS | ΔSO | ΔSR | ΔScale | Total | Expt. |
|---|---|---|---|---|---|---|---|
| $r_e$ | 2.145 | -0.004 | 0.002 | 0.0000 | -0.004 | 2.139 | 2.136[34] |
| $\omega_e$ | 451.5 | -3.8 | -2.9 | -0.8 | 4.3 | 448.3 | 444.3[34] |
| $D_e$ | 53.9 | 1.0 | -3.9 | -0.2 | 1.5 | 52.3 | 52.2[33] |

[a] The best predicted values are given under the column "Total" and are equal to CCSD(T)/aV5Z + ΔCBS + ΔCV + ΔSO + ΔDK + ΔT + ΔQ + ΔFCI and Scaled-MRCI+Q/CBS+ΔSR+ΔSO. The best theoretical estimates are the former values.

Table 2: Contributions and final predicted values for the equilibrium bond length (Å), harmonic frequency ($cm^{-1}$), dissociation, and excitation energies (kcal/mol) for the $B^3\Pi(0^+)$ state of BrCl.[a]

| MRCI+Q | aV5Z | ΔCBS | ΔSO | ΔSR | ΔScale | Total | Expt.[27] |
|---|---|---|---|---|---|---|---|
| **$B^3\Pi(0^+)$** | | | | | | | |
| $r_e$ | 2.563 | -0.009 | -0.006 | -0.001 | -0.025 | 2.522 | 2.542 |
| $\omega_e$ | 207.1 | 2.9 | 2.6 | 0.1 | 19.8 | 232.5 | 222.6 |
| $D_e$ | 7.7 | 0.3 | -5.7 | 0.0 | 1.6 | 3.9 | 4.0 |
| $T_e$ | 46.2 | 0.7 | 1.8 | -0.2 | -0.1 | 48.4 | 48.2 |

[a] The best predicted values are given under the column "Total" and are equal to Scaled-MRCI+Q/CBS+ΔSR+ΔSO (see text).

Table 3: Spectroscopic constants (Å, $cm^{-1}$, and kcal/mol) of the remaining bound excited states.[a]

| | $A'^3\Pi(2)$ | $A^3\Pi(1)$ | $1^3\Pi(0^-)$ | $2^3\Pi(0^+)$ | $1^3\Sigma^-(0^+)$ |
|---|---|---|---|---|---|
| $r_e$ | 2.519 | 2.530 | 2.538 | 3.496 | 3.200 |
| | 2.555 | | | | |
| $\omega_e$ | 235.3 | 225.2 | 217.2 | 95.2 | 114.6 |
| | 232.2 | | | | |
| $D_e$ | 9.0 | 7.3 | 4.6 | 1.1[b] | 2.0[c] |
| | 9.9 | | | | |
| $T_e$ | 43.2 | 45.0 | 47.6 | 53.8 | 60.1 |
| | 42.0 | | | | |

[a] The state labels correspond to the character of these adiabatic states at $r$ = 4.0 bohr. The spectroscopic constants were determined at the Scaled-MRCI+Q/CBS+ΔSR+ΔSO level of theory (see text). The second row of values for the A′ state are the experimental estimates.[32] [b] With respect to $Br(^2P_{3/2}) + Cl(^2P_{1/2})$. [c] With respect to $Br(^2P_{1/2}) + Cl(^2P_{3/2})$.

Table 4: Composition of the $0^+$ states in the Λ-S basis states: short bond length and avoided crossing 1.

| | **1 $0^+$** | **2 $0^+$** | **3 $0^+$** | **4 $0^+$** | **5 $0^+$** |
|---|---|---|---|---|---|
| ***r = 4.8 $a_0$*** | | | | | |
| **1 $^1\Sigma^+$** | 100% | 0% | 1% | 0% | 0% |
| **2 $^1\Sigma^+$** | 0% | 0% | 1% | 6% | 94% |
| **1 $^3\Pi$** | 0% | 100% | 0% | 0% | 0% |
| **2 $^3\Pi$** | 0% | 0% | 99% | 1% | 0% |
| **1 $^3\Sigma^-$** | 0% | 0% | 1% | 94% | 5% |
| ***r = 5.2 $a_0$*** *Before AC 1* | | | | | |
| **1 $^1\Sigma^+$** | 97% | 2% | 1% | 0% | 0% |
| **2 $^1\Sigma^+$** | 0% | 0% | 0% | 39% | 60% |
| **1 $^3\Pi$** | 2% | 96% | 2% | 0% | 0% |
| **2 $^3\Pi$** | 1% | 2% | 82% | 6% | 9% |
| **1 $^3\Sigma^-$** | 0% | 1% | 14% | 55% | 30% |
| ***r = 5.6 $a_0$*** *After AC 1* | | | | | |
| **1 $^1\Sigma^+$** | 94% | 2% | 1% | 4% | 0% |
| **2 $^1\Sigma^+$** | 0% | 2% | 23% | 27% | 49% |
| **1 $^3\Pi$** | 4% | 88% | 2% | 6% | 1% |
| **2 $^3\Pi$** | 3% | 7% | 11% | 63% | 16% |
| **1 $^3\Sigma^-$** | 0% | 2% | 63% | 1% | 34% |

Table 5: Composition of the $0^+$ states in the Λ-S basis states: avoided crossing 2.

| | **1 $0^+$** | **2 $0^+$** | **3 $0^+$** | **4 $0^+$** | **5 $0^+$** |
|---|---|---|---|---|---|
| ***r = 6.0 $a_0$*** | *Before AC 2* | | | | |
| **1 $^1\Sigma^+$** | 87% | 1% | 0% | 11% | 1% |
| **2 $^1\Sigma^+$** | 0% | 4% | 42% | 14% | 40% |
| **1 $^3\Pi$** | 5% | 70% | 2% | 23% | 1% |
| **2 $^3\Pi$** | 7% | 18% | 0% | 49% | 25% |
| **1 $^3\Sigma^-$** | 0% | 8% | 56% | 3% | 33% |
| ***r = 6.4 $a_0$*** | *AC 2* | | | | |
| **1 $^1\Sigma^+$** | 79% | 0% | 0% | 17% | 3% |
| **2 $^1\Sigma^+$** | 0% | 0% | 54% | 13% | 33% |
| **1 $^3\Pi$** | 5% | 40% | 18% | 36% | 1% |
| **2 $^3\Pi$** | 15% | 20% | 3% | 29% | 32% |
| **1 $^3\Sigma^-$** | 0% | 39% | 25% | 5% | 31% |
| ***r = 6.8 $a_0$*** | *After AC 2* | | | | |
| **1 $^1\Sigma^+$** | 70% | 0% | 3% | 20% | 8% |
| **2 $^1\Sigma^+$** | 1% | 34% | 24% | 15% | 26% |
| **1 $^3\Pi$** | 3% | 1% | 54% | 41% | 0% |
| **2 $^3\Pi$** | 27% | 3% | 16% | 17% | 38% |
| **1 $^3\Sigma^-$** | 0% | 62% | 3% | 7% | 28% |

Table 6: Composition of the $0^+$ states in the Λ-S basis states: asymptotic region.

| | **1 $0^+$** | **2 $0^+$** | **3 $0^+$** | **4 $0^+$** | **5 $0^+$** |
|---|---|---|---|---|---|
| ***r = 10.0 $a_0$*** | *Asymptotic region* | | | | |
| **1 $^1\Sigma^+$** | 36% | 28% | 2% | 2% | 31% |
| **2 $^1\Sigma^+$** | 9% | 26% | 31% | 31% | 2% |
| **1 $^3\Pi$** | 1% | 0% | 54% | 45% | 0% |
| **2 $^3\Pi$** | 43% | 1% | 2% | 10% | 44% |
| **1 $^3\Sigma^-$** | 11% | 45% | 11% | 11% | 22% |

Table 7: Calculated vertical excitation energies and transition dipole moments from the ground state.

| | $\Delta E$ ($cm^{-1}$) | $\lambda$ (nm) | $\mu_{if}$ (D) |
|---|---|---|---|
| B $^3\Pi(0^+)$ | 22700 | 441 | 0.0642 |
| 2 $^3\Pi(0^+)$ | 43300 | 231 | 0.0693 |
| 1 $^3\Sigma^-(0^+)$ | 48600 | 206 | 0.0108 |
| 2 $^1\Sigma^+(0^+)$ | 55500 | 180 | 0.0276 |
| A $^3\Pi(1)$ | 21600 | 463 | 0.0176 |
| 1 $^1\Pi(1)$ | 27300 | 366 | 0.1238 |
| 2 $^3\Pi(1)$ | 42600 | 235 | 0.0154 |
| 2 $^1\Pi(1)$ | 46600 | 215 | 0.0897 |
| 1 $^3\Sigma^+(1)$ | 48900 | 205 | 0.0033 |
| 1 $^3\Sigma^-(1)$ | 49000 | 204 | 0.0163 |
| 2 $^3\Sigma^+(1)$ | 63300 | 158 | 0.0016 |
| 1 $^3\Delta$ (1) | 64200 | 156 | 0.0009 |

Figure 1: Λ-S states of BrCl correlating with ground-state atoms

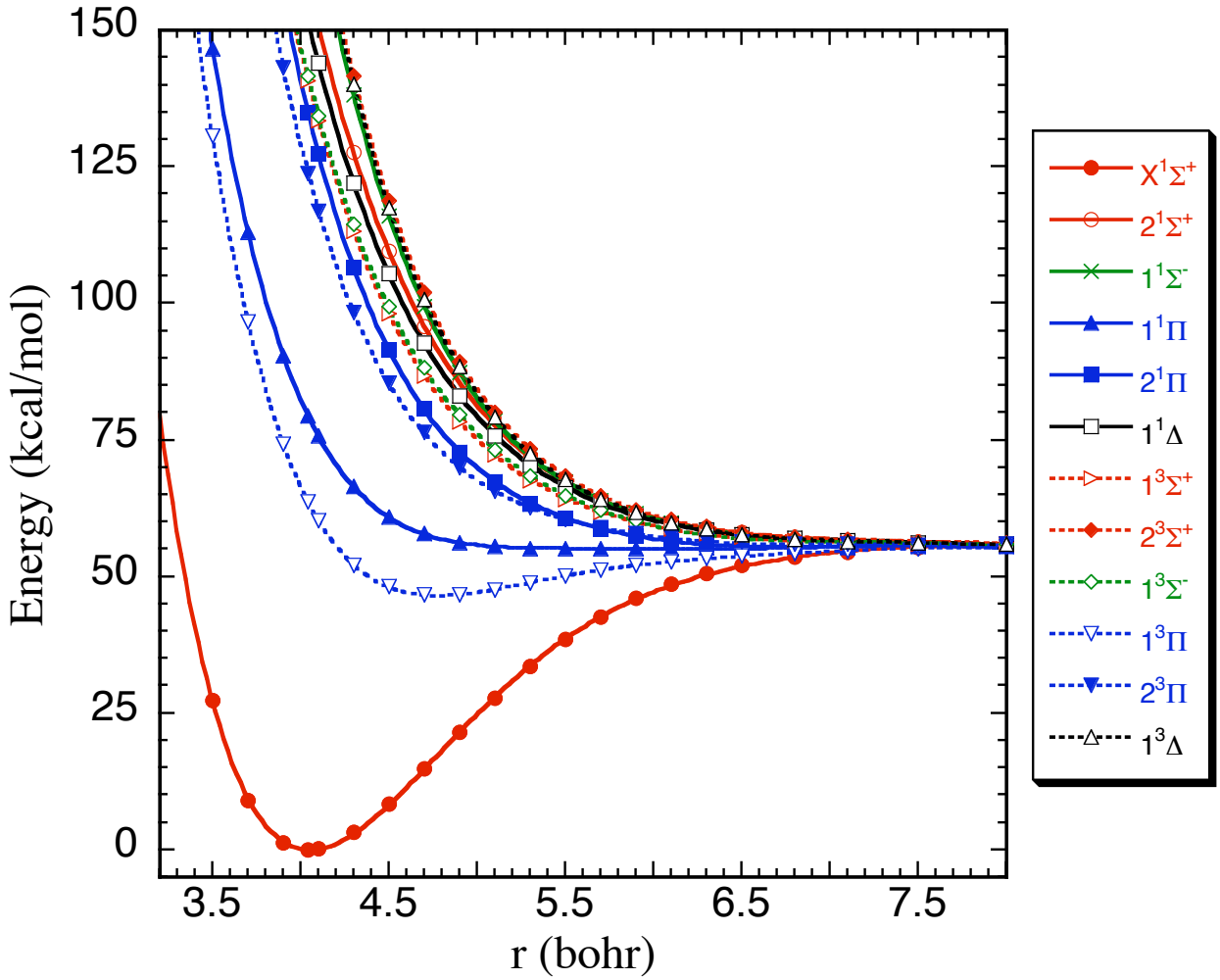

Figure 2: $\Omega = 0^+$ states

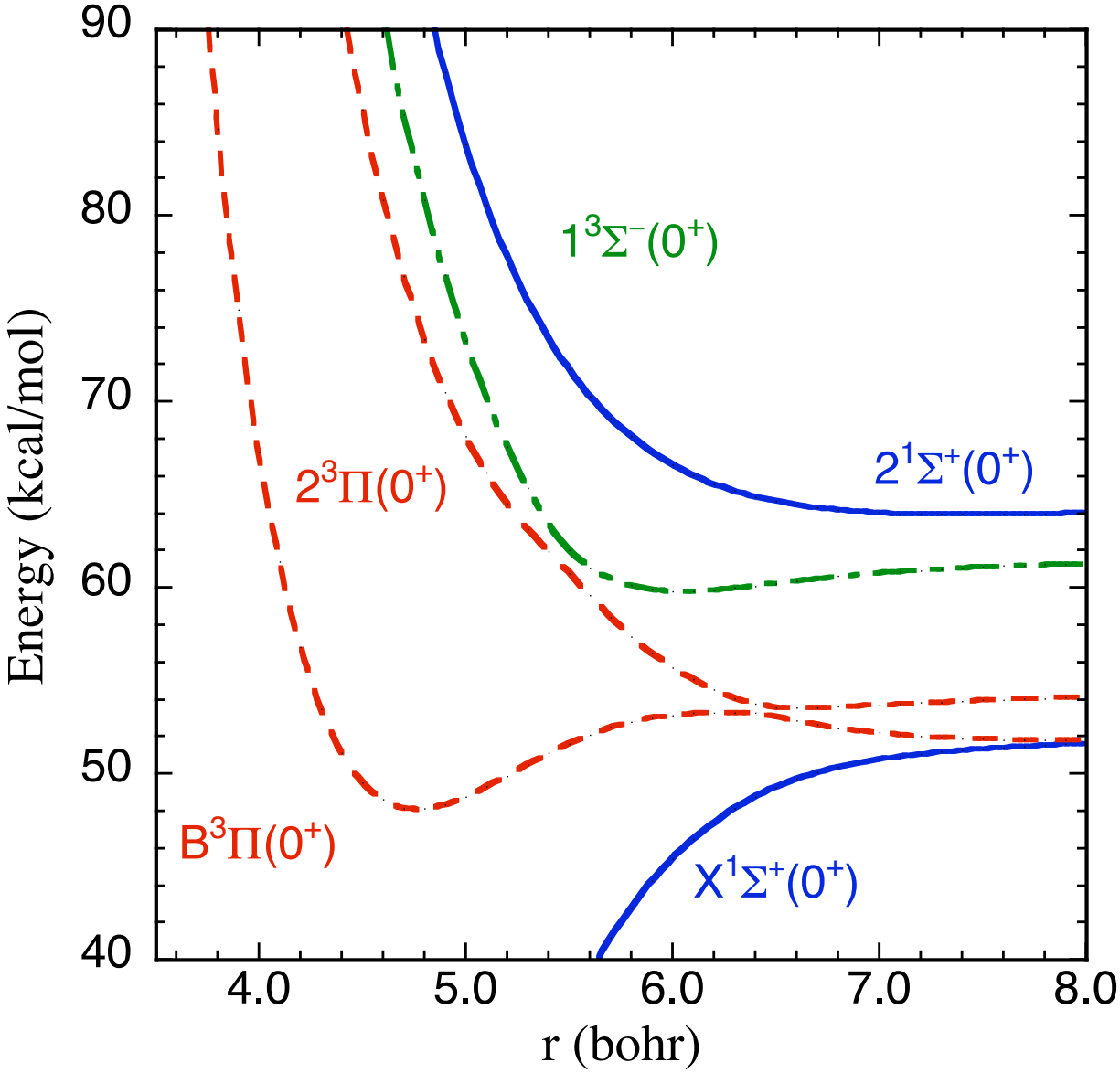

Figure 3: $\Omega = 0^-$ states

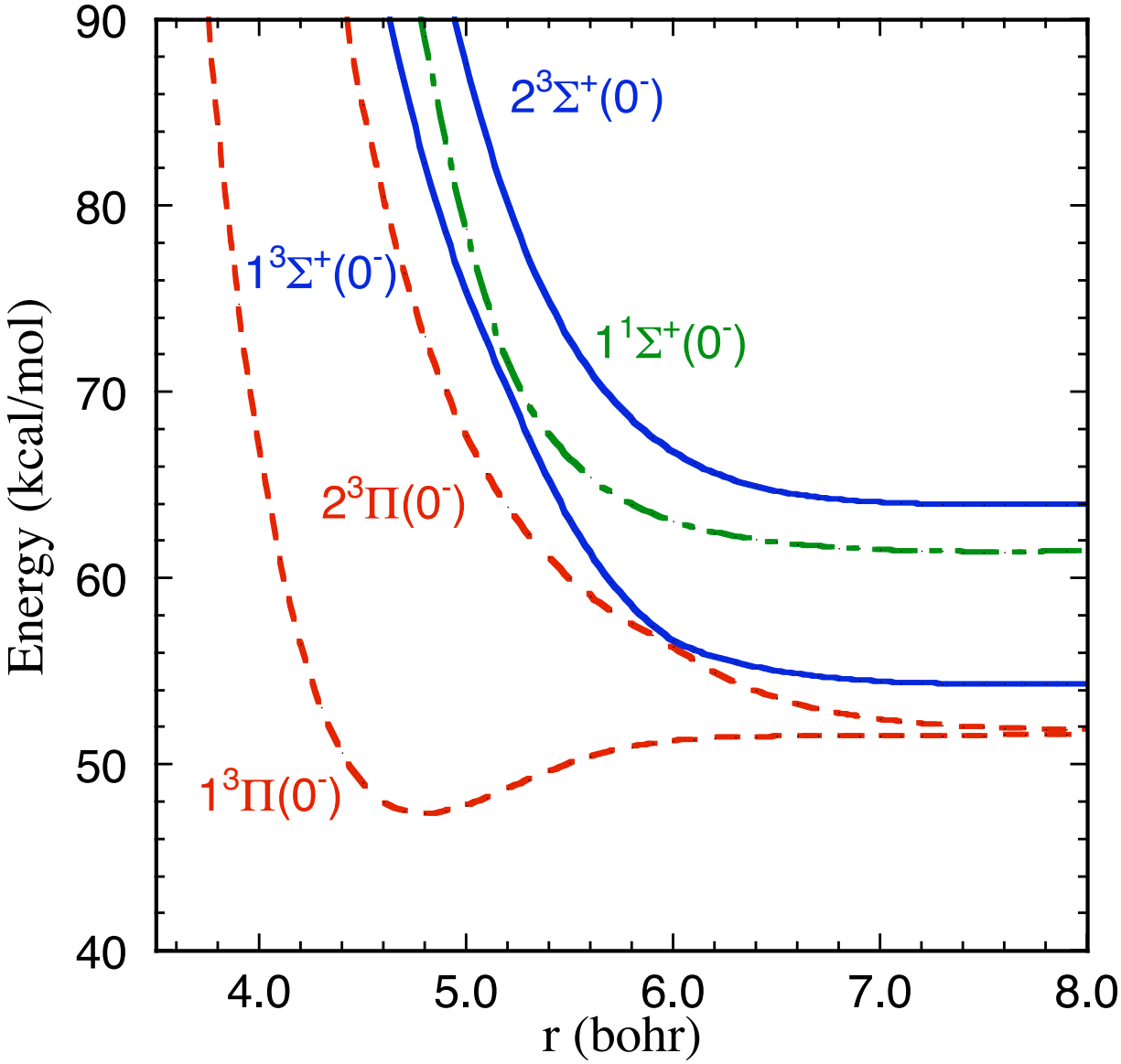

Figure 4: $\Omega = 1$ states

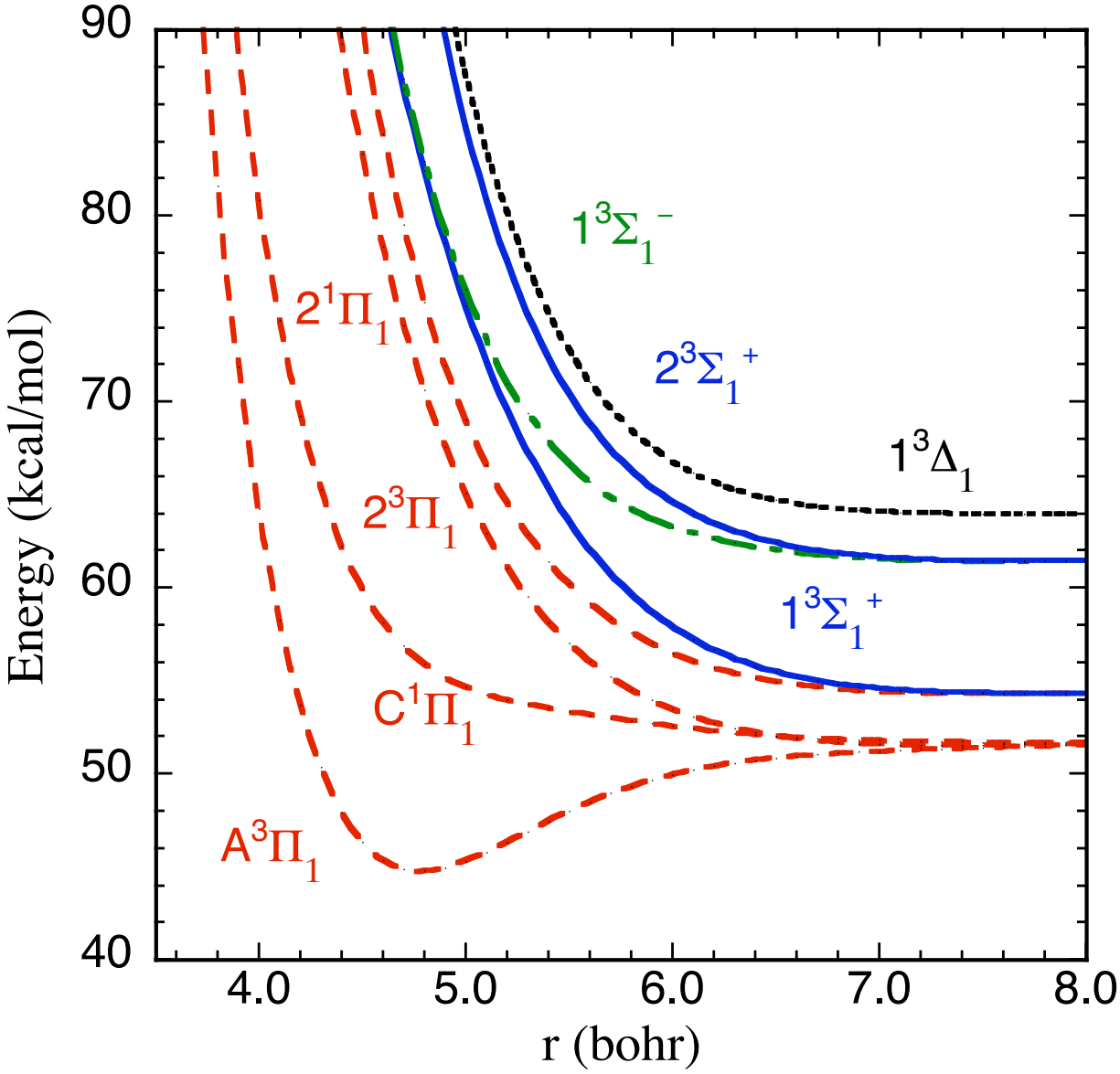

Figure 5: $\Omega = 2$ and 3 states

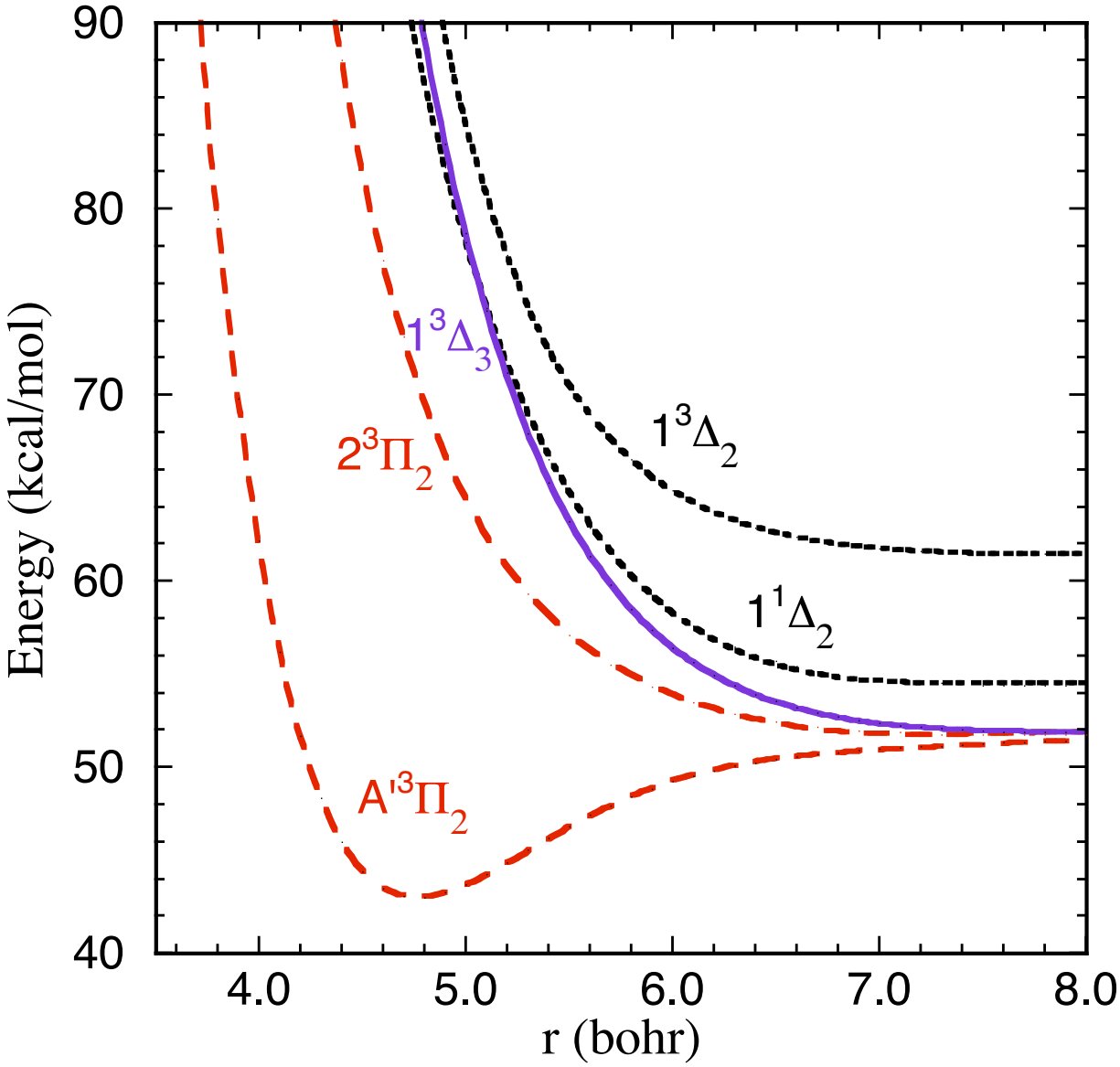

# Mercury monoxide: a systematic investigation of its ground electronic state

**Benjamin C. Shepler and Kirk A Peterson***

*Department of Chemistry, Washington State University, Pullman, Washington 99164-4630 and the Environmental Molecular Sciences Laboratory, Pacific Northwest National Laboratory, Richland, WA 99352*

**Abstract**

One of the possible key products in the oxidation and transport of atmospheric mercury is mercury monoxide, HgO. In the present work, large-scale multireference configuration interaction, as well as coupled cluster, wave functions have been used in conjunction with a series of correlation consistent basis sets to calculate the near-equilibrium potential energy functions of the first two electronic states of HgO. In the absence of spin-orbit coupling, the lowest $^1\Sigma^+$ and $^3\Pi$ states are nearly isoenergetic with a binding energy with respect to ground state atoms of only 2-3 kcal/mol at the estimated complete basis set limit. After spin-orbit coupling effects are accurately included, the resulting $X0^+$ state has a $D_0$ of just 4.0 kcal/mol, leading to a $\Delta H_f(0K)$ of 70.4 kcal/mol. These values are in stark contrast to the currently accepted experimental values. The implications of these results to atmospheric mercury chemistry are briefly discussed.

---

*Journal of Physical Chemistry A*. **107**, 1783 (2003)

## I. INTRODUCTION

Recent studies in both the Arctic and Antarctic during polar springtime have revealed episodic depletions in the concentration of tropospheric mercury.[1-6] Mercury, which prior to polar sunrise exists primarily as gaseous elemental mercury, is believed to be converted to some form of reactive gaseous mercury (RGM) or particulate mercury [Hg(p)] that is then deposited on the snowpack. It has been suggested that these mercury depletion events (MDEs) are a significant source of mercury introduction to the biosphere during this sensitive time of year and an important global sink for atmospheric mercury.[3-5] The MDEs are strongly correlated with tropospheric ozone depletions that occur at the same time of year.[1-3,5,6] The ozone depletion events are known to be caused by reactions of ozone with reactive halogen species,[7-10] and it has been suggested that reactive halogen species are also responsible for the mercury depletion events.[1-6] In particular, the reaction Hg + BrO → HgO + Br has been proposed to be a major path for the depletion of mercury in the troposphere and a major source of RGM.[2,5,8]

While HgO is well known as a solid, it is poorly characterized in the gas phase. Mercury monoxide has been tentatively identified in argon matrices[11] with a fundamental IR vibrational frequency of 676 $cm^{-1}$. An earlier mass spectrometric measurement reported a dissociation energy for HgO of 53±8 kcal/mol,[12] while JANAF cites a value of 64±15 kcal/mol.[13] The latter of these is apparently based on comparisons to lead compounds and other mercury species. Heats of formation based on these values yield a reaction enthalpy for the Hg + BrO reaction that is either slightly endothermic (2.2 kcal/mol) or slightly exothermic (–8.8 kcal/mol), respectively. Theoretical calculations of the dissociation energy of mercury monoxide, however, show even more significant variations. In particular, while the 4-component Dirac Hartree Fock (DHF) calculations of Hu et al.[14] yielded an equilibrium dissociation energy of ~40 kcal/mol, two

previous calculations[15,16] based on relativistic effective core potentials (RECPs) resulted in HgO being *unbound* with respect to dissociation to ground state atoms by more than 14 kcal/mol. All of these previous *ab initio* calculations utilized relatively small basis sets with little or no electron correlation.

In order to unambiguously determine the reaction enthalpy of the Hg+BrO reaction, large scale *ab initio* calculations have been carried out on HgO involving highly correlated wave functions and sequences of basis sets approaching the complete basis set (CBS) limit. Both RECP and all-electron calculations have been used in the calculation of the potential energy function of HgO. In the absence of spin-orbit coupling, the electronic ground state is predicted to be a $^3\Pi$ state with a $^1\Sigma^+$ state lying above by only 0.6 kcal/mol. The inclusion of spin-orbit coupling results in an $\Omega=0^+$ ground state that is bound with respect to $Hg(^1S_0) + O(^3P_2)$ products by only 4.0 kcal/mol ($D_0$). This results in a Hg+BrO → HgO+Br reaction enthalpy that is strongly endothermic.

## II. METHODOLOGY

Both singles and doubles coupled cluster with perturbative triples,[17] CCSD(T), and internally contracted multireference singles and doubles configuration interaction[18,19] (MRCI) calculations were carried out in this work. For the open-shell calculations, a variant of CCSD(T), denoted R/UCCSD(T),[20-22] was used which employs restricted open-shell Hartree-Fock (ROHF) orbitals but where some spin contamination is allowed to enter into the solution of the CCSD equations. In the present calculations the resulting spin contamination was always very small ($\leq 0.01$). The MRCI calculations included the multireference Davidson correction[23-25] for approximately including the effects of higher excitations (MRCI+Q). In order to obtain

accurate dissociation energies for HgO at the MRCI level of theory, it was found to be very important to include the Hg 6*p* orbitals in the reference function. For example, MRCI+Q calculations with standard valence (i.e., Hg 6*s* and O 2*s*2*p*) complete active space (CAS) reference functions underestimated the dissociation energy by over 3 kcal/mol for the $^1\Sigma^+$ state. The final reference function was formed from a CAS in the valence orbitals (16 electrons in 9 orbitals with the O 2*s* orbital constrained to be doubly occupied) plus additional configurations involving a maximum of two electrons in the next higher orbitals of $a_1$, $b_1$, and $b_2$ symmetry (in $C_{2v}$), which were primarily of Hg 6*p* character. This yielded 799 reference configurations for the $^1\Sigma^+$ state (742 for the $^3\Pi$ state), and the resulting internally contracted MRCI expansions involved a total number of variational parameters of just over 13 million for the $^1\Sigma^+$ and 22 million for the $^3\Pi$ state when basis sets of 5Z+diffuse quality were used (see below). The orbitals for these large MRCI calculations were taken from the CI natural orbitals of valence CAS(6,4)-MRCI calculations in order to obtain well defined Hg 6*p* orbitals across both potential curves. Those for the $^3\Pi$ state were derived from the average density matrices of analogous $^3\Pi_x$ and $^3\Pi_y$ MRCI calculations ($^3B_1$ and $^3B_2$ in $C_{2v}$, respectively). Unless otherwise noted, the frozen core approximation was employed throughout, i.e., only the 2*s* and 2*p* electrons of O and the 5*d* and 6*s* electrons of Hg were correlated.

The basis sets used in the present work corresponded to the standard cc-pV*n*Z sets for oxygen[26] augmented with extra diffuse functions,[27] denoted aug-cc-pV*n*Z, where *n* ranged from D, T, Q, and 5. New correlation consistent basis sets for mercury, denoted cc-pRV*n*Z and aug-cc-pRVnZ, have recently been developed in our laboratory and were used in the present work. These will be discussed in more detail in a separate publication.[28] The Hg basis sets

incorporate the 60 electron relativistic effective core potential (RECP) of Häussermann et al.,[29] which leaves 20 electrons (5*s*5*p*5*d*6*s*) to be explicitly treated in the *ab initio* calculations. The cc-pRV*n*Z basis sets range in size from (7*s*7*p*6*d*1*f*)/[4*s*4*p*3*d*1*f*] for the cc-pRVDZ to (14*s*14*p*11*d*4*f*3*g*2*h*1*i*)/[8*s*8*p*7*d*4*f*3*g*2*h*1*i*] for the cc-pRV5Z. The diffuse augmented variations were obtained by adding one additional even tempered function in each angular symmetry. In order to test the accuracy of the pseudopotential (PP) approximation and the effects of scalar relativity, all-electron calculations were also carried out. In these cases, two different series of basis sets were developed for mercury, one in which the exponents were optimized in calculations using the Douglas-Kroll-Hess (DK) approximation[30,31] for scalar relativity and one series in which the exponents were optimized without relativistic effects. The former will be denoted by cc-pV*n*Z-DK (*n*=D, T, Q, 5) and the latter by cc-pV*n*Z-NR (*n*=D, T, Q, 5). Similar shells of correlating functions were included in these sets as for the previously described cc-pRV*n*Z ones, but the underlying Hartree-Fock sets consisted of (32*s*26*p*19*d*13*f*) and (29*s*24*p*19*d*13*f*) base sets for -DK and -NR, respectively, which were of valence triple-ζ quality. In the DK calculations, the *sp* parts of the oxygen basis sets were recontracted based on atomic SCF-DK calculations. In all cases only the pure spherical harmonic components of the *d* through *i* polarization functions were included.

The systematic convergence behavior of the basis sets used in this work was exploited by extrapolating to the estimated complete basis set (CBS) limit. Two different extrapolation formulas were used:

$$\mathrm{E}(n) = \mathrm{E}_{\mathrm{CBS}} + Be^{-(n-1)} + Ce^{-(n-1)^2} \tag{1}$$

$$\mathrm{E}(n) = \mathrm{E}_{\mathrm{CBS}} + B/n^3 \quad . \tag{2}$$

Eq.(1)[32,33] was used with basis sets from TZ through 5Z ($n$=3-5), while Eq.(2)[34,35] was only used for the two largest sets, QZ and 5Z. In this work the average of these two values will be taken as the best estimate of the true CBS limit.

To investigate the effects of correlating the Hg 5$s$5$p$ and O 1$s$ electrons on the dissociation energies and spectroscopic constants, CCSD(T) calculations were also carried out with aug-cc-pwCV$n$Z (oxygen)[36] and cc-pRwCV$n$Z (mercury) basis sets ($n$ = T and Q) both with and without correlating the core electrons. The weighted core-valence basis sets for mercury were derived in an analogous manner as recently described[36] for the 1st and 2nd row atoms and consisted of additional 2$s$2$p$2$d$1$f$ functions for TZ and 2$s$2$p$2$d$1$f$1$g$ for the QZ set.

Spectroscopic constants were obtained via the usual Dunham analysis[37] using polynomial fits to 7 near-equilibrium bond lengths ($-0.3\ a_o \leq r - r_e \leq +0.5\ a_o$). Dissociation energies at the MRCI level were calculated relative to the energy of the $^3\Pi$ state at $r$=50 bohr. Those at the CCSD(T) level of theory were obtained relative to ground state atoms, where the O($^3$P) calculations employed partially symmetry equivalenced ($x$ and $y$ components only) Hartree-Fock orbitals.

The effects of spin-orbit coupling on the potential energy functions employed the effective 1-electron SO operator on Hg from the RECP within the interacting states method, whereby the spin-orbit coupled eigenstates were obtained by diagonalizing a matrix of $H_{el} + H_{SO}$ in a basis of pure Λ-S states. The spin-orbit matrix elements were calculated at the MRCI/aug-cc-pVQZ level of theory[38] (aug-cc-pRVQZ for Hg) with an active space similar to the large MRCI described above, but the Hg 5$d$ electrons were not correlated. The orbitals used in these calculations corresponded to state-averaged CASSCF orbitals with an active space that included the Hg 6$p$ orbitals. A total of 16 electronic states were used in the construction of $H_{el} + H_{SO}$, which

included all singlets and triplets that correlate with Hg($^1$S)+O($^3$P), Hg($^1$S)+O($^1$D), Hg($^1$S)+O($^1$S), and Hg($^3$P)+O($^3$P). Neither the repulsive quintets nor the two highest lying $^{1,3}\Sigma^-$ states were included. The diagonal elements of $H_{el} + H_{SO}$ were replaced by MRCI+Q/CBS energies for the $1^1\Sigma^+$ and $1^3\Pi$ states (Hg 5*d* electrons correlated), while the higher states were shifted by the difference of MRCI+Q/CBS (Hg 5*d* correlated) and MRCI+Q/aug-cc-pVQZ (Hg 5*d* not correlated) calculations on the $^1\Sigma^+$ state. Since a spin-orbit RECP was not included on oxygen, the asymptotic atomic energy of O was corrected by the experimental SO splitting of the O($^3$P) state, i.e., E($^3P_2 - {}^3P_{avg}$) = –0.22 kcal/mol.[39]

All of the *ab initio* calculations in this work were carried out with the MOLPRO suite of programs.[40]

## III. RESULTS

Among the low-lying electronic states of HgO, two of these, the $1^1\Sigma^+$ and $1^3\Pi$, are candidates for the electronic ground state when spin-orbit coupling is neglected. The $1^3\Pi$ state is one of two states correlating asymptotically to ground state atoms, i.e., Hg($^1$S) + O($^3$P). The other state correlating to this asymptote, the $1^3\Sigma^-$ state, is purely repulsive. The $1^1\Sigma^+$ is one of 3 states (the others are the higher-lying $1^1\Pi$ and the $1^1\Delta$ states) that correlates to Hg($^1$S) + O($^1$D). Near their equilibrium geometries, however, both the $1^1\Sigma^+$ and $1^3\Pi$ states correlate with $Hg^+(^2S)$ + $O^-(^2P)$. As discussed previously by Bauschlicher and Langhoff for ZnO,[41] these two states differ in the orientation of the *p* hole on $O^-$. The $p\sigma$ hole is favored by Pauli repulsion interactions, while the $p\pi$ hole is favored by the electrostatic interaction. In the case of the $^3\Pi$

state, the wave function changes from an ionic to a covalent charge distribution at bond distances only slightly longer than its equilibrium separation. This is essentially an avoided crossing and results in discontinuous potential energy curves at the R/UCCSD(T) level of theory. Table 1 shows the calculated spectroscopic constants for CCSD(T) and MRCI+Q as a function of basis set for both the $1^1\Sigma^+$ and $1^3\Pi$ states. The R/UCCSD(T) results for the $1^3\Pi$ state were deemed unreliable and are not shown. Potential energy curves at the MRCI+Q level of theory are plotted for both states in Figure 1 as a function of basis set. The stronger basis set dependence of the $1^1\Sigma^+$ state is clearly observed. As shown in Table 1, CCSD(T) and MRCI+Q yield essentially identical spectroscopic constants for the $^1\Sigma^+$ state and the equilibrium dissociation energies differ by only a few tenths of a kcal/mol. At the CBS limit (without including SO coupling in the molecule or atoms), this state is predicted to be bound with respect to ground state atoms by just 2.4 kcal/mol (only 1.5 kcal/mol after zero-point vibrational effects are included). The $^1\Sigma^+$ state is unbound with the DZ basis set by over 5 kcal/mol, which is consistent with earlier RECP calculations.[15,16] In the case of the $1^3\Pi$ state, the equilibrium bond length is longer than that of the $1^1\Sigma^+$ by nearly 0.3 Å with a much shallower well ($\omega_e$ ~290 $cm^{-1}$). Relative to ground state atoms, the $^3\Pi$ state is bound by 2.8 kcal/mol at the MRCI+Q/CBS level of theory (2.4 kcal/mol with ZPE corrections). Hence, before the inclusion of spin-orbit coupling, the ground state of HgO would correspond to the $1^3\Pi$ state, albeit by only a small margin (~0.4 kcal/mol without ZPE and ~0.9 kcal/mol with ZPE corrections).

Table 2 shows the effects of scalar relativity on the spectroscopic constants of the $^1\Sigma^+$ state (note that these are implicitly included via the RECP in the results described above). Scalar relativistic effects as obtained at the CCSD(T)-DK level of theory are calculated to decrease the

bond length by 0.11 Å with a concomitant increase in the harmonic frequency of 52 $cm^{-1}$. An even larger effect is observed for the dissociation energy, which is strongly decreased by scalar relativity from 23.2 to just 2.7 kcal/mol. Both of these effects are presumably due to the relativistic contraction of the 6*s* orbital of Hg, which shortens the bond length but strongly destabilizes the resulting σ bond. Comparison of the cc-pV5Z-DK results of Table 2 with the 5Z RECP values of Table 1 reveals an estimate of the accuracy of the relativistic PP approximation near the CBS limit for HgO. In the present case, the differences between the DK and PP calculations are found to be negligible for the spectroscopic constants and only ~0.5 kcal/mol for $D_e$. It should be noted, however, that the Douglas-Kroll calculations used in this work are only correct to 2nd order, so the DK scalar relativistic effects may be slightly underestimated for an element as heavy as Hg.[42]

Lastly, the effects of correlating the core electrons at the CCSD(T) level of theory using the RECPs are much more modest and result in a bond shortening of –0.009 Å, an increase in $\omega_e$ by 9 $cm^{-1}$, and nearly no change in $D_e$ (+0.02 kcal/mol) for the $^1\Sigma^+$ state. Similar calculations on the $^3\Pi$ state yielded core-valence correlation effects of just +0.0015 Å on $r_e$ and –0.25 kcal/mol on $D_e$.

Figure 2 shows the potential energy functions that were used (before adjustment) in the construction of the spin-orbit matrix within the interacting states method as described previously. In addition to the $1^1\Sigma^+$ and $1^3\Pi$ states, several other states are calculated to be clearly bound before including the effects of spin-orbit coupling, namely the low-lying $^1\Pi$ state that dissociates to Hg($^1$S)+O($^1$D), the $^3\Sigma^+$, $^3\Pi$, and $^1\Pi$ states that dissociate to Hg($^3$P)+O($^3$P), and the $^1\Sigma^+$ state that leads to Hg($^1$S)+O($^1$S). Figure 3 depicts the lowest spin-orbit coupled eigenstates of HgO.

With spin-orbit effects included, the $\Omega=0^+$ state arising from the $^1\Sigma^+$ exhibits a spin-orbit-induced avoided crossing with the $\Omega=0^+$ component of the $^3\Pi$ state and dissociates to ground state atomic products. The inclusion of spin-orbit coupling results in a $0^+$ state that is lower than the previous $^1\Sigma^+$ state by 2.4 kcal/mol. Thus, the equilibrium dissociation energy of the $0^+$ ground state is calculated to be 4.7 kcal/mol (relative to Hg $^1S_0$ + O $^3P_2$). This result cannot be reconciled with the previous DHF result by Hu et al.[14] of nearly +40 kcal/mol. Their result is presumably in error, since at the RHF level of theory the $0^+$ ($^1\Sigma^+$) state is calculated to be *unbound* in the present work by 50-60 kcal/mol (RHF/aug-cc-pRV5Z or RHF-DK/aug-cc-pV5Z-DK). The equilibrium bond length (calculated using polynomial fits near the minimum) and $v$=0-1 fundamental vibrational frequency (calculated using the program LEVEL[43]) of the $X0^+$ state are predicted in this work to be 1.922 Å and 361 $cm^{-1}$, respectively. These values do not include the effects of core-valence correlation reported above, which are expected to decrease this equilibrium bond distance by approximately 0.009 Å and only slightly increase the vibrational frequency. The vibrational frequency calculated for the final SO-coupled potential (361 $cm^{-1}$) is in strong disagreement with the tentative vibrational assignment of Butler et al.[11] in rare gas matrices, 676 $cm^{-1}$, and leads one to believe that HgO was not actually observed in their experiments. (The experimental value is also in disagreement with the calculated $^1\Sigma^+$ vibrational frequency of ~590 $cm^{-1}$.) Combining the calculated zero-point vibrational energy of 225 $cm^{-1}$ with a $D_e$ value of 4.7 kcal/mol yields a predicted $D_0$ for HgO of just 4.0 kcal/mol. This value can not be reconciled with the current experimental values of 64±15 (Ref. 13) and 53±8 (Ref. 12) kcal/mol. The former of these was obtained only by comparison with various Pb compounds and

can be safely discounted. The discrepancy with the latter experiment is difficult to explain. Certainly there is a need for further experimental studies of this species.

## IV. DISCUSSION

Accurate electronic structure methods have been used to determine the energetics and spectroscopic constants of the ground electronic state of HgO. After accounting for basis set truncation errors, electron correlation, scalar relativity, spin-orbit coupling, and vibrational zero-point energy, the $X0^+$ ground state of HgO is predicted to be bound by only 4.0 kcal/mol with respect to ground state atoms. This is in stark contrast to the JANAF value[13] of 64 ± 15 kcal/mol and a more recent mass spectrometric value[12] of 53 ± 10 kcal/mol. The much lower value for the dissociation energy of HgO has a strong impact on the predicted reactivity of Hg with BrO leading to HgO. Using the best available heats of formation[13,44] for Hg, BrO, and Br together with a $\Delta H_f(0K)$ of 70.4 kcal/mol derived from the above $D_0$, the reaction Hg + BrO → HgO + Br is now calculated to be very endothermic, $\Delta H_r(0K)$ = 51.2 kcal/mol. Hence it appears unlikely that gas phase mercury monoxide will be directly formed from the oxidation of Hg by BrO.

## V. ACKNOWLEDGEMENTS

This work was supported by the National Science Foundation (CHE-0111282). Some of this research was performed in the William R. Wiley Environmental Molecular Sciences Laboratory (EMSL) at the Pacific Northwest National Laboratory (PNNL). Operation of the EMSL is funded by the Office of Biological and Environmental Research in the U.S. Department of Energy (DOE). PNNL is operated by Battelle for the U.S. DOE under Contract DE-AC06-

76RLO 1830. The authors would like to thank Prof. Hermann Stoll (Stuttgart) for valuable discussions regarding spin-orbit coupling in Hg.

## REFERENCES


(1) Ebinghaus, R.; Kock, H. H.; Temme, C.; Einax, J. W.; Lowe, A. G.; Richter, A.; Burrows, J. P.; Schroeder, W. H. *Environ. Sci. Tech.* **2002**, *36*, 1238.

(2) Lu, J. Y.; Schroeder, W. H.; Barrie, L. A.; Steffen, A.; Welch, H. E.; Martin, K.; Lockhart, L.; Hunt, R. V.; Boila, G.; Richter, A. *Geophys. Res. Lett.* **2001**, *28*, 3219.

(3) Schroeder, W. H.; Anlauf, K. G.; Barrie, L. A.; Lu, J. Y.; Steffen, A.; Schneeberger, D. R.; Berg, T. *Nature* **1998**, *394*, 331.

(4) Steffen, A.; Schroeder, W. H.; Bottenheim, J. W.; Narayan, J.; Fuentes, J. D. *Atmos. Environ.* **2002**, *36*, 2653.

(5) Lindberg, S. E.; Brooks, S.; Lin, C.-J.; Scott, K. J.; Landis, M. S.; Stevens, R. K.; Goodsite, M.; Richter, A. *Environ. Sci. Tech.* **2002**, *36*, 1245.

(6) Berg, T.; Bartnicki, J.; Munthe, J.; Lattila, H.; Hrehoruk, J.; Mazur, A. *Atmos. Environ.* **2001**, *35*, 2569.

(7) Barrie, L. A.; Bottenheim, J. W.; Schnell, R. C.; Crutzen, P. J.; Rasmussen, R. A. *Nature* **1988**, *334*, 138.

(8) Boudries, H.; Bottenheim, J. W. *Geophys. Res. Lett.* **2000**, *27*, 517.

(9) Foster, K. L.; Plastridge, R. A.; Bottenheim, J. W.; Shepson, P. B.; Finlayson-Pitts, B. J.; Spicer, C. W. *Science* **2001**, *291*, 471.

(10) Le Bras, G.; Platt, U. *Geophys. Res. Lett.* **1995**, *22*, 599.

(11) Butler, R.; Katz, S.; Snelson, A.; Stephens, J. B. *J. Phys. Chem.* **1979**, *83*, 2578.

(12) Grade, M.; Hirschwald, H. *Ber. Bunsen-Ges. Phys. Chem.* **1982**, *86*, 899.

(13) Chase, M. W., Jr.; Davies, C. A.; Downey, J. R., Jr.; Frurip, D. J.; McDonald, R. A.; Syverud, A. N. *J. Phys. Chem. Ref. Data* **1985**, *14*, Suppl. No. 1.

(14) Hu, A.; Otto, P.; Ladik, J. *J. Mol. Struct.* **1999**, *468*, 163.

(15) Stömberg, D.; Gropen, O.; Wahlgren, U. *Chem. Phys.* **1989**, *133*, 207.

(16) Cundari, T. R.; Moody, E. W. *J. Mol. Struct.* **1998**, *425*, 43.

(17) Raghavachari, K.; Trucks, G. W.; Pople, J. A.; Head-Gordon, M. *Chem. Phys. Lett.* **1989**, *157*, 479.

(18) Werner, H.-J.; Knowles, P. J. *J. Chem. Phys.* **1988**, *89*, 5803.

(19) Knowles, P. J.; Werner, H.-J. *Chem. Phys. Lett.* **1988**, *145*, 514.

(20) Scuseria, G. E. *Chem. Phys. Lett.* **1991**, *176*, 27.

(21) Watts, J. D.; Gauss, J.; Bartlett, R. J. *J. Chem. Phys.* **1993**, *98*, 8718.

(22) Knowles, P. J.; Hampel, C.; Werner, H.-J. *J. Chem. Phys.* **1994**, *99*, 5219.

(23) Langhoff, S. R.; Davidson, E. R. *Int. J. Quantum Chem.* **1974**, *8*, 61.

(24) Blomberg, M. R. A.; Siegbahn, P. E. M. *J. Chem. Phys.* **1983**, *78*, 5682.

(25) Simons, J. *J. Phys. Chem.* **1989**, *93*, 626.

(26) Dunning, T. H., Jr. *J. Chem. Phys.* **1989**, *90*, 1007.

(27) Kendall, R. A.; Dunning, T. H., Jr.; Harrison, R. J. *J. Chem. Phys.* **1992**, *96*, 6796.

(28) Peterson, K. A. *to be published*.

(29) Häussermann, U.; Dolg, M.; Stoll, H.; Preuss, H.; Schwerdtfeger, P.; Pitzer, R. M. *Mol. Phys.* **1993**, *78*, 1211.

(30) Douglas, M.; Kroll, N. M. *Ann. Phys. (New York)* **1974**, *82*, 89.

(31) Jansen, G.; Hess, B. A. *Phys. Rev. A* **1989**, *39*, 6016.

(32) Peterson, K. A.; Woon, D. E.; Dunning, T. H., Jr. *J. Chem. Phys.* **1994**, *100*, 7410.

(33) Feller, D.; Peterson, K. A. *J. Chem. Phys.* **1999**, *110*, 8384.

(34) Helgaker, T.; Klopper, W.; Koch, H.; Noga, J. *J. Chem. Phys.* **1997**, *106*, 9639.

(35) Halkier, A.; Helgaker, T.; Jørgensen, P.; Klopper, W.; Koch, H.; Olsen, J.; Wilson, A. K. *Chem. Phys. Lett.* **1998**, *286*, 243.

(36) Peterson, K. A.; Dunning, T. H., Jr. *J. Chem. Phys.* **2002**, in press.

(37) Dunham, J. L. *Phys. Rev.* **1932**, *41*, 721.

(38) Berning, A.; Schweizer, M.; Werner, H.-J.; Knowles, P. J.; Palmieri, P. *Mol. Phys.* **2000**, *98*, 1823.

(39) Moore, C. E. *Atomic Energy Levels*; NSRDS-NBS 35, Office of Standard Reference Data, National Bureau of Standards: Washington, D.C., 1971; Vol. 1.

(40) MOLPRO is a package of *ab initio* programs written by H.-J. Werner and P.J. Knowles with contributions from J. Almlöf, R.D. Amos, A. Bernhardsson, A. Berning, P. Celani, D.L. Cooper, M.J.O. Deegan, A.J. Dobbyn, F. Eckert, S.T. Elbert, C. Hampel, G. Hetzer, T. Korona, R. Lindh, A.W. Lloyd, S.J. McNicholas, F.R. Manby, W. Meyer, M.E. Mura, A. Nicklass, P. Palmieri, K.A. Peterson, R.M. Pitzer, P. Pulay, G. Rauhut, M. Schütz, H. Stoll, A.J. Stone, R. Tarroni, P.R. Taylor, T. Thorsteinsson. Molpro2000 (2000).

(41) Bauschlicher, C. W., Jr.; Langhoff, S. R. *Chem. Phys. Lett.* **1986**, *126*, 163.

(42) Nakajima, T.; Hirao, K. *Chem. Phys. Lett.* **2000**, *329*, 511.

(43) R.J. Le Roy, LEVEL 7.1: A Computer Program for Solving the Radial Schrödinger Equation for Bound and Quasibound Levels, University of Waterloo Chemical Physics Research Report CP-642R (2000). LEVEL (2000).

(44) Wilmouth, D. M.; Hanisco, T. F.; Donahue, N. M.; Anderson, J. G. *J. Phys. Chem. A* **1999**, *103*, 8935.

**Table 1.** Calculated spectroscopic constants of $1^1\Sigma^+$ and $1^3\Pi$ HgO neglecting spin-orbit coupling.

| Method | $r_e$ (Å) | $\omega_e$ ($cm^{-1}$) | $\omega_e x_e$ ($cm^{-1}$) | $D_e$ (kcal/mol)[a] | $\Delta E_e$ (kcal/mol)[b] |
|---|---|---|---|---|---|
| $1^1\Sigma^+$ | | | | | |
| CCSD(T)/ | | | | | |
| DZ | 1.9468 | 566.8 | 3.2 | –5.75 | |
| TZ | 1.9195 | 593.9 | 3.6 | 0.04 | |
| QZ | 1.9145 | 596.7 | 3.4 | 1.59 | |
| 5Z | 1.9124 | 599.2 | 3.5 | 2.17 | |
| CBS(1) | | | | 2.52 | |
| CBS(2) | | | | 2.79 | |
| MRCI+Q/ | | | | | |
| DZ | 1.9440 | 572.7 | 3.8 | –5.42 | 6.52 |
| TZ | 1.9186 | 594.6 | 3.7 | -0.03 | 2.04 |
| QZ | 1.9145 | 596.3 | 3.6 | 1.33 | 1.20 |
| 5Z | 1.9125 | 598.8 | 3.8 | 1.84 | 0.84 |
| CBS(1) | | | | 2.14 | 0.44 |
| CBS(2) | | | | 2.38 | 0.46 |
| $1^3\Pi$ | | | | | |
| MRCI+Q/ | | | | | |
| DZ | 2.2979 | 305.1 | (c) | 0.77 | |
| TZ | 2.2410 | 294.9 | (c) | 2.01 | |
| QZ | 2.2284 | 293.9 | (c) | 2.53 | |
| 5Z | 2.2214 | 287.8 | (c) | 2.68 | |
| CBS(1) | | | | 2.77 | |
| CBS(2) | | | | 2.84 | |

[a] Calculated with respect to ground state Hg($^1$S) and O($^3$P).

[b] $E(1^1\Sigma^+) - E(1^3\Pi)$, i.e., a positive value indicates the $^3\Pi$ is lower in energy.

[c] A reliable value was not obtained due to the flatness of the potential.

**Table 2.** Effects of scalar relativity on the spectroscopic constants of $1^1\Sigma^+$ HgO at the CCSD(T) level of theory in all-electron calculations.[a]

| Method | $r_e$ (Å) | $\omega_e$ ($cm^{-1}$) | $\omega_e x_e$ ($cm^{-1}$) | $D_e$ (kcal/mol) |
|---|---|---|---|---|
| NR | | | | |
| DZ | 2.0628 | 512.2 | 2.2 | 17.56 |
| TZ | 2.0360 | 538.6 | 2.8 | 21.56 |
| QZ | 2.0291 | 547.0 | 3.0 | 22.88 |
| 5Z | 2.0268 | 548.9 | 3.0 | 23.15 |
| DK | | | | |
| DZ | 1.9425 | 566.1 | 2.9 | -3.20 |
| TZ | 1.9201 | 593.0 | 3.4 | 1.07 |
| QZ | 1.9143 | 599.5 | 3.4 | 2.40 |
| 5Z | 1.9124 | 601.4 | 3.5 | 2.69 |

[a] NR=nonrelativistic, DK=Douglas-Kroll with cc-pV*n*Z-NR or cc-pV*n*Z-DK on Hg and aug-cc-pV*n*Z or aug-cc-pV*n*Z-DK on O. See the text. All electrons are explicitly treated in these calculations but only the valence electrons were correlated.

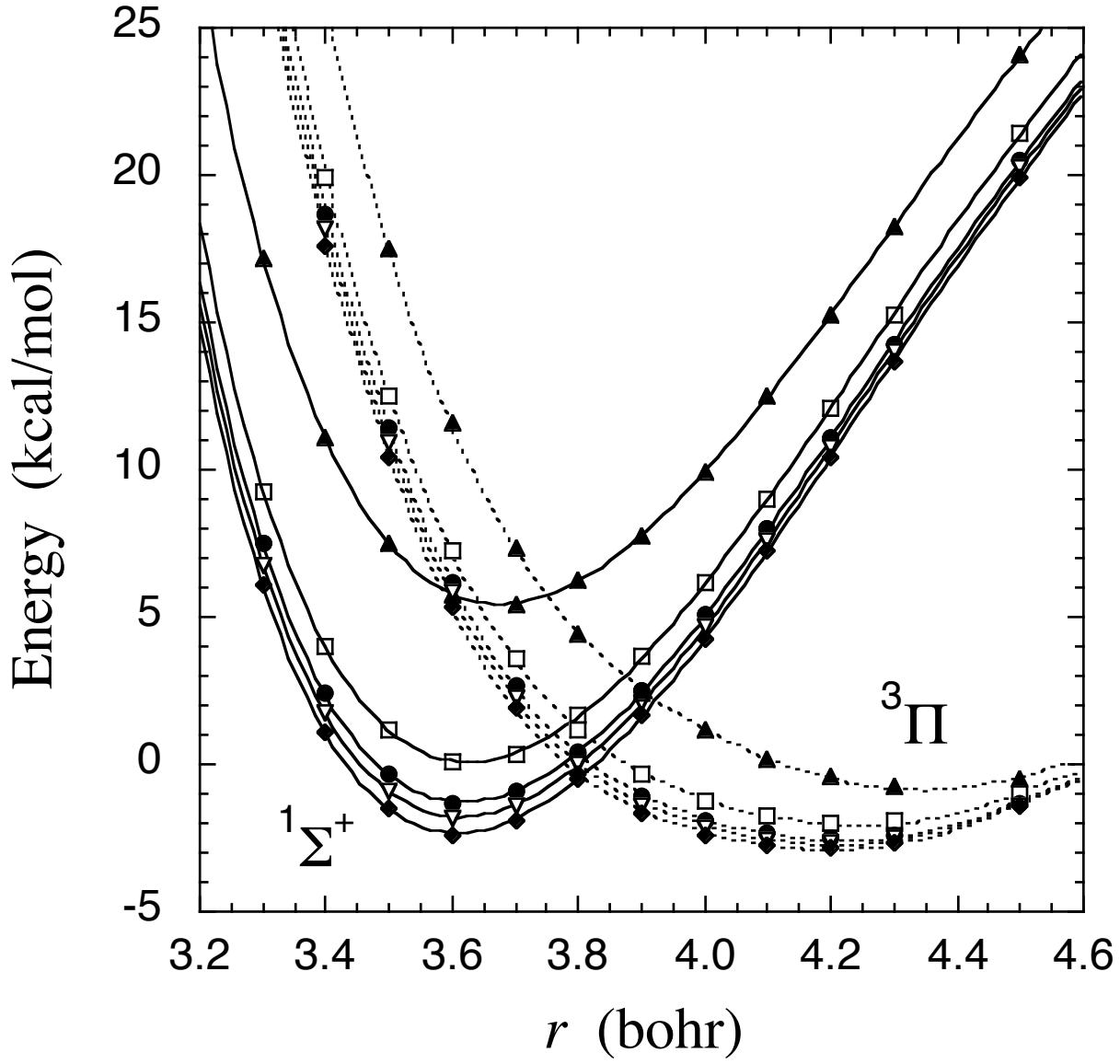


Figure 1. Potential energy curves for the lowest two electronic states of HgO calculated as a function of basis set at the MRCI+Q level of theory (neglecting spin-orbit coupling).

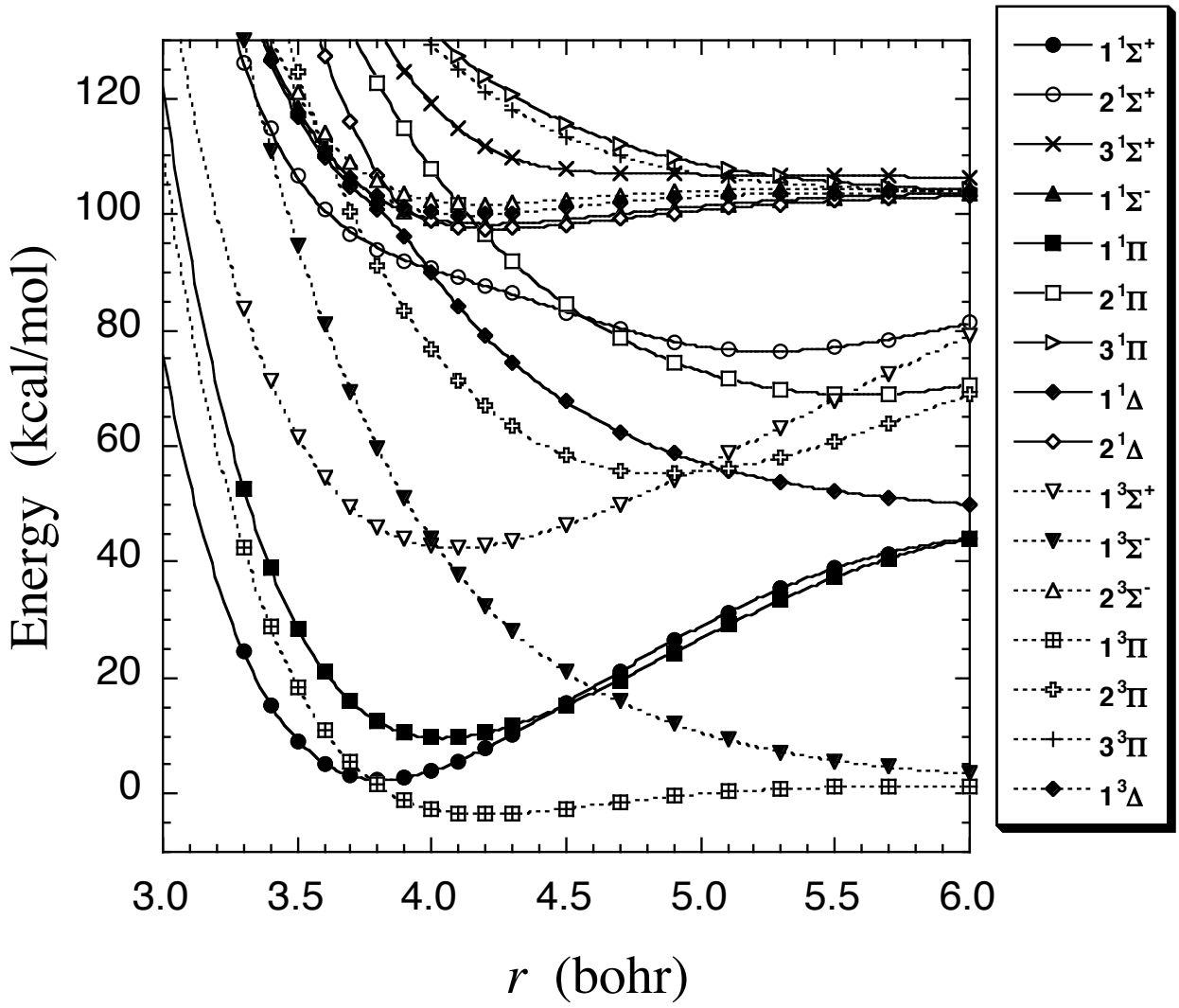


Figure 2. Potential energy curves at the MRCI+Q/aug-cc-pVQZ level of theory for the low-lying electronic states of HgO used in the calculation of spin-orbit coupling effects. The Hg 5*d* electrons were not correlated in these calculations.

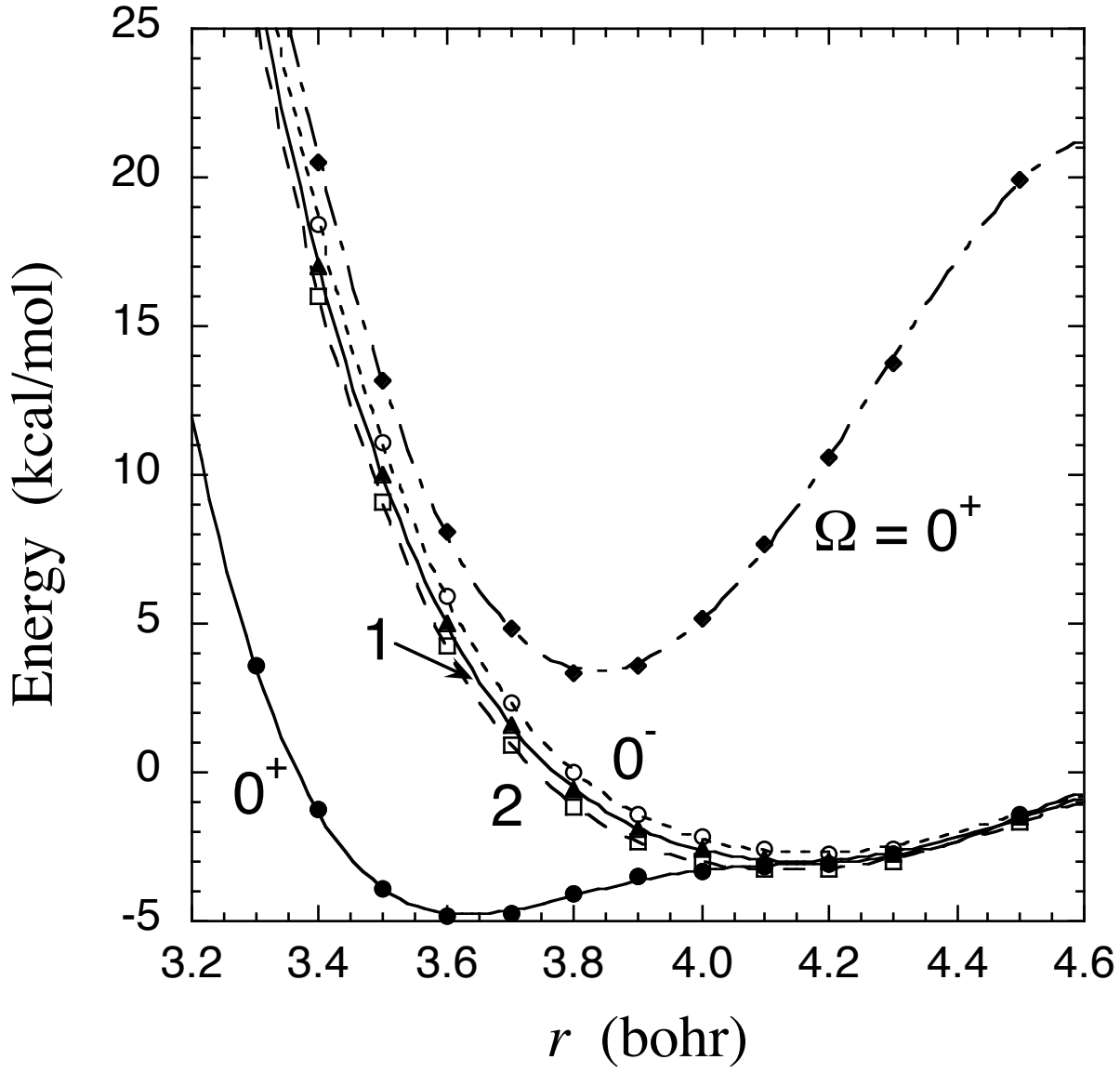


Figure 3. Potential energy curves for the lowest *spin-orbit coupled* electronic states of HgO calculated at the MRCI+Q/CBS level of theory. The states are labeled by their Ω quantum numbers.

# Hg + Br → HgBr recombination and collision-induced dissociation dynamics

**Benjamin C. Shepler, Nikolai B. Balabanov and Kirk A. Peterson***

*Department of Chemistry, Washington State University, Pullman, Washington 99164-4630*

**Abstract**

A global potential energy surface has been constructed for the system HgBr + Ar → Hg + Br + Ar to determine temperature dependant rate constants for the collision-induced dissociation (CID) and recombination of Hg and Br atoms. The surface was decomposed using the general many-body expansion. Accurate two-body potentials for HgBr, HgAr and ArBr were calculated using coupled cluster theory with single and double excitations and a perturbative treatment of triple excitations [CCSD(T)] and the multi-reference averaged coupled pair funtional (ACPF) method. Correlation consistent basis sets were used to extrapolate to the CBS limit and corrections were added to account for scalar and spin-orbit relativistic effects, core-valence correlation and the Lamb shift. The three-body potential was computed with the CCSD(T) method and triple-zeta quality basis sets. The two-body potentials were fit with a modified Lennard-Jones potential and the three-body potential was interpolated with the reproducing kernel Hilbert space method. Quasiclassical trajectories were then carried out directly on the CID of HgBr by Ar for a large sampling of initial rotational, vibrational and collision energies. The rate of Hg and Br atom recombination is a likely first step in mercury depletion events that have been observed in the arctic troposphere during polar sunrise. The effective second order rate constant for this process was determined using the rate of CID together with the principle of detailed balance and was found to be $k(T) = 1.2 \times 10^{-12}$ $cm^3$ $molecule^{-1}$ $s^{-1}$ at 260 K and 1 bar pressure.

## I. INTRODUCTION

The atmospheric chemistry of mercury is of interest because the long atmospheric residence times of gas phase $Hg^0$ makes the atmosphere the primary route by which mercury can be transported far from its anthropogenic sources.[1] Recently, the Arctic has been proposed as a sink for mercury due in part to the observation of episodic and drastic reductions of the tropospheric mercury concentration during polar sunrise.[2-4] These mercury depletion events (MDEs) are strongly correlated with tropospheric ozone depletions that are caused by reactions with photochemically produced halogen radicals.[5-8] Therefore, it has also been proposed that the mechanism for the MDEs is the result of the oxidation of $Hg^0$ through reactions with reactive halogen species.[2-4] The product of this oxidation is so-called reactive gaseous mercury (RGM), which is likely composed of divalent mercury ($Hg^{2+}$) species that are then quickly deposited on the snow-pack.[3,9]

It has been suggested that BrO and Br are the most likely reactants that initiate the oxidation of $Hg^0$ in the formation of RGM.[2,3] One can imagine several possible reactions between Hg and BrO:

$$\mathrm{Hg} + \mathrm{BrO} \rightarrow \begin{cases} \mathrm{HgBr} + \mathrm{O} & (1a) \\ \mathrm{HgO} + \mathrm{Br} & (1b) \\ \mathrm{BrHgO} & (1c) \end{cases}$$

However, based on the experimental dissociation energies of BrO ($D_0$=55.9±0.1 kcal/mol)[10] and HgBr (15.5±0.3 kcal/mol),[11] as well as an accurate ab initio dissociation energy for HgO (4.3±1.0 kcal/mol),[12,13] one would predict reactions 1a and 1b to be *endothermic* by 40.4 and 51.6 kcal/mol respectively. It is therefore unlikely that formation of HgBr or HgO by the gas-phase reaction of Hg with BrO would occur under atmospheric conditions. As for reaction 1c

the conformers Hg-Br-O and Hg-O-Br are not stable[14,15] and preliminary calculations by the authors using the coupled cluster method with single and double excitations with a perturbative estimate of triple excitations [CCSD(T)] indicate there exists only shallow van der Waals complexes with binding energies on the order of a few tenths of a kcal/mol. The Br-Hg-O conformer is strongly bound with respect to separate Hg and BrO and ab initio calculations predict reaction 1c to be *exothermic* by -20.2 kcal/mol.[16] However, there is a large barrier to insertion of Hg into the BrO bond on the order of ~40 kcal/mol making this reaction also unlikely in the atmosphere.[15] BrO may be involved in subsequent reactions steps or heterogeneous chemistry, but it cannot be responsible for the initial gas phase oxidation of $Hg^0$.

This leaves Br atom as the species most likely responsible for the initial oxidation of $Hg^0$ during mercury depletion events. Following the formation HgBr there are numerous subsequent reactions that could lead to formation of divalent mercury species that are then deposited on the snow-pack, and it is in this context that BrO may be involved. Some of the possible mercury-halogen reactions are:

$$Hg + Br \rightarrow HgBr \qquad \Delta H_r = -15.5 \text{ kcal/mol} \qquad (2)$$
$$HgBr + Br \rightarrow BrHgBr \qquad \Delta H_r = -71.8 \text{ kcal/mol} \qquad (3)$$
$$HgBr + BrO \rightarrow BrHgO + Br \qquad \Delta H_r = -4.7 \text{ kcal/mol} \qquad (4)$$
$$HgBr + BrO \rightarrow BrHgBr + O \qquad \Delta H_r = -17.1 \text{ kcal/mol} \qquad (5)$$
$$HgBr + BrO \rightarrow BrHgOBr \qquad \Delta H_r = -54.2 \text{ kcal/mol} \qquad (6)$$
$$HgBr + Br_2 \rightarrow BrHgBr + Br \qquad \Delta H_r = -26.9 \text{ kcal/mol} \qquad (7)$$

It is also possible that following formation of HgBr, non-halogen-containing oxidants like ozone are involved, i.e.:

$$HgBr + O_3 \rightarrow BrHgO + O_2 \qquad \Delta H_r = -61.9 \text{ kcal/mol} \qquad (8)$$

The heats of formation used to calculate the enthalpies of reaction for reactions 2-8 were taken from references [16-18].

These numerous pathways for the formation of divalent mercury all depend on the initial recombination of Hg and Br atoms. The hypothesis that halogen species are responsible for the mercury depletion events therefore depends on the rate of this recombination. There has been one previous experimental report of the rate constant for Hg + Br recombination of 3.2 x $10^{-12}$ $cm^3$ $molecule^{-1}$ $s^{-1}$ at 298 K and 1 atm pressure from the group of Ariya et al.,[19] and it was determined from a study of relative rates using cold vapor atomic absorption spectroscopy (CVAAS) and gas chromatography with mass spectroscopic detection (GC-MS). The same group also reported a theoretical estimate of 2.04 x $10^{-12}$ $cm^3$ $molecule^{-1}$ $s^{-1}$ for the rate constant at 298 K and 1 atm using variational transition state theory (VTST).[20] Another theoretical estimate of 1.1 x $10^{-12}$ $cm^3$ $molecule^{-1}$ $s^{-1}$ was determined from RRKM calculations.[21]

The goal of this work has been to accurately determine the rate constant of Hg + Br recombination from ab initio calculations and quassiclassical trajectories (QCT). A global potential energy surface was constructed for the system HgBr + Ar. The rate constant for the collision induced dissociation of HgBr by Ar was directly calculated with the QCT method and the rate of Hg + Br recombination was then determined using the principle of detailed balance. Details of the calculation and fitting of the surface are presented in sections IIA and IIB, respectively, while the details of the trajectory calculations are given in section IIC. The results follow in section III and then the conclusions, acknowledgements and references in sections IV, V and VI respectively. The subroutines for fitting the three-body portion of the HgBrAr potential and for evaluating the resulting potential energy surface are included in Appendix 1. The latter can be used with the POTLIB[22] interface program.

## II. METHODOLOGY

### IIA. DETAILS OF THE AB INITO CALCULATIONS

With atoms as far down in the periodic table as bromine and especially mercury, relativistic effects are large enough that their neglect does not allow for quantitative or even qualitative results. To account for scalar relativistic effects small-core energy consistent pseudopotentials of the Stuttgart-Köln type were used on the Hg and Br atoms.[23,24] The electrons left to treat explicitly were the $3s^2 3p^6 3d^{10} 4s^2 4p^5$ on Br and the $5s^2 5p^6 5d^{10} 6s^2$ on Hg. The basis sets used on Hg, Br and Ar were from the correlation consistent family of basis sets. The aug-cc-pVnZ-PP basis sets were used on Hg and Br and were optimized for use with the pseudopotentials.[24-26] The aug-cc-pV(n+d)Z basis sets that contain modified d-shells containing additional tight exponents were used on Ar.[27] Henceforth these basis sets will be denoted aVnZ.

The potential energy was decomposed using the standard many-body expansion:[28]

$$\tilde{V}(R_1,R_2,R_3) = V^{(1)} + V^{(2)}_{HgBr}(R_1) + V^{(2)}_{ArBr}(R_2) + V^{(2)}_{HgAr}(R_3) + V^{(3)}(R_1,R_2,R_3) \tag{9}$$

where $V^{(1)}$ is the sum of the energies of the separated atoms, the $V^{(2)}$'s are the two-body interactions of each pair of atoms, and $V^{(3)}$ is the three-body interaction.

$V^{(2)}$(HgBr) was computed using the internally contracted multireference averaged coupled pair functional (ACPF) method[29,30] with single and double excitations as implemented in the MOLPRO suite of ab initio programs.[31] MOLPRO was used for all calculations except where noted otherwise. The active orbitals in the ACPF calculations included all valence orbitals (Hg 5d6s and Br 4s4p) and also an extra orbital of $A_1$, $B_1$, and $B_2$ symmetry in the $C_{2v}$ point group that correlate with the Hg 6p electrons at infinite separation. Restrictions were set

such that no more than two electrons were allowed in the Hg 6p orbitals in the reference configurations. The orbitals used in the ACPF calculations were taken from complete active space self-consistent field (CASSCF)[32,33] calculations in which no restrictions were placed on the Hg 6p electrons. The basis sets aVTZ-aV5Z were used in these calculations for 29 bond lengths between 3.98 and 50 $a_0$. The total energies were then extrapolated with two formulas to obtain an estimate of the complete basis set (CBS) limit energies:

$$E(n) = E_{\mathrm{CBS}} + Be^{-(n-1)} + Ce^{-(n-1)^2} \tag{10}$$

$$E(n) = E_{\mathrm{CBS}} + B/n^3. \tag{11}$$

All three basis sets were used with extrapolation formula (10)[34,35] and only aVQZ and aV5Z were used with formula (11).[36,37] The best estimate of the CBS limit was taken as the average of the two extrapolation procedures. Coupled cluster calculations with single and double excitations and a perturbative estimate of triple excitations [CCSD(T)][38-40] were also carried out with the three basis sets and extrapolated to the CBS limit for the 13 bond lengths between 3.98 and 5.28 bohr. Restricted open-shell Hatree-Fock orbitals were used in the CCSD(T) calculations, but the spin-restrictions were relaxed in the solution of the coupled cluster equations [R/UCCSD(T)].[40-42]

A core-valence correction was also calculated for $V^{(2)}$(HgBr) with the ACPF method. In these calculations the aug-cc-pwCVTZ-PP[25,26,43] basis sets (henceforth denoted aCVTZ) were used. The core-valence correction was defined as the difference in energy between calculations in which only the valence electrons were correlated and calculations in which the core Hg 5s5p and Br 3s3p3d electrons were also correlated. The same correction was computed using the CCSD(T) method. This first core-valence correction will be denoted $\Delta E_{CV}$ for both methods.

Correlation of the Hg 4f electrons is also important, but they are replaced by the pseudopotential. Therefore all-electron calculations were carried out with the second-order Douglas-Kroll-Hess Hamiltonian (DK2). The all-electron basis sets were of augmented triple-zeta quality and corresponded to newly developed basis sets where the exponents and contraction coefficients were optimized using the DK2 Hamiltonian and are denoted aug-cc-pwCVTZ-DK. These will be referred to in this paper as aCVTZ-DK.[16,25,26] Three all-electron CCSD(T) calculations were performed with these basis sets. In the first calculation only the valence electrons were correlated, in the second calculation the valence electrons together with the Hg *5s5p* and Br *3s3p3d* electrons were correlated (where the 5*s* orbital of Hg and *3s* orbital of Br were rotated if needed above the 4*f* orbitals), and in the third the Hg *4f* electrons were also included in the correlation treatment. The contribution of the Hg *4f* electrons to the core-valence energy, $\Delta E_{CV\text{-}f}$, was calculated as the difference between the energies of the second and third calculations.

The ACPF/CBS+$\Delta E_{CV}$ two-body interaction was then scaled to match the CCSD(T)/CBS+$\Delta E_{CV}$+$\Delta E_{CV\text{-}f}$ two-body interaction potential in an approach similar to the scaling of the external correlation energy procedure of Truhlar and co-workers.[44] The scaling factor was computed as:

$$f = \frac{E_{CCSD(T)} - E_{ACPF}}{E_{ACPF} - E_{CAS}} \tag{12}$$

where $E_{CCSD(T)}$ is the energy at the CCSD(T)/CBS+$\Delta E_{CV}$+$\Delta E_{CV\text{-}f}$ level of theory $E_{ACPF}$ is the energy at the ACPF/CBS+$\Delta E_{CV}$ level of theory and $E_{CAS}$ is the CASSCF/CBS energy. The scaled energies were then calculated by the formula

$$E_{scaled} = f(E_{ACPF} - E_{CAS}) + E_{ACPF} \tag{13}$$

at each point between 3.98 and 5.28 $a_0$. At these points $E_{scaled}$ is exactly equal to the CCSD(T)/CBS+$\Delta E_{CV}$+$\Delta E_{CV\text{-}f}$ interaction energy. At points longer than 5.28 $a_0$ the scale factor is held fixed to the value it has at 5.28 $a_0$.

$V^{(2)}$(HgAr) and $V^{(2)}$(ArBr) were computed with the CCSD(T) [R/UCCSD(T) for ArBr] method and employed aVTZ through aV5Z basis sets with an extra set of diffuse functions. These are generally denoted d-aug-cc-pVnZ (d-aug-cc-pV(n+d)Z for Ar) and will be referred to as daVnZ throughout this paper. The total energies were also extrapolated to the CBS limit using formulas (10) and (11). A core-valence correction was computed as above at the CCSD(T)/aCVTZ level of theory for ArBr and HgAr, but no correction for 4f-correlation was calculated for HgAr. The standard counterpoise correction[45] was used to approximately remove the basis set superposition error (BSSE) in both the valence only and core-valence calculations on ArBr and HgAr.

To all three two-body potentials a spin-orbit correction was also added. The one-electron spin-orbit operators used were those accompanying the pseudopotentials for Hg and Br described above. A pseudopotential was also used on Ar for these calculations[46] and was again of the Stuttgart/Köln variety and it replaced the $1s^2 2s^2 2p^6$ electrons. The basis sets used were the aVTZ sets described above, but for Ar the set was recontracted in the presence of the pseudopotential. The spin-orbit calculations were carried out using the spin-orbit CI code[47] of Columbus.[48] The MRCISD method was used and employed standard full-valence active spaces with orbitals taken from CASSCF calculations employing the same active spaces. The spin-orbit correction, $\Delta E_{SO}$, was determined as the difference between calculations in which doublets and quartets (or singlets and triplets in HgAr) were allowed to mix via the spin-orbit operator and

standard MRCISD calculations. Both sets of calculations employed identical orbitals and active spaces.

One last correction was added to $V^{(2)}$(HgBr) and this was to account for the Lamb shift, which is the leading quantum electrodynamic effect not included in the parameterization of the pseudopotentials. To estimate the effect of the Lamb shift the procedure involving local model potentials of Pyykkö and Zhao was followed.[49] The leading Lamb shift contributions come from the self-energy and the vacuum polarization terms. The self-energy potential on each atom was simulated by a single Gaussian function whose coefficients were taken from Pyykkö and Zhao[49] The vacuum polarization potential was included by fitting a series of five Gaussian functions to the parameterized representation of the vacuum polarization potential given by Pyykkö and Zhao. The fitted function used for the vacuum polarization contribution was:

$$\mu = \frac{-Z}{r} \sum_i A_i e^{B_i r^2} \tag{14}$$

with coefficients $A_i$ = 3.920306e-03, 2.456215e-03, 3.415589e-03, 1.313118e-03, 6.338558e-04 and exponents $B_i$ = 4.202192e+10, 8.039480e+06, 4.197194e+08, 4.960986e+05, 6.360238e+04, for $i$=1–5, respectively. The Lamb shift correction was then determined from two all-electron ACPF/aVTZ calculations using the DK2 Hamiltonian. In the first calculation the local potentials were included when calculating the 1-electron integrals while in the second calculation they were not and the Lamb Shift correction, $\Delta E_{Lamb}$, was taken as the difference between these two calculations.

Finally, the three-body interaction was calculated at the CCSD(T)/aVTZ level of theory. The three-body interaction was calculated at 600 points on the HgBr-Ar potential energy surface with r(HgBr) ranging from 4.4-5.8 $a_0$, R(Hg-X)=5.0-15.0 $a_0$, and $\alpha$=0-180º (see Figure 1). The

counterpoise correction was again used to account for BSSE in the calculation of the 3-body interaction.

## IIB. CONSTRUCTION OF THE POTENTIAL ENERGY SURFACE

Each of the two-body interactions have been fit with the modified Lennard-Jones potential of Leroy and co-workers[50] which has the form:

$$V(R) = D_e\left[1-\left(\frac{R_e}{R}\right)^n e^{-\beta^S_{MLJ}(z)z}\right]^2 \tag{15}$$

where

$$\beta^S_{MLJ}(z) = f_S(R)\left[\sum_{m=0}\beta_m z^m - \beta_\infty\right] + \beta_\infty, \tag{16}$$

$$z = \frac{(R-R_e)}{(R+R_e)}, \tag{17}$$

$$\beta_\infty = \ln\left[2D_e(R_e)^n / C_n\right] \tag{18}$$

where $C_n$ is the London dispersion constant and $f_S$ is a switching function of the form

$$f_S(R) = 1/\left[e^{\alpha_S(R-R_S)}+1\right] \tag{19}$$

and $\alpha_S$ is a damping strength parameter and $R_S$ is the distance where the damping is half-complete. The three-body potential was interpolated using the reproducing kernel Hilbert space (RKHS) method:[51]

$$V^{(3)}(r,R,S) = \sum_{i,j,k}^{n_1,n_2,n_3} C_{ijk}q_1(r,r^i)q_1(R,R^j)q_2(S,S^k) \tag{20}$$

The coordinates used for the three-body potential were the pseudo-Jacobi coordinates shown in Figure 1 where $R$ is the distance between Ar and the midpoint of the Hg-Br bond as opposed to

its center of mass, as is the case in traditional Jacobi coordinates. For the two bond-length coordinates a distance-like kernel was used:[51]

$$q_1(x,x') = \frac{1}{14} x_>^{-7} \left(1 - \frac{7}{9}\frac{x_<}{x_>}\right) \tag{21}$$

and the angle coordinate α was first converted into the fitting coordinate

$$S = \frac{1}{2}(1 + \cos\alpha) \tag{22}$$

and then $S$ was fit using the angle-like kernel:[51]

$$q_2(x,x') = 1 + x_< x_> + 2x_<^2 x_> \left(1 - \frac{1}{3}\frac{x_<}{x_>}\right) \tag{23}$$

where $x_<$ = Min($x$, $x'$) and $x_>$ = Max($x$, $x'$). The fast algorithm for the evaluation of the RKHS surface via pre-summations[52] was employed and increased the speed of the trajectories by a factor of 10 or more depending on the collision energy. The subroutines that compute the potential energy surface and its analytical gradients were interfaced with the VENUS96 code[53] using the POTLIB2001 utility.[22]

## IIC. DETAILS OF THE QUASICLASSICAL TRAJECTORY CALCULATIONS

Reaction cross sections for the collision-induced dissociation (CID) of HgBr by collisions with Ar atom were calculated by the quasiclassical trajectory method[54] using the program VENUS96.[53] A substantial sampling of initial conditions has been investigated. The ro-vibrational levels of the HgBr potential curve computed at the scaled-ACPF/CBS+$\Delta E_{CV}$+$\Delta E_{CV\text{-}f}$+$\Delta E_{SO}$+$\Delta E_{Lamb}$ level were determined numerically using the program LEVEL.[55] At this level of theory the HgBr molecule has 68 bound vibrational levels with $j$=0 and the largest value of $j$ for which there is a bound vibrational level is $j$=564. Due to the very

low probability of a reactive collision event occurring at 298 K the initial conditions could not be sampled using a Boltzmann distribution. Trajectories were instead run for a large number of specified initial conditions. All values of $v$ from $v$=0 to the highest bound level for a given rotational quantum number were sampled in increments of 2. Trajectories were run for every 10 values of $j$ between 0-150, every 25 between $j$=150-350 and every 50 between $j$=350-550. In addition, 12 relative collision energies ($E_c$) were sampled between 0-2 kcal/mol and 15 energies between 2-10 kcal/mol. At 298 K the most probable values of $j$ and $E_c$ are 47 and 0.59 kcal/mol respectively. Of course, sets of initial conditions that did not have sufficient internal plus collisional energy to allow for dissociation were not explicitly calculated, but the cross sections were simply set to zero. By default VENUS calculates the ro-vibrational energy levels and turning points for given values of $v$ and $j$ using WKB theory, but in the present calculations the energy levels and turning points were calculated by solving the nuclear Schrödinger equation numerically with LEVEL and then inputing these values directly into VENUS. 10,000 trajectories were run for each set of initial conditions with $j$<250, and 2000 trajectories were run for initial conditions with higher $j$ values. In total over 80,000,000 trajectories were integrated.

For the majority of trajectory runs a maximum impact parameter of $b_{max}$ = 10.0 Å was used. The largest impact parameter giving rise to a reactive event was monitored for each set of trajectories and $b_{max}$ was increased to 13.0 Å for initial conditions when impact parameters yielding reactive events approached 10.0 Å. This was typically necessary for the highest bound vibrational levels when the quantum number $j$ was less than 80. A numerical integration step size of 0.2 fs was chosen and in trial calculations smaller step sizes were found to not change cross sections when a number of sets of initial conditions were tested. A number of criteria were set for determining reactive and unreactive events. Trajectories were determined to be reactive if

$r$(HgBr) exceeded 10.0 Å (the largest outer classical turning point for the ro-vibrational states considered was less than 8 Å). The first test introduced to count trajectories as unreactive was if Ar was 30 Å away from either Hg or Br and the gradient of the HgBr stretch was negative. The second possible criterion for an unreactive event was achieved if the Ar atom was greater than 300 Å from Hg or Br and $r$(Hg-Br) had not exceeded 10.0 Å. The values for these parameters were determined from extensive trial calculations with $j$=50, $v$=50-58 ($v$=58 is the maximum allowed value of $v$ when $j$=50) and various values of $E_c$.

Cross sections for each set of initial conditions was calculated as:

$$\sigma_r^{v,j}(E_c) = \pi b_{\max}^2 \frac{N_r}{N} \tag{24}$$

where $N_r$ is the number of reactive events and $N$ is the total number of trajectories. Thermally averaged cross sections were then calculated for each collision energy by summing over $\sigma_r^{v,j}$ for all ro-vibrational states and a given $E_c$ with the cross sections weighted by the probability they are occupied in a Maxwell-Boltzmann distribution:

$$\sigma_r(E_c;T) = \sum_j \sum_v \frac{\sigma_r^{v,j}(E_c)[(2j+1)e^{-(E_{vj}-E_{00})/k_BT}]}{Q} \tag{25}$$

where $E_{vj}$ is the ro-vibrational energy level, $E_{00}$ is the energy of the level with $v$=0 and $j$=0, and $Q$ is the ro-vibrational partition function:

$$Q = \sum_j \sum_v (2j+1)e^{-(E_{vj}-E_{00})/k_BT} \tag{26}$$

As was discussed above, cross sections were only computed for selected values of $v$ and $j$ so the values of cross sections not explicitly calculated were determined using 2-dimensional linear interpolation of the existing cross sections at each collision energy. The function $\sigma_r(E_c;T)$ was

then fit with cubic splines as a function of $E_c$. Finally, the rate constant for collision induced dissociation

$$\text{HgBr} + \text{Ar} \rightarrow \text{Hg} + \text{Br} + \text{Ar} \tag{27}$$

was calculated using:

$$k(T) = \left(\frac{8k_B T}{\pi\mu}\right)^{1/2} \left(k_B T\right)^{-2} \int_0^\infty \sigma_r(E_c;T) E_c e^{-E_c/k_B T} dE_c \tag{28}$$

(note that μ in the above equation is for HgBr + Ar).

Assuming the principles of detailed balance and microscopic reversibility, the 3rd order rate constant, $k_{3rd}$, for the recombination reaction:

$$\text{Hg} + \text{Br} + \text{Ar} \rightarrow \text{HgBr} + \text{Ar} \tag{29}$$

can be calculated with:

$$k_{3rd} = \frac{k_{CID}}{c^0 K_c} \tag{30}$$

where $c^0$ is the standard concentration and $K_c$ is the equilibrium constant for reaction (27) and can of course be determined from $\Delta G_r$. The experimental dissociation energy of HgBr (15.5±0.3 kcal/mol) was used with standard ideal gas forms of the partition functions to calculate $\Delta G_r$ at temperatures above 0 K. An effective second order rate constant, $k_{2nd}$, for the reaction

$$\text{Hg} + \text{Br} \rightarrow \text{HgBr} \tag{31}$$

can be determined for a given pressure of argon and temperature simply by multiplying $k_{3rd}$ by the concentration of argon at that $T$ and $P$.

## III. RESULTS AND DISCUSSION

The calculated spectroscopic constants for the ground state of HgBr and their constituent energy contributions are given in Table 1 along with the experimentally determined values. The experimental and calculated harmonic frequencies are in excellent agreement with the calculated value being only 5.5 $cm^{-1}$ larger than experiment. The calculated $D_e$ is 0.5 kcal/mol larger than the corresponding experimental determination. The estimated uncertainty in the theoretical value is ±1.0 kcal/mol, and much of this uncertainty arises from relativistic effects. The zero-field splitting in Br atom is underestimated by 0.3 kcal/mol in the current spin-orbit procedure and this is likely the upper limit of the error in the spin-orbit correction to $D_e$. Further, there have been few attempts to calculate the thermochemistry of elements as heavy as mercury to chemical accuracy (±1 kcal/mol) and the magnitude of various terms in the Dirac-Coulomb-Breit Hamiltonian as well as the leading relativistic QED contributions require further characterization. There is also likely a small amount of error associated with the use of the pseudopotentials. In a recent study[12] the dissociation energy of HgBr was found to differ by 0.1 kcal/mol when computed with the present pseudopotentials and with the all-electron 3rd order Douglas-Kroll-Hess (DK3) Hamiltonian. Unfortunately it is difficult to correct for the pseudopotential error simply by comparing these two approaches because the DK3 Hamiltonian does not include the Breit interaction, which is included in the parameterization of the pseudopotentials. Also, previous calculations indicate higher order correlation effects will increase the dissociation energy by +0.25 kcal/mol.[12] There does not appear to be a previous experimental report of the bond length of HgBr. A number of recent papers have cited an experimental bond length, but this value can be traced back to the original calculation on HgBr by Wadt.[56]

Since those first calculations there have been a number of theoretical investigations[57,58] of HgBr including recent calculations by the current group[12,16] and others.[20,21,59] Tossel[59] optimized the geometry with the CCD method and then refined the energetics with the CCSD(T) method while employing double-zeta quality basis sets. Khalizov et al.[20] optimized the geometry using the QCISD method and then carried out single-point calculations with the CCSD(T) method using a number of different basis sets. The best theoretical estimate of $D_e$ (16.30 kcal/mol) was reported previously,[12] and differs from the current value in that it also included corrections based on CCSDT and CCSDTQ calculations. However, the $r_e$ and $\omega_e$ values presented in Table 1 are the most accurate calculated to date. They improve upon the previous results[12] by including the effects of 4f-electron correlation and the Lamb shift (these corrections were previously only computed a single points). The value of $r_e$ in Table 1 should be considered the most reliable value currently available.

The calculated and experimental spectroscopic constants are provided for HgAr and ArBr in Tables 2 and 3, respectively. The effects of extrapolation to the basis set limit, core-valence correlation and spin-orbit coupling only slightly modify the spectroscopic constants for HgAr. The opposite is true for the ArBr molecule where the spin-orbit effect is relatively large. In this case the correction from extrapolation to the CBS limit and core-valence correlation together increase the dissociation energy by a modest 17 $cm^{-1}$. Spin-orbit coupling on the other hand decreases the dissociation energy by -52 $cm^{-1}$, which is a relative decrease of 25%. Overall the agreement between theory and experiment for these two weakly bound complexes is quite good.

The two-body potentials just discussed for HgBr, HgAr and ArBr are shown in Figures 2-4. The full potential energy surface, $V(r,R,\alpha)$ is depicted in Figures 5-7. Figure 5 is a contour plot in which the Hg-Br bond length is fixed at its equilibrium value of 2.494 Å while in Figure 6

the HgBr bond length has been fixed at 3.440 Å. Figure 7 is a surface plot in which the angle α has been fixed at 75°. The interaction between Ar and HgBr is fairly anisotropic and this anisotropy increases significantly as the HgBr is stretched, as is evident by examining Figures 5 and 6. There is a relatively shallow van der Waals minimum of 0.61 kcal/mol (210 $cm^{-1}$) in the HgBr-Ar potential and it has a minimum at α=79.6°, which places Ar only slightly closer to the Hg atom than the Br atom. This minimum occurs at an *R* value of 4.00 Å, and this is the distance between Ar and the center of the HgBr bond. This binding energy is slightly larger than the binding energy in both the HgAr and ArBr diatomic molecules. Even as the HgBr bond is stretched, the HgBr-Ar interaction energy remains close to 0.6 kcal/mol.

Cross sections for collision-induced dissociation of HgBr by Ar at 298 K are shown in Figures 9 and 10. In Figure 9 the *j* dependence of

$$\sigma_r^{v,j}(E_c)[(2j+1)e^{-(E_{vj}-E_{00})/k_BT} \tag{32}$$

is plotted for a number of collision energies with *v* fixed at a value of 36. Similarly, this weighted cross-section is plotted as a function of *v* for a number of collision energies with *j* fixed at 100 in Figure 10. The integrand in Eq. (28) resembles a Boltzmann distribution with a sharp peak at 0.71 kcal/mol and then drops off exponentially as $E_c$ increases, and this is shown in Figure 8. In fact, no change is observed in the rate constant if Eq. (28) is integrated past 7.5 kcal/mol, and 90% of the rate constant can be recovered if it is only integrated to 3.0 kcal/mol. It is therefore the lower energy collisions and thus necessarily the higher energy vibrational-rotational levels that are the largest contributors to the collision-induced dissociation even at 298 K. It is clear in Figures 9 and 10 that for the lowest collision energies the cross sections increase monatomically with *v* and *j* making the energy levels closest to the dissociation limit the most important. However, at the higher collision energies of relevance to 298 K (3 and 5 kcal/mol)

there is actually a peak in these cross sections and the intermediate $v$ and $j$ states become relatively more important for these collision energies.

Table 4 lists the rate constants calculated in this work by the QCT method for the collision-induced dissociation of HgBr, as well as the 3rd and effective 2nd order rate constants for the recombination of Hg and Br atoms. To determine the temperature dependence, the rate constants were computed at 12 temperatures between 200 and 400 K. The temperature dependent rate constants in Table 4 were then determined by fitting this data to an Arrhenius expression. As one would expect, the rate constant for collision-induced dissociation increases with temperature while the recombination rates show an inverse relationship. The error in the rate constants for collision-induced dissociation due to statistical error in the cross sections can be estimated from

$$\Delta\sigma^{vj} = \sigma^{vj}\left[\frac{N - N_r}{NN_r}\right]^{1/2} \tag{33}$$

and was found to give an uncertainty in $k(T)$ for collision-induced dissociation on the order of 3%. Of course, this is just the statistical error in the trajectories and does not account for the intrinsic errors in the QCT approach and any inaccuracies in the ab initio potentials. The largest source of uncertainty for the calculated rate constants for the recombination processes is a result of the uncertainty in the experimental $D_0$ of HgBr that is ±0.3 kcal/mol. This leads to an uncertainty of a factor of 1.6 for the equilibrium constant and therefore also the rates of recombination at 298 K.

The calculated 2nd order effective rate constants for recombination of HgBr at 298 K and 1 bar pressure are compared against the previous experimental and theoretical determinations in Table 5. The QCT value of $k(298) = 9.8 \times 10^{-13}$ cm$^3$ molecule$^{-1}$ s$^{-1}$ is lower than all three of the

values that were reported previously, being a factor of 3.3 slower than the experimental measurement,[19] a factor of 2 slower than the VTST estimate[20] and just slightly smaller than the value calculated with RRKM theory.[21] The range of $k(T)$ calculated in the current work resulting from the uncertainty in $D_0$ would be $1.7 \times 10^{-12} - 0.6 \times 10^{-12}$ $cm^3$ $molecule^{-1}$ $s^{-1}$ and even the maximum in this range is slower than the VTST estimate and is still a factor of 1.9 slower than experiment. In the same work that produced the experimental estimate for the rate constant of Hg + Br recombination, the rate of Hg + Cl recombination was also investigated. The rate constant for this process was reported to be $1.0 \times 10^{-11}$ $cm^3$ $molecule^{-1}$ $s^{-1}$.[19] More recently a rate constant (298 K and 1 atm) was reported for Hg + Cl recombination of $5.3 \times 10^{-13}$ $cm^3$ $molecule^{-1}$ $s^{-1}$ . This was determined in pulsed laser photolysis-pulsed laser induced fluorescence studies by Donohoue et al.[60] This might suggest the CVAAS/GC-MS rate constants of Ariya et al.[19] for Hg + Cl and Hg + Br recombination are somewhat overestimated. However, if the Hg + Cl recombination rate of Donohoue[60] is accurate to the ±50% they suggest then this also suggests that the present QCT calculations also overestimate $k(T)$. The work of Ariya et al. indicates Hg+Cl recombination is faster than Hg+Br recombination, but the recombination rate constant for Hg+Cl of Donahoue is smaller than the QCT rate constant for Hg+Br recombination. The comparison of the QCT rate constants with experiment is made complicated by the fact that the collision partner in the current calculations is Ar while the experiments were carried out in nitrogen.

The VTST result likely overestimates the rate constant. VTST results are valid only in the high-pressure limit and are generally not applicable to atom-atom recombination because there are no additional vibrational modes by which the excess energy can be equilibrated. To account for this in their calculations, the pressure dependence was introduced with a simple

collision model, but the rate constant may still be too large since the model assumed all collisions of excited HgBr with the bath gas resulted in the formation of stable HgBr. It is somewhat unclear how reliable the RRKM rate constant is despite its relative good agreement with the QCT, VTST and experimental rate constants. These RRKM calculations relied upon bond lengths, vibrational frequencies and dissociation energies calculated with the B3LYP method and double-zeta basis sets. The bond length used was 0.2 Å smaller than the current accurate ab initio calculations, and the harmonic frequency was 40 $cm^{-1}$ (20%) smaller than the experimental value and this could lead to an inaccurate density of states in the RRKM calculations.

## IV. CONCLUSIONS

An accurate global potential energy surface has been constructed for the reaction HgBr + Ar → Hg + Br + Ar. The potential energy has been decomposed using the standard many-body decomposition. In all calculations on Hg and Br relativistic pseudopotentials were used to account for scalar relativistic effects. Two-body potentials for HgAr and ArBr were computed with the CCSD(T) method, extrapolated to the complete basis set limit and corrections were added for core-valence correlation and spin-orbit coupling. The two-body potential for HgBr was computed with ACPF wavefunctions, extrapolated to the CBS limit, and corrections were added for core-valence correlation. The ACPF surface was scaled to match a CCSD(T)/CBS+CV potential energy curve in the near-equilibrium region and was then corrected for spin-orbit coupling and Lamb shift effects. The three body-potential was calculated at the CCSD(T)/aVTZ level of theory.

Quasiclassical trajectories were carried out on this surface to determine the rate constant for collision-induced dissociation of HgBr by Ar atoms. All relevant initial vibrational-rotational

energy levels were considered up to the dissociation limit for collision energies up to 10 kcal/mol. The principle of detailed balance was then used to determine the 3rd order recombination rate constant for Hg + Br + Ar → HgBr + Ar and the effective second order rate constant for Hg + Br → HgBr.

The recombination of Hg and Br atoms has been implicated in mercury depletions events in the polar troposphere during polar sunrise. During these depletion events the concentration of Hg in the lower troposphere can drop from its background levels of 1.7 ng $m^{-3}$ to as low as 0.1 ng $m^{-3}$ in a few hours. It is likely that the initiation of these mercury depletion events is the oxidation of Hg by Br radicals to form HgBr. This HgBr then likely undergoes further reactions to form divalent mercury, which is deposited on the snow pack.

The currently reported rate constants for HgBr collision-induced dissociation and recombination are somewhat smaller than previous experimental and theoretical determinations. The effective second order rate constant for Hg + Br recombination at representative Arctic conditions (260 K and 1 bar pressure) was calculated to be $k(260) = 1.20 \times 10^{-12}$ $cm^3$ $molecule^{-1}$ $s^{-1}$. The concentration of bromine radicals during mercury depletion events has been estimated to be between $10^7$-$10^8$ molecules $cm^{-3}$. If the bromine concentration is considered fixed at these values then an effective half-life for Hg is calculated to be 1.6-16 hours. Despite the slower rate constant calculated here for HgBr recombination, it is still fast enough for the oxidation of Hg by Br radicals to play a significant role in the mercury depletion events.

## V. ACKNOWLEDGEMENTS

The authors gratefully acknowledge Dr. B. Ramachandran (Louisiana Tech University) and Dr. B.C. Garrett (Pacific Northwest National Laboratory-Environmental Molecular Sciences Laboratory) for many helpful discussions concerning the trajectory calculations. The authors would also like to thank Dr. R. Duchovic (Indiana University-Purdue University Ft. Wayne) for his help with POTLIB and VENUS96.

## REFERENCES

(1) Schroeder, W. H.; Munthe, J. *Atmospheric Environment* **1998**, *32*, 809.

(2) Ariya, P. A.; Dastoor, A. P.; Amyot, M.; Schroeder, W. H.; Barrie, L.; Anlauf, K.; Raofie, F.; Ryzhkov, A.; Davignon, D.; Lalonde, J.; Steffen, A. *Tellus* **2004**, *56B*, 397.

(3) Lindberg, S. E.; Brooks, S.; Lin, C.-J.; Scott, K. J.; Landis, M. S.; Stevens, R. K.; Goodsite, M.; Richter, A. *Environmental Science and Technology* **2002**, *36*, 1245.

(4) Schroeder, W. H.; Anlauf, K. G.; Barrie, L. A.; Lu, J. Y.; Steffen, A.; Schneeberger, D. R.; Berg, T. *Nature* **1998**, *394*, 331.

(5) Barrie, L. A.; Bottenheim, J. W.; Schnell, R. C.; Crutzen, P. J.; Rasmussen, R. A. *Nature* **1988**, *334*, 138.

(6) Bottenheim, J. W.; Gallant, A. G.; Brice, K. A. *Geophysical Research Letters* **1986**, *13*, 113.

(7) Foster, K. L.; Plastridge, R. A.; Bottenheim, J. W.; Shepson, P. B.; Finlayson-Pitts, B. J.; Spicer, C. W. *Science* **2001**, *291*, 471.

(8) Spicer, C. W.; Plastridge, R. A.; Foster, K. L.; Finlayson-Pitts, B. J.; Bottenheim, J. W.; Grannas, A. M.; Shepson, P. B. *Atmospheric Environment* **2002**, *36*, 2721.

(9) Lu, J. Y.; Schroeder, W. H.; Barrie, L. A.; Steffen, A.; Welch, H. E.; Martin, K.; Lockhart, L.; Hunt, R. V.; Boila, G.; Richter, A. *Geophysical Research Letters* **2001**, *28*, 3219.

(10) Kim, H.; Dooley, K. S.; Johnson, E. R.; North, S. W. *Journal of Chemical Physics* **2006**, *124*, 134304.

(11) Tellinghuisen, J.; Ashmore, J. G. *Chemical Physics Letters* **1983**, *102*, 10.

(12) Shepler, B. C.; Balabanov, N. B.; Peterson, K. A. *Journal of Physical Chemistry A* **2005**, *109*, 10363.

(13) Shepler, B. C.; Peterson, K. A. *Journal of Physical Chemistry A* **2003**, *107*, 1783.

(14) Balabanov, N. B.; Peterson, K. A. *Journal of Chemical Physics* **2004**, *120*, 6585.

(15) Balabanov, N. B.; Shepler, B. C.; Peterson, K. A. *Journal of Physical Chemistry A* **2005**, *109*, 8765.

(16) Balabanov, N. B.; Peterson, K. A. *J. Phys. Chem. A* **2003**, *107*, 7465.

(17) Chase, M. W., Jr; Davies, C. A.; Downey, J. R., Jr; Frurip, D. J.; McDonald, R. A.; Syverud, A. N. *Journal of Physical and Chemical Reference Data* **1985**, *14*.

(18) Shepler, B. C.; Balabanov, N. B.; Peterson, K. A. *In Preparation*.

(19) Ariya, P. A.; Khalizov, A. F.; Gidas, A. *Journal of Physical Chemistry A* **2002**, *106*, 7310.

(20) Khalizov, A. F.; Viswanathan, B.; Larregaray, P.; Ariya, P. A. *Journal of Physical Chemistry A* **2003**, *107*, 6360.

(21) Goodsite, M. E.; Plane, J. M. C.; Skov, H. *Environmental Science and Technology* **2004**, *38*, 1772.

(22) Duchovic, R. J.; Volobuev, Y. L.; Lynch, G. C.; Truhlar, D. G.; Allison, T. C.; Wagner, A. F.; Carret, B. C.; Corchado, J. C. *Computer Physics Communications* **2002**, *144*, 169.

(23) Figgen, D.; Rauhut, G.; Dolg, M.; Stoll, H. *Chemical Physics* **2004**, *311*, 227.

(24) Peterson, K. A.; Figgen, D.; Goll, E.; Stoll, H.; Dolg, M. *Journal of Chemical Physics* **2003**, *119*, 11113.

(25) Peterson, K. A.; Puzzarini, C. *Theoretical Chemistry Accounts* **2005**, accepted.

(26) Peterson, K. A.; Puzzarini, C. *Theoretical Chemistry Accounts* **2005**, *114*, 283.

(27) Dunning, T. H. J.; Peterson, K. A.; Wilson, A. K. *Journal of Chemical Physics* **2001**, *114*, 9244.

(28) Murrell, J. N.; Carter, S. *Journal of Chemical Physics* **1984**, *88*, 4887.

(29) Gdanitz, R. J.; Ahlrichs, R. *Chemical Physics Letters* **1988**, *143*, 413.

(30) Werner, H.-J.; Knowles, P. J. *Theoretica Chimica Acta* **1990**, *78*, 175.

(31) Werner, H.-J. MOLPRO is a package of ab initio programs written by H.-J. Werner and P.J. Knowles, version 2002.6, R.D. Amos, A. Bernhardsson, A. Berning, P. Celani, D.L. Cooper, M.J.O. Deegan, A.J. Dobbyn, F. Eckert, C. Hampel, G. Hetzer, P.J. Knowles, T. Korona, R. Lindh, A.W. Lloyd, S.J. McNicholas, F.R. Manby, W. Meyer, M.E. Mura, A.

Nicklass, P. Palmieri, R. Pitzer, G. Rauhut, M. Schütz, U. Schumann, H. Stoll, A.J. Stone, R. Tarroni, T. Thorsteinsson, and H.-J. Werner.

(32) Knowles, P. J.; Werner, H.-J. *Chemical Physics Letters* **1985**, *115*, 259.

(33) Werner, H.-J.; Knowles, P. J. *Journal of Chemical Physics* **1985**, *82*, 5053.

(34) Feller, D.; Peterson, K. A.; de Jong, W. A.; Dixon, D. A. *Journal of Chemical Physics* **2003**, *118*, 3510.

(35) Peterson, K. A.; Woon, D. E.; Dunning, T. H., Jr. *Journal of Chemical Physics* **1994**, *100*, 7410.

(36) Halkier, A.; Helgaker, T.; Jørgensen, P.; Klopper, W.; Koch, H.; Olsen, J.; Wilson, A. K. *Chemical Physics Letters* **1998**, *286*, 243.

(37) Helgaker, T.; Klopper, W.; Koch, H.; Noga, J. *Journal of Chemical Physics* **1997**, *106*, 9639.

(38) Purvis, G. D. I.; Bartlett, R. J. *Journal of Chemical Physics* **1982**, *76*, 1910.

(39) Raghavachari, K.; Trucks, G. W.; Pople, J. A.; Head-Gordon, M. *Chemical Physics Letters* **1989**, *156*, 479.

(40) Watts, J. D.; Gauss, J.; Bartlett, R. J. *Journal of Chemical Physics* **1993**, *98*, 8718.

(41) Knowles, P. J.; Hampel, C.; Werner, H.-J. *Journal of Chemical Physics* **1994**, *99*, 5219.

(42) Scuseria, G. E. *Chemical Physics Letters* **1991**, *176*, 27.

(43) The following exponents were added to the cc-pVTZ-PP basis set of Br to form a cc-pwCVTZ-PP set: 2s (7.0742, 2p (10.1642, 2.1057), 2d (4.1557, 1.8326), 2f (8.3131, 2.1829), and 1g (2.5365).

(44) Brown, F. B.; Truhlar, D. G. *Chemical Physics Letters* **1985**, *117*, 307.

(45) Boys, S. F.; Bernardi, F. *Molecular Physics* **1970**, *19*, 553.

(46) Nicklass, A.; Dolg, M.; Stoll, H.; Preuss, H. *Journal of Chemical Physics* **1995**, *102*, 8942.

(47) Yabushita, S.; Zhang, Z.; Pitzer, R. M. *Journal of Physical Chemistry A* **1999**, *103*, 5791.

(48) Blomberg, M. R. A.; Siegbahn, P. E. M. *Journal of Chemical Physics* **1983**, *78*, 5682.

(49) Pyykko, P.; Zhao, L.-B. *Journal of Physics B: Atomic, Molecular and Optical Physics* **2003**, *36*, 1469.

(50) Hajigeorgiou, P. G.; Le Roy, R. J. *Journal of Chemical Physics* **2000**, *112*, 3949.

(51) Ho, T.-S.; Rabitz, H. *Journal of Chemical Physics* **1996**, *104*, 2584.

(52) Hollebeek, T.; Ho, T.-S.; Rabitz, H. *Journal of Chemical Physics* **1997**, *106*, 7223.

(53) Hase, W. L.; Duchovic, R. J.; Hu, X.; Komornicki, A.; Lim, K. F.; Lu, D.-h.; Peslherbe, G. H.; Swamy, K. N.; Vande Linde, S. R.; Varandas, A.; Wang, H.; Wolf, R. J. *Quantum Chemistry Program Exchange* **1996**, *16*, 671.

(54) Truhlar, D. G.; Muckerman, J. T. Reactive Scattering Cross Sections III: Quasiclassical and Semiclassical Methods. In *Atom-Molecule Collision Theory*; Bernstein, R. B., Ed.; Plenum Press: New York, 1979; pp 505.

(55) Le Roy, R. J. R.J. Le Roy, LEVEL 7.1: A Computer Program for Solving the Radial Schrödinger Equation for Bound and Quasibound Levels, University of Waterloo Chemical Physics Research Report CP-642R (2000).

(56) Wadt, W. R. *Applied Physics Letters* **1979**, *34*, 658.

(57) Kaupp, M.; von Schnering, H. G. *Inorganic Chemistry* **1994**, *33*, 4179.

(58) Liao, M.-S.; Zhang, Q.; Schwartz, W. H. E. *Inorganic Chemistry* **1995**, *34*, 5597.

(59) Tossel, J. A. *Journal of Physical Chemistry A* **2003**, *107*, 7804.

(60) Donohoue, D. L.; Bauer, D.; Hynes, A. J. *Journal of Physical Chemistry A* **2005**, *109*, 7732.

(61) Fuke, K.; Saito, T.; Kaya, K. *Journal of Chemical Physics* **1984**, 2591.

(62) Koperski, J.; Atkinson, J. B.; Krause, L. *Chemical Physics* **1994**, *186*, 401.

(63) Ohshima, Y.; Iida, M.; Endo, Y. *Journal of Chemical Physics* **1990**, *92*, 3990.

(64) Zhao, Y.; Yourshaw, I.; Reiser, G.; Arnold, C.; Neumark, D. M. *Journal of Chemical Physics* **1994**, *101*, 6538.

Table 1: Calculated and experimental spectroscopic constants of the ground state of HgBr

| Method | $r_e$ (Å) | $\omega_e$ ($cm^{-1}$) | $\omega_e x_e$ ($cm^{-1}$) | $D_e$ (kcal/mol) |
|---|---|---|---|---|
| ACPF/aug-cc-pVQZ | 2.537 | 182.2 | 0.90 | 17.20 |
| ACPF/CBS | 2.529 | 185.0 | 0.86 | 18.16 |
| CCSD(T)/CBS | 2.523 | 186.8 | 0.96 | 18.60 |
| ΔCV | -0.011 | 1.7 | 0.03 | -0.20 |
| ΔCV (Hg *f*-electrons) | -0.003 | 0.2 | 0.00 | -0.19 |
| ΔSO | -0.015 | 4.1 | 0.00 | -2.25 |
| ΔLamb-shift | -0.001 | 0.9 | -0.01 | 0.34 |
| Best Calculated Result[a] | 2.494 | 193.8 | 0.98 | 16.04 |
| Experiment[b] | --- | 188.3 | 0.97 | 15.53±0.30 |

[a)] CCSD(T)/CBS+ΔCV+ΔCV-f+ΔSO+ΔLamb. [b)] Reference 11

Table 2: Spectroscopic constants for the ground state of HgAr

| Method | $r_e$ (Å) | $\omega_e$ (cm$^{-1}$) | $D_e$ (cm$^{-1}$) |
|---|---|---|---|
| CCSD(T)/aV5Z | 4.050 | 22.8 | 127 |
| ΔCBS | -0.013 | 0.2 | 3 |
| ΔCV | -0.018 | 0.3 | 4 |
| ΔSO | -0.001 | 0.0 | 0 |
| Best Calc. | 4.019 | 23.3 | 134 |
| Exp A[a] | 4.01 | 23.5 | 142 |
| Exp B[b] | 3.99 | 24.7 | 133.7 |
| Exp C[c] | 4.053[d] | 22.1 | --- |

[a)] Reference [61] . [b)] Reference [62]. [c)] Reference [63]. [d)] This is an $r_0$.

Table 3: Spectroscopic constants for the ground state of ArBr.

| Method | $r_e$ (Å) | $\omega_e$ (cm$^{-1}$) | $D_e$ (cm$^{-1}$) |
|---|---|---|---|
| CCSD(T)/aV5Z | 3.606 | 35.0 | 184 |
| ΔCBS | -0.024 | 1.2 | 11 |
| ΔCV | -0.018 | 0.6 | 6 |
| ΔSO | 0.186 | -5.6 | -52 |
| Best Calc. | 3.750 | 31.2 | 149 |
| Exp[a)] | 3.73±0.20 | - | 133±8 |

[a)] Reference [64]

Table 4: Calculated temperature dependent rate constants for collision induced dissociation and recombination.

| reaction | $k(T)$ | units |
|---|---|---|
| HgBr + Ar → Hg + Br + Ar | $1.95 \times 10^{-20} \exp[-7670\ (1/T-1/298)]$ | $cm^3\ molecules^{-1}\ s^{-1}$ |
| Hg+Br+Ar → HgBr + Ar | $4.07 \times 10^{-32} \exp[112\ (1/T-1/298)]$ | $cm^6\ molecules^{-2}\ s^{-1}$ |
| Hg+Br → HgBr | $9.80 \times 10^{-13} \exp[401\ (1/T-1/298)]$ | $cm^3\ molecules^{-1}\ s^{-1}$ |

Table 5: Comparison of rate constants of the 2nd order recombination of Hg and Br atoms at 298 K and 1 bar pressure ($cm^3\ molecules^{-1}\ s^{-1}$).

| method | $k(T)$ |
|---|---|
| QCT (present work) | $9.8 \times 10^{-13}$ |
| VTST | $2.0 \times 10^{-12}$ |
| RRKM | $1.1 \times 10^{-12}$ |
| CVAS GC-MS | $3.2 \times 10^{-12}$ |

Figure 1: Pseudo-Jacobi coordinates used to fit the three-body potential.

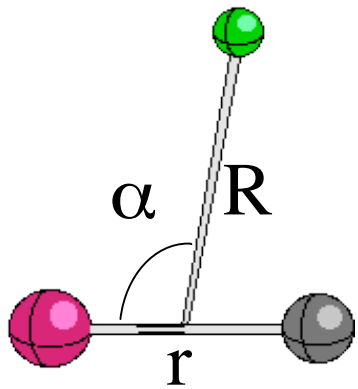


Figure 2: Ground state potential energy curve of HgBr and centrifugally distorted effective potential corresponding to J=200. Horizontal lines correspond to the v=25 level on each potential.

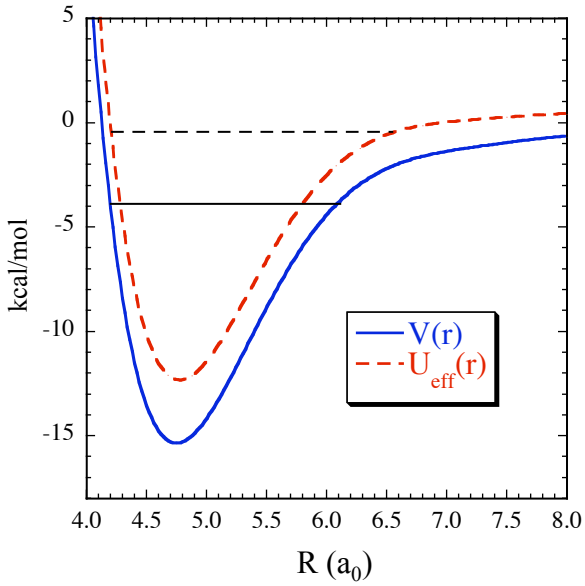

Figure 3: Ground state potential energy curve of HgAr with and without the corrections for spin-orbit coupling and core-valence correlation.

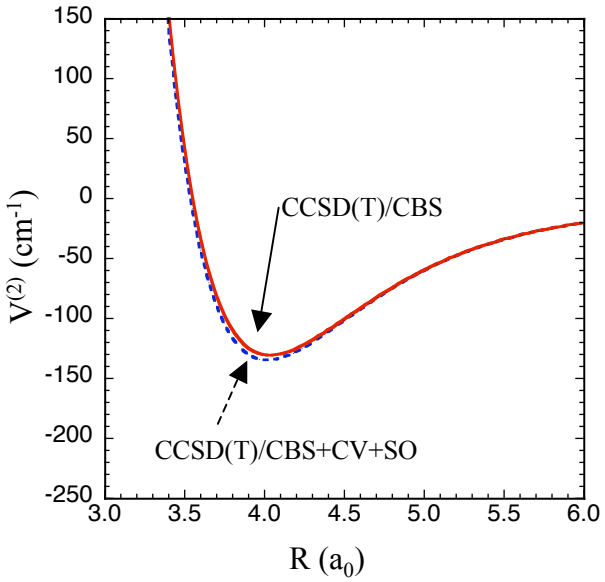


Figure 4: Ground state potential energy curve of ArBr with and without the corrections for spin-orbit coupling and core-valence correlation.

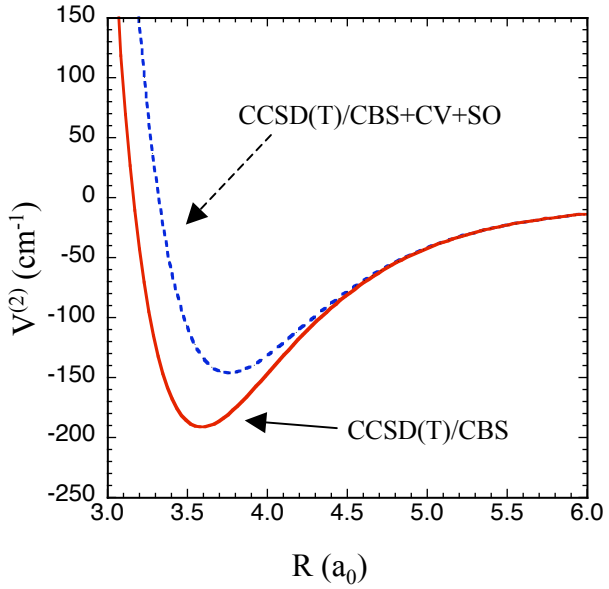

Figure 5: Contour plot of HgBr-Ar. r(HgBr)=2.494 Å

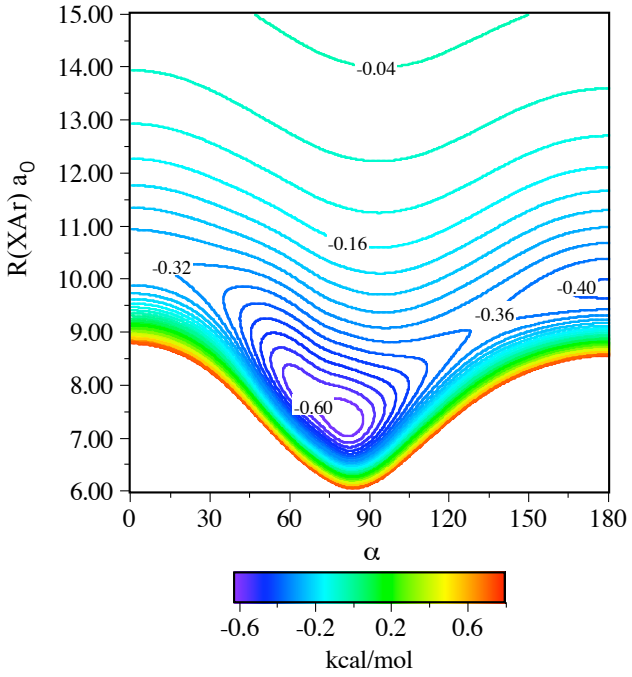


Figure 6: Contour plot of HgBr-Ar. r(HgBr)=3.440 Å

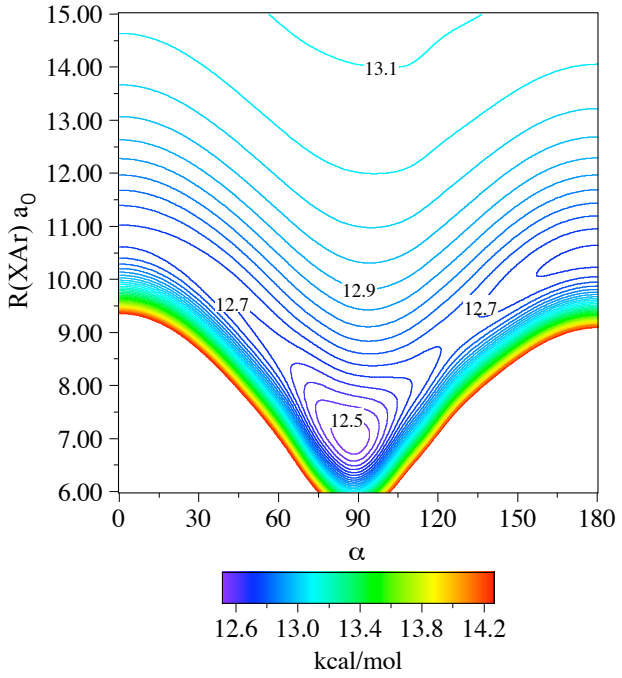

Figure 7: Surface plot of HgBr-Ar with α=75°

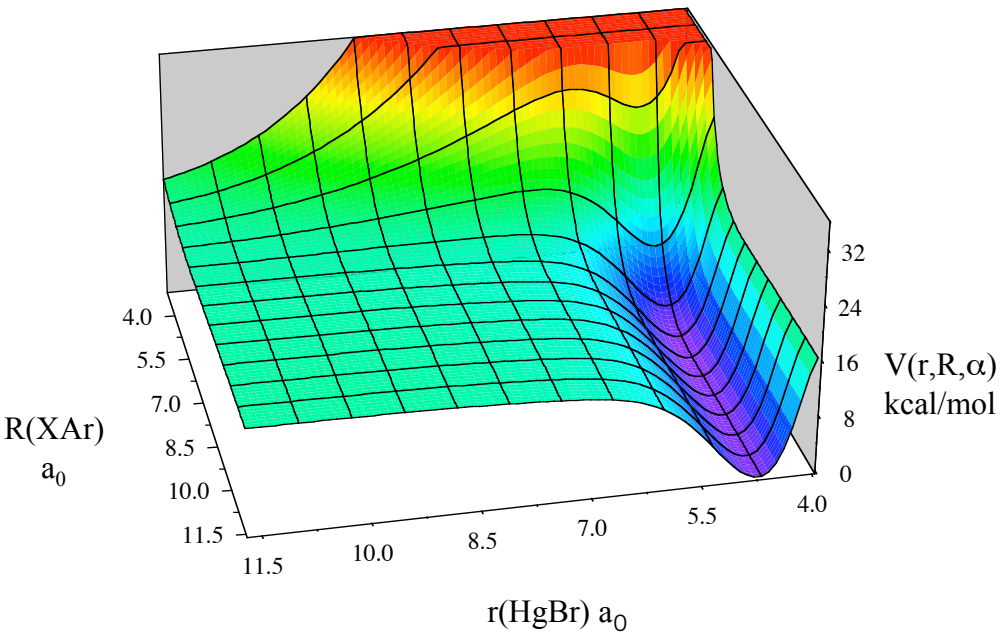


Figure 8: Thermally averaged cross section as a function of collision energy

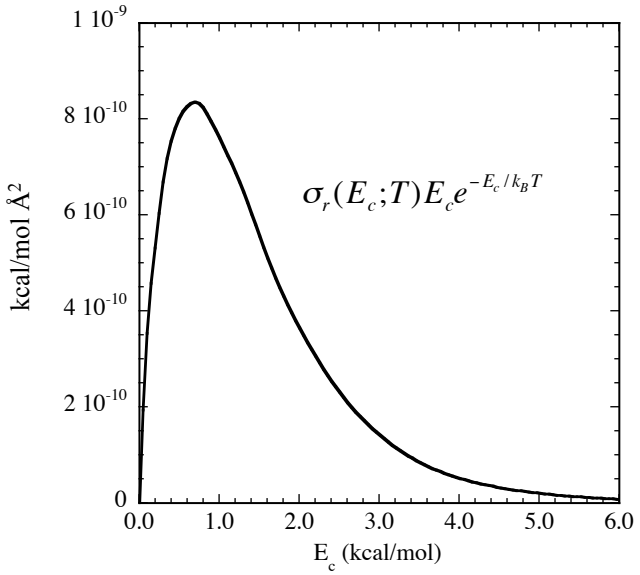

Figure 9: Boltzmann weighted cross sections as a function of j for various collision energies and v=36

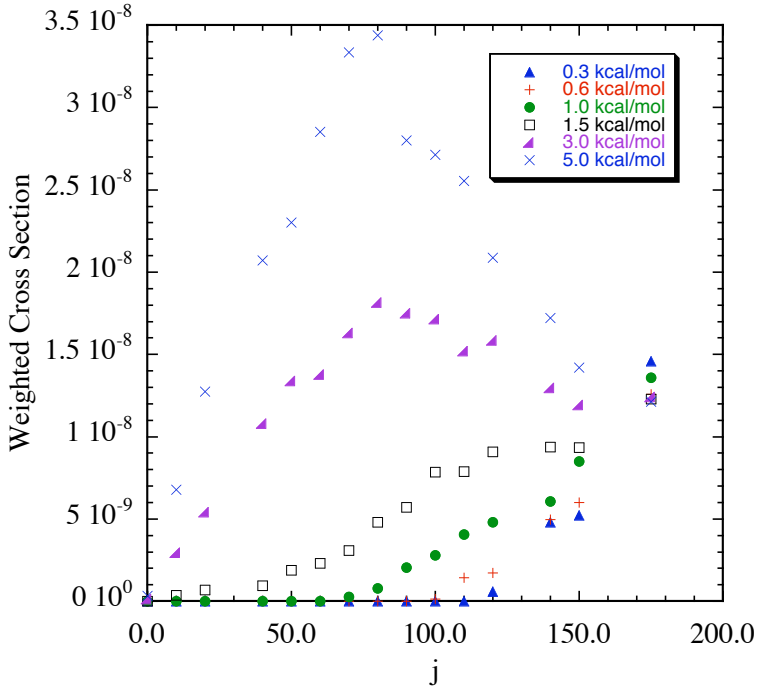


Figure 10: Boltzmann weighted cross sections as a function of v for various collision energies and j=100.

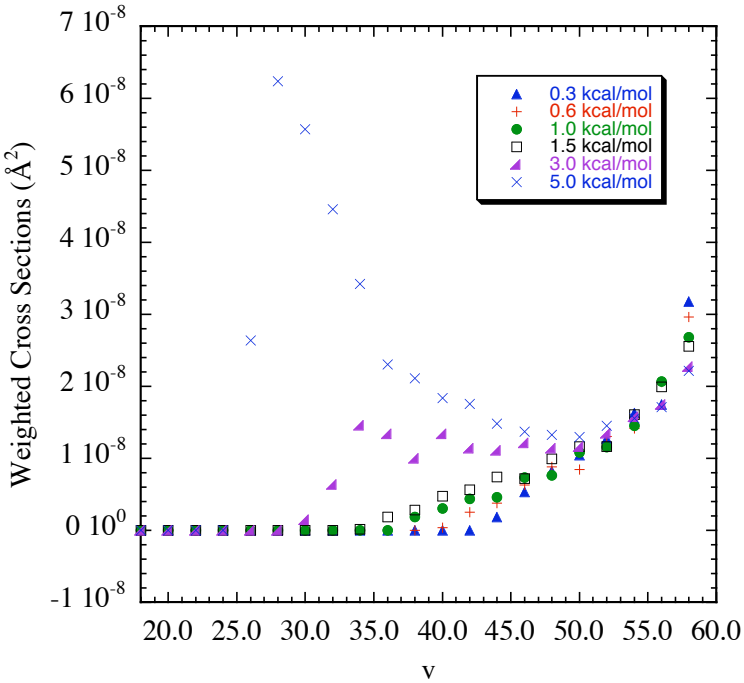

# Ab initio thermochemistry involving heavy atoms: An investigation of the reactions Hg + IX (X = I, Br, Cl, O)

**Benjamin C. Shepler, Nikolai B. Balabanov and Kirk A Peterson***

*Department of Chemistry, Washington State University, Pullman, Washington 99164-4630*

**Abstract**

Accurate 0 K enthalpies have been calculated for reactions of mercury with a series of small iodine-containing molecules ($I_2$, IBr, ICl, and IO). The calculations have been carried out with the coupled cluster singles and doubles method with a perturbative correction for connected triple excitations [CCSD(T)] using sequences of correlation consistent basis sets and accurate relativistic pseudopotentials. Corrections have been included to account for core-valence correlation, spin-orbit coupling, scalar relativity, and the Lamb shift. In a few cases coupled cluster calculations with iterative triple (CCSDT) and quadruple (CCSDTQ) excitations have been carried out to estimate the effects of higher order electron correlation. The pseudopotential calculations have also been compared to all electron calculations using 2nd and 3rd order Douglas-Kroll-Hess Hamiltonians. In addition to the reaction enthalpies, heats of formation, bond lengths, and harmonic vibrational frequencies have been calculated for the stable triatomic products $HgI_2$, HgIBr, HgICl, and HgIO. Accurate dissociation energies, equilibrium bond lengths, and harmonic vibrational frequencies have also been calculated for each of the diatomic molecules involved in this study (HgI, HgBr, HgCl, HgO, $I_2$, IBr, ICl, and IO). The reported enthalpies are expected to have accuracies of 1 kcal/mol or better.

---

*Journal of Physical Chemistry A*. **109**, 10363 (2005)

## I. INTRODUCTION

In the atmosphere, mercury exists predominately in the gas phase and zero oxidation state. Mercury in this form is fairly inert, giving it long atmospheric residence times that are on the order of 1-2 years. This allows mercury to be transported far from its anthropogenic and natural sources, and gives mercury a nearly uniform background concentration across the globe[1]. Episodic depletions of this background atmospheric mercury concentration in the arctic troposphere during polar sunrise were first observed by Schroeder et al. at Alert, Northwest Territories (83° N, 63° W)[2]. Since those first observations, mercury depletion events (MDEs) have been observed elsewhere in the Arctic[3-5], as well as the Antarctic[6]. Similar tropospheric ozone depletion events have been observed to be highly correlated with the MDEs[2-6]. Reactions of ozone with reactive photochemically produced halogen species are known to be responsible for the ozone depletion events[7-12], and it has been proposed that these halogen species are also responsible for the depletions of tropospheric mercury. The proposed mechanism of the mercury depletions is that the gas phase zero valent mercury undergoes oxidizing reactions with the photochemically produced halogen species to generate some form of reactive gaseous mercury, which is then deposited onto the snow pack. A recent study by Tarasick and Bottenheim[13] have shown that the occurrence of ozone depletion events in the arctic have been increasing since the 1960s and blame this rise on increasing global temperatures. It is likely then that the frequency of mercury depletions has been rising as well. This increase has been suggested as a partial cause of the high concentrations of mercury in Arctic biota[3,13].

When the MDEs were first observed there was very little known about the gas phase thermochemistry and kinetics of the reactions between mercury and halogen species. Since then, several theoretical[14-17] and experimental[18,19] studies have been reported for reactions of mercury

with bromine- and chlorine-containing species. Similar attention has not been given to the possible role of iodine in mercury depletion events. Goodsite et. al.[17] reported density functional theory (DFT) calculations that included the molecules HgI and HgIBr, as well as a rate constant for the recombination of Hg and I atoms using RRKM theory. Also, Calvert and Lindberg[20] performed an atmospheric modeling study of arctic tropospheric mercury that included iodine chemistry. This and other modeling studies could benefit from an accurate characterization of the reactions of mercury with iodine-containing species that might be involved.

Before the observation of MDEs, the primary interest in gaseous mercury halides was in connection with laser applications. The UV absorption[21-24] and dissociation[25-30] of $HgX_2$ and the $B^2\Sigma^+ \rightarrow X^2\Sigma^+$ transitions of HgX (X=Br, Cl, I)[31-40] have received a fair amount of attention. The infrared and Raman spectra of matrix isolated[41-44] and gas-phase[45-47] HgIX (X=Br, Cl, I) have also been characterized. Additionally, $HgI_2$ has been the focus of crossed molecular beam experiments[48-50] and femtosecond transition-state spectroscopy that focused on its photodissociation[51-54]. There have also been a small number of theoretical investigations of HgI and $HgI_2$[55-57], but these employed relatively small basis sets and modest levels of electron correlation.

Due to the relatively small body of work on mercury-iodine species, the goal of this work was to accurately compute the thermochemistry of several reactions that involve mercury and iodine that might be important in mercury depletion events. The specific reactions investigated were:

$$\mathrm{Hg} + \mathrm{IX} \rightarrow \begin{cases} \mathrm{HgX} + \mathrm{I} \\ \mathrm{HgI} + \mathrm{X} \\ \mathrm{IHgX} \end{cases}$$

where X = O, Cl, Br, and I. Currently, the enthalpies of many of these reactions are not known accurately or are not known at all. In this work, highly correlated *ab initio* calculations have been carried out on the above reactions and the heats of formation of linear IHgX (X=O, Cl, Br, I). The present study included the calculation of full near-equilibrium potential energy surfaces for each of the above diatomic and triatomic molecules to determine not only their thermochemistry, but also their spectroscopic properties. This paper will focus solely on the thermochemistry, while a future paper will address the structures and spectroscopy in more detail. Electron correlation was treated with the coupled cluster singles and doubles method with a perturbative treatment of connected triple excitations[58] [CCSD(T)] and series of correlation consistent basis sets that were used to extrapolate to the complete basis set (CBS) limit. Additionally, corrections for core-valence correlation, spin-orbit coupling, the Lamb shift, and scalar relativity were also included. A small number of coupled cluster calculations including iterative triple (CCSDT) and quadruple (CCSDTQ) excitations have also been carried out. The reported heats of reaction are expected to be the most accurate values available, and have estimated uncertainties of 1 kcal/mol. Also, the bond lengths reported here for the molecules HgX and HgIX (X=O, Cl, Br, I) should be considered the most reliable to date.

## II. METHODOLOGY

To account for the large scalar relativistic effects in the compounds under investigation, small-core energy consistent pseudopotentials of the Stuttgart/Köln type were used for Br[59], I[59], and Hg[60]. These pseudopotentials treat the valence and semi-core electrons explicitly, and the inner core electrons are replaced by the pseudopotential. The explicitly treated electrons for Br (25 $e^-$), I (25 $e^-$), and Hg (20 $e^-$) are: $3s^2 3p^6 3d^{10} 4s^2 4p^5$, $4s^2 4p^6 4d^{10} 5s^2 5p^5$, and $5s^2 5p^6 5d^{10} 6s^2$,

respectively. Correlation consistent basis sets from double-zeta to quintuple-zeta quality have recently been developed for use with these pseudopotentials, and are denoted cc-pV*n*Z-PP (*n*=D,T,Q,5)[59,61]. Augmented sets that include an extra diffuse function of each angular momentum type have also been used and are denoted aug-cc-pV*n*Z-PP[59,61]. The aug-cc-pV(*n*+*d*)Z sets[62] were used for Cl and the standard aug-cc-pV*n*Z sets[63] were used on oxygen. From this point forward the abbreviation aV*n*Z will be used to represent the above listed augmented sets for each atom. Most calculations in this study were performed with the CCSD(T) method[58] and have employed the frozen core approximation except where noted. For the open-shell molecules the calculations were performed at the ROHF/UCCSD(T)[64-66] level of theory, which uses restricted open-shell Hartree-Fock orbitals but allows for some spin-contamination in the coupled cluster calculations. Except where stated otherwise, all calculations were performed with the MOLPRO[67] suite of *ab initio* programs.

A grid of 74 points was calculated on the potential energy surface of each triatomic molecule (IHgI, IHgBr, IHgCl, and IHgO), and 7 points were calculated for each diatomic (HgI, HgBr, HgCl, HgO, $I_2$, IBr, ICl, and IO). The actual number of points that had to be explicitly calculated for the triatomic molecules was reduced by symmetry to 31 for IHgI and 50 for IHgX (X=Cl, Br, O). These grids of energies were computed for each species using all four basis sets in the series aV*n*Z (*n*=D,T,Q,5), except that in the case of the triatomic molecules the aVQZ basis set was the largest used for nonlinear geometries. Several methods for estimating the CBS limit from calculations with a series of correlation consistent basis sets have been proposed in the literature. In this work two formulas were used to extrapolate the total energies to the CBS limit:

$$E(n) = E_{\mathrm{CBS}} + Be^{-(n-1)} + Ce^{-(n-1)^2} \tag{1}$$

$$E(n) = E_{\mathrm{CBS}} + B/n^3. \tag{2}$$

The best estimate of the CBS limit was taken to be the average of the limits determined from Eqs. (1)[68,69] and (2)[70,71]. The triatomic potential energy surfaces were fit with polynomials in internal displacement coordinates using the program SURFIT[72]. Equilibrium geometries and harmonic vibrational frequencies were determined from these fits. The diatomic curves were also fit with polynomials and the usual Dunham analysis[73] was used to calculate the equilibrium geometries and harmonic frequencies. Zero-point vibrational energies (ZPE) were calculated as ZPE = $1/2\sum\omega_e$. where the $\omega_e$'s are the harmonic vibrational frequencies. Due to the heavy atoms involved, the anharmonic frequencies differed from the harmonic ones by only a few wavenumbers. Thus, the anharmonic ZPE corrections always differ from the harmonic values by less than 0.01 kcal/mol for all of the reactions in this study.

Several corrections were then applied to the valence electrons correlated CCSD(T)/CBS energies: core-valence correlation ($\Delta E_{CV}$), spin-orbit coupling ($\Delta E_{SO}$), scalar relativity ($\Delta E_{SR}$), and the Lamb shift ($\Delta E_{Lamb}$). The core-valence, spin-orbit and scalar relativistic corrections were computed for each symmetry unique point on the potential surfaces, and the corrections used in the thermochemistry calculations were defined relative to their respective minimum geometries. In the core-valence calculations aug-cc-pwCVTZ-PP[61,74] basis sets were used on Br, I, and Hg, and the aug-cc-pwCVTZ[75] sets were used for Cl and O. Two separate calculations were carried out using the core-valence basis sets to determine this correction, one calculation with the standard frozen core and a second in which both the core and valence electrons were correlated. The core-valence correction was then taken as the difference between these two results. Note, however, that the Cl *1s* electrons were kept frozen in all cases.

The Hg *4f* electrons are replaced by the pseudopotential, but energetically lie above the Hg *5s* and Br *3s* orbitals. To account for effects on the enthalpies due to the correlation of the

Hg *4f* electrons, all-electron CCSD(T) calculations have been performed with the 2nd order Douglas-Kroll-Hess Hamiltonian (DK2) [76,77] as implemented in MOLPRO. For I, Br and Hg the basis sets used in these calculations were of augmented triple-zeta quality and corresponded to newly developed all-electron core-valence correlation consistent basis sets where the exponents and contraction coefficients were optimized using the DK2 Hamiltonian and are denoted cc-pwCVTZ-DK[74] (aug-cc-pwCVTZ-DK). Standard aug-cc-pwCVTZ basis sets recontracted in atomic DK2 calculations[78] were employed for Cl and O. Three all-electron CCSD(T) calculations were performed with these basis sets at the CCSD(T)/CBS+CV+SO equilibrium geometries (CV refers to the core-valence correction described above and SO to the spin-orbit correction described below). In the first calculation only the valence electrons were correlated, in the second calculation the valence electrons together with the Hg *5s5p* and Br *3s3p3d* electrons were correlated (where the 5*s* orbital of Hg and *3s* orbital of Br were rotated if needed above the 4*f* orbitals), and in the third the Hg *4f* electrons were included in the correlation treatment. The contribution of the Hg *4f* electrons to the core-valence energy was calculated as the difference between the second and third calculations and is denoted $\Delta E_{\text{CV-}f}$.

A third correction applied to the CBS limit energy differences was to account for spin-orbit coupling. The one-electron spin-orbit operators used were those accompanying the pseudopotentials described above for Br, I, and Hg. For the spin-orbit calculations, relativistic pseudopotentials were also used for O[79] and Cl[80,81] and were again of the Stuttgart/Köln type. In the oxygen case the $1s^2$ electrons are replaced by the pseudopotential, and in the case of chlorine the $1s^2 2s^2 2p^6$ electrons are replaced. The basis sets used with the O and Cl pseudopotentials were the standard aug-cc-pVTZ basis sets (aug-cc-pV(T+*d*)Z for Cl), but they were recontracted in the presence of the pseudopotentials. The basis sets for Br, I, and Hg corresponded to the

standard aug-cc-pVTZ-PP. The spin-orbit calculations were carried out using the multireference configuration interaction with single excitations method (MRCIS) using standard full-valence complete active spaces. The spin-orbit CI[82] code in the COLUMBUS[83] suite of *ab initio* programs was used in these cases. Two calculations were again carried out for each geometry, one corresponding to a standard MRCIS without spin-orbit coupling and the second was a spin-orbit-MRCIS (SO-MRCIS) that mixed all possible singlets and triplets (or doublets and quartets) via the spin-orbit operator. The orbitals used in each of these two calculations were natural orbitals obtained from configuration interaction singles and doubles (CISD) calculations performed with MOLPRO. The spin-orbit correction at each point was then defined as the difference between the SO-MRCIS energy and the MRCIS energy. The accuracy of the spin-orbit correction calculated in this manner is quite reasonable. For example, the zero-field splittings of the I, Br, and Cl atoms were calculated to be 7157 $cm^{-1}$, 3445 $cm^{-1}$, and 912 $cm^{-1}$ respectively, which can be compared to experimental values[84] of 7603 $cm^{-1}$, 3685 $cm^{-1}$, and 912 $cm^{-1}$. Therefore, the calculated differences between the *j*-averaged levels and *j*=3/2 levels are in error with respect to experiment by -0.42 kcal/mol, -0.23 kcal/mol and 0.03 kcal/mol for I, Br, and Cl respectively. Further improvement would presumably require the correlation of the outer-core electrons in the SO-CI calculations.

The spin-orbit correction for the reaction Hg + IO → HgO + I could not be treated in the same manner. If spin-orbit coupling is not included, HgO has two low-lying excited states[85] that are nearly isoenergetic, $^1\Sigma^+$ and $^3\Pi$. When spin-orbit coupling is included, the ground state is described as an $\Omega=0^+$ state that is a mixture of the $0^+$ components of the $^3\Pi$ and $^1\Sigma^+$ states. In order to describe the relative energetics of these states in even a qualitatively correct manner, accurate inclusion of both electron correlation and basis set effects are required. The

MRCIS/aVTZ level of theory is not sufficient. These challenges were described in detail in a previous paper[85]. Therefore, the SO correction for HgO was determined using the interacting states approach in MOLPRO[86] in a similar procedure as our previous study[85], and will be discussed in detail in a future publication. Briefly, the diagonal elements of $H_{el}+H_{so}$ for several low-lying Λ-S states were computed with the internally contracted multireference configuration interaction with single and double excitations method[87,88] and included the multireference analog of the Davidson correction[89-91] (icMRCI+Q). Correlation consistent basis sets of TZ-5Z quality were used, and energies were extrapolated to the CBS limit. A correction for core-valence correlation computed at the icMRCI+Q/aVTZ level was also included. All other diagonal matrix elements and all off-diagonal matrix elements of $H_{el}+H_{so}$ were computed at the icMRCI+Q/aVTZ level of theory. The states used to construct $H_{el}+H_{so}$ included all the singlets and triplets arising from $Hg(^1S,^3P)+O(^3P,^1D,^1S)$ with the exception of the highest lying $^3\Sigma^-$ and $^1\Sigma^-$ states. The lowest energy $\Omega=0^+$ state resulting from the diagonalization of $H_{el}+H_{so}$ was taken as the ground state energy of HgO and is the energy used in the present thermochemical calculations. The ZPE and fundamental vibrational frequency of HgO was calculated for this $\Omega=0^+$ state using the program LEVEL.[92]

The fourth correction, $\Delta E_{SR}$,was to account for scalar relativistic effects in the Cl and O atoms. Scalar relativistic effects for Br, I, and Hg were included in the parameterization of the pseudopotentials. Scalar relativistic corrections for molecules containing Cl and O atoms were determined by evaluating the expectation values of the mass-velocity plus Darwin terms of the Breit-Pauli Hamiltonian with the CISD method using completely uncontracted aVTZ basis sets.

It has recently been suggested that the Lamb shift, the leading quantum electrodynamic (QED) effect not included in the parameterization of the pseudopotentials, may be of chemical

significance especially for molecules containing atoms as heavy as mercury[93,94]. To estimate the effects of the Lamb shift we follow the procedure of Pyykkö and Zhao[95] involving local model potentials. The leading Lamb shift contributions are the self-energy and vacuum polarization terms. The self-energy potential on each atom was simulated by a single Gaussian function whose coefficients and exponents were taken from Pyykkö and Zhao[95]. To simulate the vacuum polarization contribution for each atom a series of five Gaussian functions were fit to the parameterized representation of the vacuum polarization potential given by Pyykkö and Zhao[95]. The Lamb shift correction was then determined from two all-electron CCSD(T)-DK2/aug-cc-pVTZ-DK calculations carried out at the equilibrium geometries; one calculation including the local potentials when computing the one-electron integrals and the other neglecting them.

One final correction was applied, but only in the determination of the dissociation energies of a few of the diatomic molecules. In particular there has been considerable disagreement in the literature about the heat of formation and dissociation energy of the IO molecule. To further refine our predictions for these quantities, additional single-point calculations were carried out at the CCSDT/aVTZ and CCSDTQ/aVDZ levels of theory using the NWChem[96,97] suite of *ab initio* programs. To obtain an estimate of the effect of iterative triples and quadruples on some of the other molecules in this study, CCSDT and CCSDTQ calculations were also carried out on the IBr and HgBr molecules. In the case of HgBr only the VDZ basis sets were used in the CCSDTQ calculations in order to reduce the computational requirements.

As part of this study we were also interested in comparing reaction enthalpies computed with the pseudopotentials with enthalpies calculated with all electron Douglas-Kroll-Hess Hamiltonians of 2$^{nd}$ (DK2) and 3$^{rd}$ (DK3)[98] order. For I, Br and Hg the basis sets used in these

calculations corresponded to newly developed all-electron correlation consistent basis sets where the exponents and contraction coefficients were optimized using the DK2 Hamiltonian and are denoted cc-pV*n*Z-DK[59,99] (aug-cc-pV*n*Z-DK). Standard aV*n*Z basis sets recontracted in atomic DK2 calculations[78] were employed for the other atoms (aV(*n*+*d*)Z for Cl). For the DK2 enthalpies geometry optimizations using numerical gradients were carried out with the CCSD(T) method and the aug-cc-pV5Z-DK basis sets with MOLPRO. These were then compared to the CCSD(T)/aug-cc-pV5Z-PP+$\Delta E_{SR}$ enthalpies. By including $\Delta E_{SR}$ in this way we account for the neglect of scalar relativistic effects on Cl and O in the pseudopotential calculations.

For the DK3 enthalpies, calculations were carried out at the 2$^{nd}$ order Møller-Plesset perturbation theory (MP2) level with the GAMESS[100] suite of *ab initio* programs. cc-pV5Z-DK basis sets were used in these calculations with the *h* and *i* angular momentum functions removed from the Hg basis set and the *g* and *h* angular momentum functions removed from the basis sets of the other atoms. These truncations were employed since GAMESS can only handle up to *g*–type angular momentum functions. Only single-point calculations at the CCSD(T)/CBS+CV+SO equilibrium geometry were carried out. These enthalpies were then compared to (GAMESS) DK2 calculations using the same basis sets and at the same geometries. Direct comparison between the MOLPRO pseudopotential results and the DK3 calculations in GAMESS were complicated by different implementations of the open-shell MP2 method in the two program packages.

It should be noted that the DK2 method in MOLPRO and GAMESS are of slightly different implementations. Some single-point calculations using DK2 in GAMESS and MOLPRO differed by a few m$E_h$, but there was virtually no difference when energy differences were considered. For example, the reaction enthalpies of Hg + $I_2$→ $HgI_2$ and Hg + IBr → HgIBr calculated at the

MP2-DK2 level of theory differed by 0.02 and 0.01 kcal/mol respectively, depending on whether GAMESS or MOLPRO was used.

## III. RESULTS AND DISCUSSION

Table 1 shows the equilibrium bond lengths calculated at the CCSD(T)/CBS+CV+SO+SR (does not include correlation of the Hg *4f* electrons) level of theory for the four triatomic and eight diatomic molecules involved in this study. In the four cases where experimental bond lengths are available for the diatomics ($I_2$, IBr, ICl, and IO), there is excellent agreement between the calculated and experimental values. The RMS value of the difference between theory and experiment is just 0.0025 Å, and the maximum difference occurs for the ICl molecule and is just 0.0041 Å. To our knowledge, reliable experimental equilibrium geometries have not been reported for the diatomic molecules HgO, HgCl, HgBr, and HgI. A number of groups have reported previous DFT[17,57] and *ab initio*[15,16,31,101-103] calculations of the diatomic HgX (X=Cl, Br, I) bond lengths, but all involved smaller basis sets and lower levels of electron correlation than the present study. All four triatomic molecules have linear equilibrium geometries with Hg as the central atom. The only triatomic molecule for which an experimental bond length has been reported is $HgI_2$, and our calculated value of 2.546 Å is in reasonably good agreement with the experimental electron diffraction value[104] ($r_e$ = 2.554±0.003 Å), being just 0.008 Å shorter. There have been a few previous theoretical calculations of the $HgI_2$ bond length[55-57] and one study involving the geometry of HgIBr[17], but these only involved basis sets of DZ or TZ quality at the MP4[55], MP2[56], LDF[57], and B3LYP[17] levels of theory. For the species without reliable experimental values, the quantities in Table 1 should represent the best estimates to this date.

The harmonic vibrational frequencies used to compute the ZPE's are also compiled in Table 1. These are computed at the same level of theory as the bond lengths, CCSD(T)/CBS+CV+SO+SR, however when computing the CBS limit for the bending frequencies, aVDZ-aVQZ basis sets were used, while all other quantities in this table utilized aVTZ-aV5Z sets. It should be noted that CBS frequencies obtained with the two ranges of basis sets were in very close agreement for the bond stretching normal modes. In most cases the difference was less than 1 $cm^{-1}$, and only in the case of HgI was it larger than 2 $cm^{-1}$, and it was then only 2.5 $cm^{-1}$. As was the case for bond lengths, the calculated and experimental harmonic frequencies for the diatomic molecules are in excellent agreement. As opposed to the bond lengths, there do exist accurate harmonic vibrational frequencies for HgCl, HgBr, and HgI. The only molecule in this study for which there is not an accurate experimental harmonic frequency is HgO. The flatness of the potential and the multiple minima on its ground state $\Omega=0^+$ potential made the calculation of a harmonic frequency for HgO unreliable. Instead, the value listed in Table 1 for HgO is the fundamental vibrational frequency computed numerically with the program LEVEL. The ZPE for this molecule is 217.3 $cm^{-1}$, and was also determined with LEVEL. For the diatomic harmonic frequencies, the RMS of the deviation of theory from experiment is 4.8 $cm^{-1}$ with the largest differences occurring for ICl (7.5 $cm^{-1}$) and HgI (6.3 $cm^{-1}$).

Unlike the bond lengths, the vibrational frequencies of the triatomic HgIX molecules have been fairly well characterized experimentally, however at low resolution. For each mode that has been observed, there is a spread of a few wavenumbers in the experimental values. For the triatomic molecules the calculated harmonic frequencies are compared to experimental fundamental frequencies in Table 1. The comparison, however, should be reasonable due to the

small calculated anharmonicity constants of the molecules in this study. Of the molecules that have been observed experimentally, HgICl has the largest anharmonicity constants yet the largest value is only $x_{33}$=1.09 cm$^{-1}$. The calculated stretching frequencies are in general slightly higher than the experimental values. The largest difference occurs for the Hg-Cl stretch in HgICl in which the calculated $\omega_e$ is 10.4 cm$^{-1}$ higher than the largest experimental value. There is no such general trend for the bending frequencies, but they show similarly good agreement between theory and experiment. The only triatomic for which there is an absence of experimental data is HgIO. A more detailed discussion of the structure and anharmonic spectra of HgX and HgIX (X=O, Cl, Br, I) will be the focus of a future publication.

The relativistic effects on the dissociation energies of each of the molecules included in this study are presented in Table 2. In the case of the triatomic molecules the relativistic contributions correspond to the reaction HgIX→Hg+IX. The final column of this table, $\Delta E_{REL}$, represents the total of the extra relativistic corrections that were applied to the enthalpies of reaction and is equal to $\Delta E_{SO\text{-}Total}+\Delta E_{Lamb}+\Delta E_{SR}$, which are described below. Three columns of this table are devoted to the spin-orbit correction. In the first column the total calculated spin-orbit correction, $\Delta E_{SO\text{-}Total}$, is given for each of the reactions. The second column is the contribution of the zero-field splitting of the atoms, as well as those of the $^2\Pi$ IO and HgIO molecules, and is denoted $\Delta E_{SO\text{-}Zero}$. The zero-field splitting for the atoms was calculated by taking the difference between the calculated *j*-averaged levels and the $^2P_{3/2}$ levels for the halogens and the $^3P_2$ level for oxygen. The zero-field splittings of IO and HgIO were calculated as half of the splitting of the calculated $^2\Pi_{3/2}$ and $^2\Pi_{1/2}$ levels. The third column, $\Delta E_{SO\text{-}diff}$, contains the part of the spin-orbit correction not due to this zero-field splitting ($\Delta E_{SO\text{-}diff}$ =

$\Delta E_{\text{SO-Total}} - \Delta E_{\text{SO-Zero}}$) and is largely the result of second-order spin-orbit effects. For almost all of the reactions spin-orbit effects are quite large, the two exceptions are in the $D_e$ of HgCl and the reaction HgIO→Hg+IO. The zero spin-orbit correction for HgCl is due to nearly exact cancellation of the zero-field splitting of the Cl atom and the 2$^{nd}$-order spin-orbit lowering of the molecule. The spin-orbit correction in HgIO is small due to the cancellation of the large calculated zero-field splittings of IO (0.57 kcal/mol) and HgIO (0.78 kcal/mol). When the spin-orbit correction is very large, as in the $D_e$ of $I_2$, most of this correction comes from the zero-field splittings. However, for all of the reactions, except HgIO→Hg+IO, the second-order spin-orbit effects are on the order of 1 kcal/mol or more. Even for the reactions $HgI_2$→Hg+$I_2$, HgIBr→Hg+IBr, and HgICl→Hg+ICl, which involve only closed shell molecules, the spin-orbit correction is 1kcal/mol or larger. Clearly, it is important to explicitly compute a spin-orbit correction even for closed shell molecules when heavy atoms are involved if accurate results are desired (see also Refs. 105 and 106).

The fourth column of Table 2 contains the Lamb shift correction to the dissociation energies. In the four mercury-containing diatomic molecules, mercury goes from an approximately +1 oxidation state in the molecule to a zero-oxidation state in the separated atoms. The Lamb-shift correction to $D_e$ in each of these molecules is nearly the same, ranging from 0.34 kcal/mol in HgI to 0.41 kcal/mol in HgCl. Similarly, in the four triatomic molecule reactions, mercury changes from an approximately +2 oxidation state in the HgIX reactants to a zero oxidation state in the products. The Lamb shifts for all of these reactions are also very similar and approximately two times larger than the correction in the HgX diatomics. These results are similar in magnitude to the correction calculated for the first ionization potential of Hg, –0.78

kcal/mol. It is also interesting to note that the Lamb shift correction slightly increases with increasing electronegativity of the X-atom as one moves from I to Br to Cl in both the diatomic and triatomic molecules. These observations seem to support the notion that the Lamb shift will be significant in reactions involving changes in *s*-orbital occupations[94], i.e., the 6*s* orbital of mercury in these reactions. In the four dissociation energies that do not involve mercury ($I_2$, IBr, ICl, and IO), the Lamb-shift correction is never larger than 0.1 kcal/mol which seems to indicate that it is not very significant even for atoms as heavy as iodine. We have observed similarly small Lamb-shift corrections in preliminary calculations on $CdBr_2$ and CdBr.

The mass-velocity + Darwin corrections for the Cl and O atoms are presented in the fifth column of Table 2 under the heading $\Delta E_{SR}$. This correction is in general quite small, with the largest value being –0.21 for the dissociation energy of HgCl. The corrections for the other molecules are generally on the order of 0.1 kcal/mol.

Finally, the three columns in Table 2 labeled $\Delta E_{DK2\text{-}PP}$, $\Delta E_{DK3\text{-}DK2}$, $\Delta E_{DK3\text{-}PP}$ compare enthalpies calculated with pseudopotentials to all-electron calculations. The total energies one obtains with the DK2 and DK3 Hamiltonians can be quite different from each another, especially for molecules as heavy as $I_2$. For $I_2$ the MP2 energies with the truncated V5Z-DK basis set are –14222.050801 and –14226.379243 $E_h$ using the DK2 and DK3 Hamiltonians, respectively. However, when energy differences are considered, there is much less difference between DK2 and DK3. In fact, for the molecules not containing mercury, the difference between DK2 and DK3 for the reactions in Table 2 is never larger than 0.01 kcal/mol. In $I_2$, IBr, and ICl the difference between the DK2 enthalpies and the PP enthalpies are only one or two tenths of a kcal/mol. In IO the difference is much larger at –0.43 kcal/mol. The differences between the DK2 and PP enthalpies for the reactions involving mercury tend to be somewhat larger in

magnitude than in the reactions not involving mercury. However, in every case the DK3-DK2 differences are between 0.2 and 0.4 kcal/mol and opposite in sign to the DK2-PP differences. This would seem to suggest that much of the differences between the DK2 and PP calculations are due to inadequacy of the treatment of scalar relativistic effects in the DK2 Hamiltonian when atoms as heavy as mercury are involved. The column $\Delta E_{\mathrm{DK3\text{-}PP}}$ is an estimated difference between DK3 and PP enthalpies obtained by adding the two previous columns. The agreement between DK3 and PP enthalpies appears to be much better than in the DK2 case and is only larger than 0.30 kcal/mol in the HgIO reaction. However we should reiterate that DK2 seems to do well even for atoms even as heavy as iodine. As with the Lamb shift, we have observed similarly good agreement between DK2 and DK3 calculations in reactions involving $CdBr_2$ and CdBr.

There are several factors that may contribute to the remaining discrepancy between the all electron and pseudopotential enthalpies. The Dirac-Hartree-Fock calculations against which the pseudopotentials were parameterized include the Breit interaction, finite nucleus effects, and two-electron scalar relativistic effects, and these effects are not included in the DKH Hamiltonians used in this study. Also, even though large basis sets of similar quality were employed there are likely small basis set effects involved. Of course, there are also likely small errors due to the frozen core in the pseudopotential calculations, as well as the use of nodeless outer-core pseudo-orbitals. Accurately quantifying the errors due to the pseudopotential approximation for heavy elements is thus quite challenging and attempts to make such a correction have not been attempted in this work.

Table 3 contains the calculated and experimental dissociation energies, $D_0$, of the diatomic molecules involved in this study. Together with the final dissociation energies, each of

the individual corrections to the CCSD(T)/CBS energy differences are tabulated. As the results in Table 2 clearly demonstrate, it is insufficient to use only basis sets of even quadruple-zeta quality to obtain highly accurate results. The differences between the $D_e$'s calculated with the aVQZ basis and those at the CBS limit range from 1-2 kcal/mol. It should be noted that CBS limit $D_e$'s calculated with the two extrapolation formulae (that were then averaged) typically differ by just 0.2-0.3 kcal/mol with the largest difference (0.5 kcal/mol) occurring in the case of $I_2$. The inclusion of core-valence correlation also makes significant contributions. The largest total core-valence correlation correction is calculated for the $I_2$ and HgCl molecules where it is 0.75 kcal/mol in each case. The correlation of the Hg 4*f* electrons appears to be quite important, and is approximately of the same order of magnitude as the correlation of the Hg 5*s*5*p* and Br 3*s*3*p*3*d* electrons. The additional relativistic corrections, $\Delta E_{\mathrm{REL}}$, have been discussed above.

A wide range of dissociation energies and heats of formation have been reported for the IO molecule. Two independent crossed molecular beam studies of the reaction O+ICl have reported a $\Delta H_f$(0K) for IO of 32±3 kcal/mol[107] and 30±2 kcal/mol[108] ($D_0$=53 and 55 kcal/mol, respectively). These are slightly higher than those obtained from kinetics studies[109,110]; the reaction between oxygen atom and alkyl iodides places an upper bound on the $\Delta H_f$ (298K) of IO at 28.8 kcal/mol[109] ($D_0$=55.3), while kinetic investigations of the reaction IO + ClO yielded a $\Delta H_f$ (298K) for IO of 27.7±1.2 kcal/mol[110] ($D_0$=56.4 kcal/mol). Previous high quality *ab initio* investigations have predicted varying 0K heats of formation of IO, these being 31.0±1.0 kcal/mol[111], 28.9 ±1.8 kcal/mol[112], and 38.9 kcal/mol[113] ($D_0$=53.6, 55.7, 45.7 kcal/mol, respectively). In this work, without the inclusion of higher order electron correlation effects, the CCSD(T)/CBS+CV+SO+SR+LAMB dissociation energy ($D_0$) of IO is 53.135 kcal/mol. The correction for iterative triple excitations [CCSDT-CCSD(T)] calculated with the aVTZ basis sets

was calculated to add 0.50 kcal/mol. The addition of iterative quadruple excitations [CCSDTQ-CCSDT] calculated with the aVDZ basis set was found to yield an additional 0.68 kcal/mol, resulting in a total correction of 1.18 kcal/mol. Combining these values results in our best predicted value for $D_0$ of 54.31 kcal/mol. Due to the probable underestimation of spin-orbit effects in the atoms as well as errors due to the PP approximation, this value may be slightly too large. To determine the heat of formation, accurate experimental values for the $\Delta H_f$(0K) of I (25.61±0.01 kcal/mol)[114] and O (58.98±0.02 kcal/mol)[114] were combined with our predicted $D_0$ of IO to yield a predicted $\Delta H_f$(0K) for IO of 30.28 kcal/mol. Using standard ideal gas forms of the partition functions, our calculated heat of formation at 298K is 29.81 kcal/mol. This result is in good agreement with the $\Delta H_f$ values determined in the molecular beam experiments and two of the previous *ab initio* calculations, but it is considerably higher than those determined from the kinetics experiments. Based on the accuracy of the other dissociation energies in this study, and similar previous work (see, for instance, Refs.14,105,115,116 and Ref. 24 cited in Dixon et al.[117]), we believe our calculated $\Delta H_f$(0K) of IO has an accuracy better than 1 kcal/mol and is the most reliable value to date.

To gauge the effects of higher levels of electron correlation on the other reactions of this study, CCSDT and CCSDTQ corrections have also be calculated for the dissociation energies of IBr and HgBr. In both of these molecules the corrections are significantly smaller than they were in IO. For IBr the CCSDT-CCSD(T) difference is –0.22 kcal/mol and the CCSDTQ-CCSDT difference is +0.23 kcal/mol. The two corrections essentially cancel each other for a total correction of just 0.01 kcal/mol. In HgBr the total correction is somewhat higher at 0.25 kcal/mol, with 0.21 kcal/mol arising from the CCSDT-CCSD(T) difference and 0.04 kcal/mol from the CCSDTQ-CCSDT difference. These smaller corrections for IBr and HgBr are more

representative of the usual quality of CCSD(T) wavefunctions for molecules dominated by the Hartree-Fock configuration. It is likely that the large correction for higher order correlation effects is isolated to the IO molecule in this study.

Accurate and reliable experimental dissociation energies are available for $I_2$, IBr, and ICl, and in all three of these cases the agreement between theory and experiment is very good. The largest difference occurs in $I_2$, where it is only 0.47 kcal/mol. The disagreement between theory and experiment for HgBr, HgCl, and HgI is slightly higher, but in all three cases still much less than 1 kcal/mol. The experimental dissociation energy for HgI (7.83 kcal/mol)[36] has an uncertainty of 0.11 kcal/mol, while the experimental dissociation energy of HgBr (15.53 kcal/mol)[118] has a stated uncertainty of 0.29 kcal/mol. The calculated values of 8.55 kcal/mol for HgI and 16.30 kcal/mol for HgBr fall slightly outside these error bounds. In HgCl the experimental dissociation energy of 23.44 kcal/mol[35] is only a rough upper bound, and the calculated value of 22.91 kcal/mol falls below this value. There has not been a reliable experimental determination of the dissociation energy of the HgO molecule to date. The remaining differences in the experimental and calculated dissociation energies of the molecules in this study can likely be attributed to remaining inadequacies in the treatment of spin-orbit coupling, correlation treatment, the pseudopotential approximation and experimental uncertainties in HgI, HgBr, HgCl and IO.

The calculated enthalpies of reaction (0 K) along with the various corrections to the CCSD(T)/CBS limits are presented in Table 4 for the reactions Hg + IX (X=I, Br, Cl, O). Each of the corrections to the valence-only CCSD(T) enthalpies are in general small, but have non-negligible cumulative effects. The difference between energies of reaction computed with the aVQZ basis set (the second largest basis set used) and those at the CBS limit are as large as 1.2

kcal/mol, and are never smaller than 0.2 kcal/mol. As with the dissociation energies, reaction enthalpies calculated with the two CBS extrapolation formulae typically differ by just 0.1 to 0.2 kcal/mol with the largest difference of 0.3 kcal/mol in the reaction Hg + $I_2$ → HgI +I. The ZPE corrections are in general small, but are as large as 0.8 kcal/mol for the reaction Hg + IO → HgI + O. The mean value of the total CV correction to the enthalpies of reaction is 0.52 kcal/mol and is as large as 0.97 kcal/mol for the reaction Hg + IO → HgIO. The correlation of the Hg *4f* electrons is again shown to be important, often as large as 0.2 kcal/mol, but is in general smaller than the effect of correlating the Hg 5*s*5*p* and Br 3*s*3*p*3*d* electrons in these reactions. The effect of the CCSDT and CCSDTQ corrections to the bond strengths of IBr, HgBr, and IO were included in the reaction enthalpies of Table 4 where appropriate.

The reaction enthalpies are qualitatively similar to the results of a previous study[14] on the reactions Hg + ($Br_2$, BrCl, $Cl_2$, BrO, ClO). All of the abstraction reactions, i.e., Hg + XY → HgX + Y, are endothermic by 25 to 45 kcal/mol. Conversely, all of the insertion reactions, i.e., Hg + XY → XHgY, are exothermic by –35 to –40 kcal/mol. However, preliminary MRCI calculations indicate that the direct insertion reactions have large barriers on the order of 25 kcal/mol, and are therefore not likely to occur in the atmosphere. However, all of the recombination reactions such as HgX + Y→ XHgY are strongly exothermic by –60 to –80 kcal/mol and are predicted to proceed without a barrier.

Agreement between calculated and experimental enthalpies of reaction is quite good where the experimental values are available. There is only one instance where the calculated enthalpies disagree with experiment by more than 1 kcal/mol; the difference between theory and experiment is 1.6 kcal/mol for the reaction Hg + $I_2$ → $HgI_2$, with the calculated result (-34.98 kcal/mol) being more exothermic than the experimental value[114] (-33.4±0.5 kcal/mol). It is

possible, however, that the error bounds of the experimental value, which was determined from the heat of formation of the crystal and its heat of sublimation, are overly optimistic. A second reaction with a fairly large discrepancy between theory and experiment, although the difference is less than 1 kcal/mol, is Hg + ICl → HgI + Cl. In this case the calculated value (40.97 kcal/mol) is more exothermic than experiment (41.81±0.11 kcal/mol) by 0.85 kcal/mol. Due either to large uncertainties or a complete lack of experimental heat of formation data for HgIBr, HgICl, HgIO, HgO, HgCl, and IO, the currently calculated enthalpies for reactions involving these species are the best currently available.

Table 5 contains the calculated dissociation energies and 0K heats of formation for the triatomic species $HgI_2$, HgIBr, HgICl, and HgIO. To calculate these heats of formation we used the enthalpies of reaction for Hg+IX→HgIX tabulated in Table 3 together with accurate experimental heats of formation for the Hg and IX species. In the case of HgIO, the reaction Hg+I+O→HgIO was used instead of Hg+IO→HgIO because of the uncertainty in the experimental heat of formation of IO. The atomic and diatomic 0K heats of formation were taken from JANAF[114]: 15.42±0.01 kcal/mol for Hg, 25.61±0.01 kcal/mol for I, 58.98±0.02 kcal/mol for O, 4.57±0.03 kcal/mol for ICl, 11.91±0.02 kcal/mol for IBr, and 15.65±0.02 kcal/mol for $I_2$. The only triatomic species for which there exists an experimental heat of formation is $HgI_2$, and the difference between the experimental and theoretical results (1.6 kcal/mol) is of course the same as that for the reaction Hg + $I_2$ → $HgI_2$.

## IV. CONCLUSIONS

Accurate *ab initio* calculations have been performed to determine the thermochemistry of reactions between mercury and iodine-containing reactive halogen species. These calculations

have been performed using high levels of electron correlation and series of correlation consistent basis sets with accurate relativistic pseudopotentials, which allowed for extrapolations to the complete basis set limit. Corrections were also included to account for core-valence correlation, spin-orbit coupling, scalar relativity, the Lamb shift, and in some cases higher levels of electron correlation. We have calculated 0 K heats of formation for the species HgIX (X=I, Br, Cl, O) and heats of reaction for:

$$\mathrm{Hg} + \mathrm{IX} \rightarrow \begin{cases} \mathrm{HgX} + \mathrm{I} \\ \mathrm{HgI} + \mathrm{X} \\ \mathrm{IHgX} \end{cases}$$

The accuracy of the reported enthalpies is expected to be within 1 kcal/mol, which is for most of the reactions an improvement over existing experimental values. To the best of our knowledge these calculations are the first to characterize gas phase HgIO.

The heats of reaction for the present iodine-containing reactions are similar in sign and magnitude to the corresponding reactions involving only bromine and chlorine. All of the insertion reactions are found to be strongly exothermic, while the abstraction reactions are all strongly endothermic. If iodine exists in sufficient concentration in the polar tropospheres, it is possible that many of these species and reactions play a role in the episodic mercury depletion events that have recently been observed. The strongly bound IHgX species are possible contributors to reactive gaseous mercury concentrations. The formation of IHgX by direct reaction of Hg with IX is unlikely due to the large barriers indicated by preliminary MRCI+Q/aVTZ calculations. Large barriers have also been observed for the insertion of Hg into $Br_2$ in recent work on the global potential energy surface for HgBr+Br[119].

The present calculations predict the reactions of HgI+X or HgX+I to form HgIX to be strongly exothermic. Our preliminary MRCI+Q/aVTZ calculations and HgBr+Br PES results suggest these reactions will be barrierless. Other reactions involving initially formed HgX molecules can also lead to the formation of HgXY. For example the current results would predict the following reaction enthalpies (X=I; Y=I, Br, O):

$$\mathrm{HgI} + \mathrm{IBr} \rightarrow \begin{cases} \mathrm{HgI_2} + \mathrm{Br} & \Delta H_\mathrm{r} = -20.28 \ \ \mathrm{kcal/mol} \\ \mathrm{HgIBr} + \mathrm{I} & \Delta H_\mathrm{r} = -29.98 \ \ \mathrm{kcal/mol} \end{cases}$$

and

$$\mathrm{HgI} + \mathrm{IO} \rightarrow \begin{cases} \mathrm{HgI_2} + \mathrm{O} & \Delta H_\mathrm{r} = -8.14 \ \ \mathrm{kcal/mol} \\ \mathrm{HgIO} + \mathrm{I} & \Delta H_\mathrm{r} = -3.69 \ \ \mathrm{kcal/mol} \end{cases}$$

Preliminary MRCI+Q/aVTZ calculations indicate that each of these reactions should also proceed without a barrier. The current results and the results of our previous work on the reactions Hg + {$Br_2$, $Cl_2$, BrCl, BrO, ClO}[14] can be used to calculate the enthalpies of similar reactions involving any combination of I, Cl, and Br. It is hoped these accurate results can be used to advance future atmospheric modeling studies.

As part of this work, accurate dissociation energies have also been calculated for all the diatomic molecules involved in this study. In particular, an accurate heat of formation of IO has been calculated. Our results predict a $\Delta H_f$ (298K) of 29.8±1.0 kcal/mol ($D_0$ = 54.3±1.0 kcal/mol), which is slightly higher than the value reported in recent kinetics studies, but is in good agreement with earlier crossed molecular beam studies. This purely *ab initio* result is also in good agreement with the earlier predictions of both McGrath and Rowland[111] and Hassanzadeh and Irikura[112].

## V. ACKNOWLEDGEMENTS

This work was partially supported by the National Science Foundation (CHE-0111282). The authors would like to thank Prof. H. Stoll (Univ. Stuttgart) for helpful discussions concerning 4*f* correlation and the Lamb shift.

## REFERENCES


(1) Schroeder, W. H.; Munthe, J. *Atmos Environ* **1998**, *32*, 809.

(2) Schroeder, W. H.; Anlauf, K. G.; Barrie, L. A.; Lu, J. Y.; Steffen, A.; Schneeberger, D. R.; Berg, T. *Nature* **1998**, *394*, 331.

(3) Lindberg, S. E.; Brooks, S.; Lin, C.-J.; Scott, K. J.; Landis, M. S.; Stevens, R. K.; Goodsite, M.; Richter, A. *Environ Sci Technol* **2002**, *36*, 1245.

(4) Berg, T.; Sekkesæter, S.; Steinnes, E.; Valdal, A.-K.; Wibetoe, G. *Sci Total Environ* **2003**, *304*, 43.

(5) Skov, H.; Christensen, J. H.; Goodsite, M. E.; Heidam, N. Z.; Jensen, B.; Wåhlin, P.; Geernaert, G. *Environ Sci Technol* **2004**, *38*, 2373.

(6) Temme, C.; Einax, J. W.; Ebinghaus, R.; Schroeder, W. H. *Environ Sci Technol* **2003**, *37*, 22.

(7) Barrie, L. A.; Bottenheim, J. W.; Schnell, R. C.; Crutzen, P. J.; Rasmussen, R. A. *Nature* **1988**, *334*, 138.

(8) Le Bras, G.; Platt, U. *Geophys Res Lett* **1995**, *22*, 599.

(9) Boudries, H.; Bottenheim, J. W. *Geophys Res Lett* **2000**, *27*, 517.

(10) Foster, K. L.; Plastridge, R. A.; Bottenheim, J. W.; Shepson, P. B.; Finlayson-Pitts, B. J.; Spicer, C. W. *Science* **2001**, *291*, 471.

(11) Spicer, C. W.; Plastridge, R. A.; Foster, K. L.; Finlayson-Pitts, B. J.; Bottenheim, J. W.; Grannas, A. M.; Shepson, P. B. *Atmos Environ* **2002**, *36*, 2721.

(12) Lehrer, E.; Honninger, G.; Platt, U. *Atmos Chem Phys* **2004**, *4*, 2427.

(13) Tarasick, D. W.; Bottenheim, J. W. *Atmos Chem Phys* **2002**, *2*, 197.

(14) Balabanov, N. B.; Peterson, K. A. *J Phys Chem A* **2003**, *107*, 7465.

(15) Khalizov, A. F.; Viswanathan, B.; Larregaray, P.; Ariya, P. A. *J Phys Chem A* **2003**, *107*, 6360.

(16) Tossell, J. A. *J Phys Chem A* **2003**, *107*, 7804.

(17) Goodsite, M. E.; Plane, J. M. C.; Skov, H. *Environ Sci Technol* **2004**, *38*, 1772.

(18) Ariya, P. A.; Khalizov, A. F.; Gidas, A. *J Phys Chem A* **2002**, *106*, 7310.

(19) Raofie, F.; Ariya, P. A. *J Phys IV France* **2003**, *107*, 1119.

(20) Calvert, J. G.; Lindberg, S. E. *Atmos Environ* **2004**, *38*, 5105.

(21) Maya, J. *J Chem Phys* **1977**, *67*, 4976.

(22) Wilcomb, B. E.; Burnham, R.; Djeu, N. *Chem Phys Lett* **1980**, *75*, 239.

(23) Gedanken, A.; Raz, B.; Even, U.; Eliezer, I. *J Mol Spectrosc* **1969**, *32*, 287.

(24) Bell, S.; McKenzie, R. D.; Coon, J. B. *J Mol Spectrosc* **1966**, *20*, 217.

(25) Whitehurst, C.; King, T. A. *J Phys D: Appl Phys* **1987**, *20*, 1577.

(26) Wadt, W. R. *J Chem Phys* **1980**, *72*, 2469.

(27) Kushawaha, V.; Mahmood, M. *J Appl Phys* **1987**, *62*, 2173.

(28) Kushawaha, V.; Michael, A.; Mahmood, M. *J Phys B: At, Mol Opt Phys* **1988**, *21*, 2507.

(29) Azria, R.; Ziesel, J. P.; Abouaf, R.; Bouby, L.; Tronc, M. *J Phys B: At Mol Phys* **1983**, *16*, L7.

(30) Husain, J.; Wiesenfeld, J. R.; Zare, R. N. *J Chem Phys* **1980**, *72*, 2479.

(31) Wadt, W. R. *Appl Phys Lett* **1979**, *34*, 658.

(32) Viswanathan, K. S.; Tellinghuisen, J. *J Mol Spectrosc* **1983**, *98*, 185.

(33) Wieland, K. *Z Elektrochem* **1960**, *64*, 761.

(34) Tellinghuisen, J.; Ashmore, J. G. *Appl Phys Lett* **1982**, *40*, 867.

(35) Tellinghuisen, J.; Tellinghuisen, P. C.; Davies, S. A.; Berwanger, P.; Viswanathan, K. S. *Appl Phys Lett* **1982**, *41*, 789.

(36) Salter, C.; Tellinghuisen, P. C.; Ashmore, J. G.; Tellinghuisen, J. *J Mol Spectrosc* **1986**, *120*, 334.

(37) Rai, A. K.; Singh, V. B. *Indian J Phys* **1987**, *61B*, 522.

(38) Cheung, N. H.; Cool, T. A. *J Quant Spectrosc Radiat Transfer* **1979**, *21*, 397.

(39) Dreiling, T. D.; Setser, D. W. *J Chem Phys* **1983**, *79*, 5423.

(40) Greene, D. P.; Kileen, K. P.; Eden, J. G. *J Opt Soc Am B: Opt Phys* **1986**, *3*, 1282.

(41) Loewenschuss, A.; Ron, A.; Schnepp, O. *J Chem Phys* **1969**, *50*, 2502.

(42) Givan, A.; Loewenschuss, A. *J Chem Phys* **1976**, *65*, 1851.

(43) Givan, A.; Loewenschuss, A. *J Chem Phys* **1976**, *64*, 1967.

(44) Givan, A.; Loewenschuss, A. *J Mol Struct* **1978**, *48*, 325.

(45) Beattie, I. R.; Horder, J. R. *J Chem Soc A Inorg Phys Theor* **1970**, *14*, 2433.

(46) Clark, R. J. H.; Rippon, D. M. *J Chem Soc Faraday trans II* **1973**, *69*, 1496.

(47) Klemperer, W. *J Chem Phys* **1956**, *25*, 1066.

(48) Wilcomb, B. E.; Mayer, T. M.; Bernstein, R. B.; Bickes, R. W., Jr. *J Am Chem Soc* **1976**, *98*, 4676.

(49) Wilcomb, B. E.; Haberman, J. A.; Bickes, R. W. J.; Mayer, T. M.; Bernstein, R. B. *J Chem Phys* **1976**, *64*, 3501.

(50) Mayer, T. M.; Wilcomb, B. E.; Bernstein, R. B. *J Chem Phys* **1977**, *67*, 3507.

(51) Baskin, J. S.; Zewail, A. H. *J Phys Chem* **1994**, *98*, 3337.

(52) Baumert, T.; Pedersen, S.; Zewail, A. H. *J Phys Chem* **1993**, *76*, 12447.

(53) Dantus, M.; Bowman, R. M.; Gruebele, M.; Zewail, A. H. *J Chem Phys* **1989**, *91*, 7437.

(54) Pedersen, S.; Baumert, T.; Zewail, A. H. *J Phys Chem* **1993**, *97*, 12460.

(55) Howard, S. T. *J Phys Chem* **1994**, *98*, 6110.

(56) Kaupp, M.; von Schnering, H. G. *Inorg Chem* **1994**, *33*, 2555.

(57) Liao, M.; Zhang, Q.; Schwarz, W. H. E. *Inorg Chem* **1995**, *34*, 5597.

(58) Raghavachari, K.; Trucks, G. W.; Pople, J. A.; Head-Gordon, M. *Chem Phys Lett* **1989**, *156*, 479.

(59) Peterson, K. A.; Figgen, D.; Goll, E.; Stoll, H.; Dolg, M. *J Chem Phys* **2003**, *119*, 11113.

(60) Figgen, D.; Rauhut, G.; Dolg, M.; Stoll, H. *Chem Phys* **2004**, *311*, 227.

(61) Peterson, K. A.; Puzzarini, C. *Theor Chem Acc* **2005**, in press.

(62) Dunning, T. H. J.; Peterson, K. A.; Wilson, A. K. *J Chem Phys* **2001**, *114*, 9244.

(63) Kendall, R. A.; Dunning, T. H., Jr.; Harrison, R. J. *J Chem Phys* **1992**, *96*, 6796.

(64) Scuseria, G. E. *Chem Phys Lett* **1991**, *176*, 27.

(65) Watts, J. D.; Gauss, J.; Bartlett, R. J. *J Chem Phys* **1993**, *98*, 8718.

(66) Knowles, P. J.; Hampel, C.; Werner, H.-J. *J Chem Phys* **1994**, *99*, 5219.

(67) MOLRPRO is a package of ab initio programs written by H.-J. Werner and P.J. Knowles, version 2002.6, R.D. Amos, A. Bernhardsson, A. Berning, P. Celani, D.L. Cooper, M.J.O. Deegan, A.J. Dobbyn, F. Eckert, C. Hampel, G. Hetzer, P.J. Knowles, T. Korona, R. Lindh, A.W. Lloyd, S.J. McNicholas, F.R. Manby, W. Meyer, M.E. Mura, A. Nicklass, P. Palmieri, R. Pitzer, G. Rauhut, M. Schütz, U. Schumann, H. Stoll, A.J. Stone, R. Tarroni, T. Thorsteinsson, and H.-J. Werner.

(68) Peterson, K. A.; Woon, D. E.; Dunning, T. H., Jr. *J Chem Phys* **1994**, *100*, 7410.

(69) Feller, D.; Peterson, K. A. *J Chem Phys* **1999**, *110*, 8384.

(70) Halkier, A.; Helgaker, T.; Jørgensen, P.; Klopper, W.; Koch, H.; Olsen, J.; Wilson, A. K. *Chem Phys Lett* **1998**, *286*, 243.

(71) Helgaker, T.; Klopper, W.; Koch, H.; Noga, J. *J Chem Phys* **1997**, *106*, 9639.

(72) Senekowitsch, J. PhD. Thesis, Universität Frankfurt, Frankfurt, Germany, 1988.

(73) Dunham, J. L. *Phys Rev* **1932**, *41*, 721.

(74) Peterson, K. A., the additional core-correlating functions for Br and I are available upon request.

(75) Peterson, K. A.; Dunning, T. H. J. *J Chem Phys* **2002**, *117*, 1.

(76) Douglas, M.; Kroll, N. M. *Ann Phys* **1974**, *82*, 89.

(77) Jansen, G.; Hess, B. A. *Phys Rev A* **1989**, *39*, 6016.

(78) de Jong, W. A.; Harrison, R. J.; Dixon, D. A. *J Chem Phys* **2001**, *114*, 48.

(79) Metz, B.; Stoll, H.; Dolg, M., Private communication.

(80) Bergner, A.; Dolg, M.; Küchle, W.; Stoll, H.; Preuß, H. *Mol Phys* **1993**, *80*, 1431.

(81) Dolg, M. PhD. thesis, Universität Stuttgart, Stuttgart, Germany, 1989.

(82) Yabushita, S.; Zhang, Z.; Pitzer, R. M. *J Phys Chem A* **1999**, *103*, 5791.

(83) H. Lischka, R. Shepard, I. Shavitt, R. M. Pitzer, M. Dallos, Th. Müller, P. G. Szalay, F. B. Brown, R. Ahlrichs, H. J. Böhm, A. Chang, D. C. Comeau, R. Gdanitz, H. Dachsel, C. Ehrhardt, M. Ernzerhof, P. Höchtl, S. Irle, G. Kedziora, T. Kovar, V. Parasuk, M. J. M. Pepper, P. Scharf, H. Schiffer, M. Schindler, M. Schüler, M. Seth, E. A. Stahlberg, J.-G. Zhao, S. Yabushita, and Z. Zhang, COLUMBUS, an ab initio electronic structure program, release 5.8 (2001).

(84) Moore, C. E. *Atomic Energy Levels*; NSRDS-NBS 35; Office of Standard Reference Data, National Bureau of Standards: Washington DC, 1971; Vol. 1.

(85) Shepler, B. C.; Peterson, K. A. *J Phys Chem A* **2003**, *107*, 1783.

(86) Berning, A.; Schweizer, M.; Werner, H.-J.; Knowles, P.; Palmieri, P. *Mol Phys* **2000**, *98*, 1823.

(87) Knowles, P. J.; Werner, H.-J. *Chem Phys Lett* **1988**, *145*, 514.

(88) Werner, H.-J.; Knowles, P. J. *J Chem Phys* **1988**, *89*, 5803.

(89) Langhoff, S. R.; Davidson, E. R. *Int J Quantum Chem* **1974**, *8*, 61.

(90) Blomberg, M. R. A.; Siegbahn, P. E. M. *J Chem Phys* **1983**, *78*.

(91) Simons, J. *J Phys Chem* **1989**, *93*, 626.

(92) R.J. Le Roy, LEVEL 7.1: A Computer Program for Solving the Radial Schrödinger Equation for Bound and Quasibound Levels, University of Waterloo Chemical Physics Research Report CP-642R (2000).

(93) Pyykko, P.; Dyall, K. G.; Csaszar, A. G.; Tarczay, G.; Polyansky, O. L.; Tennyson, J. *Phys Rev A* **2001**, *63*, 024502.

(94) Dyall, K. G.; Bauschlicher, C. W. J.; Schwenke, D. W.; Pyykko, P. *Chem Phys Lett* **2001**, *348*, 497.

(95) Pyykko, P.; Zhao, L.-B. *J Phys B: At, Mol Opt Phys* **2003**, *36*, 1469. The fitted function used for the vacuum polarization contribution was $-Z/r * \Sigma_i A_i e^{B_i r^2}$, with coefficients $A_i$ = 3.920306e-03, 2.456215e-03, 3.415589e-03, 1.313118e-03, 6.338558e-04 and exponents $B_i$ = 4.202192e+10, 8.039480e+06, 4.197194e+08, 4.960986e+05, 6.360238e+04, for $i$=1–5, respectively.

(96) Aprà, E. W., T.L.; Straatsma, T.P.; Bylaska, E.J.; de Jong, W.; Hirata, S.; Valiev, M.; Hackler, M.; Pollack, L.; Kowalski, K.; Harrison, R.; Dupuis, M.; Smith, D.M.A; Nieplocha, J.; Tipparaju V.; Krishnan, M.; Auer, A.A.; Brown, E.; Cisneros, G.; Fann, G.; Fruchtl, H.; Garza, J.; Hirao, K.; Kendall, R.; Nichols, J.; Tsemekhman, K.; Wolinski, K.; Anchell, J.; Bernholdt, D.; Borowski, P.; Clark, T.; Clerc, D.; Dachsel, H.; Deegan, M.; Dyall, K.; Elwood, D.; Glendening, E.; Gutowski, M.; Hess, A.; Jaffe, J.; Johnson, B.; Ju, J.; Kobayashi, R.; Kutteh, R.; Lin, Z.; Littlefield, R.; Long, X.; Meng, B.; Nakajima, T.; Niu, S.; Rosing, M.; Sandrone, G.; Stave, M.; Taylor, H.; Thomas, G.; van Lenthe, J.; Wong, A.; Zhang, Z. "NWChem, A Computational Chemistry Package for Parallel Computers, Version 4.7" (2005), Pacific Northwest National Laboratory, Richland, Washington 99352-0999, USA. Richland, WA, 2005.

(97) Kendall, R. A.; Apra, E.; Bernholdt, D. E.; Bylaska, E. J.; Dupuis, M.; Fann, G. I.; Harrison, R. J.; Ju, J.; Nichols, J. A.; Nieplocha, J.; Straatsma, T. P.; Windus, T. L.; Wong, A. T. *Comput Phys Commun* **2000**, *128*, 260.

(98) Nakajima, T.; Hirao, K. *J Chem Phys* **2000**, *113*, 7786.

(99) Peterson, K. A. *Recent Advances in Electron Correlation Methodology*; In: Wilson A.K., Peterson K.A. (eds), ACS, 2005.

(100) Schmidt, M. W.; Baldridge, K. K.; Boatz, J. A.; Elbert, S. T.; Gordon, M. S.; Jensen, J. H.; Koseki, S.; Matsunaga, N.; Nguyen, K. A.; Su, S. J.; Windus, T. L.; Dupuis, M.; Montgomery, J. A. *J Comput Chem* **1993**, *14*, 1347.

(101) Kaupp, M.; von Schnering, H. G. *Inorg Chem* **1994**, *33*, 4179.

(102) Åkesson, R.; Persson, I.; Sandstrom, M.; Wahlgren, U. *Inorg Chem* **1994**, *33*, 3715.

(103) Barone, V.; Bencini, A.; Totti, F.; Uytterhoeven, M. G. *J Phys Chem* **1995**, *99*, 12743.

(104) Spiridonov, V. P.; Gershikov, A. G.; Butayev, B. S. *J Mol Struct* **1979**, *52*, 53.

(105) Feller, D.; Peterson, K. A.; de Jong, W. A.; Dixon, D. A. *J Chem Phys* **2003**, *118*, 3510.

(106) van Lenthe, E.; Snijders, J. G.; Baerends, E. J. *J Chem Phys* **1996**, *105*, 6505.

(107) Radlein, D. S. A. G.; Whitehead, J. C.; Grice, R. *Nature* **1975**, *253*, 37.

(108) Buss, R. J.; Sibener, S. J.; Lee, Y. t. *J Phys Chem* **1983**, *87*, 4840.

(109) Gilles, M. K.; Turnipseed, A. A.; Talukdar, R. K.; Rudich, Y.; Villalta, P. W.; Huey, G. H.; Burkholder, J. B.; Ravishankara, A. R. *J Phys Chem* **1996**, *100*, 14005.

(110) Bedjanian, Y.; Le Bras, G.; Poulet, G. *J Phys Chem A* **1997**, *101*, 4088.

(111) McGrath, M. P.; Rowland, F. S. *J Phys Chem* **1996**, *100*, 4815.

(112) Hassanzadeh, P.; Irikura, K. K. *J Phys Chem A* **1997**, *101*, 1580.

(113) Roszak, S.; Krauss, M.; Alekseyev, A. B.; Liebermann, H.-P.; Buenker, R. J. *J Phys Chem A* **2000**, *104*, 2999.

(114) Chase, M. W., Jr; Davies, C. A.; Downey, J. R., Jr; Frurip, D. J.; McDonald, R. A.; Syverud, A. N. *J Phys Chem Ref Data* **1985**, *14*.

(115) Boese, A. D.; Oren, M.; Atasoylu, O.; Martin, J. M. L.; Kallay, M.; Gauss, J. *J Chem Phys* **2004**, *120*, 4129.

(116) Schuurman, M. S.; Muir, S. R.; Allen, W. D.; Schaefer, H. F. I. *J Chem Phys* **2004**, *120*, 11586.

(117) Dixon, D. A.; de Jong, W. A.; Peterson, K. A.; Christe, K. O.; Schrobilgen, G. J. *J Am Chem Soc* **2005**, *127*, 8627.

(118) Tellinghuisen, J.; Ashmore, J. G. *Chem Phys Lett* **1983**, *102*, 10.

(119) Balabanov, N. B.; Shepler, B. C.; Peterson, K. A. *J Phys Chem A* **2005**, in press.

(120) Martin, F.; Bacis, R.; Churassy, S.; Verges, J. *J Mol Spectrosc* **1986**, *116*, 71.

(121) Nelander, B.; Sablinskas, V.; Dulick, M.; Braun, V.; Bernath, P. F. *Mol Phys* **1998**, *93*, 137.

(122) Willis, R. E., Jr.; Clark, W. W. I. *J Chem Phys* **1980**, *72*, 4946.

(123) Miller, C. E.; Cohen, E. A. *J Chem Phys* **2001**, *115*, 6459.

(124) Malt'sev, A. A.; Selivanov, G. K.; Yampolsky, V. I.; Zavalishin, N. I. *Nature Physical Science* **1971**, *231*, 157.

(125) Martin, F.; Churassy, S.; Bacis, R.; Field, R. W.; Verges, J. *J Chem Phys* **1983**, *79*, 3725.

(126) Wrede, E.; Laubach, S.; Schulenburg, S.; Orr-Ewing, A. J.; Ashfold, M. N. R. *Chem Phys Lett* **2000**, *326*, 22.

(127) King, G. W.; McFadden, R. G. *Chem Phys Lett* **1978**, *58*, 119.

**Table 1: Equilibrium Bond Lengths (Å) and Harmonic Frequencies ($cm^{-1}$)[a,b]**

| Species | | $r_e$ | $\omega_e$ |
|---|---|---|---|
| $X^1\Sigma^+_{0^+}$ | $I_2$ | **2.6643** | **218.1** |
| | | *2.6664*[g] | *214.5*[g] |
| $X^1\Sigma^+_{0^+}$ | IBr | **2.4673** | **272.6** |
| | | *2.4690*[h] | *268.9*[h] |
| $X^1\Sigma^+_{0^+}$ | ICl | **2.3169** | **391.8** |
| | | *2.3210*[i] | *384.3*[i] |
| $X^2\Pi_{3/2}$ | IO | **1.8666** | **685.7** |
| | | *1.8676*[j] | *681.7*[j] |
| $X^2\Sigma^+_{1/2}$ | HgI | **2.7075** | **132.4** |
| | | --- | *125.4*[l] |
| $X^2\Sigma^+_{1/2}$ | HgBr | **2.4976** | **192.7** |
| | | --- | *188.3*[m] |
| $X^2\Sigma^+_{1/2}$ | HgCl | **2.3541** | **299.8** |
| | | --- | *299.0*[n] |
| $\Omega=0^+$ | HgO | **1.9184** | **231.0**[c] |

| | | $R_e$ (Hg-I) | $R_e$ (Hg-X) | $\omega_e$ (Hg-I)[d] | $\omega_e$ (bend)[e] | $\omega_e$ (Hg-X)[f] |
|---|---|---|---|---|---|---|
| $X^1\Sigma^+_{g,0^+}$ | $HgI_2$ | **2.5460** | | **163.7** | **53.7** | **240.5** |
| | | *2.554*[k] | | *155*[o], *158*[p], *163.5*[q], *156*[k] | *63*[r], *51*[s] *51*[k] | *237.5*[q], *235*[k] |
| $X^1\Sigma^+_{0^+}$ | HgIBr | **2.5343** | **2.3785** | **188.0** | **62.2** | **278.1** |
| | | --- | --- | *182*[o], *187.6*[q] | *66*[r], *60*[s] | *266*[o], *272.0*[q] |
| $X^1\Sigma^+_{0^+}$ | HgICl | **2.5261** | **2.2558** | **206.2** | **79.5** | **388.4** |
| | | --- | --- | *196*[o], *201.5*[q] | *83.5*[r], *85*[r], *74*[s] | *371*[o], *378.0*[q] |
| $X^2\Pi_{3/2}$ | HgIO | **2.5214** | **1.9617** | **211.9** | **120.5** | **584.5** |

a) Values are calculated at the CCSD(T)/CBS+CV+SO+SR level of theory. See text for explanation.
b) Experimental values in italics. c) For HgO, this is the fundamental vibrational frequency, not the harmonic vibrational frequency. d) For $HgI_2$ this is the $\Sigma_g$ symmetric stretch. e) CBS limits for bending frequencies use DZ-QZ basis sets. f) For $HgI_2$ this is the $\Sigma_u$ asymmetric stretch. g) Reference [120]. h) Reference [121]. i) Reference [122]. j) Reference [123]. k) Reference 104 frequencies are harmonic. l) Reference 36. m) Reference 34. n) Reference 35. o) Reference 45. p) Reference 46. q) Reference 43. r) Reference 42. s) Reference [124].

**Table 2: Relativistic effects on dissociation energies (kcal/mol)[a,b]**

| Molecule | $\Delta E_{SO\text{-}TOTAL}$ | $\Delta E_{SO\text{-}ZERO}$ | $\Delta E_{SO\text{-}diff}$ | $\Delta E_{Lamb}$ | $\Delta E_{SR}$ | $\Delta E_{DK2\text{-}PP}$ | $\Delta E_{DK3\text{-}DK2}$ | $\Delta E_{DK3\text{-}PP}$ | $\Delta E_{REL}$ |
|---|---|---|---|---|---|---|---|---|---|
| HgI | -5.07 | -6.82 | 1.75 | 0.34 | --- | 0.20 | -0.17 | 0.03 | -4.73 |
| HgBr | -2.26 | -3.28 | 1.02 | 0.38 | --- | 0.33 | -0.25 | 0.08 | -1.88 |
| HgCl | 0.00 | -0.86 | 0.86 | 0.41 | -0.21 | 0.44 | -0.30 | 0.14 | 0.20 |
| HgO | 1.65 | -0.20 | 1.45 | 0.35 | -0.11 | 0.23 | -0.29 | -0.06 | 1.89 |
| $I_2$ | -12.01 | -13.64 | 1.63 | 0.09 | --- | -0.21 | -0.01 | -0.22 | -11.92 |
| IBr | -8.93 | -10.10 | 1.17 | 0.06 | --- | -0.11 | 0.00 | -0.11 | -8.87 |
| ICl | -6.46 | -7.68 | 1.22 | 0.04 | -0.14 | -0.10 | 0.00 | -0.10 | -6.56 |
| IO | -3.72 | -6.45 | 2.73 | 0.06 | -0.10 | -0.42 | -0.01 | -0.43 | -3.76 |
| $HgI_2$ | 1.34 | 0.00 | 1.34 | 0.63 | --- | -0.63 | 0.37 | -0.25 | 1.97 |
| HgIBr | 1.32 | 0.00 | 1.32 | 0.64 | --- | -0.65 | 0.39 | -0.25 | 1.96 |
| HgICl | 0.99 | 0.00 | 0.99 | 0.65 | -0.10 | -0.70 | 0.40 | -0.28 | 1.54 |
| HgIO | -0.37 | 0.21 | 0.16 | 0.57 | -0.05 | -0.94 | 0.35 | -0.59 | 0.15 |

a) $\Delta E_{SO\text{-}TOTAL}$ total spin-orbit correction, $\Delta E_{SO\text{-}ZERO}$= spin-orbit correction due to the zero-field splitting of the atoms, IO and HgIO, $\Delta E_{SO\text{-}diff}$=remaining spin-orbit effects calculated from $\Delta E_{SO\text{-}TOTAL}$-$\Delta E_{SO\text{-}ZERO}$, $\Delta E_{Lamb}$=Lamb shift correction, $\Delta E_{SR}$=mass-velocity + Darwin correction for Cl and O atoms, $\Delta E_{DK2\text{-}PP}$ = difference between reaction enthalpies calculated with pseudopotentials and the 2nd order DKH Hamiltonian, $\Delta E_{DK3\text{-}DK2}$= difference between enthalpies calculated with 2nd and 3rd or DKH Hamiltonians, $\Delta E_{DK3\text{-}PP}$= $\Delta E_{DK2\text{-}PP}$+$\Delta E_{DK3\text{-}DK2}$, $\Delta E_{REL}$= $\Delta E_{SO\text{-}TOTAL}$+$\Delta E_{Lamb}$+$\Delta E_{SR}$. b) For the triatomic molecules the reaction HgIX→Hg+IX was used.

**Table 3: Dissociation energies for the diatomic molecules of this study (kcal/mol)[a]**

| Molecule | $D_e$(QZ) | $\Delta E_e$(CBS-QZ) | $\Delta E_{ZPE}$ | $\Delta E_{CV}$ | $\Delta E_{CV\text{-}f}$ | $\Delta E_{REL}$ | $\Delta E_{CCSDTQ}$ | $D_0$(Theory) | $D_0$(Exp) |
|---|---|---|---|---|---|---|---|---|---|
| HgI | 12.41 | 0.96 | -0.19 | 0.26 | -0.16 | -4.73 | ---[j] | 8.55 | 7.83±0.11[b] |
| HgBr | 17.60 | 1.00 | -0.28 | -0.20 | -0.19 | -1.88 | 0.25 | 16.30 | 15.53±0.29[c] |
| HgCl | 22.77 | 1.12 | -0.43 | -0.55 | -0.20 | 0.20 | ---[j] | 22.91 | 23.44[d] |
| HgO | 1.77 | 1.13 | -0.62 | 0.19 | -0.04 | 1.89 | ---[j] | 4.32 | --- |
| $I_2$ | 45.34 | 2.18 | -0.31 | 0.75 | --- | -11.92 | ---[j] | 36.04 | 35.57[e] |
| IBr | 48.90 | 2.05 | -0.39 | 0.47 | --- | -8.87 | 0.01 | 42.17 | 41.93[f] |
| ICl | 54.49 | 2.04 | -0.56 | 0.10 | --- | -6.56 | ---[j] | 49.51 | 49.65[g] |
| IO | 56.22 | 1.49 | -0.98 | 0.16 | --- | -3.76 | 1.18 | 54.31 | 53[h], 56.4[i] |

a) $D_e$(QZ) = equilibrium dissociation energy calculated with the aVQZ basis set, $\Delta E_e$(CBS-QZ) = difference between aVQZ and CBS CCSD(T) equilibrum dissociation energies, $\Delta E_{ZPE}$ = zero-point energy contribution, $\Delta E_{CV}$ = core-valence contribution from Hg 5*s*5*p*, Br 3*s*3*p*3*d*, and I 4*s*4*p*4*d* $\Delta E_{CV\text{-}f}$=core-valence contribution from Hg 4*f*, $\Delta E_{REL}$ = total relativistic corrections from Table 2, $\Delta E_{CCSDTQ}$ = correction for full iterative triple and quadruple excitations. See text. b) Reference 36. c) Reference 118. d) Reference 35 this is a rough upper bound. e) $D_0$=12440.083±0.145 $cm^{-1}$ from reference [125]. f) $D_0$=14663.8±0.19 $cm^{-1}$ from reference [126]. g) $D_0$=17365.804±0.150 $cm^{-1}$ from reference [127]. h) Reference 107. i) Reference 110. j) Not determined.

**Table 4: 0K enthalpies of reaction, $\Delta H_r$ (kcal/mol), with constituent energy contributions[a]**

| Reaction | | $\Delta E_e$(QZ) | $\Delta E_e$ (CBS-QZ) | $\Delta E_{ZPE}$ | $\Delta E_{CV}$ | $\Delta E_{CV\text{-}f}$ | $\Delta E_{REL}$ | $\Delta E_{CCSDTQ}$ | $\Delta H_r$ | expt[b] |
|---|---|---|---|---|---|---|---|---|---|---|
| $Hg + I_2$ | → HgI + I | 32.92 | 1.22 | -0.12 | 0.48 | 0.16 | -7.19 | ---[e] | 27.47 | 27.74 ± 0.11 |
| | → $HgI_2$ | -32.37 | -0.25 | 0.42 | -0.88 | 0.07 | -1.97 | ---[e] | -34.98 | -33.4 ± 0.5[c] |
| Hg + IBr | → HgI + Br | 36.49 | 1.08 | -0.20 | 0.21 | 0.16 | -4.14 | 0.01 | 33.61 | 34.10 ± 0.11 |
| | → HgBr + I | 31.30 | 1.04 | -0.11 | 0.67 | 0.19 | -6.99 | -0.24 | 25.86 | 26.40 ± 0.29 |
| | → HgIBr | -36.05 | -0.43 | 0.46 | -0.64 | 0.07 | -1.96 | 0.01 | -38.54 | --- |
| Hg + ICl | → HgI + Cl | 42.08 | 1.08 | -0.36 | -0.16 | 0.16 | -1.83 | ---[e] | 40.97 | 41.82 ± 0.11 |
| | → HgCl + I | 31.73 | 0.92 | -0.13 | 0.65 | 0.20 | -6.76 | ---[e] | 26.61 | 26.21 |
| | → HgICl | -37.54 | -0.57 | 0.52 | -0.64 | 0.07 | -1.54 | ---[e] | -39.70 | --- |
| Hg + IO | → HgI + O | 43.80 | 0.54 | -0.79 | -0.10 | 0.16 | 0.97 | 1.18 | 45.76 | 45 ± 3[d] |
| | → HgO + I | 54.45 | 0.37 | -0.36 | -0.04 | 0.04 | -5.65 | 1.18 | 49.99 | --- |
| | → HgIO | -12.28 | -0.52 | 0.50 | -0.99 | 0.02 | -0.15 | 1.18 | -12.24 | --- |

a) $\Delta E_e$ = CCSD(T) electronic energy difference, $\Delta E_{ZPE}$ = zero-point energy contribution, $\Delta E_{CV}$ = core-valence contribution from Hg 5*s*5*p,* Br 3*s*3*p*3*d*, and I 4*s*4*p*4*d*, $\Delta E_{CV\text{-}f}$ =core-valence contribution from Hg 4*f*, $\Delta E_{REL}$ = relativistic corrections from Table 2, $\Delta E_{CCSDTQ}$ = correction for full iterative triple and quadruple excitations. See text. b) All experimental data taken from Table 2, except were noted. c) $\Delta H_f$ of $HgI_2$ from Reference 114. d) $\Delta H_f$ of IO derived from Reference 107. e) Not determined.

**Table 5: Dissociation energies and 0K heats of formation in kcal/mol for HgIX species[a]**

| IHgX | $D_0$(IHg+X) | $D_0$(I+HgX) | $\Delta H_f$ (calc) | $\Delta H_f$ (exp) |
|---|---|---|---|---|
| IHgI | --- | 62.47 | -3.91 | -2.35±0.50[b] |
| IHgBr | 72.15 | 64.40 | -11.21 | --- |
| IHgCl | 80.67 | 66.31 | -19.71 | --- |
| IHgO | 58.00 | 62.23 | 33.46 | --- |

a) Computed from the reaction enthalpies in Table 4 and accurate experimental heats of formation.

b) Reference 114.

# Ab initio characterization of the mercury hypohalites: XHgOY (X, Y = Br, Cl)

**Benjamin C. Shepler, Nikolai B. Balabanov and Kirk A. Peterson***

*Department of Chemistry, Washington State University, Pullman, Washington 99164-4630*

**Abstract**

Reactions between mercury and halogen species have been implicated in the increases of mercury contamination in the Arctic and the springtime atmospheric mercury depletion events that may be responsible for this contamination. One of the possible products of the reaction HgX + YO (X, Y = Br, Cl) are mercury hypohalites with the formula XHgOY. The molecules BrHgOBr, BrHgOCl, ClHgOBr, and ClHgOCl have been characterized for the first time in the gas phase by accurate ab intio calculations using the coupled cluster singles and doubles method with a perturbative correction for triple excitations [CCSD(T)] and sequences of correlation consistent basis sets. Relativistic pseudopotentials have been used to account for scalar relativistic effects and corrections have been added for core-valence correlation and spin-orbit coupling. Preliminary electronic spectra have been calculated with the linear response coupled cluster method [LR-CCSD] for BrHgOBr, and the other hypohalites should exhibit similar spectra. These hypohalites are all stable by approximately 50 kcal/mol with respect to the two possible dissociation product channels: HgX + YO and XHgO + Y.

## I. INTRODUCTION

Gas phase reactions of mercury with Br and BrO have been proposed as the cause of rapid episodic depletions of the tropospheric mercury concentration during polar sunrise.[1-5] It is expected that gaseous elemental mercury is oxidized to some form of reactive gaseous mercury (RGM) that is then deposited on the snow pack.[3,6,7] Accurate ab initio calculations[8-11] have shown that the direct gas phase reaction of Hg with BrO under atmospheric conditions can not be responsible for the mercury depletion events. The possible products of this reaction are:

$$\mathrm{Hg} + \mathrm{BrO} \rightarrow \begin{cases} \mathrm{HgO} + \mathrm{Br} & (1) \\ \mathrm{HgBr} + \mathrm{O} & (2) \\ \mathrm{HgBrO} & (3) \\ \mathrm{HgOBr} & (4) \\ \mathrm{BrHgO} & (5) \end{cases}$$

Reactions (1) and (2) are endothermic by 40.4 and 51.6 kcal/mol respectively and HgBrO and HgOBr have only shallow van der Waals minima so reactions (3) and (4) will be endothermic by approximately 55 kcal/mol ($D_0$ of BrO is 55.8 kcal/mol)[12]. Reaction (5) is exothermic by -20.2 kcal/mol, but there is a large barrier to insertion (~40 kcal/mol)[9] of Hg into the BrO bond making this reaction also unlikely to occur in the atmosphere.

It is more likely that the mercury initially undergoes recombination with bromine atoms to form HgBr as this reaction is exothermic and fast enough to account for the observed mercury depletions.[2,10,13] Once formed this HgBr has many possible routes for further reaction and one of those is the reaction with BrO. One possible product of this reaction is the formation of mercury hypohalites of the form XHgOY. Calvert and Lindberg[5] were the first to propose that these mercury hypohalites might play a role in the depletions of atmospheric mercury and suggest they are a significant component of RGM. However, these molecules have never been studied in the gas phase by theory or experiment.

The goal of this work has been to use accurate ab initio methods to characterize the mercury hypohalites BrHgOBr, BrHgOCl, ClHgOBr, and ClHgOCl. The structures and vibrational frequencies have been calculated as well as the heats of reaction for HgX + YO → XHgOY. Preliminary calculations of the electronic spectra have also been carried out for BrHgOBr, and the spectra of the other hypohalites should be similar.

## II. METHODOLOGY

To account for scalar relativistic effects small-core energy consistent pseudopotentials (PP) of the Stuttgart-Köln type were used on the Hg and Br atoms.[14,15] These pseudopotentials replace 60 electrons of the mercury atom leaving the $5s^2 5p^6 5d^{10} 6s^2$ electrons to be treated explicitly and 10 of the bromine electrons leaving the $3s^2 3p^6 3d^{10} 4s^2 4p^5$ electrons. The basis sets used were from the correlation consistent family of basis sets. The aug-cc-pVnZ-PP[15,16] basis sets were used on Hg and Br and were optimized for use with the pseudopotentials. The aug-cc-pV(n+d)Z[17] basis sets that contain modified d-shells containing additional tight exponents were used on Cl and the standard aug-cc-pVnZ[18] sets used for O. Henceforth these basis sets will be denoted aVnZ.

Geometry optimizations were carried out for BrHgOBr, BrHgOCl, ClHgOBr, ClHgOCl, HgBr, HgCl, BrO, and ClO with the coupled cluster singles and doubles method with a perturbative treatment of triple excitations [CCSD(T)] [19-21] and employed the aVQZ basis sets. For the open shell species the R/UCCSD(T)[21-23] method was used, i.e., reference wave functions were determined from ROHF calculations but the spin restriction was relaxed during the solution of the coupled cluster equations. An additional CCSD(T) calculation was then carried out at the CCSD(T)/aVQZ optimized geometries with the aV5Z basis set. The energies computed with the

aVQZ and aV5Z at the equilibrium geometry were then extrapolated to get an estimate of the energy at the complete basis set limit using formula (6).[24,25]

$$E(n) = E_{\mathrm{CBS}} + B/n^3. \tag{6}$$

A correction for core-valence correlation was then calculated at the aVQZ optimized geometry. This involved two CCSD(T) calculations with the first correlating only the valence electrons and in the second all electrons (except the Cl 1s) were correlated. The core-valence correction was then taken as the difference between these two energies. The basis sets used in these calculations were the aug-cc-pwCVTZ-PP[16,26] for Hg and Br, and aug-cc-pwCVTZ[27] for Cl and O.

The final correction was to account for spin-orbit coupling. For the Hg and Br atoms the one-electron spin-orbit operators were taken from the PPs described above. Large core PP's of the Stuttgart/Köln variety were also used on O and Cl for the SO calculations. The aVTZ basis sets were used for the Cl and O atoms, but they were recontracted in the presence of the PPs. The spin-orbit correction was computed at the CISD/aVTZ level of theory using the spin-orbit CI approach.[28] The spin-orbit correction was calculated as the energy difference between a CISD calculation without the SO operator and a SO-CISD calculation that mixed all singlet and triplet (or doublet and quartet) configurations by the effective 1-electron spin-orbit operators of the pseudopotentials.

The harmonic vibrational frequencies were calculated with second-order Møller-Plesset perturbation theory (MP2)[29] using the aVTZ basis sets. Zero point energy corrections were calculated from the harmonic frequencies as $1/2\sum\omega_e$.

Finally, the linear response coupled cluster singles and doubles method (LR-CCSD)[30] with the aVTZ basis sets has been used to compute the vertical excitation spectra of BrHgOBr. Oscillator strengths between the ground state of BrHgOBr ($X^1A'$) and singlet excited states were

also computed at the LR-CCSD/aVTZ level of theory. Oscillator strengths between the ground state and excited triplet states were computed using the full Breit-Pauli spin-orbit operator with the linear response multiconfigurational self-consistent field method (LR-MCSCF)[31] with an active space that consisted of 32 electrons in 18 orbital (full valence). The aVTZ basis sets were again used in the LR-MCSCF calculations. Also, preliminary MCSCF[32,33]/aVTZ calculations have been carried out for the ground and excited states of the reactions HgX + YO → XHgOY and XHgO + Y → XHgOY to determine if there is a barrier in either of these recombination reactions.

The spin-orbit calculations were carried out with the Columbus suite of ab initio programs.[34] The DALTON[35] computational chemistry package was used for the linear response calculations of the excitation energies and oscillator strengths. MOLPRO[36] was used for all other calculations.

## III. RESULTS AND DISCUSSION

The calculated structures (bond lengths and angles) of BrHgOBr, BrHgOCl, ClHgOBr and ClHgOCl computed at the CCSD(T)/aVQZ level of theory are provided in Table 1 and BrHgOBr is shown pictorially in Figure 1. All of the mercury hypohalites have similar structures with the primary differences being simply the fact that the Cl containing bonds are approximately 0.2 $a_0$ shorter than their Br containing counterparts. The X-Hg-O angle is nearly 180°, and is in all cases very close to 177.5°. The Hg-O-X angle is in all cases somewhat greater than 90°. The X-Hg-O-Y dihedral angle is 180° which gives the molecules $C_s$ symmetry, but with X-Hg-O being nearly linear it only requires 0.3 kcal/mol for a complete 360° rotation of this dihedral angle. The Hg-X bonds are approximately 0.2 $a_0$ shorter than their values in gas phase

HgBr (4.713 $a_0$)[10] and HgCl (4.449)[37] and the Hg-O bonds are approximately 0.15 $a_0$ longer than the bond length of gas phase HgO (3.625 $a_0$)[37]. Both the Hg-X and Hg-O bond lengths are very similar to the lengths they have in BrHgO (4.464 and 3.703 $a_0$) and ClHgO (4.230 and 3.688 $a_0$).[38] With a difference of 0.3 $a_0$ the O-Y bonds are significantly longer than the bond lengths of gas phase ClO (2.965 $a_0$)[39] and BrO (3.245 $a_0$).[40] The harmonic vibrational frequencies computed at the MP2/aVTZ level of theory are provided in Table 2.

Heats of reaction at 0K for the reactions HgX + YO → XHgOY computed at the CCSD(T)/CBS+CV+SO level of theory are presented in Table 3 along with the constituent energy corrections. The heats of reaction are all very similar at approximately -50 kcal/mol with the most exothermic reaction being HgCl + BrO → ClHgOBr at -55.77 kcal/mol and the least exothermic reaction being HgBr + ClO → BrHgOCl at -50.75 kcal/mol. The various energy corrections are also similar in size and magnitude for all four reactions. The CBS extrapolation increases the exothermicity by ~0.4 kcal/mol with the two reactions involving BrO having a slightly larger correction than the two reactions involving ClO. The core-valence correction is fairly small for these reactions never having a magnitude larger than 0.15 kcal/mol. Spin-orbit coupling is the largest correction and in all cases decreases the exothermicity of the reaction by between 0.6 – 1.5 kcal/mol. This is primarily due to the significant zero-field splitting of the BrO (975 $cm^{-1}$)[40] and ClO (322 $cm^{-1}$)[39] molecules, and the effect in the reactions involving BrO is not surprisingly several tenths of a kcal/mol larger than in ClO.

Two competing channels to the formation of XHgOY in the reaction of HgX + YO are:

$$\mathrm{HgX} + \mathrm{YO} \rightarrow \begin{cases} \mathrm{XHgY} + \mathrm{O} & (7) \\ \mathrm{XHgO} + \mathrm{Y}. & (8) \end{cases}$$

Exchange reactions of the type HgX + YO → HgO + XY are also possible, but are unlikely to occur in the atmosphere because they are all endothermic by greater than 20 kcal/mol due to the greater dissociation energies of YO and HgX than XY and HgO.[12,37,41-43] $\Delta H_r(0K)$ are given for reactions 7 and 8 along with the enthalpies for the formation of the mercury hypohalites in Table 4. An energy level diagram for these reactions in the HgBr + BrO system is shown in Figure 2. The enthalpies for reactions 7 and 8 were derived from prior accurate ab initio calculations.[37,44] In all cases the formation of the hypohalites is more exothermic than either reaction 7 or 8. Reactions between HgX + YO to form XHgY + O are all exothermic by ~20 kcal/mol. The product channel XHgO + Y on the other hand is nearly isoenergetic with the XHg + YO reactants. The two reactions of this type involving HgBr are slightly exothermic by -4.3 and -5.7 kcal/mol while the two reactions involving HgCl are endothermic by 2.7 and 1.3 kcal/mol.

The significant exothermicity for the formation of the mercury hypohalites from the reactions HgX + YO → XHgOY or XHgO + Y → XHgOY imply they could play an important role in the atmospheric mercury depletion events and be major components of RGM. However, if there is a larger barrier associated with their formation, as is the case for the Hg + BrO reaction, then the formation of mercury hypohalites under atmospheric conditions will be significantly less likely. Potential curves for the ground and low-lying excited states ($2^1A'$, $1^1A''$, $1^3A'$, $1^3A''$) for the reaction HgBr + BrO → BrHgOBr are shown in Figure 3 while the potential curves for the reaction BrHgO + Br are shown in Figure 4. In these figures all geometrical parameters have been frozen at their values in the CCSD(T)/aVQZ equilibrium structure except the Hg-O bond in Figure 3 and the O-Br bond in Figure 4. It is clear from both of these figures that reaction on the ground $X^1A'$ state *will be barrier-less* for both reactions. These figures also shows that the excited $1^3A''$ state is also stable with respect to HgBr + BrO

and slightly lower than the BrHgO + Br channel at this level of theory. There appears to be a barrier on the $1^3A''$ surface for the HgBr + BrO reaction, but it is possible that the inclusion of dynamic electron correlation and removal of the restrictions on the geometry will change this. These changes are also likely to change energy of the minimum of the $1^3A''$ state with respect to the two asymptotes. While the other excited states are not bound with respect to the BrHgO + Br channel at the MCSCF/aVTZ level of theory inclusion of electron correlation could change this as well. With atoms as heavy as bromine and mercury the effects of spin-orbit coupling should make for very interesting dynamics between the ground and excited states in both dissociation/recombination channels.

Vertical excitation energies and oscillator strengths between the ground and several low-lying excited states of BrHgOBr computed at the LR-CCSD/aVTZ level of theory (triplet oscillator strengths with LR-MCSCF/aVTZ) are given in Table 4. UV radiation with wavelengths shorter than 290 nm is unlikely to be prevalent in the troposphere, but five of the excited states ($2^1A'$, $1^1A''$, $1^3A'$, $1^3A''$, $2^3A''$) have vertical excitation energies that would place their absorption near or above this limit. It is difficult to directly compare the oscillator strengths of the singlets and triplets because they were computed at different levels of theory. The vertical excitation energy of the $1^3A''$ state would place it right at the dissociation limit of the two possible product channels. As this state is likely to have an equilibrium geometry different than the ground state this excitation energy seems to confirm that the $1^3A''$ state is likely to be stable with respect to dissociation as was suggested by the MCSCF results. An optimization on the $1^3A''$ state at the CCSD/aVDZ level of theory found an equilibrium structure of r(Hg-Br) = 4.526 $a_0$, r(Hg-O) = 3.834 $a_0$, r(O-Br) = 4.228 $a_0$, a Br-Hg-O angle of 179°, and an Hg-O-Br angle of

99°. At this level of theory the state was bound by 9.9 kcal/mol with respect to HgBr + BrO and by 3.8 kcal/mol with respect to BrHgO + Br. The structure is similar to the ground state in that the Br-Hg-O angle is nearly 180° and the Hg-O-Br angle is near 90°. The Hg-Br and Hg-O bond lengths are also comparable to the ground state but the O-Br bond is considerably stretched being 0.7 $a_0$ longer than in the ground state.

## IV. CONCLUSIONS

In this work the XHgOY (X, Y = Cl, Br) mercury hypohalites have been characterized for the first time. The geometries were optimized at the CCSD(T)/aVQZ level of theory and harmonic vibrational frequencies computed at the MP2/aVTZ level of theory. 0K reaction enthalpies for the reaction HgX + YO → XHgOY were computed at the CCSD(T)/CBS+CV+SO level of theory. Each of the mercury hypohalites was found to be bound by at least 50 kcal/mol with respect to reactants. They were also found to be bound by about the same amount with respect to the XHgO + Y dissociation channel. MCSCF/aVTZ calculations indicate that the mercury hypohalites will be formed in a barrier-less reaction from either HgX + YO or XHgO + Y reactants. The thermochemistry presented here indicates these species can be formed in the atmosphere and support the hypothesis[5] that they may be a major component of the RGM formed during mercury depletion events.

Vertical excitation spectra have been computed at the LR-CCSD level of theory for a number of low-lying excited states of the BrHgOBr molecule. The $1^3A''$ excited state is particularly interesting because it also appears to be bound with respect to the HgBr + BrO and BrHgO + Br dissociation channels by 10 and 4 kcal/mol respectively. In addition to the ground

state this excited state may also play a role in the atmospheric chemistry of mercury hypohalite species.

## REFERENCES


(1) Ariya, P. A.; Dastoor, A. P.; Amyot, M.; Schroeder, W. H.; Barrie, L. A.; Anlauf, K.; Raofie, F.; Ryzhkov, A.; Davignon, D.; Lalonde, J.; Steffen, A. *Tellus* **2004**, *56B*, 397.

(2) Ariya, P. A.; Khalizov, A. F.; Gidas, A. *Journal of Physical Chemistry A* **2002**, *106*, 7310.

(3) Lindberg, S. E.; Brooks, S.; Lin, C.-J.; Scott, K. J.; Landis, M. S.; Stevens, R. K.; Goodsite, M.; Richter, A. *Environmental Science and Technology* **2002**, *36*, 1245.

(4) Raofie, F.; Ariya, P. A. *Environmental Science and Technology* **2004**, *38*, 4319.

(5) Calvert, J. G.; Lindberg, S. E. *Atmospheric Environment* **2003**, *37*, 4467.

(6) Lindberg, S. E.; Stratton, W. J. *Environmental Science and Technology* **1998**, *32*, 49.

(7) Lu, J. Y.; Schroeder, W. H.; Barrie, L. A.; Steffen, A.; Welch, H. E.; Martin, K.; Lockhart, L.; Hunt, R. V.; Boila, G.; Richter, A. *Geophysical Research Letters* **2001**, *28*, 3219.

(8) Balabanov, N. B.; Peterson, K. A. *Journal of Physical Chemistry A* **2003**, *107*, 7465.

(9) Balabanov, N. B.; Shepler, B. C.; Peterson, K. A. *Journal of Physical Chemistry A* **2005**, *109*, 8765.

(10) Shepler, B. C.; Balabanov, N. B.; Peterson, K. A. *In preparation* **2006**.

(11) Shepler, B. C.; Peterson, K. A. *Journal of Physical Chemistry A* **2003**, *107*, 1783.

(12) Kim, H.; Dooley, K. S.; Johnson, E. R.; North, S. W. *Journal of Chemical Physics* **2006**, *124*, 134304.

(13) Khalizov, A. F.; Viswanathan, B.; Larregaray, P.; Ariya, P. A. *Journal of Physical Chemistry A* **2003**, *107*, 6360.

(14) Figgen, D.; Rauhut, G.; Dolg, M.; Stoll, H. *Chemical Physics* **2004**, *311*, 227.

(15) Peterson, K. A.; Figgen, D.; Goll, E.; Stoll, H.; Dolg, M. *Journal of Chemical Physics* **2003**, *119*, 11113.

(16) Peterson, K. A.; Puzzarini, C. *Theoretical Chemistry Accounts* **2005**, accepted.

(17) Dunning, T. H. J.; Peterson, K. A.; Wilson, A. K. *Journal of Chemical Physics* **2001**, *114*, 9244.

(18) Kendall, R. A.; Dunning, T. H., Jr.; Harrison, R. J. *Journal of Chemical Physics* **1992**, *96*, 6796.

(19) Purvis, G. D. I.; Bartlett, R. J. *Journal of Chemical Physics* **1982**, *76*, 1910.

(20) Raghavachari, K.; Trucks, G. W.; Pople, J. A.; Head-Gordon, M. *Chemical Physics Letters* **1989**, *156*, 479.

(21) Watts, J. D.; Gauss, J.; Bartlett, R. J. *Journal of Chemical Physics* **1993**, *98*, 8718.

(22) Scuseria, G. E. *Chemical Physics Letters* **1991**, *176*, 27.

(23) Knowles, P. J.; Hampel, C.; Werner, H.-J. *Journal of Chemical Physics* **1994**, *99*, 5219.

(24) Halkier, A.; Helgaker, T.; Jørgensen, P.; Klopper, W.; Koch, H.; Olsen, J.; Wilson, A. K. *Chemical Physics Letters* **1998**, *286*, 243.

(25) Helgaker, T.; Klopper, W.; Koch, H.; Noga, J. *Journal of Chemical Physics* **1997**, *106*, 9639.

(26) The following exponents were added to the cc-pVTZ-PP basis set of Br to form a cc-pwCVTZ-PP set: 2s (7.0742, 2p (10.1642, 2.1057), 2d (4.1557, 1.8326), 2f (8.3131, 2.1829), and 1g (2.5365).

(27) Peterson, K. A.; Dunning, T. H. J. *Journal of Chemical Physics* **2002**, *117*, 1.

(28) Yabushita, S.; Zhang, Z.; Pitzer, R. M. *Journal of Physical Chemistry A* **1999**, *103*, 5791.

(29) Møller, C.; Plesset, M. S. *Physical Reviews* **1934**, *46*, 618.

(30) Christiansen, O.; Koch, H.; Halkier, A.; Jorgensen, P.; Helgaker, T.; Meras, D. *Journal of Chemical Physics* **1996**, *105*, 6921.

(31) Olsen, J.; Jorgensen, P. In *Modern Electronic Structure Theory*; Yarkony, D. R., Ed.; World Scientific: Singapore, 1995; Vol. 2; pp 857.

(32) Knowles, P. J.; Werner, H.-J. *Chemical Physics Letters* **1985**, *115*, 259.

(33) Werner, H.-J.; Knowles, P. J. *Journal of Chemical Physics* **1985**, *82*, 5053.

(34) Lischka, H. H. Lischka, R. Shepard, I. Shavitt, R. M. Pitzer, M. Dallos, Th. Müller, P. G. Szalay, F. B. Brown, R. Ahlrichs, H. J. Böhm, A. Chang, D. C. Comeau, R. Gdanitz, H. Dachsel, C. Ehrhardt, M. Ernzerhof, P. Höchtl, S. Irle, G. Kedziora, T. Kovar, V. Parasuk, M. J. M. Pepper, P. Scharf, H. Schiffer, M. Schindler, M. Schüler, M. Seth, E. A. Stahlberg, J.-G. Zhao, S. Yabushita, and Z. Zhang, COLUMBUS, an ab initio electronic structure program, release 5.8 (2001).

(35) Dalton, a molecular electronic structure program, Release 1.2 (2001), written by T. Helgaker, H. J. Aa. Jensen, P. Joergensen, J. Olsen, K. Ruud, H. Aagren, A.A. Auer, K.L. Bak, V. Bakken, O. Christiansen, S. Coriani, P. Dahle, E. K. Dalskov, T. Enevoldsen, B. Fernandez, C. Haettig, K. Hald, A. Halkier, H. Heiberg, H. Hettema, D. Jonsson, S. Kirpekar, R. Kobayashi, H. Koch, K. V. Mikkelsen, P. Norman, M. J. Packer, T. B. Pedersen, T. A. Ruden, A. Sanchez, T. Saue, S. P. A. Sauer, B. Schimmelpfennig, K. O. Sylvester-Hvid, P. R. Taylor, and O. Vahtras, 2001.

(36) MOLRPRO is a package of ab initio programs written by H.-J. Werner and P.J. Knowles, version 2002.6, R.D. Amos, A. Bernhardsson, A. Berning, P. Celani, D.L. Cooper, M.J.O. Deegan, A.J. Dobbyn, F. Eckert, C. Hampel, G. Hetzer, P.J. Knowles, T. Korona, R. Lindh, A.W. Lloyd, S.J. McNicholas, F.R. Manby, W. Meyer, M.E. Mura, A. Nicklass, P. Palmieri, R. Pitzer, G. Rauhut, M. Schütz, U. Schumann, H. Stoll, A.J. Stone, R. Tarroni, T. Thorsteinsson, and H.-J. Werner.

(37) Shepler, B. C.; Balabanov, N. B.; Peterson, K. A. *Journal of Physical Chemistry A* **2005**, *109*, 10363.

(38) Balabanov, N. B.; Peterson, K. A. *Journal of Chemical Physics* **2004**, *120*, 6585.

(39) Drouin, B. J.; Miller, C. E.; Cohen, E. A.; Wagner, G.; Birk, M. *Journal of Molecular Spectroscopy* **2001**, *207*, 4.

(40) Drouin, B. J.; Miller, C. E.; Muller, H. S. P.; Cohen, E. A. *Journal of Molecular Spectroscopy* **2001**, *205*, 128.

(41) Coxon, J. A.; Ramsay, D. A. *Canadian Journal of Physics* **1976**, *54*, 1034.

(42) Gerstenkorn, S.; Luc, P. *Journal de physique* **1989**, *50*, 1417.

(43) Huber, K. P.; Herzberg, G. *Molecular Spectra and Molecular Structure IV. Constants of Diatomic Molecules*; Van Nostrand: Princeton, 1979.

(44) Balabanov, N. B.; Peterson, K. A. *Journal of Chemical Physics* **2003**, *119*, 12271.

Table 1: Bond lengths ($a_0$) and angles of the mercury hypohalites computed at the CCSD(T)/aVQZ level of theory.

| | R(XHg) | R(HgO) | R(OY) | ∠ (XHgO)° | ∠ (HgOY)° |
|---|---|---|---|---|---|
| BrHgOBr | 4.480 | 3.778 | 3.487 | 177.4 | 110.2 |
| BrHgOCl | 4.478 | 3.785 | 3.219 | 177.7 | 109.6 |
| ClHgOBr | 4.242 | 3.760 | 3.488 | 177.4 | 110.3 |
| ClHgOCl | 4.239 | 3.766 | 3.220 | 177.6 | 109.7 |

Table 2: Harmonic vibrational frequencies ($cm^{-1}$) of the mercury hypohalites computed at the MP2/aVTZ level of theory.

| ν | BrHgOBr | BrHgOCl | ClHgOBr | ClHgOCl |
|---|---|---|---|---|
| 1 | 705.9 | 778.2 | 710.8 | 781.1 |
| 2 | 524.4 | 554.7 | 532.6 | 564.9 |
| 3 | 275.7 | 277.7 | 401.4 | 403.6 |
| 4 | 132.2 | 174.6 | 143.7 | 185.4 |
| 5 | 123.4 | 124.0 | 140.4 | 140.6 |
| 6 | 51.7 | 63.3 | 65.5 | 78.1 |

Table 3: Enthalpies of reaction (0 K) for HgX + YO → XHgOY in kcal/mol. Computed at the CCSD(T)/CBS+CV+SO level of theory (see text).

| reaction | $E_e$(aV5Z) | $\Delta E_e$(CBS) | $\Delta E_e$(CV) | $\Delta E_e$(SO) | $\Delta E_{ZPE}$ | $\Delta H_r$ |
|---|---|---|---|---|---|---|
| HgBr + BrO → BrHgOBr | -55.93 | -0.44 | -0.06 | 1.54 | 1.31 | -53.57 |
| HgBr + ClO → BrHgOCl | -52.84 | -0.33 | 0.15 | 0.90 | 1.36 | -50.75 |
| HgCl + BrO → ClHgOBr | -57.92 | -0.45 | -0.09 | 1.45 | 1.25 | -55.77 |
| HgCl + ClO → ClHgOCl | -54.81 | -0.34 | 0.12 | 0.59 | 1.48 | -52.97 |

Table 4: Reaction enthalpies (0 K) for formation of mercury hypohalites and other competing reactions[a] (kcal/mol).

| Products | Reactants | $\Delta H_r$ |
|---|---|---|
| HgBr + BrO → | BrHgOBr | -53.6 |
| | BrHgBr + O | -17.6 |
| | BrHgO + Br | -4.3 |
| HgBr + ClO → | BrHgOCl | -50.8 |
| | BrHgCl + O | -18.5 |
| | BrHgO + Cl | -5.7 |
| HgCl + BrO → | ClHgOBr | -55.8 |
| | ClHgBr + O | -19.4 |
| | ClHgO + Br | 2.7 |
| HgCl + ClO → | ClHgOCl | -53.0 |
| | ClHgCl + O | -20.3 |
| | ClHgO + Cl | 1.3 |

a) Enthalpies for reactions not involving the mercury hypohalites were derived from previous accurate ab initio calculations.[8,37]

Table 5: Excitation energies and oscillator strengths for the transitions from the ground state ($X^1A'$) of BrHgOBr to excited states at wavelengths greater than 230 nm.[a]

| Excited State | ΔE (kcal/mol) | λ (nm) | f |
|---|---|---|---|
| $1\ ^3A'$ | 66.9 | 427 | $4.1 \times 10^{-5}$ |
| $2\ ^3A'$ | 109.9 | 260 | $5.8 \times 10^{-4}$ |
| $3\ ^3A'$ | 114.2 | 250 | $8.7 \times 10^{-4}$ |
| | | | |
| $1\ ^3A''$ | 54.8 | 522 | $3.6 \times 10^{-5}$ |
| $2\ ^3A''$ | 103.0 | 278 | $3.4 \times 10^{-4}$ |
| $3\ ^3A''$ | 115.2 | 248 | $7.4 \times 10^{-4}$ |
| | | | |
| $2\ ^1A'$ | 86.1 | 332 | $1.3 \times 10^{-2}$ |
| $3\ ^1A'$ | 118.4 | 242 | $7.0 \times 10^{-3}$ |
| | | | |
| $1\ ^1A''$ | 71.9 | 398 | $8.8 \times 10^{-4}$ |
| $2\ ^1A''$ | 112.2 | 255 | $5.5 \times 10^{-3}$ |
| $3\ ^1A''$ | 122.4 | 234 | $3.0 \times 10^{-3}$ |

[a)] Excitation energies computed at the LR-CCSD/aVDZ level of theory. Oscillator strengths between the singlet excited states and the ground state were also computed at the LR-CCSD/aVDZ level of theory. Oscillator strengths between the ground and triplet excited states were computed at the LR-MCSCF/aVTZ level of theory.

Figure 1: Structure of BrHgOBr

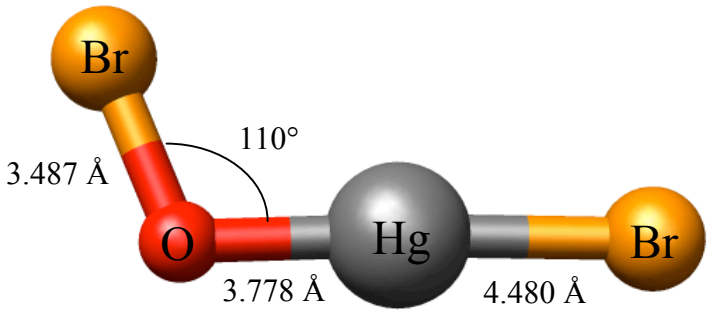

Figure 2: Energy level diagram [$\Delta H_r(0K)$] for the ground state of the HgBr+BrO reaction (kcal/mol).

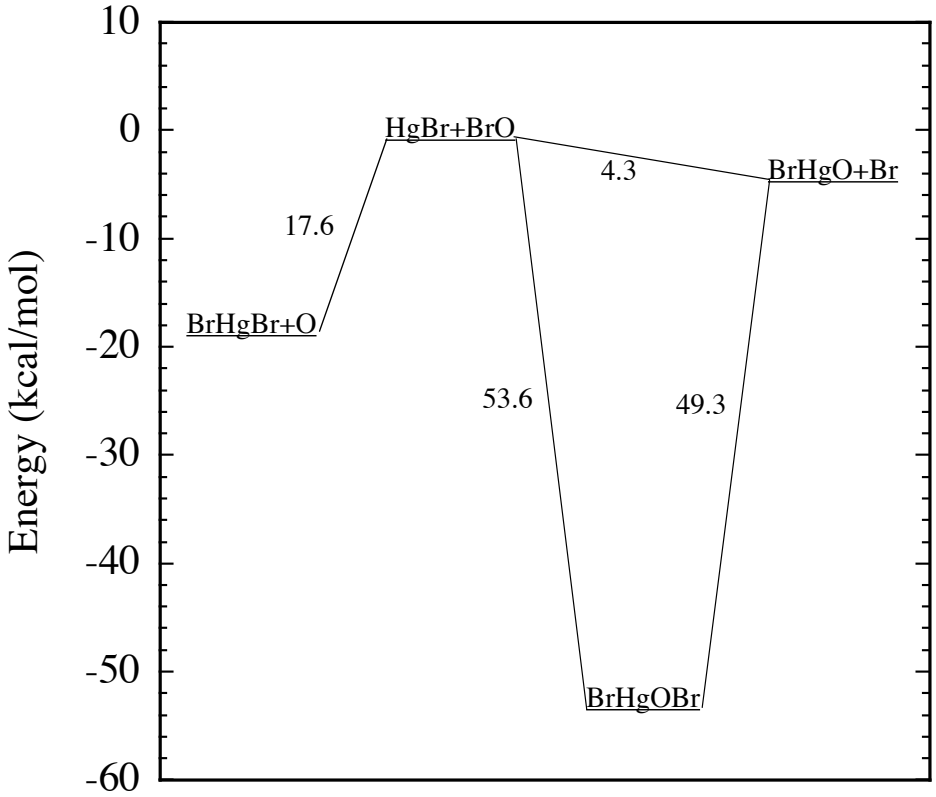

Figure 3: MCSCF/aVTZ Potential energy curves for the ground and low-lying excited states in the dissociation of BrHgOBr → BrHg + OBr[a]

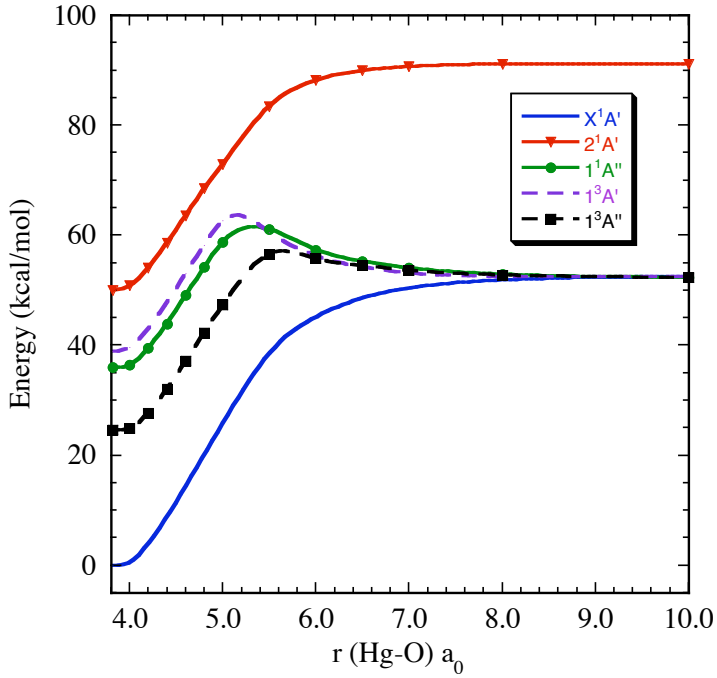


a) All other geometric parameters are fixed at their equilibrium values in ground state BrHgOBr.

Figure 4: MCSCF/aVTZ Potential energy curves for the ground and low-lying excited states in the dissociation of BrHgOBr → BrHgO + Br[a]

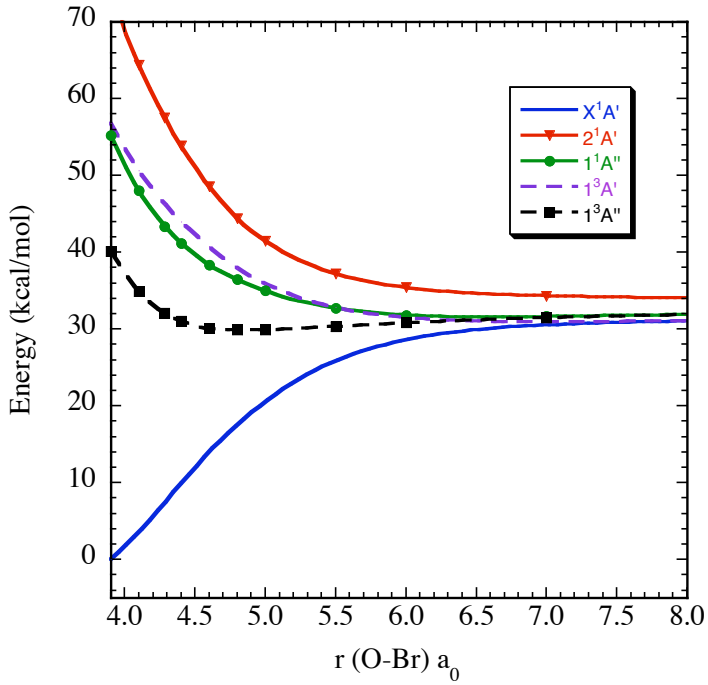


a) All other geometric parameters are fixed at their equilibrium values in ground state BrHgOBr.

# Aqueous Microsolvation of Mercury Halide Species

**Benjamin C. Shepler, Ashby D. Wright, Nikolai B. Balabanov, and Kirk A. Peterson***

*Department of Chemistry, Washington State University, Pullman, Washington 99164-4630*

**Abstract**

The effects of aqueous solvation on the thermochemistry of reactions between mercury and small halogen molecules has been investigated by the microsolvation approach using second order Møller-Plesset perturbation theory (MP2) and density functional theory (DFT). The structures, vibrational frequencies and binding energies of 1, 2 and 3 water molecules with the mercury-halide species {$HgBr_2$, HgBrCl, $HgCl_2$, HgBr, HgCl, and Hg} and the halogen species {$Br_2$, BrCl, $Cl_2$, Cl, and Br} have been computed. For the 1- and 2-water cases, binding energies have been estimated at the complete basis set (CBS) limit using sequences of correlation consistent basis sets, and higher order correlation effects were estimated from calculations with the coupled cluster singles and doubles method with a perturbative correction for connected triple excitations [CCSD(T)]. The binding energies were then used to calculate the influence of water molecules on the thermochemistry of a number of reactions between mercury and small halogen-containing molecules.

## I. INTRODUCTION

Unusual behavior has recently been observed in the polar tropospheric chemistry of mercury. Throughout the dark winter months the concentration of mercury in the polar troposphere remains near its global background concentration of 1-2 ng/m$^3$.[1] However, following polar sunrise the mercury concentration fluctuates widely, often dropping as low as 0.1 ng/m$^3$.[2-6] These fluctuations, which have been called mercury depletion events (MDEs), closely resemble ozone depletion events that are known to be caused by reactions with small halogen containing molecules like Br and BrO.[7-11] This has led to the proposal that the MDEs are a result of the oxidation of gaseous elemental mercury (the dominant form of mercury in the atmosphere) in reactions with the same halogen species.[2-5,12-14] These oxidized mercury species are then thought to be deposited on the snowpack.[3,13,14] This hypothesis has led to numerous experimental[15,16] and theoretical[17-25] studies on the gas phase kinetics and thermochemistry of possible mercury-halogen reactions that may be involved. In addition to gas phase reactions it is likely that water plays an important role in MDEs. The deposition of the oxidized mercury species on the snow and ice surfaces obviously involves water. It is also possible that clouds, water droplets and ice surfaces may catalyze the mercury oxidation.[14]

Due to the potential importance of water in MDEs, an ab initio study has been carried out to investigate the effects of aqueous microsolvation on a number of mercury and halogen-containing species. The molecules that have been studied are $HgBr_2$, $HgCl_2$, HgBrCl, HgBr, HgCl, $Br_2$, $Cl_2$, BrCl, Hg atom, Br atom, and Cl atom. The binding energies and structures with one, two and three water molecules have been determined. The effects on the gas phase thermochemistry due to the presence of one, two and three water molecules has also been examined for the following reactions:

| | | | |
|---|---|---|---|
| *Atom-Atom Recombination* | Hg + X → HgX | {X = Br, Cl} | (1) |
| *Atom-Diatom Recombination* | HgX + Y → HgXY | {X, Y = Br, Cl} | (2) |
| *Abstraction* | HgX + Y → Hg + XY | {X, Y = Br, Cl} | (3) |
| *Insertion* | Hg + XY → HgXY | {X, Y = Br, Cl}. | (4) |

The interaction of Hg atom with a single water molecule has been reported previously,[26] but the microsolvation of the other mercury species in this study have not previously appeared in the literature. There have been a number of previous investigations into water complexes involving the halogen atoms[27-29] and diatomic halogen molecules.[30-37]

## II. METHODOLOGY

Geometry optimizations were carried out for the 11 species {$HgBr_2$, $HgCl_2$, HgBrCl, HgBr, HgCl, $Br_2$, $Cl_2$, BrCl, Hg, Br, and Cl} with one, two and three water molecules. For the one and two water complexes the optimizations employed second-order Møller-Plesset perturbation theory (MP2)[38]. For the open-shell molecules unrestricted Hatree-Fock (UHF) calculations were used to determine the reference wavefunctions and the unrestricted MP2 method (UMP2) was used for the electron correlation. In all calculations the frozen-core approximation was employed that included the Br 3d electrons in the core. The basis sets used throughout this work were aug-cc-pVnZ-PP for Hg[39] and Br[40], aug-cc-pV(n+d)Z[41] for Cl, and aug-cc-pVnZ[42] for H and O (n=D, T, Q) and will henceforth be denoted aVnZ. Energy consistent relativistic pseudopotentials (PPs) of the Stuttgart-Köln variety were used on the Hg[43] and Br[40] atoms. The Hg PP leaves the $5s^2 5p^6 5d^{10} 6s^2$ electrons to be explicitly treated and the Br PP replaces all but the $3s^2 3p^6 3d^{10} 4s^2 4p^5$ electrons. The aVDZ basis sets were used in the

geometry optimiztions. For the one, two and three water molecule cases the geometries were also optimized with the B3LYP[44,45] hybrid density functional method, again employing the aVDZ basis sets. Only the Hg-atom complexes were not calculated with B3LYP. Both the MP2 and B3LYP geometry optimizations were followed by frequency calculations at the same level of theory. All geometry optimizations and frequency calculations were carried out with the Gaussian 03[46] suite of ab initio programs.

At the optimized geometries the usual counterpoise (CP) correction[47] was used in calculating the binding energies in order to to correct for basis set superposition error (BSSE). The energy of each monomer was computed at the geometry it has in the complex using its own basis functions along with the basis functions of the other monomers centered at the appropriate nuclear configurations of the complex. The counterpoise corrected interaction energy was then computed by subtracting the total energy of the complex from the sum of the energies of the monomers just described. Henceforth, interaction energies calculated in this way will be designated $\Delta E_{CP}$,

$$\Delta E_{CP} = E^*(\text{Complex})_{ab...n} - E^*(A)_{ab...n} - E^*(B)_{ab...n} \ldots - E^*(N)_{ab...n} \tag{5}$$

where the subscripts denote which n-particle basis functions are included in calculating that energy and the asterisk indicates the geometry of the complex was used. A deformation energy was also determined to account for the geometrical distortion of the monomers from their equilibrium structures. These deformation corrections were calculated by taking the difference in energy between each monomer at its equilibrium geometry and its geometry in the complex using only the monomer's basis set:

$$\Delta E(N)_{DEF} = E^*(N)_n - E(N)_n. \tag{6}$$

The binding energy is then equal to the counterpoise corrected interaction energy from Equation 5 minus the deformation energy of each monomer:

$$\Delta E_{BE} = \Delta E_{CP} - \Delta E(A)_{DEF} - \Delta E(B)_{DEF} \ldots - \Delta E(N)_{DEF} \quad (7)$$

The B3LYP counterpoise corrections and deformation energy calculations were carried out with Gaussian 03 and the MP2 values were calculated with the MOLPRO[48] suite of ab initio programs. For the open-shell molecules the restricted open-shell Hartree-Fock (RHF) method was used to determine the reference wavefunctions and the restricted MP2 (RMP2) method used to compute the correlation energy contributions.

The binding energies will be reported at 0 K, thus the zero point energy (ZPE) of each complex was needed. The zero point energy correction to the binding energy was calculated by taking $1/2\sum\omega_e$ where the $\omega_e$'s are harmonic vibrational frequencies. This term will be denoted $\Delta E_{ZPE}$.

For the one and two water molecule cases an additional correction was calculated to account for basis set incompleteness. To this end, $\Delta E_{CP}$ was computed at the MP2/aVTZ and MP2/aVQZ levels of theory using the geometries determined at the MP2/aVDZ level of theory. The three $\Delta E_{CP}$ interaction energies (computed with the aVDZ, aVTZ and aVQZ basis sets) were then extrapolated with a mixed Gaussian-exponential formula[49,50]:

$$E(n) = E_{\mathrm{CBS}} + Be^{-(n-1)} + Ce^{-(n-1)^2} \quad (8)$$

to obtain an estimate of the MP2 complete basis set (CBS) limit binding energy. In the above formula *n* is the basis set cardinal number (i.e, 2 for DZ, 3 for TZ…), *E(n)* is $\Delta E_{CP}$ with the *n*th basis set, and $E_{CBS}$ is $\Delta E_{CP}$ at the CBS limit.

A second correction to $\Delta E_{CP}$ was included to estimate the effects of higher order electron correlation and was again computed only for the 1 and 2 water complexes. The coupled cluster singles and doubles method with a perturbative estimate of connected triple excitations [CCSD(T)][51-53] was used to compute $\Delta E_{CP}$ using the aVDZ basis sets at the MP2/aVDZ optimized geometries. For the open shell species the R/UCCSD(T)[53-55] method was used, i.e., reference wavefunctions were determined from ROHF calculations but the spin restriction was relaxed in the coupled cluster calculations. The correction was then defined as the difference between the $\Delta E_{CP}$ computed with the CCSD(T)/aVDZ and MP2/aVDZ levels of theory.

Geometry optimizations and frequency calculations were not carried out using the larger basis sets or with the CCSD(T) method. Therefore, $\Delta E(N)_{DEF}$ computed at the MP2/aVDZ level of theory was used with the CBS and CCSD(T) corrected $\Delta E_{CP}$ to get the CP-corrected binding energies. The deformation energies computed with the CCSD(T) method or with larger basis sets but using the MP2/aVDZ geometries were not reliable. Also, the MP2/aVDZ ZPE corrections were used throughout to determine the 0 K binding energies.

## III. RESULTS AND DISCUSSION

### III.A. STRUCTURES

The optimized geometries of $HgBr_2$, HgBr, $Br_2$, Br atom, and Hg atom with one, two and three waters are shown in Figures I, II, III, IV, and V respectively. The geometries shown are those optimized at the MP2/aVDZ level of theory for the one and two water complexes, and at the B3LYP/aVDZ level of theory for the three water complexes. The structures for the mercury/halogen species not shown in Figures I-V are qualitatively similar to those pictured.

The optimized geometries of the $HgCl_2$ and HgBrCl complexes closely resemble the structures for $HgBr_2$ with the water molecules in the HgBrCl case preferring configurations where they are more strongly interacting with the Cl atom. The HgCl geometries closely resemble those of HgBr, Cl atom structures resembles those of Br atom, and $Cl_2$ and BrCl resemble those of $Br_2$. The lowest BrCl conformers, however, are those in which the water molecules are closest to the Br atom.

In almost every complex numerous local minima were found on the potential energy surfaces and it is the lowest energy structures that are depicted. For many of the complexes there exist local minima that lie only tenths of kcal/mol higher than the structures shown. This is especially true for the three-water complexes. The $HgBr_2$-$(H_2O)_3$ complexes pictured in Figures Ic and VIa are excellent examples of this. The conformer pictured in Figure Ic is 0.7 kcal/mol lower in energy than the conformer pictured in Figure VIa when the B3LYP/aVDZ level of theory is used in the geometry optimization. However, when the geometries are optimized at MP2/aVDZ level of theory the conformer in Figure VIa is instead found to be 0.7 kcal/mol lower in energy. For the most part, however, the B3LYP/aVDZ and MP2/aVDZ levels of theory yielded the same conformers as the global minima.

There have been a number of previous theoretical and experimental investigations in which the structures of some of the complexes considered in this study have been reported. Soldán et. al.[26] optimized the geometry of the Hg-$H_2O$ complex with a variety of methods and basis sets. Their largest basis set [10s8p7d4f] was used with a relativistic small-core ECP and the geometry optimizations were carried out with B3LYP, MP2 and quadratic configuration interaction with single and double excitations (QCISD). The current results are in good qualitative agreement with their larger basis set calculations. Both studies found the $C_s$

symmetry conformer shown in Figure IVa to be the global minimum. The MP2 Hg-H bond length of the current study was found to be 2.81 Å, which is slightly longer than the result of 2.77 Å of Soldán et al. Similarly, the B3LYP Hg-H bondlength of the current study was found to be 3.12 Å and is again longer than their value of 3.01 Å . The QCISD bond length from Ref. .26 , 3.02 Å, indicates that the current MP2/aVDZ bond length is a bit too short. The current structures could be improved by using larger basis sets and increased levels of electron correlation, but the calculations quickly become significantly more expensive for the larger complexes.

Sevilla et. al.[29] have previously reported MP2 structures using small double-zeta basis sets for Cl-$H_2O$ and Cl-$(H_2O)_3$. Roeselová and co-workers[27,28] have reported on studies of Cl-$H_2O$ and Br-$H_2O$ using the Fock-space coupled cluster singles and doubles method (FSCC) and double-zeta basis sets. The previous calculations and the current results all predict a $C_S$ symmetry minimum with the hydrogens of the water pointing away from the halogen atoms for the single water molecules. This structure is shown in Figure IVa for Br-$H_2O$. The FSCC method predicted a Br-O bond length of 2.8 Å,[28] which is identical within their reported precision to the current value of 2.80 Å. The prior MP2 Cl-O bond length in Cl-$H_2O$ was reported to be 2.70 Å[29] and the FSCC method predicted a value of 2.65 Å,[27] both of which agree well with the current value of 2.70 Å. The Cl-O-$H_1$-$H_2$ dihedral angles are also in good agreement with the FSCC method,[27] which yielded a value of 105° while the current MP2 calculations resulting in a value of 109°. The current structure for the Cl-$(H_2O)_3$ complex is not the same conformer that was reported previously, and this conformer is shown in Figure VIb. The Cl-$(H_2O)_3$ complex in this work was originally optimized with B3LYP while the previous

study used the MP2 method. Both conformers of Cl-$(H_2O)_3$ were therefore reoptimized at the MP2/aVDZ level of theory and the conformer pictured in Figure IVc was found to be lower than the conformer of Figure VIb by 2.3 kcal/mol.

The complexes of $Br_2$, $Cl_2$ and BrCl with a single water molecule have been studied previously both experimentally and theoretically. The previous studies[32,34-37] and current results indicate the equilibrium geometries have $C_s$ symmetry with the oxygen atom lying nearly on the X-X bond axis and with an obtuse X-O-H-H dihedral angle. The optimized structure of $Br_2$-$H_2O$ from this work is shown in Figure IIIa. The experimental X-O bond lengths of Legon and co-workers[35,37] for $Cl_2$-$H_2O$ and $Br_2$-$H_2O$ are 2.848 and 2.851Å, respectively, and were determined by pure rotational spectroscopy. The current values of 2.755 and 2.759 Å are shorter by 0.09 Å. The previously reported theoretical structures for $Br_2$ and $Cl_2$ with a single water molecule were determined using similar levels of theory as the current study, employing MP2 or MP3 correlation methods and approximately double- or triple-zeta quality basis sets. Thus not suprisingly these are in good qualitative agreement with the structures calculated here. The prior Cl-O bondlengths were reported to be 2.84 Å[32] and 2.76 Å[35] for $Cl_2$-$H_2O$ ; Br-O bondlengths of 2.83 Å[34] and 2.85 Å[37] for $Br_2$-$H_2O$. The Br-O bond length in BrCl-$H_2O$ has not been determined experimentally, but the MP2/aug-cc-pVDZ value of Davey and Legon[36] of 2.72 Å is only slightly longer than the present value of 2.68 Å. The difference between the current and previous double-zeta MP2 results is likely the inclusion in the present work of scalar relativistic effects via the PP's and the additional tight d-functions included in the present Cl basis set.

There has been a previous report of a multi-water-dihalogen complex, and this was for $Br_2$ with up to 7 water molecules[34]. As part of this study the authors optimized a conformer of

$Br_2$-$(H_2O)_2$ at the MP2/6-311+G(d,p) level of theory in which the two water molecules are interacting with the $Br_2$ relatively independent of one another. The structure is shown in Figure VIc. Using the MP2 method and aVDZ basis set, this conformer was found to lie 5.1 kcal/mol above the conformer pictured in Figure IIIb in which the water molecules are interacting with each other as well as the $Br_2$ molecule.

Other than the conformers just discussed, it appears that structures for the other complexes included in the present study have not been reported previously. The best estimates of the gas phase structures of the halide species should be taken from previous ab initio calculations [HgBr, HgCl (Ref. 25); $HgBr_2$, $HgCl_2$ and HgBrCl (Ref. 20)] and there exist high resolution experimental data for the bond lengths of the dihalogens.[56-59]

## III.B. INCREMENTAL BINDING ENERGIES

The incremental binding energies are shown in Tables I-III, with the HgXY complexes contained in Table I, the HgX and XY complexes contained in Table II, and the atom-water complexes contained in Table III. As mentioned in Sec. II, the B3LYP binding energies include $\Delta E_{CP}$, $\Delta E(N)_{DEF}$, and $\Delta E_{ZPE}$ computed at the B3LYP/aVDZ level of theory and the geometries were optimized at that same level of theory. Similarly, the MP2/aVDZ binding energies include $\Delta E_{CP}$, $\Delta E(N)_{DEF}$, and $\Delta E_{ZPE}$ all computed with the MP2 method and aVDZ basis set at geometries optimized at the same level of theory. For the CCSD(T)/aVDZ and MP2/CBS limit binding energies, however, only $\Delta E_{CP}$ was computed at those levels of theory and the MP2/aVDZ optimized geometries were used to compute this $\Delta E_{CP}$. The $\Delta E(N)_{DEF}$ and $\Delta E_{ZPE}$ were taken from the MP2/aVDZ calculations. The best estimate of the binding energy is defined

as the MP2/CBS binding energy plus the difference between the MP2/aVDZ and CCSD(T)/aVDZ binding energies.

A few trends in the binding energies are immediately apparent when looking at Tables I-III. With the exception of the Br-$(H_2O)_n$ and Cl-$(H_2O)_n$ complexes, all of the MP2/aVDZ binding energies overestimate the CCSD(T)/aVDZ binding energies. The MP2 energies are typically around 0.5 kcal/mol higher in energy, but in the HgBr and HgCl complexes they are nearly 1 kcal/mol higher than their CCSD(T) counterparts. The MP2/CBS binding energies in all cases represent an increase with respect to the MP2/aVDZ values. The CBS correction is generally larger than the CCSD(T) correction, and is generally between 1-2 kcal/mol with the largest value of 2.53 kcal/mol occurring in the HgBrCl-$(H_2O)_2$ complex. The two-water complexes always have a larger CBS correction than their one-water counterparts and this is not true for the CCSD(T) corrections where the one and two water complexes have comparable corrections.

It is likely that the best estimates given in Tables I-III underestimate the actual binding energies. The CCSD(T) $\Delta E_{CP}$ interaction energies were not computed at the minimum geometry on the CCSD(T)/aVDZ surface and are thus underestimated. The MP2 $\Delta E_{CP}$ values are larger than the CCSD(T) values, so the CCSD(T) correction to the MP2 binding energies will be negative and too large in magnitude due to the underestimation of the CCSD(T) $\Delta E_{CP}$. This will therefore likely lead to an underestimation of the actual binding energy. To quantify this error CCSD(T)/aVDZ optimizations have been carried out for $HgBr_2$, HgBr, and $Br_2$, and the $\Delta E_{CP}$'s calculated at these CCSD(T) geometries are 0.4, 0.2, and 0.1 kcal/mol larger than those calculated at the MP2 geometries. Similarly, the CBS $\Delta E_{CP}$'s were not computed at the global

minimum of the MP2/CBS surface and are therefore likely too small. This is a positive correction to the MP2/aVDZ binding energies and so its underestimation will again lead to calculated best estimates of the binding energies that are likely smaller than the actual binding energies.

There does not appear to be any systematic relationship between the B3LYP/aVDZ binding energies and those computed with MP2/aVDZ or CCSD(T)/aVDZ. However, for the most part all three methods agree to within 1.5 kcal/mol and often better. The two exceptions to this trend are the Cl and Br atom complexes where the B3LYP binding energies are significantly higher (1.5-3.5 kcal/mol) than those of the other two methods.

The Hg-$H_2O$ binding energies of the current study are in excellent agreement with the previous calculations of Soldán et al.[26] They reported binding energies without a ZPE correction of 0.92 kcal/mol from MP2 calculations and 0.61 kcal/mol using the CCSD(T) method, both employing a large [11s10p8d5f4g] basis set on Hg and aug-cc-pVQZ basis sets on H and O. When $\Delta E_{ZPE}$ is left out of the current binding energies for Hg-$H_2O$, the current $D_e$'s are 1.04 kcal/mol with MP2/CBS and the best estimate is 0.64 kcal/mol, which agree very well with the Soldán et al. MP2 and CCSD(T) values, respectively.

There have also been previous calculations on the binding energy of $Br_2$, BrCl and $Cl_2$ with a single water molecule. Dahl and Røeggen[32] reported a $D_e$ of 2.99 kcal/mol form MP3 calculations using approximately triple-zeta basis sets, and Davey et al.[35] reported an MP2/aug-cc-pVDZ $D_e$ of 2.82 kcal/mol for $Cl_2$-$H_2O$. These compare well with the current MP2/aVDZ $D_e$ of 2.80 kcal/mol and, due to a near cancellation of the CCSD(T) and CBS corrections, all of these values also agree well with the current best estimate for $D_e$ of 2.78 kcal/mol. The

MP2/aug-cc-pVDZ $D_e$ for BrCl-$H_2O$ was previously calculated to be 4.45 kcal/mol,[36] which is slightly lower, but still very close, to the current MP2/aVDZ $D_e$ of 4.77 kcal/mol and the best estimate of $D_e$ = 4.86 kcal/mol. Ramondo et al.[34] conducted ab inito calculations on $Br_2$-$H_2O$ with the B3LYP and MP2 methods. Their B3LYP/6-311+G(d,p) $D_e$ was calculated to be 4.06 kcal/mol, which is only slightly higher than the 3.89 kcal/mol value computed with the B3LYP/aVDZ method in this study. Similarly, Ramondo et al.'s MP2/6-311+G(d,p) $D_e$ of 3.59 kcal/mol is in good agreement with the current MP2/aVDZ value of 3.82 kcal/mol. Again, due to a cancellation of basis set effects and higher order electron correlation effects, all values for the $D_e$ of $Br_2$-$H_2O$ are in good agreement with the current best estimate of 3.92 kcal/mol.

## III.C. EFFECTS OF MICROSOLVATION ON REACTION ENTHALPIES

Last, Table IV contains the 0 K gas phase enthalpies for a number of mercury-halogen reactions that were taken from earlier ab initio investigations[19,25] along with the current effects of microsolvation. The gas phase enthalpies were computed at the CCSD(T)/CBS level of theory using relativistic PPs on Hg and Br and included corrections for core-valence correlation, spin-orbit coupling, scalar relativity and the pseudopotential approximation. They are expected to be accurate to within ±1 kcal/mol. The effect of the inclusion of water molecules on the reaction energetics was determined by including 1, 2 or 3 water molecules with one of the reactants and one of the products. When there are two species in either the reactants or products all of the water molecules are kept with the species that has the largest binding energies. The microsolvation effects are then calculated as:

$$\Delta\Delta H_r = D_0(\text{Reactant}) - D_0(\text{Product}) \quad (8)$$

where the $D_0$'s are the *total* complex binding energy. For the two and three water molecule complexes the $D_0$'s are obtained by adding the incremental binding energies found in Tables I-III. The best estimate for the binding energies is used to calculate $\Delta\Delta H_r$ for the one and two water cases. For the three water cases the third B3LYP incremental binding energy is added to the best estimates for the first two incremental binding energies. The $\Delta\Delta H_r$'s in Table IV are *not* incremental.

The atom-atom recombination reactions between Hg and Br or Cl are a likely initiation step in the oxidation of mercury during the mercury depletion events (MDEs). The gas phase recombination between these atoms proceeds without a barrier and is exothermic by 16.3 kcal/mol for HgBr and 22.9 kcal/mol for HgCl. Inclusion of water molecules on the Br or Cl atoms in the reactants and HgBr or HgCl in the products increases the exothermicity of the reactions slightly. A single water molecule yields $\Delta\Delta H_r$'s of –1.5 and –2.0 kcal/mol for HgBr and HgCl, respectively, while a second water molecule more than doubles the effects to –3.5 and –4.5 kcal/mol. The $\Delta\Delta H_r$'s with three water molecules may be less reliable in these reactions and are actually less negative with respect to the inclusion of two waters. The one and two water incremental binding energies with Br and Cl atom are greatly overestimated at the B3LYP/aVDZ level of theory with respect to the best estimate. If the 3$^{rd}$ incremental binding energy is also being overestimated it could account for the decrease in exothermicity in these atom-atom recombination reactions when increasing from two to three waters.

It has been proposed that the end result of the mercury oxidation process is the formation of Hg(II) species, and three likely contributors are $HgBr_2$, HgBrCl and $HgCl_2$. If formation of HgBr and HgCl is the first step in the oxidation, then one way to form these Hg(II) species

would be the atom-diatom recombination reactions given in Table IV, i.e., HgX + Y → XHgY. These reactions are also known to proceed without a barrier[24] and are all strongly exothermic by 73-83 kcal/mol. The addition of water molecules also yields an increase in the exothermicity, but the effects are somewhat smaller (0.5-2.5 kcal/mol) than for the atom-atom recombination reactions. There also appears to be little significant difference between the 1, 2 and 3 water cases, and the change in exothermicity seems to be nearly converged with the addition of a single water molecule. Of course, this could certainly change as more waters are included.

A reaction that can compete with the atom-diatom recombination reactions and formation of Hg(II) species are abstraction reactions, i.e., HgX + Y → Hg + XY. As shown in Table 4 these reactions are also exothermic, but at ~30 kcal/mol they are significantly less so than the atom-diatom recombination reactions. This series of reactions are actually made *less* exothermic by the inclusion of water molecules, and there is a significant increase in the solvation effect between one and three water molecules. The presence of water would seem to favor formation of the divalent mercury species, at least with respect to these abstraction reactions.

The final set of reactions that is considered are insertion reactions of the type Hg + XY → XHgY. This single step oxidation of Hg(0) to Hg(II) is exothermic by about 45 kcal/mol for $Br_2$, BrCl and $Cl_2$. These reactions, however, are unlikely to occur directly in the gas phase because of large barriers to insertion. Multireference configuration interaction (MRCI) calculations have shown the Hg + $Br_2$ → $HgBr_2$ reaction to have a barrier of 27.2 kcal/mol.[24] The inclusion of water molecules again has the result of making these reactions more exothermic and the effects are slightly larger than for the other series of reactions. Presence of a single water molecule increases the exothermicity by 2.5, 1.7 and 3.2 kcal/mol for $Br_2$, BrCl and $Cl_2$, respectively, and a second water molecule more than doubles the effect to 4.9, 4.6, and 7.3

kcal/mol. Addition of a third water molecule further increases the exothermicity. It is highly likely that presence of water will also stabilize the transition state with respect to reactants. If the stabilization of the transition state is significant, then it is possible that these insertion reactions are sufficiently catalyzed by the presence of ice surfaces and water droplets to play a role in the mercury depletion events.

## IV. CONCLUSIONS

Ab initio calculations have been carried out to determine the structures and binding energies of one, two and three water molecules with a series of small mercury and halogen containing species {$HgBr_2$, HgBrCl, $HgCl_2$, HgBr, HgCl, $Br_2$, BrCl, $Cl_2$, Hg, Br, and Cl}. These calculations were undertaken to determine the effects of microsolvation on reactions between mercury and halogen molecules that may play an important role in polar tropospheric mercury depletion events. Geometry optimizations were carried out with the MP2 and B3LYP methods using double-zeta basis sets augmented with diffuse functions. For the one and two water molecule complexes additional calculations were performed with series of correlation consistent basis sets to estimate binding energies at the complete basis set limit. A further correction for higher order electron correlation effects was calculated using the CCSD(T) method. The counterpoise correction was applied to all binding energies to account for BSSE.

Theoretical structures and binding energies have been reported previously for Hg atom, the halogen atoms and the dihalogen molecules with one water molecule and for the halogen atoms with multiple water molecules. For these complexes the current binding energies are among the most accurate currently available. For the other complexes in this study it is believed this is the first time the structures or binding energies have been reported.

The effects of solvation on four series of reactions have been investigated. The atom-atom abstraction reactions, i.e., Hg + X → HgX (X = Br, Cl) that have been proposed as a first step in the mercury depletion events were found to increase in exothermicity due to the presence of water molecules. Likewise, the atom-diatom recombination reactions of the form HgX + Y → XHgY (X, Y = Br, Cl) were also found to increase in exothermicity with the inclusion of water molecules. HgX + Y → Hg + XY abstraction reactions, which may compete with the atom-diatom recombination, were found to be less exothermic when water molecules were present. Finally, the insertion reactions Hg + XY → XHgY were found to be significantly more exothermic when microsolvation was included.

## V. REFERENCES


(1) Schroeder, W. H.; Munthe, J. *Atmospheric Environment* **1998**, *32*, 809.

(2) Schroeder, W. H.; Anlauf, K. G.; Barrie, L. A.; Lu, J. Y.; Steffen, A.; Schneeberger, D. R.; Berg, T. *Nature* **1998**, *394*, 331.

(3) Lindberg, S. E.; Brooks, S.; Lin, C.-J.; Scott, K. J.; Landis, M. S.; Stevens, R. K.; Goodsite, M.; Richter, A. *Environmental Science and Technology* **2002**, *36*, 1245.

(4) Temme, C.; Einax, J. W.; Ebinghaus, R.; Schroeder, W. H. *Environmental Science and Technology* **2003**, *37*, 22.

(5) Skov, H.; Christensen, J. H.; Goodsite, M. E.; Heidam, N. Z.; Jensen, B.; Wåhlin, P.; Geernaert, G. *Environmental Science and Technology* **2004**, *38*, 2373.

(6) Berg, T.; Bartnicki, J.; Munthe, J.; Lattila, H.; Hrehoruk, J.; Mazur, A. *Atmospheric Environment* **2001**, *35*, 2569.

(7) Barrie, L. A.; Bottenheim, J. W.; Schnell, R. C.; Crutzen, P. J.; Rasmussen, R. A. *Nature* **1988**, *334*, 138.

(8) Le Bras, G.; Platt, U. *Geophysical Research Letters* **1995**, *22*, 599.

(9) Boudries, H.; Bottenheim, J. W. *Geophysical Research Letters* **2000**, *27*, 517.

(10) Foster, K. L.; Plastridge, R. A.; Bottenheim, J. W.; Shepson, P. B.; Finlayson-Pitts, B. J.; Spicer, C. W. *Science* **2001**, *291*, 471.

(11) Spicer, C. W.; Plastridge, R. A.; Foster, K. L.; Finlayson-Pitts, B. J.; Bottenheim, J. W.; Grannas, A. M.; Shepson, P. B. *Atmospheric Environment* **2002**, *36*, 2721.

(12) Ariya, P. A.; Dastoor, A. P.; Amyot, M.; Schroeder, W. H.; Barrie, L. A.; Anlauf, K.; Raofie, F.; Ryzhkov, A.; Davignon, D.; Lalonde, J.; Steffen, A. *Tellus* **2004**, *56B*, 397.

(13) Lu, J. Y.; Schroeder, W. H.; Barrie, L. A.; Steffen, A.; Welch, H. E.; Martin, K.; Lockhart, L.; Hunt, R. V.; Boila, G.; Richter, A. *Geophysical Research Letters* **2001**, *28*, 3219.

(14) Gauchard, P.-A.; Aspmo, K.; Temme, C.; Steffen, A.; Ferrari, C.; Berg, T.; Strom, J.; Kaleschke, L.; Dommergue, A.; Bahlman, E.; Magand, O.; Planchon, F.; Ebinghaus, R.; Banic, C.; Nagorski, S.; Baussand, P.; Boutron, C. *Atmospheric Environment* **2005**, *39*, 7620.

(15) Ariya, P. A.; Khalizov, A. F.; Gidas, A. *Journal of Physical Chemistry A* **2002**, *106*, 7310.

(16) Raofie, F.; Ariya, P. A. *Environmental Science and Technology* **2004**, *38*, 4319.

(17) Khalizov, A. F.; Viswanathan, B.; Larregaray, P.; Ariya, P. A. *Journal of Physical Chemistry A* **2003**, *107*, 6360.

(18) Tossell, J. A. *Journal of Physical Chemistry A* **2003**, *107*, 7804.

(19) Balabanov, N. B.; Peterson, K. A. *Journal of Physical Chemistry A* **2003**, *107*, 7465.

(20) Balabanov, N. B.; Peterson, K. A. *Journal of Chemical Physics* **2003**, *119*, 12271.

(21) Balabanov, N. B.; Peterson, K. A. *Journal of Chemical Physics* **2004**, *120*, 6585.

(22) Calvert, J. G.; Lindberg, S. E. *Atmospheric Environment* **2004**, *38*, 5105.

(23) Goodsite, M. E.; Plane, J. M. C.; Skov, H. *Environmental Science and Technology* **2004**, *38*, 1772.

(24) Balabanov, N. B.; Shepler, B. C.; Peterson, K. A. *Journal of Physical Chemistry A* **2005**, *109*, 8765.

(25) Shepler, B. C.; Balabanov, N. B.; Peterson, K. A. *Journal of Physical Chemistry A* **2005**, *109*, 10363.

(26) Soldan, P.; Lee, E. P. F.; Wright, T. G. *Journal of Physical Chemistry A* **2002**, *106*, 8619.

(27) Roeselova, M.; Jacoby, G.; Kaldor, U.; Jungwirth, P. *Chemical Physics Letters* **1998**, *293*, 309.

(28) Roeselova, M.; Kaldor, U.; Jungwirth, P. *Journal of Physical Chemistry A* **2000**, *104*, 6523.

(29) Sevilla, M. D.; Summerfield, S.; Eliezer, I.; Rak, J.; Symons, M. C. R. *Journal of Physical Chemistry A* **1997**, *101*, 2910.

(30) Engdahl, A.; Nelander, B. *Journal of Chemical Physics* **1986**, *84*, 1981.

(31) Johnsson, K.; Engdahl, A.; Ouis, P.; Nelander, B. *Journal of Physical Chemistry* **1992**, *96*, 5778.

(32) Dahl, T.; Roeggen, I. *Journal of the American Chemical Society* **1996**, *118*, 4152.

(33) Liu, Z. F.; Siu, C. K.; Tse, J. S. *Chemical Physics Letters* **1999**, *311*, 93.

(34) Ramondo, F.; Sodeau, J. R.; Roddis, T. B.; Williams, N. A. *Physical Chemistry Chemical Physics* **2000**, *2*, 2309.

(35) Davey, J. B.; Legon, A. C.; Thumwood, J. M. A. *Journal of Chemical Physics* **2001**, *114*, 6190.

(36) Davey, J. B.; Legon, A. C. *Physical Chemistry Chemical Physics* **2001**, *3*, 3006.

(37) Legon, A. C.; Thumwood, J. M. A.; Waclawik, E. R. *Chemistry a European Journal* **2002**, *8*, 940.

(38) Møller, C.; Plesset, M. S. *Physical Reviews* **1934**, *46*, 618.

(39) Puzzarini, C.; Peterson, K. A. *Chemical Physics* **2005**, *311*, 177.

(40) Peterson, K. A.; Figgen, D.; Goll, E.; Stoll, H.; Dolg, M. *Journal of Chemical Physics* **2003**, *119*, 11113.

(41) Dunning, T. H. J.; Peterson, K. A.; Wilson, A. K. *Journal of Chemical Physics* **2001**, *114*, 9244.

(42) Kendall, R. A.; Dunning, T. H., Jr.; Harrison, R. J. *Journal of Chemical Physics* **1992**, *96*, 6796.

(43) Figgen, D.; Rauhut, G.; Dolg, M.; Stoll, H. *Chemical Physics* **2004**, *311*, 227.

(44) Becke, A. D. *Journal of Chemical Physics* **1993**, *98*, 5648.

(45) Stephens, P. J.; Devlin, F. J.; Chabalowski, C. F.; Frisch, M. J. *Journal of Physical Chemistry* **1994**, *98*, 11623.

(46) Gaussian 03, 2003.

(47) Boys, S. F.; Bernardi, F. *Molecular Physics* **1970**, *19*, 553.

(48) MOLRPRO is a package of ab initio programs written by H.-J. Werner and P.J. Knowles, version 2002.6, R.D. Amos, A. Bernhardsson, A. Berning, P. Celani, D.L. Cooper, M.J.O. Deegan, A.J. Dobbyn, F. Eckert, C. Hampel, G. Hetzer, P.J. Knowles, T. Korona, R. Lindh, A.W. Lloyd, S.J. McNicholas, F.R. Manby, W. Meyer, M.E. Mura, A. Nicklass, P. Palmieri, R. Pitzer, G. Rauhut, M. Schütz, U. Schumann, H. Stoll, A.J. Stone, R. Tarroni, T. Thorsteinsson, and H.-J. Werner.

(49) Peterson, K. A.; Woon, D. E.; Dunning, T. H., Jr. *Journal of Chemical Physics* **1994**, *100*, 7410.

(50) Feller, D.; Peterson, K. A. *Journal of Chemical Physics* **1999**, *110*, 8384.

(51) Purvis, G. D. I.; Bartlett, R. J. *Journal of Chemical Physics* **1982**, *76*, 1910.

(52) Raghavachari, K.; Trucks, G. W.; Pople, J. A.; Head-Gordon, M. *Chemical Physics Letters* **1989**, *156*, 479.

(53) Watts, J. D.; Gauss, J.; Bartlett, R. J. *Journal of Chemical Physics* **1993**, *98*, 8718.

(54) Scuseria, G. E. *Chemical Physics Letters* **1991**, *176*, 27.

(55) Knowles, P. J.; Hampel, C.; Werner, H.-J. *Journal of Chemical Physics* **1994**, *99*, 5219.

(56) Bermejo, D.; Jimenez, J. J.; Martinez, R. Z. *Journal of Molecular Spectroscopy* **2002**, *212*, 186.

(57) Focsa, C.; Li, H.; Bernath, P. F. *Journal of Molecular Spectroscopy* **2000**, *200*, 104.

(58) Uehara, H.; Konno, T.; Ozaki, Y.; Horiai, K.; Nakagawa, K.; Johns, J. W. C. *Canadian Journal of Physics* **1994**, *72*, 1145.

(59) Huber, K. P.; Herzberg, G. *Molecular Spectra and Molecular Structure IV. Constants of Diatomic Molecules*; Van Nostrand: Princeton, 1979.

**TABLE I: Incremental binding energies ($D_0$) for HgXY + $nH_2O$ (kcal/mol)**

| Species | Theory | Basis set | n=1 | n=2 | n=3 |
|---|---|---|---|---|---|
| $HgBr_2$ | B3LYP | aVDZ | 3.18 | 4.31 | 7.31 |
| | MP2 | aVDZ | 4.37 | 5.81 | |
| | CCSD(T) | aVDZ | 3.88 | 5.40 | |
| | MP2 | CBS | 5.94 | 7.74 | |
| | Best Estimate[a] | | 5.45 | 7.34 | |
| HgBrCl | B3LYP | aVDZ | 3.44 | 6.36 | 5.98 |
| | MP2 | aVDZ | 4.67 | 6.36 | |
| | CCSD(T) | aVDZ | 4.17 | 5.94 | |
| | MP2 | CBS | 6.27 | 8.25 | |
| | Best Estimate[a] | | 5.76 | 7.83 | |
| $HgCl_2$ | B3LYP | aVDZ | 3.83 | 6.13 | 6.05 |
| | MP2 | aVDZ | 4.89 | 6.29 | |
| | CCSD(T) | aVDZ | 4.39 | 5.88 | |
| | MP2 | CBS | 5.81 | 8.82 | |
| | Best Estimate[a] | | 5.30 | 8.41 | |

a) See the text for explanation

**TABLE II: Incremental binding energies ($D_0$) for HgX and XY + $nH_2O$ (kcal/mol)**

| Species | Method | Basis | n=1 | n=2 | n=3 |
|---|---|---|---|---|---|
| HgBr | B3LYP | aVDZ | 2.27 | 6.74 | 6.19 |
| | MP2 | aVDZ | 3.33 | 6.43 | |
| | CCSD(T) | aVDZ | 2.73 | 5.48 | |
| | MP2 | CBS | 4.71 | 8.24 | |
| | Best Estimate[a] | | 4.10 | 7.29 | |
| HgCl | B3LYP | aVDZ | 2.82 | 7.41 | 6.41 |
| | MP2 | aVDZ | 4.02 | 7.08 | |
| | CCSD(T) | aVDZ | 3.16 | 6.12 | |
| | MP2 | CBS | 5.54 | 8.99 | |
| | Best Estimate[a] | | 4.68 | 8.02 | |
| $Br_2$ | B3LYP | aVDZ | 2.70 | 4.49 | 5.14 |
| | MP2 | aVDZ | 2.82 | 3.99 | |
| | CCSD(T) | aVDZ | 2.32 | 3.64 | |
| | MP2 | CBS | 3.42 | 5.32 | |
| | Best Estimate[a] | | 2.92 | 4.97 | |
| BrCl | B3LYP | aVDZ | 3.70 | 4.93 | 4.99 |
| | MP2 | aVDZ | 3.97 | 3.93 | |
| | CCSD(T) | aVDZ | 3.32 | 3.50 | |
| | MP2 | CBS | 4.71 | 5.33 | |
| | Best Estimate[a] | | 4.06 | 4.90 | |
| $Cl_2$ | B3LYP | aVDZ | 1.61 | 3.86 | 5.48 |
| | MP2 | aVDZ | 2.13 | 3.25 | |
| | CCSD(T) | aVDZ | 1.78 | 3.02 | |
| | MP2 | CBS | 2.45 | 4.57 | |
| | Best Estimate[a] | | 2.11 | 4.34 | |

a) See the text for explanation

**TABLE III: Incremental binding energies ($D_0$) for atoms + $nH_2O$ (kcal/mol)**

| Species | Theory | Basis set | n=1 | n=2 | n=3 |
|---|---|---|---|---|---|
| Hg | B3LYP | aVDZ | --- | --- | --- |
| | MP2 | aVDZ | 0.24 | 3.09 | |
| | CCSD(T) | aVDZ | -0.17 | 2.75 | |
| | MP2 | CBS | 0.69 | 4.04 | |
| | Best Estimate[a] | | 0.29 | 3.70 | |
| Br | B3LYP | aVDZ | 3.95 | 5.46 | 6.91 |
| | MP2 | aVDZ | 1.73 | 3.93 | |
| | CCSD(T) | aVDZ | 1.92 | 3.94 | |
| | MP2 | CBS | 2.46 | 5.27 | |
| | Best Estimate[a] | | 2.65 | 5.28 | |
| Cl | B3LYP | aVDZ | 5.21 | 5.97 | 7.26 |
| | MP2 | aVDZ | 1.70 | 3.54 | |
| | CCSD(T) | aVDZ | 1.93 | 3.91 | |
| | MP2 | CBS | 2.46 | 5.14 | |
| | Best Estimate[a] | | 2.68 | 5.51 | |

a) See the text for explanation

**TABLE IV: Effects of microsolvation on reaction enthalpies (kcal/mol)**

| Reaction | | $\Delta H_r$ gas phase[a] | $\Delta\Delta H_r$ n=1 | $\Delta\Delta H_r$ n=2 | $\Delta\Delta H_r$ n=3 |
|---|---|---|---|---|---|
| *Atom-Atom Recombination* | | | | | |
| Hg + Br → | HgBr | -16.3 | -1.5 | -3.5 | -2.7 |
| Hg + Cl → | HgCl | -22.9 | -2.0 | -4.5 | -3.7 |
| *Atom-Diatom Recombination* | | | | | |
| HgBr + Br → | $HgBr_2$ | -73.0 | -1.4 | -1.4 | -2.5 |
| HgBr + Cl → | HgBrCl | -81.8 | -1.7 | -2.2 | -2.0 |
| HgCl + Br → | HgBrCl | -75.0 | -1.1 | -0.9 | -0.5 |
| HgCl + Cl → | $HgCl_2$ | -83.8 | -0.6 | -1.0 | -0.7 |
| *Abstraction* | | | | | |
| HgBr + Br → | Hg + $Br_2$ | -30.6 | 1.2 | 3.5 | 4.6 |
| HgBr + Cl → | Hg + BrCl | -36.5 | 0.0 | 2.4 | 3.6 |
| HgCl + Br → | Hg + BrCl | -29.7 | 0.6 | 3.7 | 5.2 |
| HgCl + Cl → | Hg + $Cl_2$ | -35.1 | 2.6 | 6.3 | 7.2 |
| *Insertion* | | | | | |
| Hg + $Br_2$ → | $HgBr_2$ | -42.4 | -2.5 | -4.9 | -7.1 |
| Hg + BrCl → | HgBrCl | -45.3 | -1.7 | -4.6 | -5.6 |
| Hg + $Cl_2$ → | $HgCl_2$ | -48.7 | -3.2 | -7.3 | -7.8 |

a) Atom-atom recombinations taken from Ref. 25 with other enthalpies from Ref. 19.

**Figure I: Microsolvated structures of $HgBr_2$**

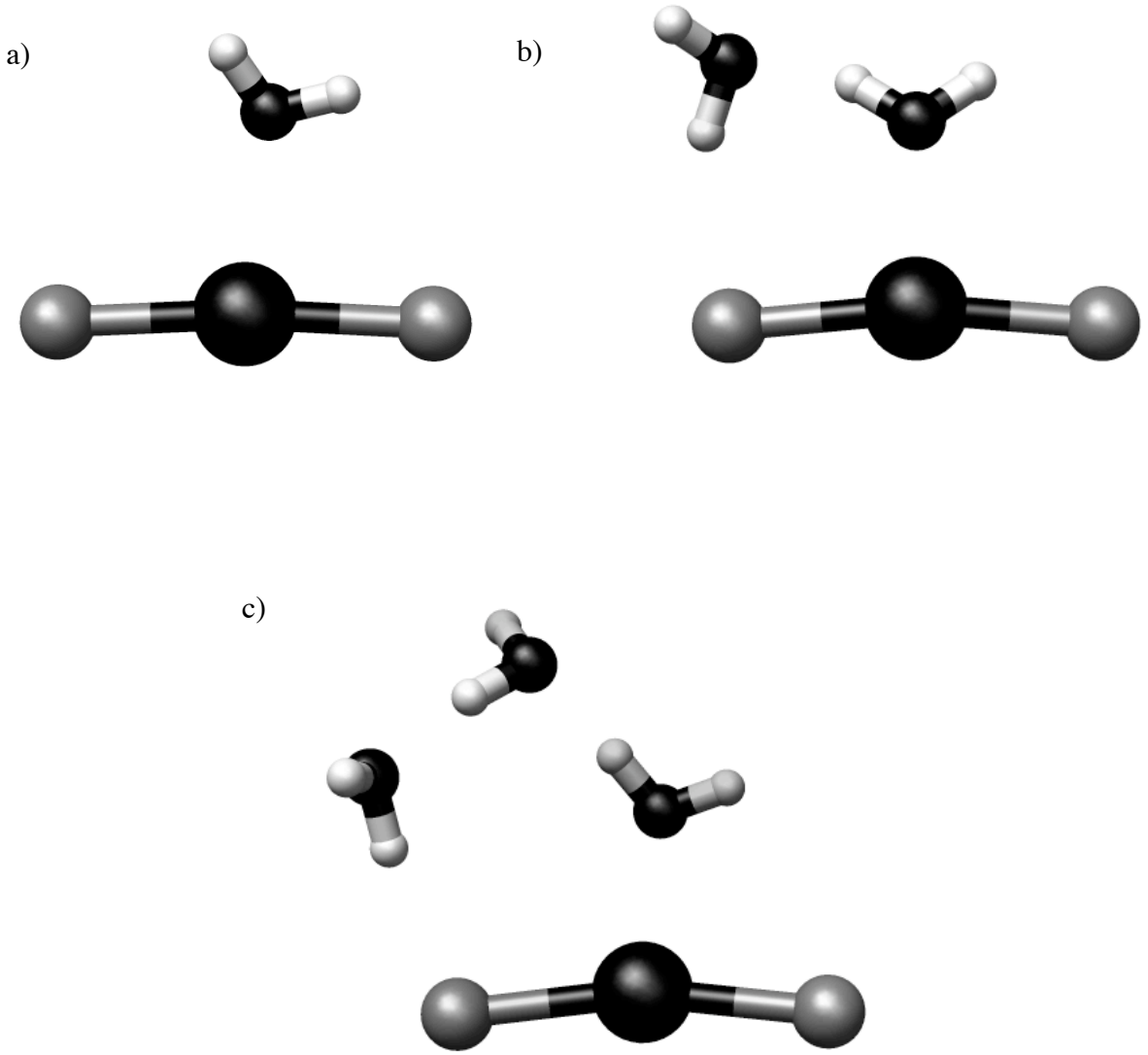

**Figure II: Microsolvated structures of HgBr**

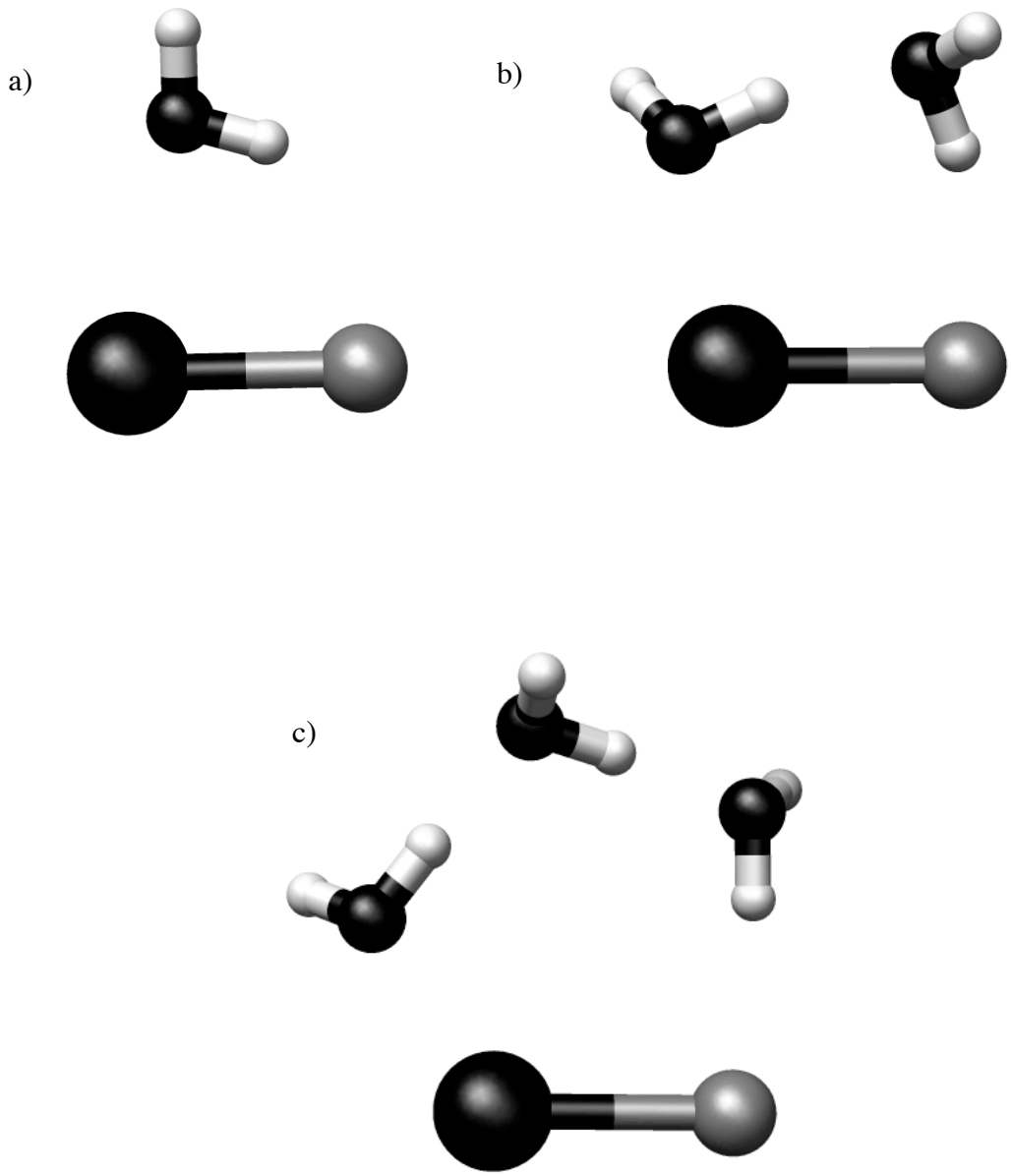

**Figure III: Microsolvated structures of $Br_2$**

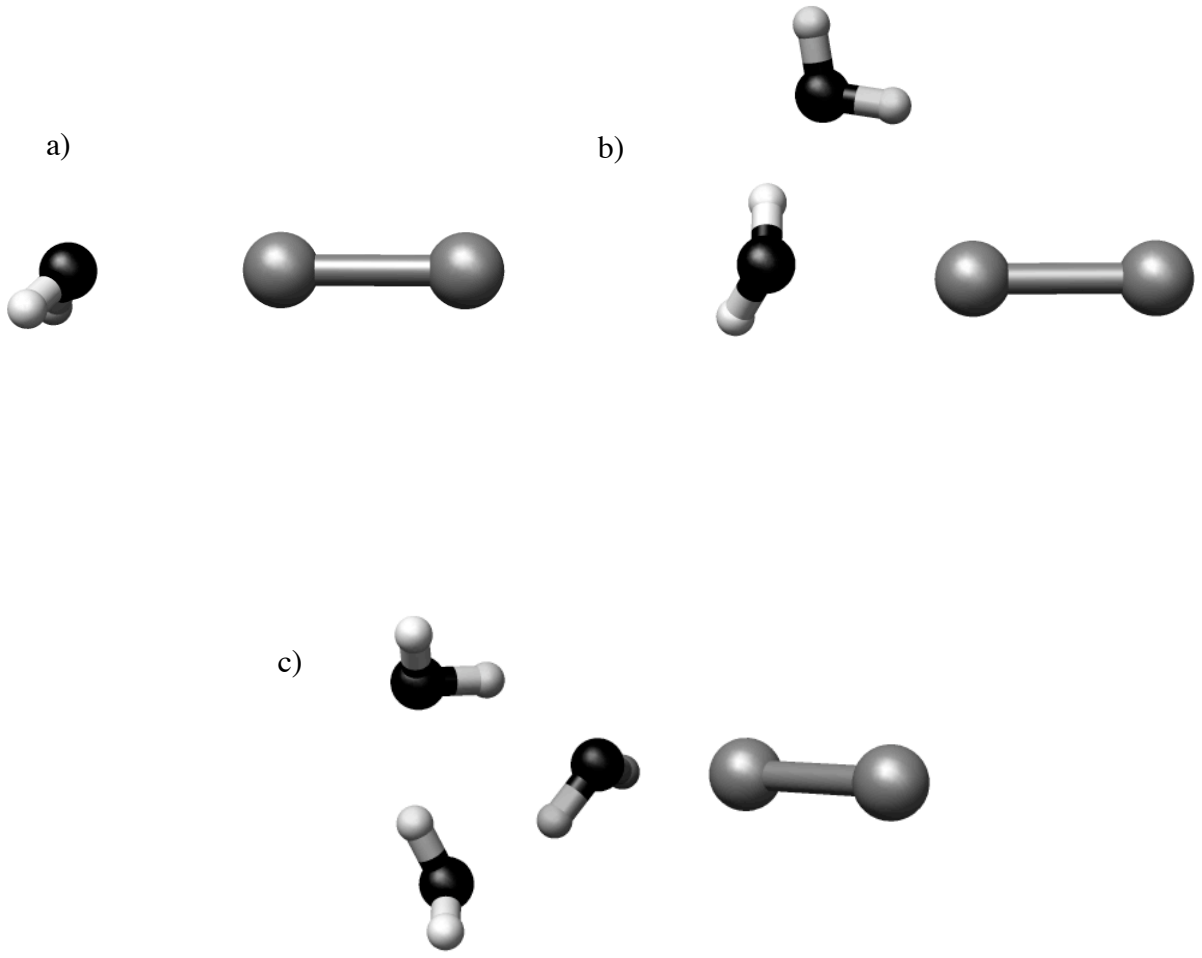

**Figure IV: Microsolvated structures of Br atom**

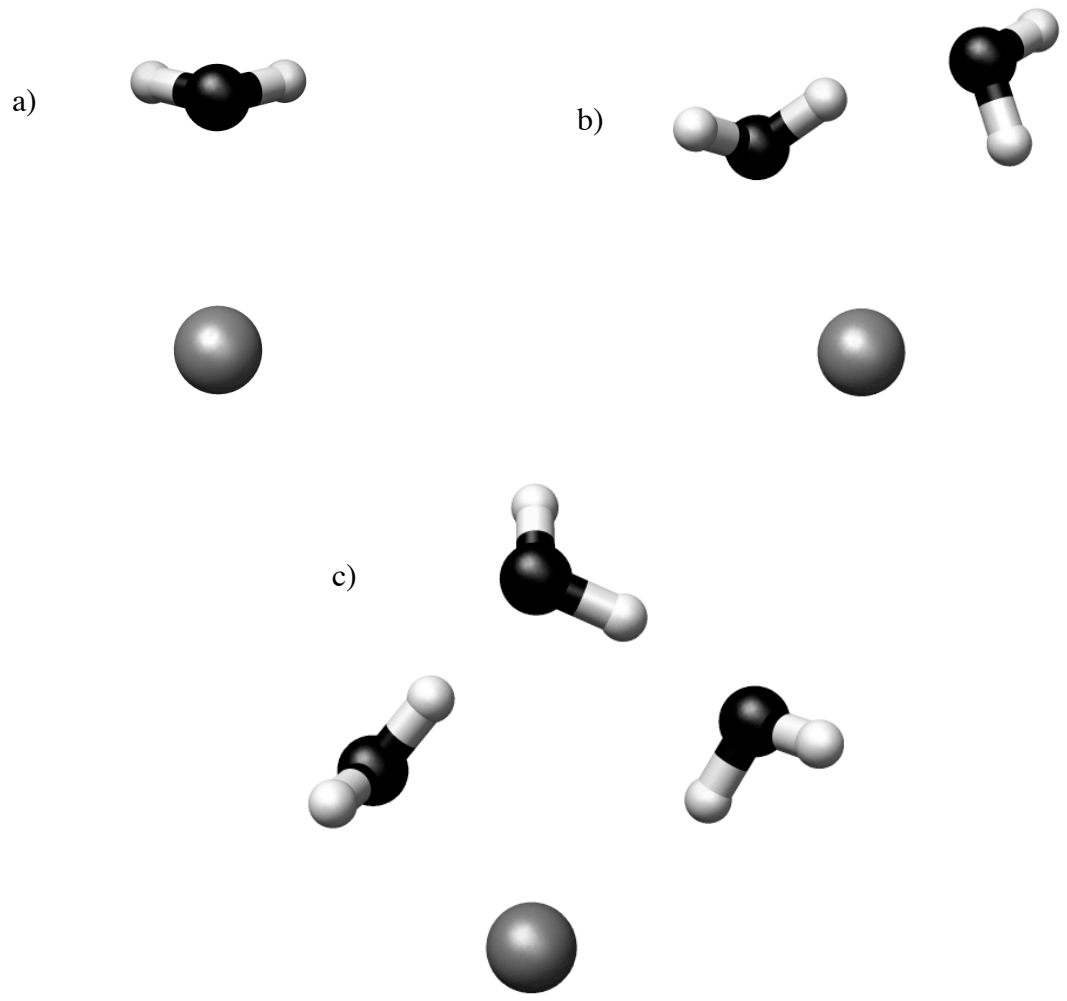

**Figure V: Microsolvated structures of Hg atom**

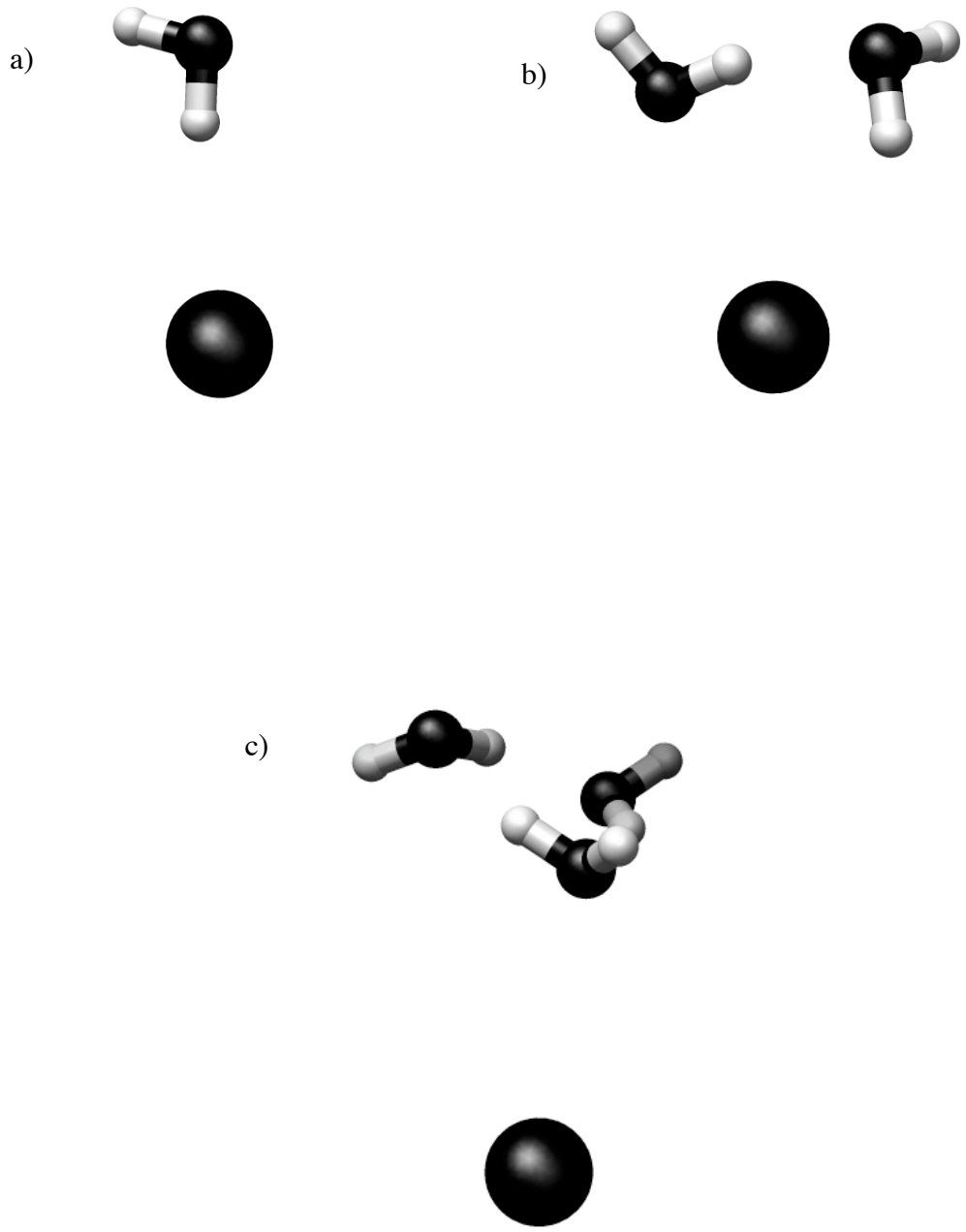

**Figure VI: Alternate conformers**

a)

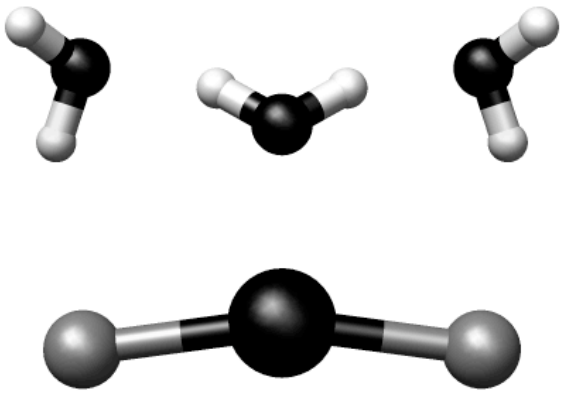

b)

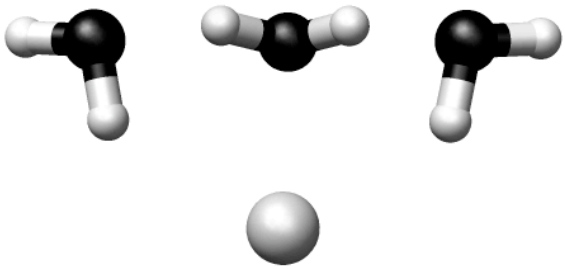

c)

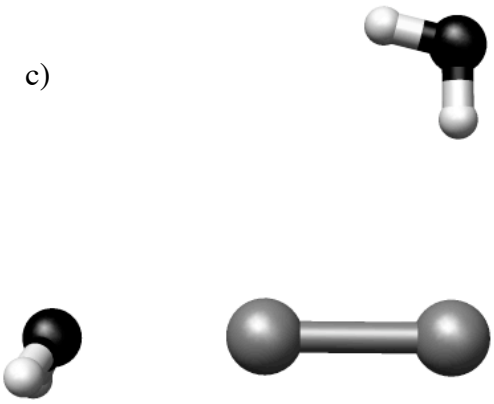

# Chemically Accurate Thermochemistry of Cadmium: An ab Initio Study of Cd + XY (X=H, O, Cl, Br; Y=Cl, Br)

**Benjamin C. Shepler and Kirk A. Peterson***

*Department of Chemistry, Washington State University, Pullman, Washington 99164-4630*

Using a composite coupled cluster method employing sequences of correlation consistent basis sets for complete basis set (CBS) extrapolations and with explicit treatment of core-valence correlation and scalar and spin-orbit relativistic effects, the 0 K enthalpies of a wide range of cadmium-halide reactions, namely Cd + (HCl, HBr, ClO, BrO, $Cl_2$, BrCl, $Br_2$) have been determined to an estimated accuracy of ±1 kcal/mol. In addition, accurate equilibrium geometries, harmonic frequencies, and dissociation energies have been calculated at the same level of theory for all the diatomic (e.g., CdH, CdO, CdCl, CdBr) and triatomic (CdHCl, CdHBr, CdClO, CdBrO, $CdCl_2$, CdBrCl, $CdBr_2$) species involved in these reactions, some for the very first time. Like their mercury analogs, all of the abstraction reactions are predicted to be endothermic while the insertion reactions are strongly exothermic with the formation of stable linear, Cd-centric complexes. With the exception of CdH and the reactions involving this species, the present results for the remaining Cd-containing systems are believed to be the most accurate to date.

*Journal of Physical Chemistry A.* submitted.

## I. INTRODUCTION

There has recently been a great deal of interest in the reactions between mercury and reactive halogen species (see, for example, Refs. 1-3 and references therein). These reactions have been of interest due to their likely involvement in recently observed depletions of atmospheric mercury concentrations in the polar troposphere during polar spring[4-7] and also these reactions' more general involvement in the global cycling of mercury[8,9]. Cadmium is a toxic heavy metal similar to mercury in that it has long atmospheric residence times and also exhibits long range transport from its original emission sources[10]. The major natural source of Cd in the atmosphere is volcanic emission[10,11]. The major anthropogenic sources of atmospheric cadmium are comparable to or greater than the natural sources, and the most significant of these are waste incineration and non-ferrous metals production[10]. Due to the similarity of the chemistry between mercury and cadmium, it is likely that reactions between cadmium and reactive halogen species play an important role in the global cycling of cadmium. Unlike mercury, however, cadmium exists predominately in the particulate phase in the atmosphere[10,11]. A fundamental understanding of cadmium's gas phase chemistry is valuable in the understanding of the formation of these particles and also to form a basis for future studies into the heterogeneous chemistry of cadmium. Gas phase reactions between cadmium and small halogen containing species are also likely to be important in combustion chemistry and thus relevant to the primary ways in which cadmium is introduced into the atmosphere.

Despite this potential importance of reactions between cadmium and small halide molecules, very little is known about their gas phase properties and specifically the thermochemistry of cadmium halides. To broaden the current knowledge of such reactions, this work reports an ab initio investigation of the thermochemistry, equilibrium geometries, and vibrational frequencies

of species relevant to the reactions Cd + {HCl, HBr, ClO, BrO, $Cl_2$, $Br_2$, and BrCl}, which include the following cadmium-containing products: the diatomic molecules CdH, CdO, CdCl, CdBr and the triatomic species CdHCl, CdHBr, CdClO, CdBrO, $CdCl_2$, $CdBr_2$, and CdBrCl. The reactions of Cd with HCl and HBr should be particularly important in combustion chemistry. The gas phase properties of CdHCl and CdHBr are also of particular interest since ZnHCl was recently the first gaseous metal hydrochloride to be observed experimentally[12] and CdHCl has recently been studied in argon matrices.[13] Diatomic cadmium halides have also received some prior attention due to their lasing properties[14] analogous to their mercury counterparts.

While accurate thermochemical information was not previously available for many of the species and reactions in this study, there have been a few experimental investigations of gas phase and matrix isolated cadmium dihalides. Klemperer[15] first reported the gas phase infrared (IR) spectra of $CdBr_2$ and $CdCl_2$ in 1956. Givan, Loewenschuss, and co-workers[16-19] conducted a number of IR and Raman studies of matrix isolated $CdBr_2$, $CdCl_2$, and CdBrCl in the 1970s. There have also been a number of electron diffraction studies that allowed for estimates of the bond lengths in $CdCl_2$ [20] and $CdBr_2$.[21] Further, an early mass spectrometric investigation of CdBrCl allowed researchers to calculate a rough value for its heat of formation.[22]

The diatomic cadmium halides CdBr and CdCl have received considerably less experimental attention and have been limited to studies focused on their electronic spectroscopy.[14,23,24] CdO has been observed in matrices via IR, Raman and UV-Vis spectroscopy[25,26] and has also been studied in the gas phase via mass spectrometry.[27] Unlike the other diatomic cadmium molecules in this study, CdH has been very well characterized in the gas phase.[28]

A number of the molecules in this study have been previously studied theoretically using relatively modest levels of electron correlation and basis sets. The first such calculations were carried out by Stromberg et al.[29] who reported small configuration interaction calculations on $CdCl_2$ using effective core potentials and double-zeta basis sets. Since those first calculations a number of studies have been carried out on CdCl, CdBr, $CdCl_2$, and $CdBr_2$ using semiempirical[30], DFT[31,32], and MP2[33] methods with triple-zeta or smaller basis sets. CdHCl has been previously studied with B3LYP and triple-zeta quality basis sets.[13]

In this work we have used a composite thermochemical approach similar to that used in previous investigations in our group, as well as by Feller, Dixon, and co-workers (c.f., Refs. 34-42 and references therein). Closely related procedures include the recently proposed HEAT method,[43] the W*n* methods of Martin and co-workers,[44] and the focal point technique of Schaefer and co-workers.[45] The present procedure, which has been shown to yield enthalpies accurate to within 1 kcal/mol or better, generally involves calculations with coupled cluster theory with extrapolations of these total energies to the complete basis set limit. Further corrections such as core-valence correlation and relativistic effects are then added based on the specific nature of the problem under study. In this work the additional corrections we include are for core-valence correlation, spin-orbit coupling, scalar relativistic effects, and the pseudopotential approximation. The presently reported heats of reaction are expected to be the most accurate to date for nearly all of the reactions studied. Additionally, with the exception of CdH, the calculated equilibrium structures for all of the cadmium-containing molecules, i.e., CdHCl, $CdCl_2$, CdBrCl, $CdBr_2$, CdO, CdCl, and CdBr, should be the most reliable values currently available. To the best of our knowledge this is the first report, either experimental or theoretical, for the gas phase molecules CdBrO, CdClO, and CdHBr.

## II. METHODOLOGY

In preparation for a subsequent study of their spectroscopic properties, near-equilibrium potential energy surfaces consisting of 74 points around the equilibrium geometries were computed for each of the triatomic molecules. Symmetry considerations reduced the number of points that were explicitly calculated for $CdCl_2$ ($D_{\infty h}$) and $CdBr_2$ ($D_{\infty h}$) to 26, and for the other triatomic molecules ($C_{\infty v}$ with Cd as the central atom) the number of points was reduced to 50. The potential surfaces were fit to polynomials in internal displacement coordinates using the program SURFIT.[46] Equilibrium geometries, harmonic frequencies, and anharmonicity constants were then determined from the resulting polynomial coefficients. For the diatomic molecules a series of seven points were computed about $r_e$, and the resulting curves were also accurately fit to polynomials. The usual Dunham[47] analysis was utilized to determine the spectroscopic constants. In each case anharmonic zero point vibrational energies (ZPEs) were determined from the quartic forcefields using the calculated harmonic frequencies and anharmonicity constants.[48]

The first series of calculations that were carried out determined the reaction enthalpies and dissociation energies with the coupled cluster singles and doubles method with a perturbative treatment of triple excitations[49-51] [CCSD(T)] at the complete basis set (CBS) limit. The frozen core approximation was applied in these cases. For all open shell molecules and atoms the R/UCCSD(T)[51-53] method was used, i.e., restricted open shell Hartree-Fock (ROHF) calculations were used to determine the reference wavefunctions but the spin restriction was relaxed in the coupled cluster calculations. In the open shell atomic calculations the orbitals were symmetry equivalenced between all three components ($P_x$, $P_y$, and $P_z$) of the ground state terms. All of the coupled cluster calculations were carried out with the MOLPRO 2002.6 suite of electronic structure programs.[54]

The basis sets used in this work are from the systematically convergent correlation consistent family of basis sets. Basis sets of double-ζ through quintuple-ζ quality, augmented with an additional diffuse function of each angular momentum type, were used in these first series of calculations. For oxygen and hydrogen the basis sets corresponded to the aug-cc-pV*n*Z sets[55]; for chlorine the aug-cc-pV(*n*+*d*)Z sets[56] that contain modified *d*-shells containing additional tight exponents; for cadmium[39] and bromine[57] the aug-cc-pV*n*Z-PP sets with energy consistent small-core relativistic pseudopotentials (PPs) of the Stuttgart/Köln type.[57,58] The relativistic PP for cadmium replaced 28 electrons leaving the $4s^2 4p^6 4d^{10} 5s^2$ electrons to be treated explicitly and that for bromine replaced 10 electrons leaving the $3s^2 3p^6 3d^{10} 4s^2 4p^5$ electrons to be treated. A summary of the electrons excluded from the core and the active atomic orbitals associated with the different basis sets employed in this study is provided in Table 1. The group of basis sets just described will be simply denoted aVnZ (n=D, T, Q, 5) throughout the remainder of the paper. For geometries corresponding to linear structures all four basis sets from aVDZ to aV5Z were used, but for bent triatomic geometries the largest basis set employed was aVQZ. The systematic convergence of these basis sets was exploited to obtain an estimate of the CBS limit for the total energies using two extrapolation formulas:

$$E(n) = E_{\mathrm{CBS}} + Be^{-(n-1)} + Ce^{-(n-1)^2} \tag{1}$$

$$E(n) = E_{\mathrm{CBS}} + B/n^3. \tag{2}$$

In Eq.(1)[59,60] the three largest basis sets used at that geometry were used in the extrapolation while for the second formula[61,62] two basis sets were used. Total energies were used in each case. The best estimate of the CBS limit was taken as the average of the two extrapolation procedures and the spread in these two limits provided an approximate uncertainty in the basis

set extrapolation, since Eq.(1) generally underestimates the true limit while on average Eq. (2) overestimates.[42]

After obtaining CCSD(T) potential surfaces at the CBS limit, the first correction taken into account was for core-valence correlation, ΔCV. When including correlation of the core electrons, triple-ζ basis sets of the weighted core-valence type were used. For oxygen and chlorine the aug-cc-pwCVTZ[63] sets were utilized, while the aug-cc-pwCVTZ-PP basis sets were employed for cadmium[39] and bromine.[64] Henceforth these sets will be denoted awCVTZ. At each geometry two CCSD(T) calculations were carried out with these awCVTZ basis sets, one in which only the valence electrons were correlated and a second with all electrons correlated except the 1s electrons of chlorine. A core-valence correction was then calculated for each point on the potential surface by taking the difference of these two resulting energies. The ΔCV corrections were only determined for linear geometries.

The next contribution considered was for spin-orbit coupling, ΔSO, where aVTZ basis sets were used throughout. For Cd and Br the one-electron spin-orbit operators were taken from the PPs used in the calculations described above. In the cases of O and Cl, PPs were also used in the SO calculations. Both the Cl[65,66] and O[67] PPs were of the large core, Stuttgart/Köln variety, leaving just the valence electrons to be explicitly treated. The Cl and O basis sets used in these cases corresponded to the aVTZ sets described above, but were recontracted in the presence of the PPs. The multireference configuration interaction method with single excitations (MRCIS) was used with standard valence complete active spaces to determine the spin-orbit corrections. This combination of method and basis set was found to give accurate results in our previous work on the thermochemistry of mercury halides[41]. As in that work, the spin-orbit CI code[68] implemented in the COLUMBUS suite of *ab initio* programs[69] was used. The spin-orbit-MRCIS

(SO-MRCIS) calculations utilized sets of natural orbitals determined from single reference configuration interaction singles and doubles (CISD) calculations carried out with MOLPRO. The spin-orbit correction was calculated as the energy difference between a MRCIS calculation without the SO operator and a SO-MRCIS calculation that mixed all singlet and triplet (or doublet and quartet) configurations. The ΔSO corrections were also only determined for linear geometries.

While small-core relativistic PPs provide a convenient and accurate technique to account for relativistic effects in atoms and molecules, the loss of nodal structure in the orbitals can introduce small errors in such calculations (c.f., Refs. 70,71). To approximately account for this effect, energy differences calculated with the PP approach using the aVTZ basis sets have been compared to values determined using the all-electron Douglas-Kroll-Hess (DKH) Hamiltonian.[72,73] In these latter all-electron calculations, the Cd basis set corresponded to a newly developed aug-cc-pVTZ-DK set[39] where the exponents and contraction coefficients were optimized using the DKH Hamiltonian. Standard aug-cc-pVTZ basis sets[74] recontracted[75] in atomic DKH calculations were employed for the other atoms (H, O, Cl, Br). These combinations of basis sets will henceforth be denoted as aVTZ-DK. Comparison of the energies calculated at the CCSD(T)/aVTZ and DKH-CCSD(T)/aVTZ-DK levels of theory yielded the final correction ΔDK. It is important to note that this contribution includes not only corrections due to the pseudopotential approximation but also the small scalar relativistic effects arising from the atoms not treated by PPs (H, O, and Cl).

One possible remaining concern is that the DKH Hamiltonian does not treat scalar relativistic effects to a sufficient level of accuracy for the Cd-containing molecules to reliably compare the all-electron energy differences (and geometries) with the PP results. This was

investigated by calculating reaction energies using the second- (DK2) and third-order (DK3) Douglas-Kroll Hamiltonians[76] for the reactions $Cd+Br_2 \rightarrow CdBr_2$, $CdBr+Br \rightarrow CdBr_2$, and $Cd+Br \rightarrow CdBr$. These calculations were performed at the MP2 level of theory using aVTZ-DK basis sets with the GAMESS[77] suite of electronic structure programs. In all three of these reactions the differences between the DK2 and DK3 results were less than 0.01 kcal/mol. These results are consistent with our previous study,[41] where it was found that while for mercury there were non-negligible differences between DK2 and DK3 dissociation and reaction energies, DK2 was sufficient up through iodine.

## III. RESULTS AND DISCUSSION

### A. Molecular Structures

Table 2 contains the calculated and experimental equilibrium bond lengths for the 11 diatomic and 7 triatomic molecules involved in this study. The best theoretical values were determined at the CCSD(T)/CBS level of theory with contributions due to core-valence correlation (ΔCV), spin-orbit coupling (ΔSO), and a correction for the pseudopotential approximation and scalar relativity on the light atoms (ΔDK). Table 2 shows the best directly calculated value, CCSD(T)/aV5Z, as well as the effect of the CBS extrapolations (ΔCBS), the effects of each of the other three corrections noted above, and the final predicted results (aV5Z+ΔCBS+ΔCV+ΔSO+ΔDK). In every case the CCSD(T)/aV5Z bond lengths are longer than the best estimates, and in some cases considerably so. The corrections for basis set incompleteness and core-valence correlation have the largest effects and always result in bond length shortening. With the exception of H-containing bonds, the CBS extrapolation typically results in a shortening of about -0.002 Å relative to the aV5Z bond lengths, with some molecules

($Cl_2$, $Br_2$, and $BrCl_2$) having ΔCBS values as large as –0.004 Å. The typical magnitude of the core valence correction on the bond lengths was even larger, with an average value of –0.007 Å for the 23 bond lengths listed in Table 2. The largest core valence corrections were for the Br-containing bonds due to the relatively large effect of correlating the 3d electrons.

In contrast to the two previously discussed corrections to the valence-only CCSD(T)/aV5Z bond lengths, the contributions due to molecular spin-orbit coupling were significantly smaller. In only six cases was the magnitude of this correction larger than 0.001 Å. The largest was for $Br_2$ (-0.0021 Å) and BrO (-0.0024 Å). It was perhaps a little surprising that the heavier Cd atom did not result in larger spin-orbit effects, but this presumably reflects the lack of 5p character in these systems. The ΔDK corrections (scalar relativity on H, Cl and O and the pseudopotential approximation) were also very small and never larger than about 0.001 Å.

Accurate experimental values appear to only be available for CdH and the non-Cd containing molecules. In these cases each of the calculated values agree, in general, very well with experiment. The largest differences occur for ClO ($\Delta r_e$=0.0041Å), BrO ($\Delta r_e$=0.0034Å) and CdH ($\Delta r_e$=0.0092 Å). However ClO, BrO, and CdH were the only molecules in this study where the $T_1$ diagnostic[78] was larger than 0.03, and hence much of these differences with experiment are likely due to higher order electron correlation effects. In fact, recent CCSDT and CCSDTQ calculations on ClO and BrO by the present authors have shown that more extensive electron correlation completely removes the remaining discrepancy with experiment in these cases.[79] Even with the relatively high CCSD $T_1$ diagnostic for CdH, the disagreement in the calculated and experimental bond lengths was a little surprising since, as discussed below, the harmonic frequencies and dissociation energies agree with experiment to within 2 $cm^{-1}$ and 0.1 kcal/mol,

respectively. The potential curve of this molecule is rather flat, however, which makes the $r_e$ value very sensitive to relatively small contributions like higher electron correlation effects. To further investigate some of the sources of this error, all-electron DK calculations were also carried out for ΔCV using aug-cc-pwCVTZ-DK basis sets. This yielded a core-valence correction for $r_e$ of just –0.0040 Å for CdH in comparison to the PP value as shown in Table 2 of –0.0064 Å. This decreases the disagreement with experiment to 0.0066 Å, much of which could now presumably be accounted for by higher electron correlation effects upon comparison to the ClO and BrO results. Larger basis set (aug-cc-pwCVQZ-PP) core-valence calculations were also carried out on CdH, but this yielded negligible differences in ΔCV for $r_e$ (<0.0001 Å) from the aug-cc-pwCVTZ-PP value. It should also be noted that DK calculations for ΔCV were also carried out for CdBr and $CdBr_2$ to determine if this would lead to systematically better agreement with experiment for the other equilibrium bond lengths of this study, but the differences from the PP results in these cases were only 0.001 Å. This was not deemed large enough to warrant the recalculation of ΔCV for the remaining molecules of this study. Additionally, the difference in ΔCV computed with pseudopotentials or DK for $\omega_e$ was only 2 $cm^{-1}$ for CdBr and the ΔCV's for the latter molecule's dissociation energy only differed by 0.07 kcal/mol.

All of the triatomic molecules of this study were found to have linear equilibrium geometries with Cd as the central atom, in agreement with previous theoretical and experimental investigations. However, as can be seen in Table 3, these species generally have fairly small bending force constants and only CdHBr and CdHCl have bending harmonic frequencies larger than about 100 $cm^{-1}$. Only the molecules $CdCl_2$ and $CdBr_2$ have experimentally reported bond

lengths and for both molecules the values come from X-ray diffraction experiments.[20,21,80-82] The experimental bond lengths for $CdCl_2$ are fairly disparate, having values of 2.21 Å, 2.266 Å, and 2.8282 Å. The presently calculated value of 2.249 Å lies within this range, but does not agree particularly well with any of the experimental values. In the case of $CdBr_2$ our predicted value of 2.377 Å also falls within the range of the two sets of experimental bond lengths, 2.372 Å and 2.394 Å. Unlike $CdCl_2$, the calculated $CdBr_2$ value is in good agreement with one of the experimental results. Due to the high level of the current calculations, our predicted bond length of 2.249 Å for $CdCl_2$ is certainly the most reliable to date and has an expected uncertainty of about ±0.005 Å.

In addition to the experimental data there have been a small number of previous theoretical predictions of bond lengths for the cadmium molecules in this study. Configuration interaction (CI) calculations carried out by Stromberg et al.[29] yielded a bond length of 2.32 Å for $CdCl_2$ in what were sophisticated calculations for the time. In 1995 Liao et. al.[31] reported density functional theory (DFT) calculations employing double-zeta quality basis sets to predict bond lengths for CdCl (2.38 Å), CdBr (2.52 Å), $CdCl_2$ (2.28 Å), and $CdBr_2$ (2.41 Å). These values are in qualitative agreement with our current values, but are larger by 0.03 to 0.05 Å. These results seem reasonable in light of the differences in electron correlation and basis set completeness. Also in the mid-1990's Kaupp and von Schnering[33] carried out MP2 calculations with double-zeta basis sets and determined bond lengths of 2.369 Å for CdCl and 2.292 Å for $CdCl_2$ in approximate agreement with the previously mentioned DFT calculations. CdO was also studied by DFT methods at approximately the same time by Chertihin and Andrews,[26] and their resulting bond length of 1.924 Å was also slightly longer but in qualitative agreement with

our predicted value of 1.903 Å. More recently Zhao et al.[32] have carried out DFT calculations on $CdCl_2$ and $CdBr_2$ and these were of similar quality to the other earlier work.

In the case of CdH, theoretical bond lengths have been previously reported using multireference second-order configuration interaction[83] (MR-SOCI) (1.761 Å), MP2[33] (1.739 Å), and 4-component CCSD[84] (1.778 Å). The MR-SOCI value of Balasubramanian[83] agrees very well with experiment, but this is probably partly due to a fortuitous cancellation of errors since their calculated harmonic frequencies and dissociation energies were not in as close agreement. Last, the CdHCl molecule was previously studied via DFT using triple-zeta quality basis sets[13] and those calculations predicted a H-Cd bond length of 1.673 Å and a Cd-Cl bond length of 2.362 Å, which are both considerably longer than the values calculated here (1.639 Å and 2.267 Å, respectively).

In general, the predicted equilibrium structures of the present work are a considerable improvement over the previously calculated results for the Cd-containing molecules of the present study. With the exception of CdH, the predicted bond lengths of this work are expected to be accurate to within about ±0.005 Å.

**B. Vibrational Frequencies**

The harmonic vibrational frequencies are compiled along with the available experimental values in Table 3. The theoretical anharmonic zero point energies are also shown. Accurate experimental harmonic frequencies have been reported for all of the diatomic molecules except CdO. In general the agreement between theory and experiment is excellent. The largest differences are again for ClO and BrO, which only differ from experiment by +9.6 $cm^{-1}$ and +6.6 $cm^{-1}$, respectively. The fact that the harmonic frequencies are too large for ClO and BrO is consistent with their theoretical bond lengths being too short. Chertihin and Andrews[26] derived a

gas-phase fundamental vibrational frequency for CdO of 650±10 $cm^{-1}$ based on matrix-isolated infrared studies of the products observed from reactions of laser ablated Cd atoms with $O_2$. The bands actually observed were at 645.1 $cm^{-1}$ and 654.4 $cm^{-1}$ for what they believed to be CdO in solid argon and solid nitrogen, respectively. Using the theoretical harmonic frequency for CdO in Table 3 and a calculated anharmonicity constant, $\omega_e x_e$ =3.9 $cm^{-1}$, yields a theoretical fundamental vibrational frequency of 607 $cm^{-1}$, which is 43 $cm^{-1}$ lower than the experimental estimate. The specific reason for this large disagreement is not entirely clear. It is possible the experimental bands were strongly blue shifted due to matrix interactions or even other molecules in the matrices.

For the most part experimental high resolution gas phase vibrational frequencies also do not exist for the triatomic molecules in this study. The experimental values for $CdCl_2$, $CdBr_2$, and CdBrCl correspond to fundamental vibrational frequencies taken from matrix isolated infrared and Raman experiments.[16-19] The theoretical gas phase harmonic frequencies of Table 3 are in good qualitative agreement with these fundamentals. The largest differences are observed for $CdCl_2$ where the symmetric and antisymmetric stretches differ by 15 $cm^{-1}$ and 20 $cm^{-1}$, respectively. As one might expect, the theoretical values are larger in all cases (except the $CdCl_2$ bending mode) due primarily to red shifting of the experimental values from matrix interactions and to a lesser extent the neglect of anharmonicities in the theoretical values; the calculated anharmonicities were in all cases small and generally much less than 1 $cm^{-1}$. CdHCl has also recently been investigated in matrices with IR and UV-Vis spectroscopic methods.[13] The experimental values for this molecule in Table 3 correspond to the harmonic vibrational frequencies. Again, the theoretical and experimental values are in good qualitative agreement,

with the theoretical gas-phase values being larger than the experimental matrix isolated frequencies. Neither CdHBr, CdClO, nor CdBrO have been previously studied by theory or experiment.

Previous theoretical work has yielded harmonic vibrational frequencies for many of these cadmium-containing molecules. CdCl and CdBr frequencies have been previously calculated by DFT, yielding values of 305 and 214 $cm^{-1}$, respectively.[31] These results differ from the experimental values by 30 and 16 $cm^{-1}$, respectively while the current CCSD(T) results differ by just 4 and 3 $cm^{-1}$. A CdO harmonic frequency has also been calculated with DFT,[26] which yielded a value of 598 $cm^{-1}$, 16 $cm^{-1}$ smaller than the currently predicted value shown in Table 3. Consistent with the DFT bond lengths that were much too long compared to the present results, the DFT harmonic frequencies are generally significantly smaller than the CCSD(T)/CBS+CV+SO results. DFT harmonic frequencies have also been calculated for $CdCl_2$,[31,32] $CdBr_2$,[31,32] CdBrCl,[32] and CdHCl,[13] and these are also significantly smaller than the currently calculated values, as well as the experimental matrix isolation results. The previous MR-SOCI[83] calculations on CdH resulted in a harmonic frequency of 1524 $cm^{-1}$, while 4-component CCSD[84] yielded a value of 1370 $cm^{-1}$. By comparison, the current CdH harmonic frequency obtained with our composite approach was calculated to be 1462 $cm^{-1}$, which is nearly identical to the experimental (harmonic) infrared value of 1461 $cm^{-1}$.

**C. Dissociation energies and reaction enthalpies**

The dissociation energies, $D_0$, for the 11 diatomic molecules of this work are shown with their individual contributions in Table 4, where they are also compared to the best available experimental values. The latter were available for the seven non-cadmium-containing

molecules, as well CdH. In all of these cases the agreement between theory and experiment is excellent. Differences are larger than 0.2 kcal/mol only for $Br_2$, ClO, and BrO. Even in these cases the differences are only +0.26, –0.22, and –0.23 kcal/mol, respectively. It should be noted that the ClO and BrO dissociation energies include corrections from CCSDTQ calculations taken from ref. 79. Huber and Herzberg[85] give uncertain values for the dissociation energies of CdO (an upper bound of 88 kcal/mol vs. the calculated value of 21.71 kcal/mol), CdBr (21-37 kcal/mol vs. the calculated value of 34 kcal/mol), and CdCl (~49 kcal/mol vs. the calculated value of 43.6 kcal/mol). To our knowledge there do not exist reliable experimental dissociation energies for these molecules.

As with the bond lengths, the largest corrections to the dissociation energies are from basis set incompleteness and core-valence correlation. The effect of increasing the basis set from quintuple-zeta to the CBS limit is estimated to generally increase the dissociation energies by about 0.5-1 kcal/mol. The exception to this trend is CdH where the difference between the aV5Z $D_e$ and the CBS limit was calculated to be just 0.02 kcal/mol. The basis set convergence is very fast for this molecule; the difference in $D_e$ between aVTZ and aVQZ is only 0.4 kcal/mol, while the average for the other 10 molecules is 2.2 kcal/mol. The core-valence corrections follow no clear trend and range from +0.44 to –0.91 kcal/mol, with the covalent molecules having core-valence effects tending to increase dissociation energies while the more ionic molecules tend to have negative core-valence corrections.

As observed in Table 4, the corrections to the diatomic $D_e$'s for spin-orbit coupling can be rather large, especially for molecules that contain bromine. The majority of this effect, however, is due to the zero-field splitting of the atoms, as well as first-order splittings in the $^2\Pi$ states of ClO and BrO. It is probable that the magnitude of the spin-orbit correction is

underestimated in the present calculations. The zero-field splitting of the atoms can give some estimate of the error in the spin-orbit corrections. The difference between the calculated *J*-averaged level and the *J*=3/2 level for the Br and Cl atoms are 3.28 and 0.87 kcal/mol. The experimental values for these differences are 3.51 and 0.84 kcal/mol. Thus, the spin-orbit correction is too small for Br atom by 0.23 kcal/mol and would suggest that the magnitude of the negative spin-orbit correction in the dissociation energies is slightly underestimated. This may partly explain the dissociation energies for $Br_2$ and BrCl being larger than the experimental values by 0.27 and 0.13 kcal/mol.

As with the bond lengths, the effect due to scalar relativity on H, O, and Cl together with the correction for the PP approximation (ΔDK) is relatively small but non-negligible. Scalar relativistic effects on $D_e$ from Cl amount to about –0.2 kcal/mol (see, for example, HCl, ClO, and $Cl_2$, which do not involve pseudopotentials), while the corrections for the pseudopotential approximation are estimated to be at most a few tenths of a kcal/mol.

Reaction enthalpies at 0K are given in Table 5 for the gas phase reactions

$$\mathrm{Cd} + \mathrm{XY} \rightarrow \begin{cases} \mathrm{CdX} + \mathrm{Y} \\ \mathrm{CdY} + \mathrm{X} \\ \mathrm{XCdY} \end{cases}$$

where X={Cl, Br} and Y={H, O, Cl, Br}. For most of the reactions it is not possible to compare with experiment because reliable experimental heats of formation are not available for most of the cadmium halide molecules. It was possible, however, to derive accurate experimental enthalpies for Cd + HBr → CdH + Br and Cd + HCl → CdH + Cl based on the accurate experimental dissociation energies for CdH, HCl, and HBr. The agreement between theory and

experiment for these two reactions is excellent, with differences of just +0.07 and +0.14 kcal/mol, respectively.

Experimental heats of formation at 298 K for $CdBr_2$ and $CdCl_2$ are given in Ref. 86, who cite Ref. 87, but no uncertainties are provided nor is it stated by what means the enthalpies are determined. Converting these values to 0 K, however, using standard ideal gas forms of the partition functions and combined with accurate 0 K heats of formation for Cd(g) (28.20 ± 0.05 kcal/mol)[88,89] and $Br_2$ (10.92 ± 0.03 kcal/mol),[90] yielded experimental 0 K enthalpies for Cd + $Cl_2 \rightarrow CdCl_2$ and Cd + $Br_2 \rightarrow CdBr_2$, of –73.8 and –70.1 kcal/mol, respectively. These differ from our calculated values (see Table 5) by –3.2 kcal/mol and +1.0 kcal/mol, respectively. Based on the agreement between theory and experiment for the diatomic dissociation energies and the Cd + HCl and Cd + HBr reactions, it is expected that the final theoretical reaction enthalpies in Table 5 should be accurate to at least 1 kcal/mol. Hence, the cited experimental heat of formation for $CdCl_2$ may have a relatively large uncertainty.

The enthalpies in Table 5 are qualitatively similar to previous work on the reactions between Hg and the same halogen species[34] (not including HCl and HBr). All of the abstraction reactions (Cd + XY → CdX + Y) are endothermic, while the insertion reactions (Cd + XY → XCdY) are exothermic. One major difference between the mercury and cadmium reactions is that the abstraction reactions with cadmium are significantly less endothermic than the mercury cases due to the larger dissociation energies of the cadmium halides compared to the mercury halides. All of the mercury abstraction reactions involving $Br_2$, $Cl_2$, and BrCl were calculated to be endothermic by 30 – 40 kcal/mol, while the analogous cadmium reactions are only endothermic by 10 – 20 kcal/mol. Similarly, the enthalpies of the cadmium abstraction reactions involving BrO and ClO are 15 – 20 kcal/mol smaller than their mercury counterparts. High level

ab initio calculations on the global potential energy surface of Hg + $Br_2$ have shown that the abstraction reactions proceed without a barrier,[3] and this is presumably also the case for cadmium.

The cadmium-halide reactions are also similar to the mercury cases in that all of the processes forming insertion complexes are strongly exothermic. However, following the same trend as the abstraction reactions, the cadmium insertion reactions are all 25 – 30 kcal/mol more exothermic than the analogous mercury cases. Large potential energy barriers have been previously calculated for the insertion of mercury into BrO and $Br_2$,[3] i.e., the barrier height for Hg + $Br_2$ is 27.2 kcal/mol.[3] It is likely that there are also barriers to insertion in the cadmium reactions, but the stronger exothermicity may result in significantly lower values.

Finally, Table 6 lists the bond dissociation energies and 0 K heats of formation for the 7 triatomic cadmium molecules. The heats of formation were calculated using the insertion reaction enthalpies for each triatomic species along with accurate experimental heats of formation for Cd and the halide-containing diatomics. The 0 K heats of formation that were used were: 28.20±0.05 kcal/mol for Cd,[88,89] 28.18±0.01 kcal/mol for Br,[90] 28.590±0.001 kcal/mol for Cl,[90] 10.92±0.03 kcal/mol for $Br_2$,[90] 5.24±0.02 kcal/mol for BrCl (derived from the $D_0$ of Tellinghuisen[91]), 24.14±0.03 kcal/mol for ClO,[92] 31.3±0.1 kcal/mol for BrO (derived from the $D_0$ of Kim et al.[93]), –22.016±0.004 kcal/mol for HCl,[94] and –6.805±0.06 for HBr.[94] Of course, the resulting differences between the experimental and theoretical heats of formation of $CdBr_2$ and $CdCl_2$ shown in Table 6 are identical to those shown in Table 5 for the insertion reaction enthalpies. A value of $\Delta H_f$ for CdBrCl has been previously determined from mass spectrometry

measurements, 0.4 ± 1 kcal/mol[22]. This is in substantial disagreement, however, with our presently predicted value (–39.4 kcal/mol) and does not seem reliable.

The DFT calculations of Liao et al.[31] have yielded bond energies for CdCl (48.2 kcal/mol), CdBr (39.4 kcal/mol), BrCd-Br (59.3 kcal/mol), and ClCd-Cl (68.5 kcal/mol). By comparison, the current calculations predict bond energies of 43.6 kcal/mol for CdCl, 34.2 kcal/mol for CdBr, 80.9 kcal/mol for BrCd-Br, and 91.1 kcal/mol for ClCd-Cl. Thus the DFT results for CdCl and CdBr are reasonably close to the present values, with DFT overestimating the bond strengths by 5-6 kcal/mol. Their particular choice of DFT (X$\alpha$), however, underestimates the bond dissociation energies of the triatomics species by ~22 kcal/mol in both cases. The MR-SOCI dissociation energy of CdH from Ref. 83 (15.8 kcal/mol) slightly underestimates the current and experimental values by 0.8 and 0.9 kcal/mol, respectively, while 4-component CCSD calculations[84] (18.2 kcal/mol) yielded a value that was slightly too large by about 0.4 kcal/mol.

## IV. CONCLUSIONS

Accurate ab initio calculations have been carried out to determine the thermochemistry of reactions between cadmium and reactive halogen species, as well as to determine the structures and vibrational frequencies of all the species involved. The specific reactions that have been investigated are

$$\mathrm{Cd} + \mathrm{XY} \rightarrow \begin{cases} \mathrm{CdX} + \mathrm{Y} \\ \mathrm{CdY} + \mathrm{X} \\ \mathrm{XCdY} \end{cases}$$

where X={Cl, Br} and Y={H, O, Cl, Br}. The cadmium molecules that have been characterized include the diatomic species CdH, CdO, CdCl, CdBr and the triatomics CdHCl, CdHBr, CdClO,

CdBrO, $CdCl_2$, $CdBr_2$, and CdBrCl. All of the triatomic molecules have linear equilibrium geometries with Cd as the central atom.

Electron correlation has been treated with the CCSD(T) method with a series of correlation consistent basis sets that allowed for extrapolation to the complete basis set limit. Accurate relativistic pseudopotentials have been used on the Cd and Br atoms to account for the major scalar and spin-orbit relativistic effects. Additional calculations were carried out using the one-component all-electron DKH Hamiltonian to estimate the errors associated with the pseudopotential approximation, as well as to recover the effects due to scalar relativity on the H, O, and Cl atoms. Additive corrections for core-valence correlation and spin-orbit coupling were also incorporated into the final results.

It is expected that the dissociation and reaction enthalpies of this work have been calculated to within 1 kcal/mol. Experimental enthalpies currently exist for only four of the reactions in this study and, with the exception of Cd + HBr → CdH + Br and Cd + HCl → CdH + Cl, the currently calculated enthalpies are believed to be the most accurate to date. With the exception of CdH, the bond lengths for the molecules of this study have been determined to within ±0.005 Å where experimental values are available. With this one exception, the predicted equilibrium geometries for the cadmium-containing molecules are the most reliable values currently available and are expected to be accurate to within ±0.005 Å.

The enthalpies in the present study are qualitatively similar to previous calculations involving mercury and reactive halogen species. All of the abstraction reactions considered are endothermic, while the insertion reactions are strongly exothermic. The abstraction reactions involving cadmium, however, are several kcal/mol less endothermic than the corresponding mercury reactions, while the cadmium insertion reactions are more exothermic than their

mercury counterparts. The mercury abstraction reactions are known to proceed without a barrier while the insertion reactions have relatively large barriers. It is probable that the cadmium reactions follow this same trend.

## V. ACKNOWLEDGEMENTS

The authors would like to thank Dr. David Feller for his critical reading of the manuscript and helpful comments.

**REFERENCES**


(1) Raofie, F.; Ariya, P. A. *Environ. Sci. Tech.* **2004**, *38*, 4319.

(2) Calvert, J. G.; Lindberg, S. E. *Atmos. Environ.* **2004**, *38*, 5105.

(3) Balabanov, N. B.; Shepler, B. C.; Peterson, K. A. *J. Phys. Chem. A* **2005**, *109*, 8765.

(4) Schroeder, W. H.; Anlauf, K. G.; Barrie, L. A.; Lu, J. Y.; Steffen, A.; Schneeberger, D. R.; Berg, T. *Nature* **1998**, *394*, 331.

(5) Lindberg, S. E.; Brooks, S.; Lin, C.-J.; Scott, K. J.; Landis, M. S.; Stevens, R. K.; Goodsite, M.; Richter, A. *Environ. Sci. Tech.* **2002**, *36*, 1245.

(6) Temme, C.; Einax, J. W.; Ebinghaus, R.; Schroeder, W. H. *Environ. Sci. Tech.* **2003**, *37*, 22.

(7) Skov, H.; Christensen, J. H.; Goodsite, M. E.; Heidam, N. Z.; Jensen, B.; Wåhlin, P.; Geernaert, G. *Environ. Sci. Tech.* **2004**, *38*, 2373.

(8) Berg, T.; Bartnicki, J.; Munthe, J.; Lattila, H.; Hrehoruk, J.; Mazur, A. *Atmos. Environ.* **2001**, *35*, 2569.

(9) Ariya, P. A.; Dastoor, A. P.; Amyot, M.; Schroeder, W. H.; Barrie, L. A.; Anlauf, K.; Raofie, F.; Ryzhkov, A.; Davignon, D.; Lalonde, J.; Steffen, A. *Tellus* **2004**, *56B*, 397.

(10) Williams, C. R.; Harrison, R. M. *Experientia* **1984**, *40*, 29.

(11) Bewers, J. M.; Barry, P. J.; MacGregor, D. J. *Adv. Environ. Sci. Tech.* **1987**, *19*, 1.

(12) Yu, S.; Shayesteh, A.; Fu, D.; Bernath, P. F. *J. Phys. Chem. A* **2005**, *109*, 4092.

(13) Macrae, V. A.; Green, J. C.; Greene, T. M.; Downs, A. J. *J. Phys. Chem. A* **2004**, *108*, 9500.

(14) Ediger, M. N.; McCown, A. W.; Eden, J. G. *Appl. Phys. Lett.* **1982**, *40*, 99.

(15) Klemperer, W. *J. Chem. Phys.* **1956**, *25*, 1066.

(16) Loewenschuss, A.; Ron, A.; Schnepp, O. *J. Chem. Phys.* **1969**, *50*, 2502.

(17) Strull, A.; Givan, A.; Loewenschuss, A. *J. Mol. Spectrosc.* **1976**, *62*, 283.

(18) Givan, A.; Loewenschuss, A. *Spectrochim. Acta A* **1978**, *34A*, 765.

(19) Givan, A.; Loewenschuss, A. *J. Mol. Struct.* **1978**, *48*, 325.

(20) Haaland, A.; Martinsen, K.-G.; Tremmel. *Acta Chem. Scand.* **1992**, *46*, 589.

(21) Petrov, V. M.; Utkin, A. N.; Girichev, G. V.; Ivanov, A. A. *Zh. Strukt. Khim.* **1985**, *26*, 52.

(22) Bloom, H.; Anthony, R. G. *Aus. J. Chem.* **1972**, *25*, 23.

(23) Wieland, K. *Helv. Phys. Acta* **1929**, *2*, 46.

(24) Gosavi, R. K.; Greig, G.; Young, P. J.; Strausz, O. P. *J. Chem. Phys.* **1971**, *54*, 983.

(25) Prochaska, E. S.; Andrews, L. *J. Chem. Phys.* **1980**, *72*, 6782.

(26) Chertihin, G. V.; Andrews, L. *J. Chem. Phys.* **1997**, *106*, 3457.

(27) Grade, M.; Hirschwald, H. *Ber. Bunsen-Ges. Phys. Chem.* **1982**, *86*, 899.

(28) Urban, R.-D.; Magg, U.; Birk, H.; Jones, H. *J. Chem. Phys.* **1990**, *92*, 14.

(29) Stromberg, D.; Gropen, O.; Wahlgren, U. *Chem. Phys.* **1989**, *133*, 207.

(30) Pankratov, A. N. *J. Serb. Chem. Soc.* **2002**, *67*, 339.

(31) Liao, M.; Zhang, Q.; Schwarz, W. H. E. *Inorg. Chem.* **1995**, *34*, 5597.

(32) Zhao, J.; Zhang, Y.; Kan, Y.; Zhu, L. *Spectrochim. Acta A* **2004**, *60*, 679.

(33) Kaupp, M.; von Schnering, H. G. *Inorg. Chem.* **1994**, *33*, 4179.

(34) Balabanov, N. B.; Peterson, K. A. *J. Phys. Chem. A* **2003**, *107*, 7465.

(35) Feller, D.; Peterson, K. A.; de Jong, W. A.; Dixon, D. A. *J. Chem. Phys.* **2003**, *118*, 3510.

(36) Feller, D.; Dixon, D. A. *J. Phys. Chem. A* **2003**, *107*, 9641.

(37) Dixon, D. A.; de Jong, W. A.; Peterson, K. A.; Christe, K. O.; Schrobilgen, G. J. *J. Am. Chem. Soc.* **2005**, *127*, 8627.

(38) Puzzarini, C.; Peterson, K. A. *Chem. Phys.* **2005**, *311*, 177.

(39) Peterson, K. A.; Puzzarini, C. *Theor. Chem. Acc.* **2005**, *114*, 283.

(40) Pollack, L.; Windus, T. L.; de Jong, W. A.; Dixon, D. A. *J. Phys. Chem. A* **2005**, *109*, 6934.

(41) Shepler, B. C.; Balabanov, N. B.; Peterson, K. A. *J. Phys. Chem. A* **2005**, *109*, 10363.

(42) Feller, D.; Peterson, K. A.; Crawford, T. D. *J. Chem. Phys.* **2006**, *124*, 054107.

(43) Tajti, A.; Szalay, P. G.; Csaszar, A. G.; Kallay, M.; Gauss, J.; Valeev, E. F.; Flowers, B. A.; Vazquez, J.; Stanton, J. F. *J. Chem. Phys.* **2004**, *121*, 11599.

(44) Boese, A. D.; Oren, M.; Atasoylu, O.; Martin, J. M. L. *J. Chem. Phys.* **2004**, *120*, 4129.

(45) Schuurman, M. S.; Muir, S. R.; Allen, W. D.; Schaefer, H. F., III. *J. Chem. Phys.* **2004**, *120*, 11586.

(46) Senekowitsch, J. PhD. Thesis, Universität Frankfurt, Frankfurt, Germany, 1988.

(47) Dunham, J. L. *Phys. Rev.* **1932**, *41*, 721.

(48) *Vibration-rotation structure in asymmetric and symmetric top molecules.*; Mills, I. M., Ed.; Academic: New York, 1972; Vol. 1.

(49) Purvis, G. D. I.; Bartlett, R. J. *J. Chem. Phys.* **1982**, *76*, 1910.

(50) Raghavachari, K.; Trucks, G. W.; Pople, J. A.; Head-Gordon, M. *Chem. Phys. Lett.* **1989**, *156*, 479.

(51) Watts, J. D.; Gauss, J.; Bartlett, R. J. *J. Chem. Phys.* **1993**, *98*, 8718.

(52) Scuseria, G. E. *Chem. Phys. Lett.* **1991**, *176*, 27.

(53) Knowles, P. J.; Hampel, C.; Werner, H.-J. *J. Chem. Phys.* **1994**, *99*, 5219.

(54) Werner, H.-J. MOLPRO is a package of ab initio programs written by H.-J. Werner and P.J. Knowles, version 2002.6, R.D. Amos, A. Bernhardsson, A. Berning, P. Celani, D.L. Cooper, M.J.O. Deegan, A.J. Dobbyn, F. Eckert, C. Hampel, G. Hetzer, P.J. Knowles, T. Korona, R. Lindh, A.W. Lloyd, S.J. McNicholas, F.R. Manby, W. Meyer, M.E. Mura, A. Nicklass, P. Palmieri, R. Pitzer, G. Rauhut, M. Schütz, U. Schumann, H. Stoll, A.J. Stone, R. Tarroni, T. Thorsteinsson, and H.-J. Werner.

(55) Kendall, R. A.; Dunning, T. H., Jr.; Harrison, R. J. *J. Chem. Phys.* **1992**, *96*, 6796.

(56) Dunning, T. H. J.; Peterson, K. A.; Wilson, A. K. *J. Chem. Phys.* **2001**, *114*, 9244.

(57) Peterson, K. A.; Figgen, D.; Goll, E.; Stoll, H.; Dolg, M. *J. Chem. Phys.* **2003**, *119*, 11113.

(58) Figgen, D.; Rauhut, G.; Dolg, M.; Stoll, H. *Chem. Phys.* **2004**, *311*, 227.

(59) Peterson, K. A.; Woon, D. E.; Dunning, T. H., Jr. *J. Chem. Phys.* **1994**, *100*, 7410.

(60) Feller, D.; Peterson, K. A. *J. Chem. Phys.* **1999**, *110*, 8384.

(61) Halkier, A.; Helgaker, T.; Jørgensen, P.; Klopper, W.; Koch, H.; Olsen, J.; Wilson, A. K. *Chem. Phys. Lett.* **1998**, *286*, 243.

(62) Helgaker, T.; Klopper, W.; Koch, H.; Noga, J. *J. Chem. Phys.* **1997**, *106*, 9639.

(63) Peterson, K. A.; Dunning, T. H. J. *J. Chem. Phys.* **2002**, *117*, 1.

(64) Peterson, K. A.

(65) Bergner, A.; Dolg, M.; Küchle, W.; Stoll, H.; Preuß, H. *Mol. Phys.* **1993**, *80*, 1431.

(66) Dolg, M. PhD. thesis, Universität Stuttgart, Stuttgart, Germany, 1989.

(67) Metz, B.; Stoll, H.; Dolg, M., Private communication.

(68) Yabushita, S.; Zhang, Z.; Pitzer, R. M. *J. Phys. Chem. A* **1999**, *103*, 5791.

(69) Lischka, H. H. Lischka, R. Shepard, I. Shavitt, R. M. Pitzer, M. Dallos, Th. Müller, P. G. Szalay, F. B. Brown, R. Ahlrichs, H. J. Böhm, A. Chang, D. C. Comeau, R. Gdanitz, H. Dachsel, C. Ehrhardt, M. Ernzerhof, P. Höchtl, S. Irle, G. Kedziora, T. Kovar, V. Parasuk, M. J. M. Pepper, P. Scharf, H. Schiffer, M. Schindler, M. Schüler, M. Seth, E. A. Stahlberg, J.-G. Zhao, S. Yabushita, and Z. Zhang, COLUMBUS, an ab initio electronic structure program, release 5.8 (2001).

(70) Dolg, M. *Chem. Phys. Lett.* **1996**, *250*, 75.

(71) Dolg, M. *J. Chem. Phys.* **1996**, *104*, 4061.

(72) Douglas, M.; Kroll, N. M. *Ann. Phys.* **1974**, *82*, 89.

(73) Jansen, G.; Hess, B. A. *Phys. Rev. A* **1989**, *39*, 6016.

(74) Wilson, A. K.; Peterson, K. A.; Woon, D. E.; Dunning, T. H., Jr. *J. Chem. Phys.* **1999**, *110*, 7667.

(75) de Jong, W. A.; Harrison, R. J.; Dixon, D. A. *J. Chem. Phys.* **2001**, *114*, 48.

(76) Nakajima, T.; Hirao, K. *J. Chem. Phys.* **2000**, *113*, 7786.

(77) Schmidt, M. W.; Baldridge, K. K.; Boatz, J. A.; Elbert, S. T.; Gordon, M. S.; Jensen, J. H.; Koseki, S.; Matsunaga, N.; Nguyen, K. A.; Su, S. J.; Windus, T. L.; Dupuis, M.; Montgomery, J. A. *J. Comp. Chem.* **1993**, *14*, 1347.

(78) Lee, T. J.; Taylor, P. R. *Int. J. Quantum Chem. Symp.* **1989**, *23*, 199.

(79) Peterson, K. A.; Shepler, B. C. **2006**.

(80) Kulikov, V. A.; Ugarov, V. V.; Rambidi, N. G. *Zh. Strukt. Khim.* **1980**, *21*, 201.

(81) Akishin, P. A.; Spiridonov, V. P. *Kristallografiya* **1957**, *2*, 475.

(82) Nogt, N.; Haaland, A.; Martinsen, K.-G.; Vogt, J. *Acta Chem. Scand.* **1993**, *47*, 937.

(83) Balasubramanian, K. *J. Chem. Phys.* **1990**, *93*, 8061.

(84) Eliav, E.; Kaldor, U.; Hess, B. A. *J. Chem. Phys.* **1998**, *108*, 3409.

(85) Huber, K. P.; Herzberg, G. *Molecular Spectra and Molecular Structure IV. Constants of Diatomic Molecules*; Van Nostrand: Princeton, 1979.

(86) Knacke, O.; Kubaschewski, O.; Hesselmann, K. *Thermochemical Properties of Inorganic Substances*; Springer: Berlin, 1991.

(87) Glushko, P.; Medvedev, V. A. *Termicheskue Konstanty Veshchestv parts I-VIII*; Akademyia Nauk: Moskow, 1965-1981.

(88) Cox, J. D.; Wagman, D. D.; Medvedev, V. A. *CODATA Key Values for Thermodynamics*; Hemisphere Publishing Corp: New York, 1984.

(89) Hultgren, R.; Desai, P. D.; Hawkins, D. T.; Gleiser, M.; Kelley, K. K.; Wagman, D. D. *Selected Values of Thermodynamic Properties of the Elements*; American Society for Metals: Metals Park, 1973.

(90) Chase, M. W., Jr; Davies, C. A.; Downey, J. R., Jr; Frurip, D. J.; McDonald, R. A.; Syverud, A. N. *J. Phys. Chem. Ref. Data* **1985**, *14*.

(91) Tellinghuisen, J. *J. Phys. Chem. A* **2003**, *107*, 753.

(92) Coxon, J. A.; Ramsay, D. A. *Can. J. Phys.* **1976**, *54*, 1034.

(93) Kim, H.; Dooley, K. S.; Johnson, E. R.; North, S. W. *J. Chem. Phys.* **2006**, *124*, 134304.

(94) Shenyavskaya, E. A.; Yungman, V. S. *J. Phys. Chem. Ref. Data* **2004**, *33*, 923.

(95) Uehara, H.; Horiai, K.; Akiyama, K. *Bull. Chem. Soc. Jpn.* **2004**, *77*, 1821.

(96) Coxon, J. A.; Hajigeorgiou, P. G. *J. Mol. Spectrosc.* **2000**, *203*, 49.

(97) Coxon, J. A.; Hajigeorgiou, P. G. *J. Mol. Spectrosc.* **1991**, *150*, 1.

(98) Bermejo, D.; Jimenez, J. J.; Martinez, R. Z. *J. Mol. Spectrosc.* **2002**, *212*, 186.

(99) Focsa, C.; Li, H.; Bernath, P. F. *J. Mol. Spectrosc.* **2000**, *200*, 104.

(100) Uehara, H.; Konno, T.; Ozaki, Y.; Horiai, K.; Nakagawa, K.; Johns, J. W. C. *Can. J. Phys.* **1994**, *72*, 1145.

(101) Drouin, B. J.; Miller, C. E.; Cohen, E. A.; Wagner, G.; Birk, M. *J. Mol. Spectrosc.* **2001**, *207*, 4.

(102) Drouin, B. J.; Miller, C. E.; Muller, H. S. P.; Cohen, E. A. *J. Mol. Spectrosc.* **2001**, *205*, 128.

(103) Nishimiya, N.; Yukiya, T.; Ohtsuka, T.; Suzuki, M. *J. Mol. Spectrosc.* **1997**, *182*, 309.

(104) Gerstenkorn, S.; Luc, P. *J. Phys. (Paris)* **1989**, *50*, 1417.

(105) Tellinghuisen, J. *J. Chem. Phys.* **2003**, *118*, 2016.

(106) Wilmouth, D. M.; Hanisco, T. F.; Donahue, N. M.; Anderson, J. G. *J. Phys. Chem. A* **1999**, *103*, 8935.

TABLE 1: Basis Set and Pseudopotential Details.

| Element | | Basis | Exclude from PP Core | Active AOs |
|---|---|---|---|---|
| H,O | FC | aug-cc-pVnZ | | 1s (H), 2s2p (O) |
| | CV | aug-cc-pwCVTZ | | 1s (H), 1s2s2p (O) |
| | FC | aug-cc-pVTZ-DK | | 1s (H), 2s2p (O) |
| Cl | FC | aug-cc-pV(n+d)Z | | 3s3p |
| | CV | aug-cc-pwCVTZ | | 2s2p3s3p |
| | FC | aug-cc-pV(T+d)Z-DK | | 3s3p |
| Br | FC | aug-cc-pVnZ-PP | $3s^2 3p^6 3d^{10} 4s^2 4p^5$ | 4s4p |
| | CV | aug-cc-pwCVTZ-PP | $3s^2 3p^6 3d^{10} 4s^2 4p^5$ | 3s3p3d4s4p |
| | FC | aug-cc-pVTZ-DK | | 4s4p |
| Hg | FC | aug-cc-pVnZ-PP | $4s^2 4p^6 5d^{10} 5s^2$ | 5d5s |
| | CV | aug-cc-pwCVTZ-PP | $4s^2 4p^6 5d^{10} 5s^2$ | 4s4p5d5s |
| | FC | aug-cc-pVTZ-DK | | 5d5s |

TABLE 2: Calculated CCSD(T) Equilibrium Bond Lengths (Å). [a]

| Species | | | aV5Z | ΔCBS[b] | ΔCV | ΔSO | ΔDK | Theory | Expt. |
|---|---|---|---|---|---|---|---|---|---|
| $X^1\Sigma^+_{0^+}$ | HCl | | 1.2759 | -0.0003 | -0.0014 | 0.0000 | -0.0001 | 1.2741 | 1.2746[95 c, 85,96] |
| $X^1\Sigma^+_{0^+}$ | HBr | | 1.4190 | -0.0000 | -0.0049 | 0.0004 | -0.0005 | 1.4140 | 1.4145[85,97] |
| $X^1\Sigma^+_{g,0^+}$ | $Cl_2$ | | 1.9926 | -0.0033 | -0.0035 | 0.0001 | 0.0015 | 1.9873 | 1.9880[85,98] |
| $X^1\Sigma^+_{g,0^+}$ | $Br_2$ | | 2.2922 | -0.0034 | -0.0097 | 0.0021 | 0.0008 | 2.2819 | 2.2810[85,99] |
| $X^1\Sigma^+_{0^+}$ | BrCl | | 2.1431 | -0.0036 | -0.0061 | 0.0013 | 0.0007 | 2.1354 | 2.1361[85,100] |
| $X^2\Pi_{3/2}$ | ClO | | 1.5702 | -0.0029 | -0.0028 | -0.0006 | 0.0018 | 1.5657 | 1.5689[101] |
| $X^2\Pi_{3/2}$ | BrO | | 1.7220 | -0.0024 | -0.0034 | -0.0024 | 0.0002 | 1.7140 | 1.7172[85,102] |
| $X^2\Sigma^+_{1/2}$ | CdH | | 1.7602 | -0.0002 | -0.0064[d] | -0.0014 | -0.0002 | 1.7519[d] | 1.7611[28,c] |
| $X^1\Sigma^+_{0^+}$ | CdO | | 1.9112 | -0.0020 | -0.0070 | -0.0006 | 0.0013 | 1.9030 | |
| $X^2\Sigma^+_{1/2}$ | CdCl | | 2.3397 | -0.0023 | -0.0050 | -0.0004 | -0.0004 | 2.3329 | |
| $X^2\Sigma^+_{1/2}$ | CdBr | | 2.4752 | -0.0022 | -0.0094 | -0.0002 | 0.0010 | 2.4664 | |
| $X^1\Sigma^+_{g,0^+}$ | $CdCl_2$ | | 2.2572 | -0.0019 | -0.0063 | -0.0005 | 0.0002 | 2.2487 | 2.21[81], 2.266[82],2.282[20] |
| $X^1\Sigma^+_{g,0^+}$ | $CdBr_2$ | | 2.3886 | -0.0017 | -0.0103 | -0.0003 | 0.0006 | 2.3768 | 2.372[80], 2.394[21] |
| $X^1\Sigma^+_{0^+}$ | CdBrCl | $r_e$(CdBr) | 2.3834 | -0.0018 | -0.0103 | -0.0003 | 0.0006 | 2.3716 | |

| | | | | | | | | |
|---|---|---|---|---|---|---|---|---|
| | | $r_e$ (CdCl) | 2.2622 | -0.0019 | -0.0063 | -0.0005 | 0.0001 | 2.2537 |
| $X^1\Sigma^+_{0^+}$ | HCdCl | $r_e$ (CdCl) | 2.2753 | -0.0019 | -0.0059 | -0.0006 | -0.0004 | 2.2665 |
| | | $r_e$ (CdH) | 1.6467 | -0.0002 | -0.0072 | -0.0006 | 0.0000 | 1.6388 |
| $X^1\Sigma^+_{0^+}$ | HCdBr | $r_e$ (CdBr) | 2.4034 | -0.0017 | -0.0101 | -0.0005 | 0.0002 | 2.3914 |
| | | $r_e$ (CdH) | 1.6529 | -0.0001 | -0.0073 | -0.0006 | -0.0003 | 1.6446 |
| $X^2\Pi_{3/2}$ | CdClO | $r_e$ (CdCl) | 2.2543 | -0.0019 | -0.0067 | -0.0006 | 0.0003 | 2.2455 |
| | | $r_e$ (CdO) | 1.9811 | -0.0015 | -0.0066 | -0.0011 | 0.0010 | 1.9730 |
| $X^2\Pi_{3/2}$ | CdBrO | $r_e$ (CdBr) | 2.3808 | -0.0018 | -0.0107 | -0.0005 | 0.0006 | 2.3685 |
| | | $r_e$ (CdO) | 1.9855 | -0.0015 | -0.0064 | -0.0012 | 0.0010 | 1.9775 |

[a] See the text for the definition of the individual contributions. The best predicted value is given by aV5Z + ΔCBS + ΔCV + ΔSO + ΔDK. Expected uncertainty in the theoretical values is ±0.005 Å.

[b] Difference between the estimated CBS limit and the aV5Z value. See the text.

[c] Calculated from $U_{01}$.

[d] The best theoretical estimate for ΔCV is –0.0040 Å, which yields an $r_e$ of 1.7543 Å.

TABLE 3: Harmonic Vibrational Frequencies and Zero Point Energies ($cm^{-1}$).

| Species | | $\omega_e$ (Theory)[a] | $\omega_e$ (Expt.) | Anharmonic ZPE (Theory) |
|---|---|---|---|---|
| HCl | | 2997.7 | 2990.9[85,95] | 1485.8 |
| HBr | | 2650.7 | 2649.6[103] | 1314.2 |
| $Cl_2$ | | 565.2 | 559.7[85,98] | 282.0 |
| $Br_2$ | | 328.3 | 325.3[85,99] | 163.9 |
| BrCl | | 449.0 | 444.3[85,100] | 224.1 |
| ClO | | 865.1 | 855.5[101] | 431.2 |
| BrO | | 739.5 | 732.9[102] | 368.6 |
| CdH | | 1462.7 | 1460.9[28] | 718.9 |
| CdO | | 614.4 | 645.1[26] | 306.2 |
| | | | 654.4[26] | |
| CdCl | | 334.7 | 331.0[85] | 167.0 |
| CdBr | | 233.2 | 230.0[23] | 116.4 |
| | | | 231.0[24,85] | |
| $CdCl_2$ | ($\Sigma_g$) | 344.3 | 329.8[17] | 477.1 |
| | ($\Pi_u$) | 87.0 | 88.0[18] | |
| | ($\Sigma_u$) | 439.0 | 419 [16] | |
| $CdBr_2$ | ($\Sigma_g$) | 213.9 | 209.1[17] | 334.5 |
| | ($\Pi_u$) | 63.5 | 62 [18] | |
| | ($\Sigma_u$) | 329.5 | 319 [16] | |
| CdBrCl | (CdBr) | 255.4 | 246.6[17] | 406.4 |
| | (bend) | 75.6 | 72.0[18] | |

| | | | | |
|---|---|---|---|---|
| | (CdCl) | 407.8 | 392.9[17] | |
| CdHCl | (CdCl) | 381.3 | 364.5[13] | 1559.0 |
| | (bend) | 422.1 | 432.3[13] | |
| | (CdH) | 1920.5 | 1890.0[13] | |
| CdHBr | (CdBr) | 270.0 | | 1480.9 |
| | (bend) | 407.6 | | |
| | (CdH) | 1903.5 | | |
| CdClO | (CdCl) | 381.9 | | 598.3 |
| | (bend) | 111.2 | | |
| | (CdO) | 594.9 | | |
| CdBrO | (CdBr) | 269.8 | | 528.7 |
| | (bend) | 101.3 | | |
| | (CdO) | 584.8 | | |

[a] Calculated at the CCSD(T)/CBS + ΔCV + ΔSO level of theory. See the text.

TABLE 4: CCSD(T) dissociation energies ($D_0$) of the diatomic molecules of the present work compared to the available experimental values (kcal/mol).[a]

| Species | aV5Z | ΔCBS[b] | ΔCV | ΔSO | ΔDK | $\Delta E_{ZPE}$ | Theory | Expt. |
|---|---|---|---|---|---|---|---|---|
| HCl | 107.25 | 0.35 | 0.06 | -0.86 | -0.25 | -4.25 | 102.29 | 102.24[85,94] |
| HBr | 92.78 | 0.29 | 0.44 | -3.18 | 0.07 | -3.76 | 86.63 | 86.62[94] |
| $Cl_2$ | 58.98 | 1.02 | -0.02 | -1.72 | -0.18 | -0.81 | 57.26 | 57.18[85] |
| $Br_2$ | 51.19 | 0.88 | 0.32 | -6.26 | 0.05 | -0.47 | 45.71 | 45.45[85,104] |
| BrCl | 55.33 | 0.93 | 0.09 | -3.94 | -0.11 | -0.64 | 51.66 | 51.53[91,105,d] |
| ClO | 63.83 | 0.84 | 0.12 | -0.61 | -0.23 | -1.23 | 63.21[c] | 63.43[85,92] |
| BrO | 57.31 | 0.68 | 0.04 | -2.18 | -0.09 | -1.05 | 55.57[c] | 55.21[106], 55.8[93] |
| CdH | 17.81 | 0.01 | -0.21 | 0.13 | -0.10 | -2.06 | 15.58 | 15.64[85] |
| CdO | 22.30 | 0.50 | -0.58 | -0.12 | -0.39 | -0.88 | 20.83 | |
| CdCl | 45.12 | 0.56 | -0.91 | -0.78 | -0.38 | -0.48 | 43.14 | |
| CdBr | 37.25 | 0.55 | -0.44 | -3.04 | -0.11 | -0.33 | 33.88 | |

[a] See the text for the definition of the individual contributions. The best predicted value is given by aV5Z + ΔCBS + ΔCV + ΔSO + ΔDK + $\Delta E_{ZPE}$.

[b] Difference between the estimated CBS limit and the aV5Z value. See the text.

[c] These contain additional contributions of +0.49 and +0. 83 kcal/mol for ClO and BrO, respectively, for the effects of iterative triple and quadruple excitations to the CCSD(T) values. See Ref. 79.

[d] $D_e$ was converted to $D_0$ using the experimental anharmonic zero point energy. See Table 3 for the experimental references.

TABLE 5: Calculated 0 K reaction enthalpies compared to the available experimental values (kcal/mol). [a]

| Reaction | | $\Delta E_e$ (aV5Z) | $\Delta CBS$[b] | $\Delta CV$ | $\Delta SO$ | $\Delta DK$ | $\Delta E_{TQ}$[c] | $\Delta E_{ZPE}$ | $\Delta H_r$ | Expt. |
|---|---|---|---|---|---|---|---|---|---|---|
| $Cd + Br_2$ | → CdBr + Br | 13.94 | 0.33 | 0.76 | -3.22 | 0.16 | --- | -0.14 | 11.82 | |
| | → $CdBr_2$ | -69.75 | -0.29 | 0.26 | -0.03 | 0.24 | --- | 0.49 | -69.08 | -70.08[86] |
| $Cd + Cl_2$ | → CdCl + Cl | 13.86 | 0.46 | 0.89 | -0.94 | 0.20 | --- | -0.33 | 14.14 | |
| | → $CdCl_2$ | -78.66 | -0.19 | 0.85 | -0.12 | 0.55 | --- | 0.56 | -77.00 | -73.80[86] |
| Cd + BrCl | → CdBr + Cl | 18.08 | 0.38 | 0.53 | -0.90 | 0.00 | --- | -0.31 | 17.77 | |
| | → CdCl + Br | 10.21 | 0.37 | 1.00 | -3.16 | 0.27 | --- | -0.16 | 8.53 | |
| | → CdBrCl | -73.97 | -0.26 | 0.50 | 0.00 | 0.38 | --- | 0.52 | -72.83 | |
| Cd + BrO | → CdBr + O | 20.06 | 0.13 | 0.48 | 0.86 | 0.02 | 0.83 | -0.72 | 21.64 | |
| | → CdO + Br | 35.01 | 0.18 | 0.62 | -2.06 | 0.30 | 0.83 | -0.18 | 34.70 | |
| | → BrCdO | -45.98 | -0.27 | 0.24 | 1.09 | 0.24 | 0.83 | 0.46 | -43.39 | |
| Cd + ClO | → CdCl + O | 18.71 | 0.28 | 1.03 | 0.17 | 0.15 | 0.49 | -0.76 | 20.07 | |
| | → CdO + Cl | 41.53 | 0.34 | 0.70 | -0.49 | 0.16 | 0.49 | -0.36 | 42.38 | |
| | → CdClO | -47.92 | -0.13 | 0.77 | 0.27 | 0.38 | 0.49 | 0.48 | -45.67 | |

| | | | | | | | | | | |
|---|---|---|---|---|---|---|---|---|---|---|
| Cd + HBr | → CdBr + H | 55.53 | -0.26 | 0.88 | -0.14 | 0.18 | --- | -3.42 | 52.76 | |
| | → CdH + Br | 74.97 | 0.28 | 0.65 | -3.31 | 0.17 | --- | -1.70 | 71.06 | 70.99[d] |
| | → CdHBr | -16.82 | -0.35 | 0.13 | -0.17 | 0.14 | --- | 0.48 | -16.60 | |
| Cd + HCl | → CdCl + H | 62.13 | -0.21 | 0.97 | -0.08 | 0.13 | --- | -3.77 | 59.17 | |
| | → CdH + Cl | 89.44 | 0.34 | 0.27 | -0.99 | -0.15 | --- | -2.19 | 86.72 | 86.60[d] |
| | → CdHCl | -11.45 | -0.31 | 0.20 | -0.16 | 0.10 | --- | 0.21 | -11.42 | |

[a] See the text for the definition of the individual contributions. The best predicted value is given by aV5Z + ΔCBS + ΔCV + ΔSO + ΔDK + $\Delta E_{TQ}$ + $\Delta E_{ZPE}$.

[b] Difference between the estimated CBS limit and the aV5Z value. See the text.

[c] Contributions from CCSDT and CCSDTQ calculations on ClO and BrO. See Ref. 79.

[d] Calculated from the experimental dissociation energies in Table 4.

Table 6: Dissociation energies and 0 K heats of formation in kcal/mol for triatomic cadmium halides[a]

| XCdY | $D_0$(XCd+Y) | $D_0$(X+CdY) | $\Delta H_f$ (Calc.) | $\Delta H_f$ (Expt.) |
|---|---|---|---|---|
| BrCdBr | --- | 80.90 | -29.96 | -30.96[86] |
| ClCdCl | --- | 91.14 | -48.80 | -45.60[86] |
| BrCdCl | 90.60 | 81.36 | -39.39 | |
| BrCdO | 65.03 | 78.09 | 16.77 | |
| ClCdO | 65.74 | 88.05 | 6.67 | |
| HCdBr | 87.66 | 69.36 | 4.80 | |
| HCdCl | 98.14 | 70.59 | -5.24 | |

a) Calculated from the reaction enthalpies in Table 5. See the text.

# Appendix 1**

# On the spectroscopic and thermochemical properties of ClO, BrO, IO, and their anions

**Kirk A. Peterson* and Benjamin C. Shepler**

*Department of Chemistry, Washington State University, Pullman, Washington 99164-4630*

**Abstract**

A coupled cluster composite approach has been used to accurately determine the spectroscopic constants, bond dissociation energies, and heats of formation for the $X^2\Pi_{3/2}$ states of the halogen oxides ClO, BrO, and IO, as well as their negative ions $ClO^-$, $BrO^-$, and $IO^-$. After determining the valence electrons correlated, complete basis set (CBS) limit CCSD(T) values, corrections were added for core-valence correlation, relativistic effects (scalar and spin-orbit), the pseudopotential approximation (BrO and IO), iterative connected triple excitations (CCSDT), and iterative quadruples (CCSDTQ). The final *ab initio* equilibrium bond lengths and harmonic frequencies for ClO and BrO differ from their accurate experimental values by an average of just 0.0005 Å and 0.8 $cm^{-1}$, respectively. The bond length of IO is overestimated by 0.0040 Å, presumably due to an underestimation of molecular spin-orbit coupling effects. The predicted bond lengths and harmonic frequencies for the closed-shell anions are expected to be accurate to within 0.002 Å and 3 $cm^{-1}$, respectively. The dissociation energies of the radicals have been determined by both direct calculation and through use of negative ion thermochemical cycles, which made use of a small amount of accurate experimental data. The resulting values of $D_0$, 63.5, 55.8, and 54.3 kcal/mol for ClO, BrO, and IO, respectively, are the most accurate *ab*

*initio* values to date, and those for ClO and BrO differ from their experimental values by just 0.1 kcal/mol. These dissociation energies lead to heats of formation, $\Delta H_f$(298 K), of 24.2±0.3, 29.6±0.4, and 29.8±0.6 kcal/mol for ClO, BrO, and IO, respectively. Also, the final calculated electron affinities are all within 0.2 kcal/mol of their experimental values.

** The dissertation author was a contributor, but not this manuscripts primary author.
To be submitted to the *Journal of Physical Chemistry A*

## I. INTRODUCTION

The importance of the halogen oxides ClO, BrO, and IO in atmospheric catalytic ozone depletion chemistry, particularly in the stratosphere,[1] has motivated numerous high level experimental and theoretical studies on these species. In the cases of the BrO and IO radicals, these species represent about 40% and 90% of inorganic bromine and iodine, respectively, in the stratosphere. High resolution spectroscopy studies have led to very accurate determinations of the molecular constants in the $X_1{}^2\Pi_{3/2}$ ground states of all three radicals (Refs. 2-10 and references therein) while studies of the near-ultraviolet $A_1{}^2\Pi_{3/2}$–$X_1{}^2\Pi_{3/2}$ electronic transitions of ClO and BrO have led to accurate values of their ground state dissociation energies and heats of formation.[11-13] A reliable spectroscopic determination of the IO dissociation energy has yet to be reported, and hence its value has more experimental uncertainty than its chlorine or bromine analogs.

The halogen oxides are known to be challenging species to describe with ab initio electronic structure methods. Accurate results require high levels of electron correlation, either by coupled cluster or multireference configuration interaction methods, as well as large 1-particle basis sets and inclusion of relativistic effects. Because of the availability of a nearly complete set of accurate molecular constants for all three species, these molecules provide a unique set of benchmark systems involving isovalent open shell radicals between 3 rows of the periodic table. In the present work all three radicals are treated at the same level of theory using a systematic coupled cluster composite method[14-19] that attempts to account for all major sources of error in an ab initio calculation.

In order to provide more insight into the resulting accuracy of the neutral radical results, analogous calculations have also been carried out on the closed-shell halogen oxide anions. Far

fewer experimental and theoretical studies have been previously carried out on these species, with most studies focusing on the accurate determination of the halogen oxide electron affinities.[20-29] The present work provides the most accurate predictions for the spectroscopic constants of these species to this date, as well as a secondary route for the calculation of the neutral dissociation energies.

## II. COMPUTATIONAL METHODS

The base set of calculations on both the radicals and anions involved a valence electrons correlated, coupled cluster singles and doubles calculation with a perturbative treatment of connected triples, CCSD(T).[30,31] The open shell calculations utilized the RHF-UCCSD(T) variant, i.e., R/UCCSD(T), and were based on restricted open-shell Hartree-Fock (ROHF) orbitals.[32-36] The orbitals in the atomic calculations were fully symmetry equivalenced. These CCSD(T) calculations employed a series of three correlation consistent basis sets ranging from triple- to quintuple-ζ, namely aug-cc-pV*n*Z for oxygen,[37,38] aug-cc-pV(*n*+*d*)Z for chlorine,[39,40] and aug-cc-pV*n*Z-PP for bromine and iodine,[41] where *n* = T, Q, and 5. Relativistic Douglas-Kroll-Hess (DKH) contracted versions of the O and Cl basis sets were used for ClO/$ClO^-$ since the DKH Hamiltonian[42,43] was used throughout in these cases. The aug-cc-pV*n*Z-PP basis sets for Br and I included small-core energy consistent relativistic pseudopotentials that were optimized in multiconfigurational Dirac-Hartree-Fock calculations.[41] In the following these basis sets will be collectively refered to as aV*n*Z where *n*=T, Q, 5. In each case calculations were carried out at a total of 7 bond distances unequally distributed around the approximate equilibrium geometries of each species ($r - r_e$ = –0.3, -0.2, -0.1, 0.0, +0.1, +0.3, +0.5 $a_o$) and the resulting energies were fit to 6th-order polynomials in displacement coordinates. The fitted

coefficients were then used in subsequent Dunham analyses.[44] To exploit the systematic basis set convergence characteristics of the correlation consistent basis sets, the total energies at each bond length were extrapolated to the complete basis set (CBS) limit using[45-47]

$$\mathrm{E}(n) = \mathrm{E}_{\mathrm{CBS}} + Be^{-(n-1)} + Ce^{-(n-1)^2} \quad (n = 3, 4, 5) \tag{1}$$

and

$$\mathrm{E}(n) = \mathrm{E}_{\mathrm{CBS}} + B/n^3 \quad (n = 4, 5) \ . \tag{2}$$

The best CBS estimate was taken as the average of these two results, and the spread was accepted as an estimate of the uncertainty in the extrapolation procedure.[15] The CBS energies were then fit and subjected to the same Dunham analysis as above.

The contributions to the total energies due to core-valence correlation, namely 1s for O, 2s2p for Cl, 3s3p3d for Br, and 4s4p4d for I, were calculated at the CCSD(T) level of theory with core-valence basis sets of quadruple-ζ quality, aug-cc-pwCVQZ for O and Cl (Ref. [48]) and aug-cc-pwCVQZ-PP for Br and I.[49] The DKH-contracted versions of the Cl and O basis sets were used in the cases of ClO/$ClO^-$. In all cases the core-valence basis sets were used in both valence-only and all-electrons correlated (except 1*s* of Cl) calculations, and the difference in energies defined the total core-valence correction.

The second contribution to the CCSD(T)/CBS energies was specific to BrO/$BrO^-$ and IO/$IO^-$ and was designed to correct both for the pseudopotential approximation and the scalar relativistic effects due to oxygen in these molecules. In this case all-electrons correlated DKH CCSD(T) calculations were carried out using DKH-contracted aug-cc-pwCVTZ basis sets,[50,51] and these total energies were compared to those from analogous PP-based calculations using aug-cc-pwCVTZ-PP basis sets[49] on Br and I (with the standard aug-cc-pwCVTZ set[48] on O).

The effects due to molecular and atomic spin-orbit coupling were recovered by use of the double-group spin-orbit configuration interaction (SO-CI) method[52] as implemented in the COLUMBUS program suite.[53] In these calculations the spin-orbit parameters accompanying the pseudopotentials described above were used throughout and an accurate PP was also used on the oxygen atom.[54] The aug-cc-pVTZ-PP basis sets were used on Br and I, while the aug-cc-pVTZ basis set recontracted in the presence of the PP was used for O. The SO correction was defined by the difference in two calculations, a full valence, complete active space (CAS) reference, multireference singles and doubles CI (MRCISD) calculation that did not include the spin-orbit operator and an analogous MRCISD that mixed (via the spin-orbit operator) either doublet and quartet states in the case of the neutral radicals or singlet and triplet states for the closed-shell anions. In each case CASSCF orbitals were used. Analogous calculations were also carried out for all of the atomic species of this work. This procedure differed slightly from other recent work from our laboratory[16] where CISD natural orbitals were used in conjunction with MRCIS calculations. The final results, however, differed only slightly, e.g., by less than 0.1 kcal/mol for the spin-orbit correction to $D_e$ for IO.

The last correction was for the effects of higher electron correlation beyond the CCSD(T) level of theory. The differences between perturbative and full iterative connected triple excitations,[55-58] CCSDT – CCSD(T), were calculated with the aug-cc-pVTZ basis sets (-DK for $ClO/ClO^-$, standard and –PP for $BrO/BrO^-$ and $IO/IO^-$), while the effects of iterative connected quadruples,[55,59-61] CCSDTQ – CCSDT, employed the analogous double-ζ basis sets. A total of 5 bond distances were sampled in each case for each species, the CCSD(T) $r_e$ obtained with the specified basis set (DZ or TZ) and displacements from this value of –0.04, –0.02, +0.02, and +0.04 $a_o$. The CCSD(T), CCSDT, and CCSDTQ potential curves were then fit to cubic

polynomials to determine the minimum energies, equilibrium bond lengths, and harmonic frequencies. Last, an estimate of the full configuration interaction (FCI) results were obtained with the aug-cc-pVDZ basis sets by carrying out a continued fraction (cf) extrapolation[15,62] with the CCSD, CCSDT, and CCSDTQ energies.

All of the CCSD(T) calculations of this work were carried out with the MOLPRO suite of ab initio programs.[63] The CCSDT and CCSDTQ calculations were carried out primarily with the string-based MRCC program of Kállay[64] as interfaced to MOLPRO. The CCSDT calculations on ClO were performed with the NWChem program.[65,66]

## III. RESULTS

The calculated results for the $X_1{}^2\Pi_{3/2}$ states of ClO, BrO, and IO are shown in Table 1 where they are also compared to the available experimental data. Only modest changes in $r_e$, $\omega_e$, and $D_e$ are observed between the aV5Z basis set and the CBS limit, however the difference for $D_e$ is as high as 0.83 kcal/mol for BrO. Core-valence correlation is calculated to have a minor impact on the dissociation energies, but it yields relatively large bond length shortenings, especially for IO where $r_e$ decreases by 0.0089 Å upon 4s4p4d electron correlation. As expected, the inclusion of spin-orbit coupling increases in importance from ClO to IO. It should be noted that the effects of SO coupling on $D_e$ shown in Table 1 are significantly different from what one might estimate based only on the experimental zero-field splittings. This is due to strong second-order effects, especially for IO. Of particular interest in Table 1 are the contributions of iterative triple and quadruple excitations in the coupled cluster treatment compared to CCSD(T). The difference between CCSDT and CCSD(T), ΔT, is relatively large due to the not insubstantial amount of

nondynamical correlation in these molecules as indicated by the somewhat large $T_1$ diagnostics, which run as large as about 0.07 for IO. In each case iterative triples increase the bond lengths by about 0.003 Å, decrease the harmonic frequencies, and increase the dissociation energies, the latter by 0.10 to 0.55 kcal/mol. In regards to the equilibrium bond lengths, the effects of iterative connected quadruple excitations, ΔQ, are small, less than 0.001 Å. Their effect on the dissociation energies, however, is substantial, ranging from +0.56 to +0.70 kcal/mol. The contributions for IO are slightly different from those reported previously[16] due to the different bond lengths used. It should particularly be noted that in each case the iterative triples and quadruples corrections are both in the same direction compared to the CCSD(T) results, i.e., they both increase the dissociation energies over the CCSD(T) values and hence a fortuitous cancellation of the CCSDT–CCSD(T) and CCSDTQ–CCSDT contributions does not occur in these cases as is often observed (see, e.g., the results for IBr in Ref. [16]). Finally, the effects of correlation beyond CCSDTQ, as estimated by the continued fraction approximation, are small and amount to only about 0.1 kcal/mol for $D_e$ and are essentially negligible for $r_e$ and $\omega_e$. The final results for the spectroscopic constants of ClO and BrO are in excellent agreement with experiment - within 0.001 Å for $r_e$, 1.5 $cm^{-1}$ for $\omega_e$, and about 0.1 kcal/mol for $D_e$. The final calculated $r_e$ for IO, 1.8716 Å, is 0.004 Å longer than experiment while we is larger by just 2.8 $cm^{-1}$. This calculated value for $r_e$ is nearly identical to our recently reported value[16] if the ΔDK correction from this work is included. This agreement is a bit fortuitous, however, since the smaller core-valence correlation contribution of Ref. [16] is offset by the effects of iterative triples and quadruples of the present work. The discrepancy with experiment is presumably due to the underestimation of spin-orbit coupling effects. The present calculations yield a bond length shortening due to spin-orbit couping of 0.0056 Å, however the value estimated from experiment

(determined as one-half the difference in bond lengths between the two states) would correspond to a SO correction of –0.0086 Å. This additional -0.003 Å would bring our ab initio result to within 0.001 Å of experiment.

In order to obtain further insight into the accuracy of the current SO calculations, the excited $X_2{}^2\Pi_{1/2}$ state of each radical has also been investigated. These results are shown in Table 2 where they are compared to the accurate experimental values. The equilibrium state separation is reproduced to with 2% (9 $cm^{-1}$) for ClO, but it is underestimated for BrO and IO by about 12%. The shifts in the equilibrium bond lengths and harmonic frequencies between the two components, however, is very well reproduced in all three cases. In fact the near perfect agreement between theory and experiment for $\Delta r_e$ of IO contrasts the calculated SO correction for $r_e$ in the $X_1{}^2\Pi_{3/2}$ state, which as mentioned above was too small. The origin of this apparent inconsistency is currently not clear.

Coupled cluster results for the spectroscopic constants of the halogen oxide anions are shown in Table 3 where they are also compared to the available experimental values. The magnitudes of the basis set extrapolation and core-valence correlation contributions are observed to be very similar to those calculated for the neutral radicals. Not surprisingly, the effects due to spin-orbit coupling are relatively small for these closed-shell species, except of course for the electron affinity which involves the open shell radicals. It is very interesting to note the effects of iterative triple and quadruple excitations on the CCSD(T) spectroscopic constants and energetics. For the equilibrium bond lengths and harmonic frequencies, the ΔT and ΔQ corrections both have the same sign, just as in the case of the neutrals, but the iterative triples correction for $r_e$ is an order of magnitude smaller than ΔQ, which reflects the relatively small $T_1$ diagnostics for the

anions and hence higher accuracy of the perturbative triples approximation. The effects of iterative quadruples on the bond lengths, +0.002–+0.003 Å, are rather larger than expected, but recent work in our laboratory on the isovalent BrCl molecule yielded a nearly identical correction.[67] In contrast to the neutral radicals, the iterative triples and quadruples corrections to CCSD(T) for the dissociation energies are opposite in sign for the anions. While these two terms do not completely cancel, they do result in relatively small overall corrections (~0.3 kcal/mol) to the CCSD(T) results. In the case of the electron affinities, the effects of iterative triples dominate the correlation corrections to the CCSD(T) results, amounting to –0.6 to –1.0 kcal/mol. The final ab initio values for $r_e$ and $\omega_e$ of the negative ions are all within the relatively large error bars of the values derived from photoelectron spectroscopy.[23,24] Based on our results for the neutral radicals, as well as other related systems, the final ab initio results [CCSD(T)/aV5Z + ΔCBS + ΔCV + ΔSO + ΔDK + ΔT + ΔQ + ΔFCI] should have conservative uncertainties of about 0.002 Å and 3 $cm^{-1}$ for $r_e$ and $\omega_e$, respectively. The dissociation energies and electron affinities shown in Table 3 are in excellent agreement with experiment, exhibiting deviations from the accurate experimental values of just 0.1-0.2 kcal/mol. The present results for $ClO^-$ and $BrO^-$ are also in very good agreement with the previous coupled cluster calculations of Kim et al.[25] and Francisco et al.,[22] respectively. The calculations of Kim et al., which included correlation up through CCSDT with CBS extrapolations, yields a nearly identical electron affinity for ClO as the present work after molecular spin-orbit corrections are included to their result.

Table 4 summarizes the dissociation energies and resulting heats of formation calculated in the present work compared to experiment for the neutral halogen monoxide radicals. The ab

initio dissociation energies have been derived using two schemes, (a) by direct calculation as given in Table 1 and (b) via the negative ion thermochemical cycle

$$D_0(XO) = D_0(XO^-) + EA(X) - EA(XO) \qquad (X=Cl, Br, I) \qquad (3)$$

where the electron affinities were taken from the accurate experimental results.[21,23,24,68,69] While it is our belief that the second route leads to the most accurate dissociation energies in these cases since it minimizes errors due to spin-orbit effects, the two sets of $D_0$ values agree to within 0.1 kcal/mol in each case. The thermal corrections to the heats of formation at 0 K (to yield $\Delta H_f$ values at 298 K) have been determined using standard expressions for the ideal gas partition functions and experimental spectroscopic data where available.

Based on the spreads in the CBS extrapolation procedure and the experimental error bars in the electron affinities, best estimates of 63.5±0.3, 55.8±0.4, and 54.3±0.6 kcal/mol have been determined for the $D_0$ values of ClO, BrO, and IO, respectively. The values for ClO and BrO clearly emcompass the experimental values, while our predicted $D_0$ for BrO tends to favor the most recent experimental determination by North and co-workers[12] although our error bars do not exclude the smaller value obtained by Wilmouth et al.[13] As in our previous work,[16] our final predicted $D_0$ for IO is in good agreement with the experimental crossed molecular beam measurements based on the O+ICl reaction,[70,71] although these latter values have rather large stated uncertainties. The top end of our predicted range also just overlaps with the lower end of the experimental error bars derived from the most recent kinetics experiments,[1,72] but only after updating their result with the most recent OClO dissociation energy.[73] This revision also significantly decreases the uncertainty in their experimental heat of formation and resulting dissociation energy. In addition, the presently predicted heat of formation for IO at 298 K,

29.8±0.6 kcal/mol, can be compared to the values calculated previously by Hassanzadeh and Irikura,[74] 28.4±1.8 kcal/mol, and McGrath and Rowland,[75] 30.5±1.0 kcal/mol. Actually the level of agreement is remarkable given the very large differences in basis sets, correlation treatments, and methods for recovery of relativistic effects.

## IV. CONCLUSIONS

The spectroscopic and thermochemical properties of the halogen monoxides and their anions have been determined using high level electronic structure calculations that included explicit extraplations to the complete basis set limit and full configuration interaction level of theory with additional corrections due to core-valence correlation and spin-orbit coupling. The resulting molecular constants exhibit excellent agreement with experiment for the neutral species and provide very reliable predictions for the anions. The final *ab initio* equilibrium bond lengths and harmonic frequencies for ClO and BrO differ from their accurate experimental values by an average of just 0.0005 Å and 0.8 $cm^{-1}$, respectively. The bond length of IO is overestimated by 0.0040 Å, presumably due to an underestimation of molecular spin-orbit coupling effects. The predicted bond lengths and harmonic frequencies for the closed-shell anions are expected to be accurate to within 0.002 Å and 3 $cm^{-1}$, respectively. The dissociation energies of the radicals have been determined by both direct calculation and through use of negative ion thermochemical cycles, which made use of a small amount of accurate experimental data. The resulting values of $D_0$, 63.5, 55.8, and 54.3 kcal/mol for ClO, BrO, and IO, respectively, are the most accurate *ab initio* values to date, and those for ClO and BrO differ from their experimental values by just 0.1 kcal/mol. These dissociation energies lead to heats of formation, $\Delta H_f$(298 K), of 24.2±0.3, 29.6±0.4, and 29.8±0.6 kcal/mol for ClO, BrO, and IO, respectively. Also, the final calculated

electron affinities are all within 0.2 kcal/mol of their experimental values. The inclusion of full iterative triple and quadruple excitations in the coupled cluster treatment was found to be critical for obtaining this high level of accuracy.

**REFERENCES**


(1) Bedjanian, Y.; Poulet, G. *Chem. Rev.* **2003**, *103*, 4639.

(2) Burkholder, J. B.; Hammer, P. D.; Howard, C. J.; Maki, A. G.; Thompson, G.; Chackerian, C. *J. Mol. Spectrosc.* **1987**, *124*, 139.

(3) Drouin, B. J.; Miller, C. E.; Cohen, E. A.; Wagner, G.; Birk, M. *J. Mol. Spectrosc.* **2001**, *207*, 4.

(4) Drouin, B. J.; Miller, C. E.; Muller, H. S. P.; Cohen, E. A. *J. Mol. Spectrosc.* **2001**, *205*, 128.

(5) McKellar, A. R. W. *J. Mol. Spectrosc.* **1981**, *86*, 43.

(6) Orlando, J. J.; Burkholder, J. B.; Bopegedera, A. M. R. P.; Howard, C. J. *J. Mol. Spectrosc.* **1991**, *145*, 278.

(7) Durie, R. A.; Legay, F.; Ramsay, D. A. *Can. J. Phys.* **1060**, *38*, 444.

(8) Newman, S. M.; Howie, W. H.; Lane, I. C.; Upson, M. R.; Orr-Ewing, A. J. *J. Chem. Soc. Faraday Trans.* **1998**, *94*, 2681.

(9) Wennberg, P. O.; Brault, J. W.; Hanisco, T. F.; Salawitch, R. J.; Mount, G. H. *J. Geophys. Res.* **1997**, *102*, 8887.

(10) Miller, C. E.; Cohen, E. A. *J. Chem. Phys.* **2001**, *115*, 6459.

(11) Coxon, J. A.; Ramsay, D. A. *Can. J. Phys.* **1976**, *54*, 1034.

(12) Kim, H.; Dooley, K. S.; Johnson, E. R.; North, S. W. *J. Chem. Phys.* **2006**, *124*, 134304.

(13) Wilmouth, D. M.; Hanisco, T. F.; Donahue, N. M.; Anderson, J. G. *J. Phys. Chem. A* **1999**, *103*, 8935.

(14) Feller, D.; Peterson, K. A.; de Jong, W. A.; Dixon, D. A. *J. Chem. Phys.* **2003**, *118*, 3510.

(15) Feller, D.; Peterson, K. A.; Crawford, T. D. *J. Chem. Phys.* **2006**, *124*, 054107.

(16) Shepler, B. C.; Balabanov, N. B.; Peterson, K. A. *J. Phys. Chem. A* **2005**, *109*, 10363.

(17) Dixon, D. A.; de Jong, W. A.; Peterson, K. A.; Christe, K.; Schrobilgen, G. J. *J. Am. Chem. Soc.* **2005**, *127*, 8627.

(18) Feller, D.; Dixon, D. A. *J. Phys. Chem. A* **2003**, *107*, 9641.

(19) Pollack, L.; Windus, T. L.; de Jong, W. A.; Dixon, D. A. *J. Phys. Chem. A* **2005**, *109*, 6934.

(20) Brinkmann, N. R.; Tschumper, G. S.; Schaefer, H. F. *J. Chem. Phys.* **1999**, *110*, 6240.

(21) Distelrath, V.; Boesl, U. *Faraday Discuss.* **2000**, *115*, 161.

(22) Francisco, J. S.; Parthiban, S.; Lee, T. J. *J. Chem. Phys.* **1998**, *109*, 10818.

(23) Gilles, M. K.; Polak, M. L.; Lineberger, W. C. *J. Chem. Phys.* **1991**, *95*, 4723.

(24) Gilles, M. K.; Polak, M. L.; Lineberger, W. C. *J. Chem. Phys.* **1992**, *96*, 8012.

(25) Kim, S.-J.; Kim, Y.-J.; Shin, C.-H.; Mhin, B.-J.; Crawford, T. D. *J. Chem. Phys.* **2002**, *117*, 9703.

(26) Ma, N. L.; Cheung, Y.-S.; Ng, C. Y.; Li, W.-K. *Mol. Phys.* **1997**, *91*, 495.

(27) Midda, S.; Das, A. K. *J. Mol. Struct. (Theochem)* **2005**, *713*, 101.

(28) Minaev, B.; Loboda, O.; Vahtras, O.; Ågren, H.; Bilan, E. *Spectrochim. Acta A* **2002**, *58*, 1039.

(29) Xie, Y.; Schaefer, H. F.; Wang, Y.; Fu, X.-Y.; Liu, R.-Z. *Mol. Phys.* **2000**, *98*, 879.

(30) Hampel, C.; Peterson, K. A.; Werner, H.-J. *Chem. Phys. Lett.* **1992**, *190*, 1.

(31) Raghavachari, K.; Trucks, G. W.; Pople, J. A.; Head-Gordon, M. *Chem. Phys. Lett.* **1989**, *156*, 479.

(32) Knowles, P. J.; Hampel, C.; Werner, H.-J. *J. Chem. Phys.* **1994**, *99*, 5219.

(33) Knowles, P. J.; Hampel, C.; Werner, H.-J. *J. Chem. Phys.* **2000**, *112*, 3106.

(34) Scuseria, G. E. *Chem. Phys. Lett.* **1991**, *176*, 27.

(35) Deegan, M. J. O.; Knowles, P. J. *Chem. Phys. Lett.* **1994**, *227*, 321.

(36) Watts, J. D.; Gauss, J.; Bartlett, R. J. *J. Chem. Phys.* **1993**, *98*, 8718.

(37) Dunning, T. H., Jr. *J. Chem. Phys.* **1989**, *90*, 1007.

(38) Kendall, R. A.; Dunning, T. H., Jr.; Harrison, R. J. *J. Chem. Phys.* **1992**, *96*, 6796.

(39) Dunning, T. H. J.; Peterson, K. A.; Wilson, A. K. *J. Chem. Phys.* **2001**, *114*, 9244.

(40) Woon, D. E.; Dunning, T. H., Jr. *J. Chem. Phys.* **1993**, *98*, 1358.

(41) Peterson, K. A.; Figgen, D.; Goll, E.; Stoll, H.; Dolg, M. *J. Chem. Phys.* **2003**, *119*, 11113.

(42) Douglas, M.; Kroll, N. M. *Ann. Phys. (New York)* **1974**, *82*, 89.

(43) Jansen, G.; Hess, B. A. *Phys. Rev. A* **1989**, *39*, 6016.

(44) Dunham, J. L. *Phys. Rev.* **1932**, *41*, 721.

(45) Peterson, K. A.; Woon, D. E.; Dunning, T. H., Jr. *J. Chem. Phys.* **1994**, *100*, 7410.

(46) Halkier, A.; Helgaker, T.; Jørgensen, P.; Klopper, W.; Koch, H.; Olsen, J.; Wilson, A. K. *Chem. Phys. Lett.* **1998**, *286*, 243.

(47) Helgaker, T.; Klopper, W.; Koch, H.; Noga, J. *J. Chem. Phys.* **1997**, *106*, 9639.

(48) Peterson, K. A.; Dunning, T. H. J. *J. Chem. Phys.* **2002**, *117*, 1.

(49) Balabanov, N. B.; Peterson, K. A. *Journal of Chemical Physics* **2003**, *119*, 12271.

(50) de Jong, W. A.; Harrison, R. J.; Dixon, D. A. *J. Chem. Phys.* **2001**, *114*, 48.

(51) Wilson, A. K.; Peterson, K. A.; Woon, D. E.; Dunning, T. H., Jr. *J. Chem. Phys.* **1999**, *110*, 7667.

(52) Yabushita, S.; Zhang, Z.; Pitzer, R. M. *J. Phys. Chem. A* **1999**, *103*, 5791.

(53) Columbus. H. Lischka, R. Shepard, I. Shavitt, R. M. Pitzer, M. Dallos, Th. Müller, P. G. Szalay, F. B. Brown, R. Ahlrichs, H. J. Böhm, A. Chang, D. C. Comeau, R. Gdanitz, H. Dachsel, C. Ehrhardt, M. Ernzerhof, P. Höchtl, S. Irle, G. Kedziora, T. Kovar, V. Parasuk, M. J. M. Pepper, P. Scharf, H. Schiffer, M. Schindler, M. Schüler, M. Seth, E. A. Stahlberg, J.-G. Zhao, S. Yabushita, and Z. Zhang, COLUMBUS, an ab initio electronic structure program, release 5.8 (2001).

(54) Metz, B.; Stoll, H.; Dolg, M., Private communication.

(55) Kállay, M.; Surján, P. R. *J. Chem. Phys.* **2001**, *115*, 2945.

(56) Noga, J.; Bartlett, R. J. *J. Chem. Phys.* **1987**, *86*, 7041.

(57) Scuseria, G. E.; Schaefer, H. F. *Chem. Phys. Lett.* **1988**, *132*, 382.

(58) Watts, J. D.; Bartlett, R. J. *J. Chem. Phys.* **1993**, *93*, 6104.

(59) Kucharski, S. A.; Bartlett, R. J. *Theor. Chim. Acta* **1991**, *80*, 387.

(60) Kucharski, S. A.; Bartlett, R. J. *J. Chem. Phys.* **1992**, *97*, 4282.

(61) Oliphant, N.; Adamowicz, L. *J. Chem. Phys.* **1991**, *94*, 1229.

(62) Goodson, D. Z. *J. Chem. Phys.* **2002**, *116*, 6948.

(63) Molpro-long. MOLPRO, a package of ab initio programs designed by H.-J. Werner and P. J. Knowles, version 2002.6, R. D. Amos, A. Bernhardsson, A. Berning, P. Celani, D. L. Cooper, M. J. O. Deegan, A. J. Dobbyn, F. Eckert, C. Hampel, G. Hetzer, P. J. Knowles, T. Korona, R. Lindh, A. W. Lloyd, S. J. McNicholas, F. R. Manby, W. Meyer, M. E. Mura, A. Nicklass, P. Palmieri, R. Pitzer, G. Rauhut, M. Schütz, U. Schumann, H. Stoll, A. J. Stone, R. Tarroni, T. Thorsteinsson, and H.-J. Werner., 2002.

(64) MRCC. MRCC, a string-based quantum chemical program suite written by M. Kállay. See also M. Kállay, P. R. Surján, J. Chem. Phys. 115 2945 (2001) as well as: http://www.mrcc.hu., 2006.

(65) NWChem. Aprà, E.; Windus, T.L.; Straatsma, T.P.; Bylaska, E.J.; de Jong, W.; Hirata, S.; Valiev, M.; Hackler, M.; Pollack, L.; Kowalski, K.; Harrison, R.; Dupuis, M.; Smith, D.M.A;

Nieplocha, J.; Tipparaju V.; Krishnan, M.; Auer, A.A.; Brown, E.; Cisneros, G.; Fann, G.; Fruchtl, H.; Garza, J.; Hirao, K.; Kendall, R.; Nichols, J.; Tsemekhman, K.; Wolinski, K.; Anchell, J.; Bernholdt, D.; Borowski, P.; Clark, T.; Clerc, D.; Dachsel, H.; Deegan, M.; Dyall, K.; Elwood, D.; Glendening, E.; Gutowski, M.; Hess, A.; Jaffe, J.; Johnson, B.; Ju, J.; Kobayashi, R.; Kutteh, R.; Lin, Z.; Littlefield, R.; Long, X.; Meng, B.; Nakajima, T.; Niu, S.; Rosing, M.; Sandrone, G.; Stave, M.; Taylor, H.; Thomas, G.; van Lenthe, J.; Wong, A.; Zhang, Z. "NWChem, A Computational Chemistry Package for Parallel Computers, Version 4.7" (2005), Pacific Northwest National Laboratory, Richland, Washington 99352-0999, USA. Richland, WA, 2005.

(66) Hirata, S. *J. Phys. Chem. A* **2003**, *107*, 9887.

(67) Shepler, B. C. Ab initio investigation of the thermochemistry, spectroscopy and dynamics of reactions between mercury and reactive halogen species. Ph.D. thesis, Washington State University, 2006.

(68) Blondel, C.; Cacciani, P.; Delsart, C.; Trainham, R. *Phys. Rev. A* **1989**, *40*, 3698.

(69) Hotop, H.; Lineberger, W. C. *J. Phys. Chem. Ref. Data* **1985**, *14*, 731.

(70) Buss, R. J.; Sibener, S. J.; Lee, Y. t. *J. Phys. Chem.* **1983**, *87*, 4840.

(71) Radlein, D. S. A. G.; Whitehead, J. C.; Grice, R. *Nature* **1975**, *253*, 37.

(72) Bedjanian, Y.; Le Bras, G.; Poulet, G. *J. Phys. Chem. A* **1997**, *101*, 4088.

(73) Davis, H. F.; Lee, Y. T. *J. Chem. Phys.* **1996**, *105*, 8142.

(74) Hassanzadeh, P.; Irikura, K. K. *J. Phys. Chem. A* **1997**, *101*, 1580.

(75) McGrath, M. P.; Rowland, F. S. *J. Phys. Chem.* **1996**, *100*, 4815.

(76) Chase, M. W., Jr.; Davies, C. A.; Downey, J. R., Jr.; Frurip, D. J.; McDonald, R. A.; Syverud, A. N. *J. Phys. Chem. Ref. Data* **1985**, *14*, Suppl. No. 1.

Table 1: Contributions and final predicted values for equilibrium bond lengths (Å), harmonic frequencies ($cm^{-1}$), and dissociation energies (kcal/mol) of the $X^2\Pi_{3/2}$ states of ClO, BrO, and IO with comparison to experiment.[a]

| | CCSD(T)/ aV5Z | ΔCBS | ΔCV | ΔSO | ΔDK | ΔT | ΔQ | ΔFCI | Total | Expt.[b] |
|---|---|---|---|---|---|---|---|---|---|---|
| ClO | | | | | | | | | | |
| $r_e$ | 1.5711 | -0.0029 | -0.0033 | -0.0007 | --- | 0.0031 | 0.0009 | 0.0001 | 1.5683 | 1.5689 |
| $\omega_e$ | 856.6 | 3.8 | 3.6 | 2.2 | --- | -6.5 | -2.6 | -0.3 | 856.7 | 855.5 |
| $D_e$ | 63.58 | 0.83 | 0.06 | -0.61 | --- | 0.10 | 0.56 | 0.06 | 64.60 | 64.65(1) |
| BrO | | | | | | | | | | |
| $r_e$ | 1.7220 | -0.0024 | -0.0043 | -0.0026 | 0.0000 | 0.0032 | 0.0008 | 0.0001 | 1.7168 | 1.7172 |
| $\omega_e$ | 729.7 | 3.2 | 3.6 | 4.7 | -0.7 | -4.5 | -2.3 | -0.3 | 733.4 | 732.9 |
| $D_e$ | 57.31 | 0.68 | -0.05 | -2.05 | -0.10 | 0.32 | 0.60 | 0.07 | 56.77 | 56.9(1) |
| IO | | | | | | | | | | |
| $r_e$ | 1.8810 | -0.0030 | -0.0089 | -0.0056 | 0.0048 | 0.0030 | 0.0004 | 0.0000 | 1.8716 | 1.8676 |
| $\omega_e$ | 672.9 | 1.9 | 5.5 | 9.4 | -3.1 | -1.3 | -0.8 | -0.1 | 684.5 | 681.7 |
| $D_e$ | 57.04 | 0.67 | 0.14 | -3.35 | -0.51 | 0.55 | 0.70 | 0.09 | 55.33 | |

[a] The best predicted values are given under the column "Total" and are equal to CCSD(T)/aV5Z + ΔCBS + ΔCV + ΔSO + ΔDK + ΔT + ΔQ + ΔFCI; ΔCBS = difference between CCSD(T) CBS and aV5Z values, ΔCV = core-valence correlation correction obtained with aug-cc-pwCVQZ (awCVQZ) basis sets, ΔSO = contribution from molecular and atomic spin-orbit coupling, ΔDK = difference between all-electron DKH CCSD(T)/awCVTZ calculations and pseudopotential-based CCSD(T)/awCVTZ with all-electrons correlated (not shown for ClO since the DK Hamiltonian was used throughout, except for the SO calculations), ΔT = difference between CCSDT and CCSD(T) results with aVTZ, ΔQ = difference between CCSDTQ and CCSDT results with aVDZ. The FCI

correction, ΔFCI, was calculated by extrapolating the CCSD, CCSDT, and CCSDTQ energies (aVDZ basis) using the continued fraction approximation (see text).

[b] References 3,4,10 and references therein. See Table 4 for a number of experimental $D_0$ values for IO.

Table 2: Calculated values for the spin-orbit constants ($A_e$, $cm^{-1}$) and shifts in the equilibrium bond lengths ($\Delta r_e$, Å) and harmonic frequencies ($\Delta\omega_e$, $cm^{-1}$) relative to the $X_1{}^2\Pi_{3/2}$ states for the $X_2{}^2\Pi_{1/2}$ states of ClO, BrO, and IO with comparison to experiment.

| | $A_e$ | $\Delta r_e$ | $\Delta\omega_e$ |
|---|---|---|---|
| ClO | | | |
| Theory (this work) | -313 | +0.0014 | –4.1 |
| Expt.[3] | -321.96 | +0.00121 | –3.3 |
| BrO | | | |
| Theory (this work) | -856 | +0.0066 | –13.3 |
| Expt.[4] | -975.43 | +0.00684 | –14.9 |
| IO | | | |
| Theory (this work) | -1812 | +0.0171 | –32.8 |
| Expt.[10,23] | -2091(40) | +0.01706 | –36.4 |

Table 3: Contributions and final predicted values for equilibrium bond lengths (Å), harmonic frequencies ($cm^{-1}$), and dissociation energies (kcal/mol) of the $X^1\Sigma^+$ states of $ClO^-$, $BrO^-$, and $IO^-$ with comparison to experiment.[a]

| | CCSD(T)/ aV5Z | ΔCBS | ΔCV | ΔSO | ΔDK | ΔT | ΔQ | ΔFCI | Total | Expt.[b] |
|---|---|---|---|---|---|---|---|---|---|---|
| $ClO^-$ | | | | | | | | | | |
| $r_e$ | 1.6835 | –0.0036 | –0.0036 | 0.0000 | --- | +0.0007 | +0.0025 | +0.0004 | 1.6798 | 1.673(8) |
| $\omega_e$ | 667.2 | +3.3 | +2.4 | 0.0 | --- | –1.5 | –2.5 | –0.2 | 668.6 | 665(25) |
| $D_e$ | 32.71 | +0.64 | +0.13 | –0.15 | --- | –0.33 | +0.61 | +0.07 | 33.68 | 33.60(4) |
| $EA_e$ | 52.75 | +0.33 | –0.08 | –0.47 | --- | –0.57 | +0.15 | +0.02 | 52.12 | 52.26(3) |
| $BrO^-$ | | | | | | | | | | |
| $r_e$ | 1.8131 | –0.0030 | –0.0035 | +0.0001 | +0.0003 | +0.0004 | +0.0022 | +0.0003 | 1.8099 | 1.814(9) |
| $\omega_e$ | 598.4 | +3.1 | +2.4 | –0.1 | –0.8 | –1.3 | –2.2 | –0.2 | 599.2 | 575(25) |
| $D_e$ | 33.00 | +0.50 | –0.15 | –0.16 | –0.25 | –0.36 | +0.66 | +0.08 | 33.32 | 33.5(2) |
| $EA_e$ | 55.83 | +0.40 | –0.10 | –1.67 | –0.03 | –0.75 | +0.13 | +0.02 | 53.84 | 54.07(14) |
| $IO^-$ | | | | | | | | | | |
| $r_e$ | 1.9402 | –0.0034 | –0.0059 | +0.0012 | +0.0048 | +0.0002 | +0.0024 | +0.0004 | 1.9399 | 1.929(10) |
| $\omega_e$ | 595.9 | +2.6 | +0.4 | –0.8 | –2.1 | +0.1 | –2.5 | –0.4 | 593.0 | 581(25) |
| $D_e$ | 39.50 | +0.52 | –0.20 | –0.27 | –0.56 | –0.40 | +0.72 | +0.10 | 39.40 | --- |
| $EA_e$ | 58.87 | +0.46 | –0.22 | –3.45 | 0.00 | –1.00 | +0.09 | +0.01 | 54.77 | 54.71(14) |

[a] See the footnotes to Table 1. Vibration-rotation and anharmonicity constants are available from the authors on request. The dissociation energies are given relative to $X^-(^1S_0) + O(^3P_2)$.

[b] Taken from references 21,23,24. Values in parentheses denote the stated experimental uncertainty in the last digit. The experimental $EA_e$ values were derived from the adiabatic $EA_0$s using the accurate *ab initio* zero-point energies. The experimental $D_e$ values were derived using the experimental molecular and atomic electron affinities (Refs. 21,24,68,69) and $D_0$(XO) values (Ref. 11 for ClO and Ref. 12 for BrO).

Table 4. A summary of calculated dissociation energies and heats of formation for the $X^2\Pi_{3/2}$ ground states of ClO, BrO, and IO with comparison to the available experimental results (in kcal/mol).

| | $D_0$ | | | $\Delta H_f$ (0 K) | | $\Delta H_f$ (298 K) | |
|---|---|---|---|---|---|---|---|
| | direct[a] | via $XO^-$ [b] | Expt | ab initio[c] | Expt | ab initio[c] | Expt |
| ClO | 63.4 | 63.5±0.3 | 63.43±0.01[11] | 24.1±0.3 | 24.15±0.03[11] | 24.2±0.3 | 24.29±0.03[11] |
| BrO | 55.7 | 55.8±0.4 | 55.9±0.1[12]<br>55.2±0.4[13] | 31.4±0.4 | 31.3±0.1[12]<br>32.0±0.4[13] | 29.6±0.4 | 29.5±0.1[12]<br>30.2±0.4[13] |
| IO | 54.4 | 54.3±0.6 | 53±3,[71] 55±2[70]<br>55.3±0.5[d] | 30.3±0.6 | 32±3,[71]<br>30±2[70]<br>29.3±0.5[d] | 29.8±0.6 | 31±3,[71]<br>29±2[70]<br>28.8±0.5[d] |

[a] Derived from the ab initio results of Table 1.

[b] Ab initio results utilizing the relation $D_0(XO) = D_0(XO^-) + EA(X) - EA(XO)$ with experimental electron affinities taken from Refs. 21,23,24,68,69.

[c] Calculated from the dissociation energies based on the negative ion cycles. See footnote b. The following reference thermodynamic data (Ref. 76) was utilized throughout (in kcal/mol): $\Delta H_f$(O) = 58.98±0.02 (0K), 59.55±0.02 (298K); $\Delta H_f$(Cl) = 28.590±0.001 (0K), 28.992±0.002 (298K); $\Delta H_f$(Br) = 28.18±0.01 (0K), 26.74±0.01 (298K); $\Delta H_f$(I) = 25.61±0.01 (0K), 25.52±0.01 (298K).

[d] The heat of formation derived in Ref. 72 (27.7±1.2 kcal/mol at 298 K) from the kinetics of the IO + ClO reaction has been revised upwards by 1.1 kcal/mol with a concomitant decrease in its uncertainty by using a more recent determination[73] of $\Delta H_f$ (OClO), 23.53±0.24 kcal/mol at 298 K, and the $\Delta H_f$ (ClO) derived from Ref. 11.

# Appendix 2**

# Accurate global potential energy surface and reaction dynamics for the ground state of $HgBr_2$

**Nikolai B. Balabanov, Benjamin C. Shepler, and Kirk A. Peterson***

*Department of Chemistry, Washington State University, Pullman, Washington 99164-4630*

**Abstract**

A global potential energy surface (PES) for the $^1A'$ ground state of $HgBr_2$ has been constructed in order to determine the rate constants for atmospherically important reactions involving the mercury and bromine species. The total energy of $HgBr_2$ was calculated by the multireference configuration interaction level of theory with series of correlation consistent basis sets up to quadruple-ζ quality with subsequent extrapolation to the complete basis set limit. An additive correction for spin-orbit coupling was also included. The global PES was represented piecewise by interpolating three separate parts of the surface with the reproducing kernel Hilbert space method and connecting them smoothly by switch functions. Quasiclassical trajectory calculations carried out on the surface yielded 298 K thermal rate constants of $3.88\times10^{-11}$ $cm^3/(mol\cdot sec)$ for the abstraction reaction $HgBr+Br \rightarrow Hg+Br_2$, $2.98\times10^{-11}$ $cm^3/(mol\cdot sec)$ for the recombination reaction $Br + HgBr \rightarrow HgBr_2$, and $3.97\times10^{-11}$ $cm^3/(mol\cdot sec)$ for the exchange reaction $Br+HgBr \rightarrow BrHg+Br$. The insertion reaction $Hg+Br_2 \rightarrow HgBr_2$ was found to have a high barrier of 27.2 kcal/mol and a very small rate constant of just $2.74\times10^{-31}$ $cm^3/(mol\cdot sec)$ determined by the microcanonical variational transition state theory method. The implications of the obtained results to the description of the mechanism of recently observed polar tropospheric mercury depletion events are briefly discussed.

---

** The dissertation author was a contributor, but not this manuscripts primary author.

*Journal of Physical Chemistry A*. **109**, 8765 (2005)

# Accurate Global Potential Energy Surface and Reaction Dynamics for the Ground State of $HgBr_2$

**Nikolai B. Balabanov,† Benjamin C. Shepler,‡ and Kirk A. Peterson***

*Department of Chemistry, Washington State University, Pullman, Washington 99164-4630*

*Received: June 23, 2005; In Final Form: July 29, 2005*

A global potential energy surface (PES) for the $^1A'$ ground state of $HgBr_2$ has been constructed in order to determine the rate constants for atmospherically important reactions involving mercury and bromine. The total energy of $HgBr_2$ was calculated by the multireference configuration interaction level of theory with series of correlation consistent basis sets up to quadruple-ζ quality with subsequent extrapolation to the complete basis set limit. An additive correction for spin−orbit coupling was also included. The global PES was represented piecewise by interpolating three separate parts of the surface with the reproducing kernel Hilbert space method and connecting them smoothly by switch functions. Quasiclassical trajectory calculations carried out on the surface yielded 298 K thermal rate constants of $3.89 \times 10^{-11}$ cm$^3$/(mol•s) for the abstraction reaction $HgBr + Br \rightarrow Hg + Br_2$, $2.98 \times 10^{-11}$ cm$^3$/(mol•s) for the recombination reaction $Br + HgBr \rightarrow HgBr_2$, and $3.97 \times 10^{-11}$ cm$^3$/(mol•s) for the exchange reaction $Br + HgBr \rightarrow BrHg + Br$. The insertion reaction $Hg + Br_2 \rightarrow HgBr_2$ was found to have a high barrier of 27.2 kcal/mol and a very small rate constant of just $2.74 \times 10^{-31}$ cm$^3$/(mol•s) determined by the microcanonical variational transition state theory method. The implications of the obtained results to the description of the mechanism of recently observed polar tropospheric mercury depletion events are briefly discussed.

## I. Introduction

The contamination of remote polar regions, which are generally thought to be ecologically safe, has been of growing concern due to the recent discovery of mercury depletion events[1] (MDEs). These periodic rapid depletions of atmospheric gaseous mercury (predominantly in elemental $Hg^0$ form) were observed in both the Arctic[1,2] and Antarctic[3,4] during polar springtime. The periods of nearly complete removal of mercury from the atmosphere is always accompanied by an increase in concentration of mercury compounds on snow and ice surfaces.[2,5,6] It was also observed[1] that MDEs mimic the analogous depletions of ozone[7] occurring at the polar regions in this same period of time. Since there is strong evidence that ozone depletions are due to its reaction with halogen radicals generated photochemically from sea salts after polar sunrise,[8] the oxidation of elemental mercury by halogen radicals is also considered to be one of the major mechanisms for MDEs.[2,5,9,10] The reactions of elemental gaseous mercury and halogens probably produce what are called reactive gaseous mercury (RGM) species that apparently quickly deposit on snow and ice packs.[2,5,9,10]

One of the most likely reactions that can occur during the MDEs is oxidation of elemental mercury by bromine radicals. This might be described by a set of elemental reactions such as

$$Br_2 + h\nu \rightarrow 2Br \quad (1)$$

$$Hg + Br \rightarrow HgBr \quad (2)$$

$$HgBr + Br \rightarrow HgBr_2 \quad (3)$$

where $HgBr_2$ is one of the most probable RGM species that might deposit on the surface. Of course, the bimolecular reaction 3 might also be accompanied by abstraction of a bromine atom

$$HgBr + Br \rightarrow Hg + Br_2 \quad (4)$$

or by the exchange of the bromine atom

$$HgBr(1) + Br(2) \rightarrow Br(1) + HgBr(2) \quad (5)$$

Theoretically the RGM species $HgBr_2$ can also be produced via a direct insertion reaction of the mercury atom into the $Br_2$ bond

$$Hg + Br_2 \rightarrow HgBr_2 \quad (6)$$

The main focus of the present paper is on the high level theoretical determination of the rate constants of reactions 3−6. For this purpose an accurate ab initio global potential energy surface (PES) of $HgBr_2$ was constructed and the reaction rate constants were then evaluated with use of quasiclassical trajectory (QCT) calculations or by variational transition state theory (VTST). Reaction 2, which is the prerequisite for reactions 3−5, will be carefully examined in another publication.[11] The details of the ab initio electronic structure calculations are described in section II, those of construction of the global potential surface of $HgBr_2$ are given in section III, the description of the calculations of the rate constants can be found in section IV, and the comparison of the obtained results with known experimental[12] and previous theoretical[13] data on the rate constants of reactions 3 and 6 and the discussion of their atmospheric implications is presented in section V. The conclusions drawn from the present work are summarized in section VI.

## II. Details of the Ab Initio Calculations

In the electronic structure calculations the Br 1s−2p and Hg 1s−4f electrons were described by relativistic small core

* Corresponding author. E-mail: kipeters@wsu.edu.
† E-mail: nick@mail.wsu.edu.
‡ E-mail: bshepler@wsu.edu.

10.1021/jp053415l CCC: $30.25 © 2005 American Chemical Society
Published on Web 09/13/2005

pseudopotentials of the Stuttgart-Köln type.[14,15] The remaining Br (3s3p3d4s4p) and Hg (5s5p5d6s) electrons were explicitly treated with series of augmented correlation consistent basis sets, aug-cc-pV*n*Z-PP, constructed for use with these pseudopotentials.[14,16] The quality of basis sets ranged from double-$\zeta$ to quadruple-$\zeta$ ($n$ = D, T, Q) and only the pure spherical d-, f-, g-, and h-type angular momentum functions were employed in the calculations. The total number of basis functions for the $HgBr_2$ system consisted of 118 for double-$\zeta$, 198 for triple-$\zeta$, and 313 for the quadruple-$\zeta$ calculations. All calculations were performed in $C_s$ effective symmetry.

The total energies of the $HgBr_2$ ground electronic state were calculated by the internally contracted multireference configuration interaction (singles and doubles) method[17,18] with the multireference Davidson correction for an approximate treatment of the effect of higher excitations[19−21] (icMRCI+Q). The orbitals for the icMRCI+Q calculations were determined by the state-averaged complete active space self-consistent field (CASSCF) method by averaging four lowest $^1A'$ and two lowest $^3A'$ electronic states with equal weights. The active space in these CASSCF calculations consisted of eight molecular orbitals originating from the Hg 6s, $6p_x$, $6p_y$, $6p_z$ and Br $4p_x$, $4p_z$ AOs (assuming $HgBr_2$ is lying in the *xz* plane). The Hg 5d and Br 4s, $4p_y$ were always kept doubly occupied in the CASSCF procedure. The CASSCF wave function consisted of 980 configuration state functions (CSFs) for singlet states and 1176 CSFs for triplet states. This choice of active space and number of states included in the averaging procedure allowed us to obtain well-defined molecular orbitals over different regions of the $HgBr_2$ potential energy surface.

In the icMRCI+Q calculations, the active space consisted of orbitals arising from Hg 5d, 6s, and 6p and Br 4p AOs. The CSFs in the reference space were generated with the restrictions that the Hg 5d and Br $4p_y$ orbitals were doubly occupied and the Hg $6p_x$, $6p_y$, and $6p_z$ orbitals had a maximum occupation of a single electron in any one CSF. When used with the aug-cc-pVQZ-PP basis, the largest basis set employed in this work, the icMRCI wave function consisted of about 8.5 million variational parameters, which effectively took into account more than 327 million uncontracted CSFs. All CASSCF and icMRCI+Q calculations described above were carried out with the MOLPRO suite[22] of quantum chemistry programs.

After calculating the icMRCI+Q energy with each basis set (DZ, TZ, QZ), the complete basis set limits of the icMRCI+Q total energies were then obtained by averaging the CBS limits found by two extrapolations: a mixed exponential and Gaussian form[23]

$$E_n = E_{CBS} + A\mathrm{e}^{-(n-1)} + B\mathrm{e}^{-(n-1)^2} \tag{7}$$

using $n$ = 2 (DZ), 3 (TZ), and 4 (QZ) and a 2-point $n^{-3}$ formula[24−26]

$$E_n = E_{CBS} + \frac{A}{n^3} \tag{8}$$

which utilized energies for $n$ = 3 (TZ) and 4 (QZ). Total energies were used in both cases.

Finally, corrections for the spin-obit interaction, $\Delta E_{SO}$, were added to the icMRCI+Q/CBS energies. $\Delta E_{SO}$ was obtained as the difference in energy of the lowest spin−orbit state and the energy of the lowest singlet state of $HgBr_2$. The spin−orbit energy was obtained by the spin−orbit MRCI method[27] taking into account only single electron excitations (SO-MRCIS) with the aug-cc-pVTZ-PP basis sets. The energy of the lowest singlet state was found with the same method, but without the SO interaction. Both these calculations were carried out with the COLUMBUS package,[28−31] but utilized the orbitals obtained in the MOLPRO CASSCF calculations as described above. The active space in the (SO-) MRCIS work consisted of the Hg 6s5d and Br 4s4p orbitals. In the spin−orbit calculations the effective spin−orbit potentials that are part of the relativistic core potentials on Br[14] and Hg[15] were used, and the wave function was constructed with the inclusion of both singlet and triplet CSFs.

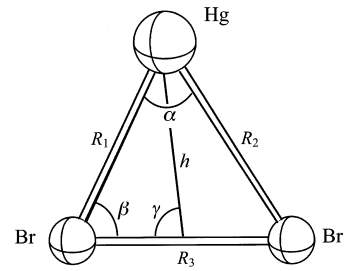


**Figure 1.** Notation of coordinates for $HgBr_2$ used in sampling and fitting the PES.

## III. Construction of an Analytical PES

**A. Sampling.** The potential energy surface of $HgBr_2$ was divided into three regions corresponding to the abstraction reaction HgBr + Br → Hg + $Br_2$, insertion reaction Hg +$Br_2$ → $HgBr_2$, and recombination reaction Br + HgBr → $HgBr_2$. Each of these sections was sampled by a regular three-dimensional grid in its natural internal coordinates. The definition of the internal coordinates $R_1$, $R_2$, $R_3$, $h$, α, $\beta$, and $\gamma$ are shown in Figure 1; i.e., $R_1$ and $R_2$ are the two HgBr distances, $R_3$ is the BrBr distance, $h$ is the distance from the Hg atom to the center of mass (CM) of $Br_2$, α is the valence angle Br−Hg−Br, $\beta$ is the larger of the two Hg−Br−Br valence angles, and $\gamma$ is the smaller of the two Br−CM−Hg angles.

For the recombination reaction part of the surface, the internal coordinates were $R_1$, $R_2$, and α. A grid of 1296 configurations was generated by choosing $R_1$ and $R_2$ to be {3.5, 3.7, 3.9, 4.05, 4.2, 4.35, 4.50, 4.65, 4.8, 4.95, 5.15, 5.4, 6.0, 7.0, 8.5, 10.0, 15.0, and 30.0}$a_0$, and α to be {179.9, 160, 140, and 120}°. However the icMRCI+Q/CBS + Δ*SO* energies were calculated only for the 420 symmetry unique points with both $R_1$ and $R_2$ ≥ 4.2$a_0$. The energies for shorter distances were explicitly determined only at the icMRCI+Q/aug-cc-pVTZ-PP level of theory and only for α = 179.9°. The final energies $E(X_1, X_2, \alpha)$ for the points with $X_1(=R_1)$ or $X_2(=R_2) \leq 4.05a_0$ were then estimated by first calculating the factor $\xi$, which is independent of α

$$\xi = \frac{E^{TZ}(X_1,X_2) - E^{TZ}(R_1^*,R_2^*)}{E^{TZ}(R_1,R_2) - E^{TZ}(R_1^*,R_2^*)} \tag{9a}$$

where $(R_1,R_2)$ is a point on the edge of the rectangle [4.2:30.0] × [4.2:30.0] closest to $(X_1,X_2)$ and $(R_1^*, R_2^*)$ is the analogous point on the edge of the rectangle [4.35:30.0] × [4.35:30.0], each at α = 179.9°. The value of $E(X_1,X_2, \alpha)$ was then obtained by

$$E(X_1,X_2,\alpha) = E(R_1^*,R_2^*,\alpha) + \xi[E(R_1,R_2,\alpha) - E(R_1^*,R_2^*,\alpha)] \quad (9b)$$

It should be stressed that this particular extrapolation procedure mainly accounted for the basis set dependence of these short range data points since all of the collinear points were explicitly calculated with the aug-cc-pVTZ-PP basis set. In particular, these points had relatively high energies and were only necessary to include in the final fit to improve the behavior of the RKHS interpolation at short range.

For the abstraction reaction, the natural internal coordinates are $R_1$, $R_3$, and $\beta$. The $R_1$ distance ran over the array {4.2, 4.4, 4.6, 4.8, 5.0, 5.3, 6.0, 7.5, 9.0, 13.0, and 25.0}$a_0$, $R_3$ distances were chosen from {4.1, 4.3, 4.5, 4.7, 5.0, 5.3, 6.0, 7.5, 9.0, 13.0, and 25.0}$a_0$, and $\beta$ = {179.9, 160, 140, and 120}°, which gave 484 geometries.

The points for the insertion reaction region were sampled in Jacobi coordinates $h$, $R_3$, and $\gamma$. The values for the median $h$ were chosen from {3.0, 4.0, 4.5, 5.0, 5.5, 6.0, 7.0, 8.0, 10.0, and 15.0}$a_0$, the $R_3$ distance ran over {4.0, 5.0, 5.5, 6.0, 6.5, 7.0, 8.0, 9.5, 13.0, and 20.0}$a_0$, and the angle $\gamma$ was selected from {45, 60, 75, 90}°, which resulted in 400 symmetry-unique points.

To describe the two-body interaction of the Hg and Br atoms, calculations were carried out for the $HgBr_2$ molecule with one of the Hg−Br distances always kept at 50$a_0$. The values of the other Hg−Br distance were chosen from {3.2, 3.4, 3.6, 3.8, 4.0, 4.1, 4.2, 4.4, 4.5, 4.6, 4.7, 4.8, 4.9, 5.0, 5.2, 5.7, 6.3, 7.0, 8.0, 9.0, 10.0, 11.0, 13.0, 15.0, and 30}$a_0$. The points corresponding to distances ≥4.0$a_0$ were explicitly calculated at the icMRCI+Q/CBS + ΔSO level, while the remaining points in the short distance region were obtained by extrapolation via the exponential function $A + B\exp(-R) + C\exp(-2R)$. The coefficients in the latter equation were obtained by fitting to the shortest three data points. Similar calculations were performed to obtain energies of the Br−Br diatom interaction. The Br−Br distance was sampled from {2.9, 3.1, 3.3, 3.5, 3.7, 3.9, 4.0, 4.1, 4.2, 4.3, 4.4, 4.5, 4.6, 4.7, 4.9, 5.3, 6.0, 7.0, 8.5, 10.0, 13.0, and 30.0}$a_0$. The energies for the five shortest distances were obtained by exponential extrapolation as in Hg−Br.

Finally, a small grid was also sampled around the near-equilibrium geometry of $HgBr_2$ to improve the analytical representation of the PES in this region. A total of 22 points (14 symmetry unique) were sampled in ($R_1$, $R_2$, α) internal coordinates in the range 4.41−4.81$a_0$ for distances and 160−180° for the valence angle α.

**B. Fitting.** The data of regular grids for the recombination, abstraction, and insertion reaction regions were first decomposed using the general many-body expansion,[32] i.e.

$$\tilde{V}(R_1,R_2,R_3) = V^{(1)} + V^{(2)}_{HgBr}(R_1) + V^{(2)}_{HgBr}(R_2) + V^{(2)}_{BrBr}(R_3) + V^{(3)}(R_1,R_2,R_3) \quad (10)$$

where $V^{(1)}$ is the sum of energies of two separated Br atoms and the Hg atom, $V^{(2)}$ is the energy of the two-body interaction of the corresponding pair of atoms, and $V^{(3)}$ is the three-body interaction energy.

Diatomic interaction terms $V^{(2)}$ were interpolated via the one-dimensional reproducing kernel Hilbert space method[33] (RKHS)

$$V^{(2)}(R) = \sum_{i=1}^{n} C_i q(R,R^i) \quad (11)$$

where $q$ is a distancelike reproducing kernel[33]

$$q(x,x') = \frac{1}{14} x_>^{-7}\left\{1 - \frac{7}{9}\frac{x_<}{x_>}\right\} \quad (12)$$

and $x_< = \min(x,x')$ and $x_> = \max(x,x')$.

The regular grids of three-body energies for abstraction, recombination, and insertion on the global PES were interpolated separately with the multidimensional RKHS formula[33]

$$V^{(3)}_{region}(S_1,S_2,S_3) = \sum_{i,j,k=1}^{n_1,n_2,n_3} C_{ijk} q_1(S_1,S_1^i) q_2(S_2,S_2^j) q_3(S_3,S_3^k) \quad (13)$$

where $S_i$ and $q_i$ ($i$ = 1, 2, 3) are fitting coordinates and one-dimensional reproducing kernels, respectively, that are appropriate for each region. For the recombination and abstraction regions, kernels $q_1$ and $q_2$ in eq 13 were distancelike reproducing kernels given by eq 12, while $q_3$ was an anglelike reproducing kernel[33]

$$q(x,x') = 1 + x_< x_> + 2x_<^2 x_>\left\{1 - \frac{1}{3}\frac{x_<}{x_>}\right\} \quad (14)$$

The fitting coordinates for the recombination piece were chosen to be

$$S_1 = 1 - \exp(-aR_1)$$
$$S_2 = 1 - \exp(-aR_2)$$
$$S_3 = \frac{1}{2}(1 + \cos\alpha) \quad (15)$$

and for the abstraction piece, the corresponding coordinates were

$$S_1 = 1 - \exp(-aR_1)$$
$$S_2 = 1 - \exp(-aR_2)$$
$$S_3 = \frac{1}{2}(1 + \cos\beta) \quad (16)$$

where $a > 0$ was a parameter (~0.1). It was found that the use of exponential coordinates $S_1$ and $S_2$ of form (15) and (16) instead of the original $R_1$, $R_2$, and $R_3$ distances in the RKHS formula (13) produced significantly smaller $C_{ijk}$ coefficients.

For the insertion reaction piece, the $q_1$ kernel in eq 13 was a Taylor spline reproducing kernel[34]

$$q(x,x') = 2x_<^2 x_>\left\{1 - \frac{1}{3}\frac{x_<}{x_>}\right\} \quad (17)$$

$q_2$ was a distancelike kernel (eq 12), and $q_3$ was an anglelike kernel (eq 14). The fitting coordinates for the insertion region were chosen as

$$S_1 = \cosh^{-1}(bh)$$
$$S_2 = 1 - \exp(-aR_3)$$
$$S_3 = \sin^2\gamma \quad (18)$$

where $b$ was a parameter (~0.25). The use of the inverse hyperbolic cosine function for the description of the median $h$ is dictated by the properties of the three-body potential of $HgBr_2$: it is an even function relative to the $h$ coordinate, vanishes when $h \to \infty$, and has a minimum or maximum at $h$=0.

The three functions of the form of eq 13 for the insertion, abstraction, and recombination reaction regions were then combined into one global surface via the relation

$$V^{(3)} = \chi(R_1,R_2,R_3)[\Omega_+(\beta;\beta',\kappa_\beta)V^{(3)}_{abs} + \Omega_-(\beta;\beta',\kappa_\beta) \times \{\Omega_+(\alpha;\alpha',\kappa_\alpha)V^{(3)}_{ins} + \Omega_-(\alpha;\alpha',\kappa_\alpha)V^{(3)}_{rec}\}] \quad (19)$$

where

$$\Omega_\pm(\phi;\phi',\kappa) = \frac{1}{2}[1 \pm \tanh(\kappa(\phi - \phi')\}] \quad (20)$$

is a pair of functions for a smooth switch[35] between the intervals $(-\infty,\phi']$ and $[\phi',\infty)$. It is worthwhile to note that $\Omega_+ + \Omega_- \equiv 1$ and parameter $\kappa$ controls the strength of the switch. The values for the parameters were accepted as follows: $\alpha' = 115°$, $\beta' = 115°$, $\kappa_\alpha = 0.3$, and $\kappa_\beta = 0.3$. The $\chi$ function in eq 19 is designed to vanish at long range and is described in terms of switch functions (eq 20) as

$$\chi(R_1,R_2,R_3) = \prod_{i=1}^{3}\Omega_+(R_i;R_i',\kappa_R) \quad (21)$$

where $R_i' = 15.0a_0$ and $\kappa_R = 0.5$. The $\chi$ term is introduced in order to equivalence the long distance parts of the three-body terms obtained through interpolation of the three separate grids.

The small grid sampled around the near-equilibrium geometry of $HgBr_2$ was fitted with a polynomial function of the form

$$V_{eq}(Q_1,Q_2,Q_3) = \sum_{i,j,k} C_{ijk}(Q_1)^i(Q_2)^j(Q_3)^k \quad (22)$$

where the coordinates $Q_i$ were

$$Q_1 = R_1 - R_{1e}$$
$$Q_2 = R_2 - R_{2e}$$
$$Q_3 = \alpha - 180° \quad (23)$$

The SURFIT program[36] was used to obtain the equilibrium distances ($R_{1e}$, $R_{2e}$) and the $C_{ijk}$ coefficients in eq 22.

The final global $HgBr_2$ potential energy surface was then described by the formula

$$V(R_1,R_2,R_3) = \Omega_+(\rho;\rho',\kappa_\rho)V_{eq}(R_1,R_2,R_3) + \Omega_-(\rho;\rho',\kappa_\rho)\tilde{V}(R_1,R_2,R_3) \quad (24)$$

where

$$\rho = \sqrt{(R_1 - R_{1e})^2 + (R_2 - R_{2e})^2 + (\alpha - 180)^2 + \lambda} \quad (25)$$

In eq 25, $\lambda$ is a small parameter (0.001) introduced to avoid a discontinuity in the analytical first derivatives at the equilibrium geometry of $HgBr_2$. The values for the parameters of the switch function were chosen as $\rho' = 1$ and $\kappa_\rho = 1$.

It should be mentioned that after connecting different parts into one global surface, the final analytical function does not exactly interpolate all of the original data. However, nearly all of the significant errors are located at very high energies on the repulsive wall, and all the data around the minimum energy paths for reactions 3−6 are accurately reproduced by the fit. The overall root-mean-square error of the final fit relative to the original data (2202 total points, 1069 symmetry unique) was just 0.12 kcal/mol. It should also be noted that the RKHS formula (eq 13) was never directly used to compute the three-body potential energies in our calculations. Instead the fast algorithm for evaluation of the RKHS surface as described in ref 37 was employed. Switching to the fast summation technique resulted in speeding up the evaluation of the potential energy and its analytical partial derivatives by a factor of ∼10 for the insertion and abstraction regions and up to 17 times for the recombination part. This significantly decreased the time for running trajectories. The code that computes the $HgBr_2$ potential energy and its gradient was interfaced to the POLYRATE[38] and VENUS96[39] dynamics programs using the POTLIB2001[40] utility package and is available upon request from the authors.

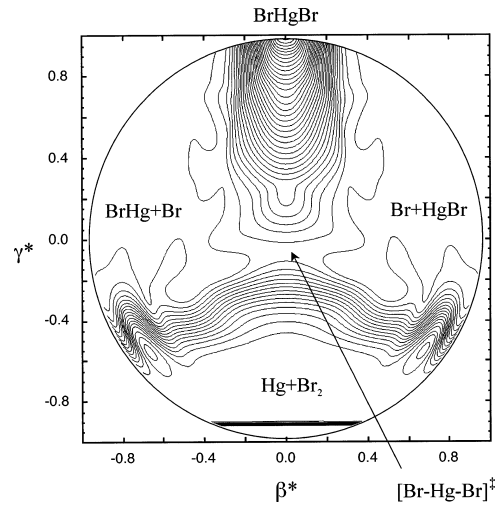


**Figure 2.** Relaxed triangle equipotential contour plot of the $HgBr_2$ PES given relative to the Br + Hg+Br energy in kcal/mol. Contours are equally spaced by 2 starting at −90 and finishing at −15. The plot is shown in the coordinates $\beta^* = \sqrt{3}\,(R_1^2 - R_2^2)/Q$ and $\gamma^* = (2R_3^2 - R_1^2 - R_2^2)/Q$, where $Q = R_1^2 + R_2^2 + R_3^2$ is varied to minimize the potential energy at the given point $(\beta^*,\gamma^*)$, where $(\beta^*)^2+(\gamma^*)^2 \leq 1$. Notations of the coordinates $R_1$, $R_2$, $R_3$ are found in Figure 1. At the transition state $\beta^* = 0$ and $\gamma^* = -0.135$.

**C. Characteristics of the Analytical PES.** Figure 2 presents a relaxed triangle plot[41] of the $HgBr_2$ potential energy surface using hyperspherical-like symmetrical coordinates.[42] More detailed plots of the insertion, abstraction, and recombination reactions in their natural coordinates are shown in Figures 3−5, respectively. In general the surface features two symmetrical valleys corresponding to the HgBr + Br → Hg + $Br_2$ abstraction reaction(s), a van der Waals well along the minimum energy path (MEP) of the abstraction reaction, a global minimum corresponding to the linear Br−Hg−Br insertion complex, and a saddle point corresponding to the barrier for the insertion reaction Hg + $Br_2$ → $HgBr_2$. The geometrical configuration of the saddle point is symmetrical with $R_1$(Hg−Br) = $R_2$(Hg−Br) = 2.853 Å and α(Br−Hg−Br) = 55.74°. The barrier for the insertion reaction 6 obtained from the present PES is 27.2 kcal/mol relative to the energy of the Hg+$Br_2$ reactants. Both reaction 4 for abstraction of the bromine atom from HgBr and the recombination reaction 3 to linear Br−Hg−Br are barrierless, and the corresponding MEPs go through linear geometrical configurations. The van der Waals minimum along the abstraction reaction MEP is located at $R_1$(Hg−Br) = 3.138 Å and $R_3$-(Br−Br) = 2.307 Å with a binding energy for the Hg−$Br_2$ adduct of 1.97 kcal/mol. Additional calibration calculations at

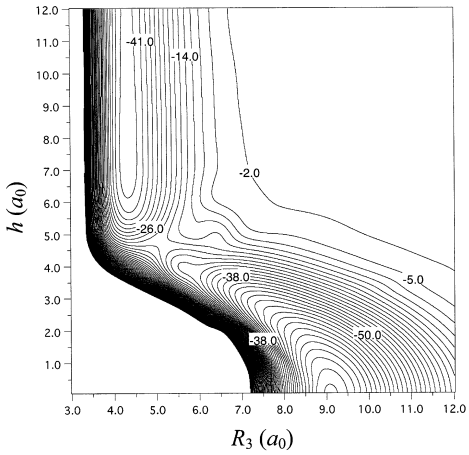


**Figure 3.** Equipotential contour plot of the $HgBr_2$ PES for fixed $\gamma = 90°$ in $(h,R_2,\gamma)$ Jacobi coordinates (Hg + $Br_2$ insertion reaction). The contours are equally spaced by 2 kcal/mol; the total energy is relative to completely separated ground-state atoms.

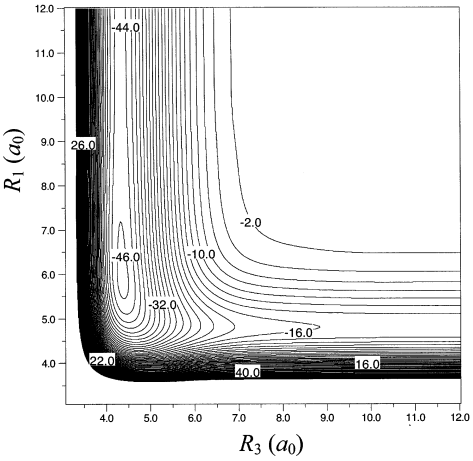


**Figure 4.** Equipotential contour plot of the $HgBr_2$ PES for fixed $\beta = 180°$ in $(R_1,R_3,\beta)$ valence coordinates (Hg + $Br_2$ abstraction reaction). The contours are equally spaced by 2 kcal/mol; the total energy is relative to completely separated ground-state atoms.

the CCSD(T)/CBS level of theory using DZ through QZ basis sets indicate that this binding energy is too small at this level of theory by only about 0.6 kcal/mol. The van der Waals interaction energy of Hg and $Br_2$ is comparable to the value of 1.34 kcal/mol for the Hg−$I_2$ complex determined in a crossed beam study of the rainbow scattering of Hg by $I_2$ by Wilcomb et al.[43]

To evaluate the accuracy of the constructed $HgBr_2$ global potential surface, we performed an analysis of the stationary points and asymptotes with the POLYRATE program in order to compare their structures and energies to the results of our previous accurate ab initio calculations[44,45] of the thermochemistry and structures of mercury bromides and/or available experimental data. The results are given in Tables 1 and 2. The

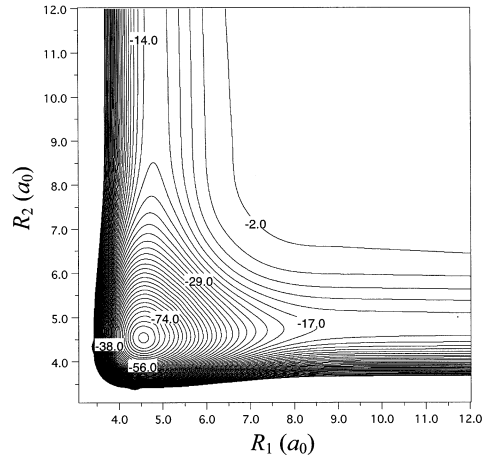


**Figure 5.** Equipotential contour plot of the $HgBr_2$ PES for fixed $\alpha = 180°$ in $(R_1,R_2,\alpha)$ valence coordinates (HgBr + Br recombination reaction). The contours are equally spaced by 3 kcal/mol; the total energy is relative to completely separated ground-state atoms.

**TABLE 1: Equilibrium Structures ($R$, Å) and Harmonic Frequencies ($\omega_i$, $cm^{-1}$) at Stationary Points and Asymptotes on the IcMRCI+Q/CBS+SO Potential Energy Surface of $HgBr_2$**

| point | parameter | current surface | best estimate |
|---|---|---|---|
| Hg + $Br_2$ | $R_e$(BrBr) | 2.288 | 2.281[a] |
| | $\omega_e$ | 325.0 | 325.31[a] |
| HgBr + Br | $R_e$(HgBr) | 2.544 | 2.527[b] |
| | $\omega_e$ | 185.8 | 188.25[c] |
| $HgBr_2$ (min) | $R_e$(HgBr) | 2.404 | 2.377[d] |
| | $\omega_1$ ($\Sigma^+$) | 231.6 | 226.9[d] |
| | $\omega_2$ ($\Pi$) | 71.6 | 69.6[d] |
| | $\omega_3$ ($\Sigma^-$) | 302.5 | 297.8[d] |
| Hg−$Br_2$ (TS) | $R_e$(HgBr) | 2.853 | |
| | $\alpha$(BrHgBr) | 55.74 | |
| | $\omega_1$ ($A_1$) | 152.6 | |
| | $\omega_2$ ($A_1$) | 189.4i | |
| | $\omega_3$ ($B_2$) | 55.7 | |

[a] Reference 62. [b] Reference 44. [c] Reference 63. [d] Reference 45.

**TABLE 2: Heats of Reactions $\Delta H_r$(0K), Kcal/Mol**

| reaction | current surface | best previous theoretical result[a] | experiment[b] |
|---|---|---|---|
| HgBr + Br → Hg + $Br_2$ | −28.9 | −30.6 | −29.91 ± 0.37 |
| HgBr + Br → $HgBr_2$ | −73.4 | −72.4 | −72.33 ± 2.34 |
| Hg + $Br_2$ → $HgBr_2$ | −44.4 | −42.4 | −42.42 ± 2.05 |

[a] Reference 44. [b] Using $\Delta H_f$(0K) = 15.42 ± 0.01 kcal/mol for Hg, $\Delta H_f$(0K) = 28.18 ± 0.01 kcal/mol for Br, $\Delta H_f$(0K) = 10.92 ± 0.03 kcal/mol for $Br_2$, and $\Delta H_f$(0K) = −16.08 ± 2.01 kcal/mol for $HgBr_2$ from JANAF data.[64] An experimental $\Delta H_f$(0K) = 28.07 ± 0.34 kcal/mol for HgBr was calculated using the $D_0$(HgBr) = 15.53±0.32 kcal/mol from ref 65.

current surface accurately reproduces the equilibrium BrBr distance and harmonic frequency of $Br_2$ and the harmonic frequencies in the HgBr and $HgBr_2$ molecules. The equilibrium HgBr distances in both HgBr and $HgBr_2$, however, are somewhat longer by ∼0.03 Å than those obtained previously[44,45] by the CCSD(T) method. These differences cannot be explained by just the neglect of core-valence correlation effects in the present study, since according to our previous work the core-valence effect on the HgBr distance in $HgBr_2$ consists of just

0.009 Å. Therefore, the reason for the discrepancies is mostly due to differences in the treatment of electron correlation by the icMRCI+Q method used in the present study compared to the CCSD(T) method used previously.[44,45] Apparently, the icMRCI+Q method of this work does not recover as much electron correlation around the single determinant dominated regions of the $HgBr_2$ molecule as compared to the CCSD(T) method.

The enthalpy of the insertion reaction calculated from the current PES is at the lower end of the uncertainty interval of the corresponding experimental value and 2.0 kcal/mol lower than the accurate CCSD(T) value obtained in our previous work.[44] The icMRCI+Q/CBS+SO enthalpies for abstraction and recombination are in very good agreement with the experimental enthalpies and differ by less than 1 kcal/mol from the accurate theoretical values obtained in our previous study.[44] Generally, the global potential energy surface of $HgBr_2$ constructed in the present work reproduces the best estimates for the energies and spectroscopic parameters of the species involved in these reactions, and we believe it to be very suitable for an accurate investigation of the dynamics of reactions 3−6.

## IV. Details of Rate Constant Calculations

The thermal rate constants of the reactions HgBr + Br → *products* were determined by the QCT method. There are several schemes for investigation of reaction rates using the QCT approach and a general description of the QCT methodology can be found in the literature (cf., ref 46). In the present study the thermal rate constants were determined by

$$k(T) = \sum_{v,j} k^{vj}(T) \frac{(2j+1)\exp\{-E_{vj}/k_B T\}}{Q_{vr}(T)} \tag{26}$$

where $Q_{vr}$ is the rovibrational partition function and $E_{vj}$ is the HgBr rovibrational energy for vibrational and rotational quantum numbers $v$ and $j$ found by the standard formula

$$E_{vj} = \omega_e\left(v+\frac{1}{2}\right) - \omega_e x_e\left(v+\frac{1}{2}\right)^2 + B_e j(j+1) - \alpha_e\left(v+\frac{1}{2}\right)j(j+1) - D_e[j(j+1)]^2 \tag{27}$$

where the spectroscopic constants of the HgBr molecule are $\omega_e = 186.6\ \mathrm{cm}^{-1}$, $\omega_e x_e = 0.75\ \mathrm{cm}^{-1}$, $B_e = 0.045925\ \mathrm{cm}^{-1}$, $\alpha_e = 0.00032\ \mathrm{cm}^{-1}$, and $D_e = 1.10 \times 10^{-8}\ \mathrm{cm}^{-1}$ calculated from the two-body HgBr potential of the current work.

The reaction rates $k^{vj}$(T) for each ($v$, $j$) rovibrational energy level were found by

$$k^{vj}(T) = g_e\left(\frac{8k_B T}{\pi\mu_{\mathrm{HgBr+Br}}}\right)^{1/2}\sigma^{vj} \tag{28}$$

where $g_e$ is the electronic degeneracy number; $g_e = 1/8$ for the recombination reaction 3 and abstraction reaction 4 and $g_e = 1$ for the exchange reaction 5. In addition, $k_B$ is the Boltzmann constant, $\mu_{\mathrm{HgBr+Br}}$ is the reduced mass, and $\sigma^{vj}$ is the reaction cross section

$$\sigma^{vj} = \pi b_{\max}\frac{N_r^{vj}}{N} \tag{29}$$

In eq 29 $b_{\max}$ is the maximum impact parameter, $N_r^{vj}$ is the number of reactive trajectories for a given reactant ($v$, $j$) rovibrational level, and $N$ is the total number of trajectories.

**TABLE 3: Definition of Trajectory Termination Criteria for HgBr + Br**

| no. | product[a] | criteria[b] |
|---|---|---|
| 1 | BrHg + Br | $R_1 < 3.5$ and $R_2 > 12.0$ and $-16.0 < V < -1.0$ |
| 2 | Hg + $Br_2$ | $R_3 < 3.5$ and $h > 12.0$ and $-46.0 < V < -1.0$ |
| 3 | Br + HgBr | $R_1 > 12.0$ and $R_2 < 3.5$ and $-16.0 < V < -1.0$ |
| 4 | Br + Hg+Br | $R_1, R_2, R_3 > 12.0$ and $V > -1.0$ |
| 5 | BrHgBr | $V < -50.0$ and *time* $> 10^{-11}$ s |

[a] Channel No. 1 corresponds to a nonreactive trajectory while channel No. 3 describes the exchange reaction. [b] Distances $R_1$, $R_2$, $R_3$, and $h$ are in Å; see Figure 1 and text for the notation of coordinates. Potential energy $V$ is in kcal/mol, given relative to the Br + Hg + Br separated energy. The test for termination started after $2.5 \times 10^{-12}$ s. See text for more details.

With a probability of 95%, the statistical error of the rate constants $k^{vj}$ does not exceed

$$\Delta k^{vj} = 2k^{vj}\left[\frac{(N - N_r^{vj})}{NN_r^{vj}}\right]^{1/2} \tag{30}$$

The sum of the $\Delta k^{vj}$ values analogous to eq 26 gives then the estimate to the total error $\Delta k(T)$ of the rate constant $k$(T).

The QCT calculations were carried out with the VENUS96 program.[39] The initial translational energies were generated by sampling a Maxwell−Boltzmann distribution, and the maximum impact parameter $b_{\max} = 9.0$ Å was found in trial calculations for the ($v = 0$, $j = 0$) rovibrational level of HgBr. We have verified that larger values of $b_{\max}$ did not significantly alter the reaction cross sections for the higher $v$ and $j$ states investigated in this study. The termination of trajectories was determined by both geometrical and energy criteria for the abstraction and exchange reaction channels, and a criterion based on the time spent in the Br−Hg−Br complex well for the recombination reaction (see Table 3). The test for termination criteria was always initiated after $2.5 \times 10^{-12}$ s after the start of a trajectory. The trajectory calculations were performed for HgBr vibrational quantum numbers $v = 0, 1, 2, ..., 5$ and rotational quantum numbers $j = 0, 10, 20, ..., 200$. The total number of trajectories, $N$, was chosen to be 10 000 for the runs with vibrational quantum numbers $v = 0$, 1, and 2, and $N = 6000$ for the remainder of the calculations. The full set of $k^{vj}$ ($j = 0, 1, 2, ..., 200$) was obtained by fitting the function $k^{vj} = \exp(-\alpha j^2) \times \sum_{i=1}^{3} c_i j^{i-1}$ to the partial data weighted by $1/\Delta k^{vj}$ in the least squares procedure. Similarly, the full set of errors $\Delta k^{vj}$ was obtained by interpolation of known errors at $j = 0, 10, 20, ..., 200$ by natural cubic splines.

Because of the high barrier for the insertion Hg + $Br_2$ → $HgBr_2$, one could expect a very small reaction probability for this channel at $T = 298$ K. Hence the calculation of the rate constant using the QCT method would demand very large numbers of trajectories, which would be very computationally intensive. Therefore, the rate constant for the insertion reaction was calculated by canonical (CVT), improved canonical (ICVT), and microcanonical ($\mu$VT) variational transition state theory[47−53] with use of the POLYRATE program.[38] The analogous VTST calculations were also carried out for the abstraction and recombination reactions in order to compare with the QCT results.

Finally, assuming microscopic reversibility, the rate constants $k_r$ for the reverse reactions of reactions 3, 4, and 6 were estimated from the detailed balance principle $K_{eq} = k_f/k_r$, where $K_{eq}$ is the corresponding equilibrium constant found using the harmonic approximation with the POLYRATE program and $k_f$ is the calculated forward rate constant for reaction 3, 4, or 6.

**TABLE 4: Thermal (298 K) Reaction Rate Constants of the Present Work**[a]

| | reaction[b] | QCT | CVT | ICVT | $\mu$VT |
|---|---|---|---|---|---|
| A | $HgBr + Br \rightarrow Hg + Br_2$ | $3.89 \pm 0.17$ (−11) | 6.15 (−11) | 5.30 (−11) | 4.52 (−11) |
| B | $HgBr + Br \rightarrow HgBr_2$ | $2.98 \pm 0.14$ (−11) | 1.27 (−10) | 1.22 (−10) | 1.05 (−10) |
| C | $Hg + Br_2 \rightarrow HgBr_2$ | | 2.76 (−31) | 2.76 (−31) | 2.74 (−31) |
| D | $BrHg + Br \rightarrow Br + HgBr$ | $3.97 \pm 0.35$ (−11) | | | |
| E | $Hg + Br_2 \rightarrow HgBr + Br$ | $3.4 \pm 0.15$ (−31) | 5.4 (−31) | 4.6 (−31) | 3.9 (−31) |
| F | $HgBr_2 \rightarrow HgBr + Br$ | $5.5 \pm 0.26$ (−39) | 2.4 (−38) | 2.3 (−38) | 2.0 (−38) |
| G | $HgBr_2 \rightarrow Hg + Br_2$ | | 5.9 (−39) | 5.9 (−39) | 5.8 (−39) |

[a] The rate constants of reactions A−E have units of $cm^3/(mol\cdot s)$, while those of the unimolecular reactions F and G have units of $s^{-1}$. Numbers in parentheses denote powers of 10. [b] The rate constants for the reactions E−G were calculated from the detailed balance principle using equilibrium constants of $K = 1.146839 \times 10^{20}$ for reaction A, $K = 5.407325 \times 10^{27}$ for reaction B, and $K = 4.71417 \times 10^{7}$ for reaction C.

## V. Results and Discussion

The results of the calculations of rate constants at a temperature of $T = 298.15$ K are summarized in Table 4. As expected, the thermal rate constant for the insertion $Hg + Br_2 \rightarrow HgBr_2$ is very small. Three variants of variational transition state theory yielded essentially the same result of $k = 2.74 \times 10^{-31}$ $cm^3/(mol\cdot s)$. The ICVT transition state for this reaction is located slightly toward the reactants side from the insertion saddle point on the $HgBr_2$ PES at the minimum energy path coordinate $s = -0.1787a_o$ (by definition, $s = -\infty$ at the reactants, $s = 0$ at the saddle point, and $s = \infty$ at the products), which corresponds to valence coordinates of $R_1^{\ddagger}(HgBr) = R_2^{\ddagger}(HgBr) = 2.857$ Å, and $\alpha^{\ddagger}(Br-Hg-Br) = 56.4°$.

In the case of the abstraction reaction $HgBr + Br \rightarrow Hg + Br_2$, the ICVT collinear transition state is found at $R_1^{\ddagger}(HgBr) = 2.561$ Å and $R_3^{\ddagger}(BrBr) = 3.803$ Å. The microcanonical VTST rate constant for this reaction is just slightly higher than that obtained via the QCT calculations. The ICVT collinear transition state for the recombination reaction $Br + HgBr \rightarrow HgBr_2$ is located at $R_1^{\ddagger}(HgBr) = 2.539$ and $R_2^{\ddagger}(HgBr) = 4.567$ Å. Energetically the transition state for the recombination reaction lies ~0.5 kcal/mol higher, i.e., closer to the $Br + HgBr$ reactants, than the transition state for the abstraction reaction. Correspondingly, all forms of VTST theory applied in the current study predict that the rate constant for recombination is about a factor of 2 faster than that for abstraction.

Unlike VTST, the QCT calculations predict the rate constant for the recombination reaction to be slightly slower than that for the abstraction reaction. The QCT rate constant for recombination is also 4 times less than the corresponding $\mu$VT value. To explain this larger difference in the QCT and VTST rate constants, one should take into account that the two competing channels, the recombination $Br + HgBr \rightarrow HgBr_2$ and exchange $Br + HgBr \rightarrow BrHg + Br$, both pass through the same variational transition state and are indistinguishable by VTST. In the QCT calculations, however, these two channels have been counted separately. Also, while the VTST theory predicts a high-pressure limit for the rate constant, the QCT rate constant corresponds to a low-pressure limit. A proper accounting for pressure in the QCT calculations could be carried out via introduction of a collision partner. A nonreactive interaction with a collider (Ar, $N_2$) would release the excess energy of trajectories in highly excited rovibrational states of $HgBr_2$ and thus increase the number of reactive trajectories trapped inside the well of the $HgBr_2$ complex. This would decrease the number of trajectories leading to the exchange reaction of the bromine atom. Consequently, after the pressure is taken into account, the rate constant will be higher for recombination, $Br + HgBr \rightarrow HgBr_2$, and lower for exchange, $Br + HgBr \rightarrow BrHg + Br$. We hope to address this issue in a future publication.[11]

The reaction of Hg with $Br_2$ was previously examined in the experimental kinetics study of Ariya et al.[12] that utilized cold-vapor atomic absorption spectroscopy and mass spectroscopic detection techniques. The measurements of the reaction kinetics in that work was complicated, however, due to strong surface catalysis effects on the walls of the reaction chamber, and nearly all the elemental mercury disappeared before it could be detected in the mass spectrometer. Therefore, the authors of that study[12] were only able to predict an upper limit for the $Hg + Br_2$ reaction rate, $k < (0.9 \pm 0.2) \times 10^{-16}$ $cm^3/(mol\cdot s)$. According to our theoretical calculations, the gas-phase reactions of both $Hg + Br_2 \rightarrow HgBr_2$ and $Hg + Br_2 \rightarrow HgBr + Br$ have much smaller rate constants of $k = 2.7 \times 10^{-31}$ $cm^3/(mol\cdot s)$ and $k = 3.4 \times 10^{-31}$ $cm^3/(mol\cdot s)$, respectively.

Goodsite et al.[13] has carried out a theoretical study of a number of reactions involving Hg with Br, I, and OH with use of Rice−Ramsberg−Kassel−Marcus (RRKM) theory.[54] The RRKM model utilized in ref 13 effectively accounted for pressure by including the collision of reagents with $N_2$ molecules. At a temperature of 298 K and a pressure of 1 atm of $N_2$, the RRKM rate coefficient for the recombination reaction $Br + HgBr \rightarrow HgBr_2$ was found to be $k = 2.5 \times 10^{-10}$ $cm^3/(mol\cdot s)$, which is higher than predicted in our VTST calculations (high-pressure limit) $k = 1.05 \pm 0.14 \times 10^{-10}$ $cm^3/(mol\cdot s)$. The possible reason for this inconsistency is that the RRKM calculations of ref 13 were based on equilibrium distances, vibrational frequencies, and a bond energy of $HgBr_2$ estimated at a relatively low level of theory (the B3LYP method and double-$\zeta$ basis sets), which has quite large errors compared to the high level ab initio results[44,45] and/or experimental data (see refs 44 and 45) that could lead to an inaccurate density of states in the RRKM calculations.

Since the observation of mercury depletion events,[1] the mechanism of these phenomena, specifically the chemistry of gas-phase mercury, has been addressed in a number of publications.[2,9,10,12,13,55−58] Most of the researchers agree that conversion of elemental gaseous mercury to its reactive form is mainly due to reaction with active halogen species. One of the possible reaction paths for creation of RGM is successive oxidation of mercury by halogen atoms, predominately bromine, by reactions 2 and 3. The results of the present study strongly support this mechanism. The reaction of HgBr with Br to form the RGM species $HgBr_2$ is fast, while dissociation of the $HgBr_2$ complex to either $Hg + Br_2$ or back to $HgBr + Br$ is extremely slow. However it should be noted that the recombination reaction has two competitive channels with comparable rate coefficients, i.e., abstraction of bromine atom that reintroduces mercury and molecular bromine in the atmosphere, and the exchange reaction of the bromine atom. These channels should be considered in kinetic simulations.

Another popular choice in explaining and modeling MDE mechanisms is the reaction of Hg with BrO radicals.[2,9,59,60] BrO

radicals have been shown to be produced via the ozone destruction reaction $Br + O_3 \rightarrow BrO + O_2$ in the same locations as the observation of MDEs.[2] There is a strong anti-correlation between the concentrations of mercury and BrO.[2] In a kinetic study by Raofie and Aryia,[59] the rate constant of the reaction Hg + BrO was estimated to be $10^{-15} < k < 10^{-13}$ cm$^3$/(mol·s). Although in the current study we investigated the global PES of $HgBr_2$, preliminary calculations in our laboratory indicate that the topology of the HgBrO PES is similar, and therefore, general conclusions from the $HgBr_2$ case should also be valid for HgBrO. The two abstraction channels $Hg + BrO \rightarrow HgO + Br$ and $Hg + BrO \rightarrow HgBr + O$ are strongly endothermic[44,61] by 50.2 and 39.5 kcal/mol, respectively, and these reactions are likely to have small rates just like the $Hg + Br_2 \rightarrow HgBr + Br$ reaction. The insertion reaction, $Hg + BrO \rightarrow BrHgO$, is exothermic[44] by −20.2 kcal/mol; however, our preliminary calculations at the icMRCI+Q level with triple-$\zeta$ correlation consistent basis sets also shows the presence of a large barrier (~40 kcal/mol) like in $HgBr_2$, which implies a very low reaction probability. These factors indicate that reaction of Hg with BrO might have a more complex mechanism in order to explain the high reaction rate found in the experiments. There are also alternatives for the BrO influence on mercury oxidation. For example, Calvert and Lindberg[56] suggested the following reactions involving BrO:

$$HgBr + BrO \rightarrow HgBr_2 + O \quad (31)$$

$$HgBr + BrO \rightarrow BrHgO + Br \quad (32)$$

Analogously, for $Br_2$ one could consider

$$HgBr + Br_2 \rightarrow HgBr_2 + Br \quad (33)$$

From the heat of formation of BrHgO ($\Delta H_f(0K) = 27.2$ kcal/mol) accurately calculated in our previous theoretical study[44] together with experimental heats of formation $\Delta H_f(0K) = 28.18$ kcal/mol for Br(g), $\Delta H_f(0K) = 58.98$ kcal/mol for O(g), $\Delta H_f(0K) = 10.92$ kcal/mol for $Br_2$(g), $\Delta H_f(0K) = 31.96$ kcal/mol BrO, and $\Delta H_f(0K) = -16.08$ kcal/mol for $HgBr_2$ (see ref 44 for references), the enthalpies of reactions 31−33 are −17.1, −4.7, and −26.9 kcal/mol, respectively. Preliminary calculations carried out in our group predict that reactions 31 and 33 are barrierless. It should also be mentioned that the kinetics of the reaction of Hg with $Br_2$/BrO could be affected by the presence of water aerosols[57] and surfaces.[12] The effects of microsolvation on the thermochemistry and reaction dynamics of the interaction of mercury with halogenated species XY (X = Br, Cl; Y = Br, Cl, O) are currently being investigated by theoretical methods in our laboratory.

## VI. Conclusions

An ab initio global potential energy surface for the ground state of $HgBr_2$ was constructed. The reference points are calculated at the icMRCI+Q/CBS+SO level of theory and the surface is represented by a smooth piecewise connection of three sections interpolated by the RKHS method. The quasiclassical trajectory calculations performed on the obtained global surface show that reaction of HgBr with a Br atom has nearly the same rate at 298 K $\{k = (3.0-4.0) \times 10^{-11}$ cm$^3$/(mol·s)$\}$ for all three possible product channels: BrHgBr, $Hg + Br_2$ and Br + HgBr. The insertion reaction, $Hg + Br_2 \rightarrow BrHgBr$, has a large barrier and very small rate constant at 298 K of $k = 2.74 \times 10^{-31}$ cm$^3$/(mol·s). The results of the present study support a mechanism whereby the reaction of mercury with halogen atoms is one of the main initiating steps for atmospheric oxidation of mercury that leads to the observed depletion events in the polar troposphere. The obtained kinetic data are expected to be valuable for future kinetics studies and model simulations.

**Acknowledgment.** This work was partially supported by the National Science Foundation (Grant No. CHE-0111282). The authors gratefully acknowledge Prof. B. Ramachandran (Louisiana Tech University) for his help with the trajectory calculations. The authors would also like to thank Prof. R. Duchovic (Indiana Univ.—Purdue Univ. Ft. Wayne) for his help with Venus and Potlib.

## References and Notes

(1) Schroeder, W. H.; Anlauf, K. G.; Barrie, L. A.; Lu, J. Y.; Steffen, A.; Schneeberger, D. R.; Berg, T. *Nature (London)* **1998**, *394*, 331.
(2) Lindberg, S. E.; Brooks, S.; Lin, C.-J.; Scott, K. J.; Landis, M. S.; Stevens, R. K.; Goodsite, M.; Richter, A. *Environ. Sci. Technol.* **2002**, *36*, 1245.
(3) Ebinghaus, R.; Kock, H. H.; Temme, C.; Einax, J. W.; Lowe, A. G.; Richter, A.; Burrows, J. P.; Schroeder, W. H. *Environ. Sci. Technol.* **2002**, *36*, 1238.
(4) Temme, C.; Einax, J. W.; Ebinghaus, R.; Schroeder, W. H. *Environ. Sci. Technol.* **2003**, *37*, 22.
(5) Steffen, A.; Schroeder, W. H.; Bottenheim, J. W.; Narayan, J.; Fuentes, J. D. *Atmos. Environ.* **2002**, *36*, 2653.
(6) Berg, T.; Sekkesaeter, S.; Steinnes, E.; Valdal, A.-K.; Wibetoe, G. *Sci. Total Environ.* **2003**, *304*, 43.
(7) Boudries, H.; Bottenheim, J. W. *Geophys. Res. Lett.* **2000**, *27* (4), 517.
(8) Oltmans, S. J.; Schnell, R. C.; Sheridan, P. J.; Peterson, R. E.; Li, S.-M.; Winchester, J. W.; Tans, P. P.; Sturges, W. T.; Kahl, J. D.; Barrie, L. A. *Atmos. Environ.* **1988**, *23*, 2431.
(9) Ariya, P. A.; Dastoor, A. P.; Amyot, M.; Schroeder, W. H.; Barrie, L.; Anlauf, K.; Raofie, F.; Ryzhkov, A.; Davignon, D.; Lalonde, J.; Steffen, A. *Tellus B* **2004**, *56B* (5), 397.
(10) Skov, H.; Christensen, J. H.; Goodsite, M. E.; Heidam, N. Z.; Jensen, B.; Wahlin, P.; Geernaert, G. *Environ. Sci. Technol.* **2004**, *38*, 2373.
(11) Shepler, B. C.; Peterson, K. A. *in preparation.*
(12) Ariya, P. A.; Khalizov, A.; Gidas, A. *J. Phys. Chem. A* **2002**, *106*, 7310.
(13) Goodsite, M. E.; Plane, J. M. C.; Skov, H. *Environ. Sci. Technol.* **2004**, *38*, 1772.
(14) Peterson, K. A.; Figgen, D.; Goll, E.; Stoll, H.; Dolg, M. *J. Chem. Phys.* **2003**, *119*, 11113.
(15) Figgen, D.; Rauhut, G.; Dolg, M.; Stoll, H. *Chem. Phys.* **2005**, *311* (1−2), 227.
(16) Peterson, K. A.; Puzzarini, C. *Theor. Chem. Acc.* **2005**, in press.
(17) Knowles, P. J.; Werner, H.-J. *Chem. Phys. Lett.* **1988**, *145* (6), 514.
(18) Werner, H.-J.; Knowles, P. J. *J. Chem. Phys.* **1988**, *89*, 5803.
(19) Langhoff, S. R.; Davidson, E. R. *Int. J. Quantum Chem.* **1974**, *8*, 61.
(20) Blomberg, M. R. A.; Siegbahn, P. E. M. *J. Chem. Phys.* **1983**, *78*, 5682.
(21) Simons, J. *J. Phys. Chem.* **1989**, *93*, 626.
(22) MOLPRO, a package of ab initio programs designed by Werner, H.-J.; Knowles, P. J. version 2002.6. Amos, R. D.; Bernhardsson, A.; Berning, A.; Celani, P.; Cooper, D. L.; Deegan, M. J. O.; Dobbyn, A. J.; Eckert, F.; Hampel, C.; Hetzer, G.; Knowles, P. J.; Korona, T.; Lindh, R.; Lloyd, A. W.; McNicholas, S. J.; Manby, F. R.; Meyer, W.; Mura, M. E.; Nicklass, A.; Palmieri, P.; Pitzer, R.; Rauhut, G.; Schütz, M.; Schumann, U.; Stoll, H.; Stone, A. J.; Tarroni, R.; Thorsteinsson, T.; Werner, H.-J. 2002.
(23) Peterson, K. A.; Woon, D. E.; Dunning, T. H., Jr. *J. Chem. Phys.* **1994**, *100*, 7410.
(24) Helgaker, T.; Klopper, W.; Koch, H.; Noga, J. *J. Chem. Phys.* **1997**, *106*, 9639.
(25) Halkier, A.; Helgaker, T.; Jørgensen, P.; Klopper, W.; Koch, H.; Olsen, J.; Wilson, A. K. *Chem. Phys. Lett.* **1998**, *286*, 243.
(26) Klopper, W.; Bak, K. L.; Jorgensen, P.; Olsen, J.; Helgaker, T. *J. Phys. B* **1999**, *32*, R103.
(27) Yabushita, S.; Zhang, Z.; Pitzer, R. M. *J. Phys. Chem. A* **1999**, *103*, 5791.
(28) Lischka, H.; Shepard, R.; Brown, F. B.; Shavitt, I. *Int. J. Quantum Chem. Symp.* **1981**, *15*, 91.
(29) Shepard, R.; Shavitt, I.; Pitzer, R. M.; Comeau, D. C.; Pepper, M.; Lischka, H.; Szalay, P. G.; Ahlrichs, R.; Brown, F. B.; Zhao, J. G. *Int. J. Quantum Chem. Symp.* **1988**, *22*, 149.

(30) Lischka, H.; Shepard, R.; Pitzer, R. M.; Shavitt, I.; Dallos, M.; Muller, T.; Szalay, P. G.; Seth, M.; Kedziora, G. S.; Yabushita, S.; Zhang, Z. *Phys. Chem. Chem. Phys.* **2001**, *3* (5), 664.
(31) Lischka, H.; Shepard, R.; Shavitt, I.; Pitzer, R. M.; Dallos, M.; Müller, T.; Szalay, P. G.; Brown, F. B.; Ahlrichs, R.; Böhm, H. J.; Chang, A.; Comeau, D. C.; Gdanitz, R.; Dachsel, H.; Ehrhardt, C.; Ernzerhof, M.; Höchtl, P.; Irle, S.; Kedziora, G.; Kovar, T.; Parasuk, V.; Pepper, M. J. M.; Scharf, P.; Schiffer, H.; Schindler, M.; Schüler, M.; Seth, M.; Stahlberg, E. A.; Zhao, J.-G.; Yabushita, S.; Zhang, Z.; COLUMBUS, an ab initio electronic structure program, release 5.8, 2001.
(32) Murrell, J. N.; Carter, S. *J. Chem. Phys.* **1984**, *88*, 4887.
(33) Ho, T.-S.; Rabitz, H. *J. Chem. Phys.* **1996**, *104*, 2584.
(34) Ho, T.-S.; Hollebeek, T.; Rabitz, H.; Chao, S. D.; Skodje, R. T.; Zyubin, A. T.; Mebel, A. M. *J. Chem. Phys.* **2002**, *116*, 4124.
(35) Murrell, J. N.; Carter, S.; Farantos, S. C.; Huxley, P.; Varandas, A. J. C. *Molecular Potential Energy Functions*; John Wiley and Sons: Chichester, U.K., 1984.
(36) Senekowitsch, J. Ph.D. Thesis, Universität Frankfurt, Frankfurt, Germany, 1988.
(37) Hollebeek, T.; Ho, T.-S.; Rabitz, H. *J. Chem. Phys.* **1997**, *106*, 7223.
(38) Corchado, J. C.; Chuang, Y.-Y.; Fast, P. L.; Villà, J.; Hu, W.-P.; Liu, Y.-P.; Lynch, G. C.; Nguyen, K. A.; Jackels, C. F.; Melissas, V. S.; Lynch, B. J.; Rossi, I.; Coitiño, E. L.; Fernandez-Ramos, A.; Pu, J.; Steckler, R.; Garrett, B. C.; Isaacson, A. D.; Truhlar, D. G. POLYRATE-version 8.7.2; University of Minnesota: Minneapolis, MN, 2002.
(39) Hase, W. L.; Duchovic, R. J.; Hu, X.; Komornicki, A.; Lim, K. F.; Lu, D.-h.; Peslherbe, G. H.; Swamy, K. N.; Vande Linde, S. R.; Varandas, A.; Wang, H.; Wolf, R. J. *Quantum Chemistry Program Exchange* **1996**, *16*, 671.
(40) Duchovic, R. J.; Volobuev, Y. L.; Lynch, G. C.; Truhlar, D. G.; Allison, T. C.; Wagner, A. F.; Garrett, B. C.; Corchado, J. C. *Comput. Phys. Commun.* **2002**, *144*, 169.
(41) Varandas, A. J. C. *Chem. Phys. Lett.* **1987**, *138* (5), 455.
(42) Mead, C. A.; Truhlar, D. G. *J. Chem. Phys.* **1979**, *70*, 2284.
(43) Wilcomb, B. E.; Haberman, J. A.; Bickes, R. W., Jr.; Mayer, T. M.; Bernstein, R. B. *J. Chem. Phys.* **1976**, *64*, 3501.
(44) Balabanov, N. B.; Peterson, K. A. *J. Phys. Chem. A* **2003**, *107*, 7465.
(45) Balabanov, N. B.; Peterson, K. A. *J. Chem. Phys.* **2003**, *119*, 12271.
(46) Peslherbe, G. H.; Wang, H.; Hase, W. L. *Adv. Chem. Phys.* **1999**, *105*, 171.
(47) Garrett, B. C.; Truhlar, D. G. *J. Phys. Chem.* **1979**, *83*, 1052.
(48) Garrett, B. C.; Truhlar, D. G.; Grev, R. S. In *Potential Energy Surfaces and Dynamics* Calculations; Truhlar, D. G., Ed.; Plenum: New York, 1980; p 587.
(49) Garrett, B. C.; Truhlar, D. G.; Grev, R. S.; Magnuson, A. W. *J. Phys. Chem.* **1980**, *84*, 1730.
(50) Garrett, B. C.; Truhlar, D. G.; Grev, R. S.; Magnuson, A. W. *J. Phys. Chem.* **1983**, *87*, 4554.
(51) Isaacson, A. D.; Truhlar, D. G. *J. Chem. Phys.* **1982**, *76*, 1380.
(52) Truhlar, D. G.; Isaacson, A. D.; Garrett, B. C. In *Theory of Chemical Reaction Dynamics*; Baer, M., Ed.; CRC Press: Boca Raton, FL, 1985; Vol. 4; p 65.
(53) Tucker, S. C.; Truhlar, D. G. In *New Theoretical Concepts for Understanding Organic Reactions*; Bertran, J., Csizmadia, I. G., Eds.; Kluwer: Dordrecht, The Netherlands, 1989.
(54) Steinfeld, J. I.; Francisco, J. S.; Hase, W. L. *Chemical Kinetics and Dynamics*; Prentice Hall: Englewood Cliffs, NJ, 1989.
(55) Calvert, J. G.; Lindberg, S. E. *Atmos. Environ.* **2003**, *37*, 4467.
(56) Calvert, J. G.; Lindberg, S. E. *Atmos. Environ.* **2004**, *38*, 5105.
(57) Tossel, J. A. *J. Phys. Chem. A* **2003**, *107*, 7804.
(58) Sheu, G.-R.; Mason, R. P. *J. Atmos. Chem.* **2004**, *48*, 107.
(59) Raofie, F.; Ariya, P. A. *J. Phys. IV* **2003**, *107*, 1119.
(60) Raofie, F.; Ariya, P. A. *Environ. Sci. Technol.* **2004**, *38*, 4319.
(61) Shepler, B. C.; Peterson, K. A. *J. Phys. Chem. A* **2003**, *107*, 1783.
(62) Focsa, C.; Li, H.; Bernath, P. F. *J. Mol. Spectrosc.* **2000**, *200* (1), 104.
(63) Tellinghuisen, J.; Ashmore, J. G. *Appl. Phys. Lett.* **1982**, *40*, 867.
(64) Chase, M. W., Jr.; Davies, C. A.; Downey, J. R., Jr.; Frurip, D. J.; McDonald, R. A.; Syverud, A. N. *J. Phys. Chem. Ref. Data* **1985**, *14*, Suppl. No. 1.
(65) Tellinghuisen, J.; Ashmore, J. G. *Chem. Phys. Lett.* **1983**, *102* (1), 10.